

---

# IN-SITU MEASUREMENT METHODS FOR CHARACTERISATION AND DIAGNOSIS OF AIRBORNE SOUND TRANSMISSION THROUGH MULTI- LAYERED BUILDING PARTITIONS

---

Ph.D. Thesis

Author

**NIKHILESH PATIL**

Supervisor

**ANDY MOORHOUSE**

*A thesis submitted in fulfilment of the requirements for the degree of Doctor of Philosophy*

Acoustics Research Centre, University of Salford, UK

March 2018

---

# DECLARATION OF AUTHORSHIP

---

I, NIKHILESH PATIL, declare that this thesis and the work presented in it are my own and has been generated by me as the result of my own original research.

“IN-SITU MEASUREMENT METHODS FOR CHARACTERISATION AND DIAGNOSIS OF AIRBORNE SOUND TRANSMISSION THROUGH MULTI-LAYERED BUILDING PARTITIONS”

I confirm that:

1. This work was done wholly or mainly while in candidature for a research degree at University of Salford, UK;
2. Where any part of this thesis has previously been submitted for a degree or any other qualification at this University or any other institution, this has been clearly stated;
3. Where I have consulted the published work of others, this is always clearly attributed;
4. Where I have quoted from the work of others, the source is always given. With the exception of such quotations, this thesis is entirely my own work;
5. I have acknowledged all main sources of help;
6. Where the thesis is based on work done by myself jointly with others, I have made clear exactly what was done by others and what I have contributed myself;

Signed: .....

Date: .....

---

# ACKNOWLEDGEMENTS

---

I started my research work at University of Salford three years ago with a drive to learn acoustics and develop solutions for silent technologies. University of Salford presented as the best opportunity to me at the time and I am happy that I decided to study here away from my home country.

I would like to thank my supervisor Prof. Andy Moorhouse who has been a great teacher, and mentor for my PhD studies, and helped me gain practical experience through technical work in the acoustics laboratories. His professional guidance, direction and insight has certainly helped me steer my studies and work in the right direction. I would also like to thank Dr. Andy Elliott who has been a mentor as well and provided me with commercial research opportunities for work. It was a great learning experience to work alongside him.

I also feel proud in maintaining a steady focus of my vision, and keeping track of my life in UK away from my home country. I am very thankful to my parents for believing in me, supporting my decision to study in UK as well as providing assistance in times of need. I am also thankful to my grandparents, cousins and family for all their wishes and support. Without their guidance and support, I would not be the person I am today.

Lastly, but not the least, I would like to thank my friends and colleagues who have been by my side and motivated me and helped me in some way towards my studies and life. In addition, special mention to all the lab colleagues who helped me gain hands on training for practical equipment and skills.

---

# ABSTRACT

---

The thesis concerns with the development of novel measurement methods for characterisation and diagnosis of airborne sound transmission through building partitions. Using standard tests, the airborne sound insulation of partitions can be measured as the Sound Reduction Index 'SRI'. While the SRI provides the frequency dependence of sound insulation (or transmission), the local/spatial sound transmission through various paths in the partition is not known. If the contributions of different paths in the partition can be measured then any weak paths of sound insulation can be diagnosed. This would be especially useful in the case of multi-layered partitions where the sound insulation depends on the sound transmission through point connections/ribs/studs/frame, etc. present in the structure. While different theoretical models are in place to predict the sound insulation in presence of such elements, the experimental diagnosis of their sound transfer contributions remains fairly unexplored.

Similar diagnosis problems are encountered by automotive industry while dealing with structure borne sources in the vehicle. In practice, Transfer Path Analysis (TPA) methods are extensively used in such cases for diagnosing the contributions of different structure borne sources at vehicle interiors. Application of such TPA methods for diagnosing airborne sound transmission is challenging on various counts. Firstly, the airborne source applies a continuous excitation on the receiver as opposed to structure borne sources which are typically discrete. Secondly, for our study, the path contributions are desired which is difficult than measuring source characterisations. To address these issues, a novel TPA application Inverse-Airborne Source Contribution Analysis (I-ASCA) is devised which employs a patch based discretisation of the source receiver interface for the diagnosis of airborne sound transmission through partitions. Using such discretisation, the airborne excitation on the partition can be inversely characterised by blocked forces and the source contributions can be measured. Additionally, a new methodology Inverse Path Contribution Analysis (I-PCA) is outlined which allows for measurement of path contributions. These



methodologies applied to the case of single and double layer partitions excited by airborne source and the accuracy of the methods was found to be within 2-3 dB of the measured response in general up to a maximum of 1 kHz under the tested grid size. The accuracy of the method is thus strictly linked to the discretisation size. A sampling criterion of  $\lambda_b/2$  was found to be sufficient which is less demanding than sampling criterion utilised by finite element methods. The methods can be applied to >1 kHz range if the discretisation can be made finer.

To improve the practical application of the methods, the Direct-Airborne Source Contribution Analysis (D-ASCA) is presented which allows for direct characterisation of the airborne excitation using contact pressures. The method is much faster than I-ASCA in providing source contributions however path contributions cannot be measured using this method and the accuracy of the method is also found to be within 2-3 dB.

D-ASCA application has been presented for the case of commercial single and double casement windows. Using careful assumptions, it is possible to estimate the path contributions of the glazing and frame in the windows from the source contributions. The diagnosis allows comparing the path contributions in frequency regions up to 1 kHz and the weak path is identified. This shows the potential of the method in identifying the weak elements of sound insulation which can be used as a complement to the SRI data and can provide cues for improving the sound insulation of the partition.

Lastly, an in-situ measurement method for airborne sound insulation measurement is presented which can be applied when a pressure doubling occurs at the surface. A novel approach has been presented to assess whether pressure doubling occurs on the surface and calculating the blocked pressures. This allows one to measure SRI in-situ using diagnostic measurements without the need of a separate standard test for measuring SRI. This showcases the versatility of the approaches in that the frequency dependence (SRI) and spatial dependence (path contributions) of sound insulation/transmission can be measured within a single approach.

---

# CONTENTS

---

|  |      |
|--|------|
| Declaration Of Authorship.....                                     | I    |
| Acknowledgements.....  | II   |
| Abstract.....  | III  |
| Contents.....  | V    |
| List of Figures .....  | IX   |
| Abbreviations .....  | XVI  |
| Symbols.....   | XVII |
| 1 INTRODUCTION .....   | 1    |
| 1.1 Structure borne noise .....                                    | 3    |
| 1.2 Airborne noise .....   | 4    |
| 1.3 Sound insulation .....   | 4    |
| 1.3.1 Airborne sound insulation measurement.....                   | 5    |
| 1.4 Motivations .....  | 6    |
| 2 LITERATURE SURVEY .....  | 8    |
| 2.1 Sound transmission through building elements.....              | 8    |
| 2.1.1 Measuring airborne sound insulation .....                    | 11   |
| 2.1.2 Implication of diffuse field assumption.....                 | 14   |
| 2.1.3 Quantifying uncertainty in SRI.....                          | 15   |
| 2.2 Literature survey on SRI measurement of building elements..... | 16   |
| 2.2.1 Experimental techniques – improving repeatability .....      | 17   |
| 2.2.2 Alternative methods towards SRI measurement .....            | 18   |
| 2.2.3 Prediction methods .....                                     | 20   |
| 2.3 Factors influencing SRI of a partition.....                    | 20   |
| 2.3.1 Mass effects.....  | 21   |
| 2.3.2 Source factors .....   | 21   |
| 2.3.3 Structure borne transmission and flanking.....               | 22   |
| 2.3.4 Effect of structural elements.....                           | 23   |
| 2.4 Transfer Path Analysis (TPA) .....                             | 25   |
| 2.4.1 Source Characterisation.....                                 | 26   |
| 2.4.2 Structure borne sources .....                                | 26   |
| 2.4.3 Power based quantities.....                                  | 30   |

|       |  |    |
|-------|--|----|
| 2.4.4 | Airborne source characterisation.....                        | 31 |
| 2.4.5 | TPA – diagnostic contributions.....                          | 33 |
| 2.5   | Diagnostic methods in building acoustics .....               | 34 |
| 2.5.1 | Objectives of study.....                                     | 35 |
| 2.6   | Discussion.....  | 36 |
| 3     | DIAGNOSIS OF AIRBORNE SOUND TRANSMISSION – TPA METHODS ..... | 38 |
| 3.1   | Diagnosis of airborne sound insulation.....                  | 38 |
| 3.2   | Diagnostic descriptor.....                                   | 40 |
| 3.2.1 | Transmitted pressure and velocity .....                      | 41 |
| 3.2.2 | Vibroacoustic FRF .....                                      | 42 |
| 3.3   | Diagnostic analysis – TPA.....                               | 43 |
| 3.3.1 | Source-interface-receiver model.....                         | 43 |
| 3.3.2 | FRF measurements .....                                       | 46 |
| 3.3.3 | Operational measurements.....                                | 47 |
| 3.3.4 | Source characterisation and diagnostic contributions .....   | 48 |
| 3.3.5 | Application of iTPA to airborne problems .....               | 49 |
| 3.4   | Airborne source contribution analysis –Methodology.....      | 54 |
| 3.4.1 | Validation of I-ASCA methodology .....                       | 57 |
| 3.4.2 | Sampling considerations .....                                | 57 |
| 3.5   | I-ASCA: Test setup and measurements.....                     | 59 |
| 3.5.1 | I-ASCA – pressure validation results .....                   | 61 |
| 3.5.2 | I-ASCA – source contribution results .....                   | 67 |
| 3.6   | Path contribution analysis .....                             | 69 |
| 3.6.1 | I-PCA – methodology.....                                     | 72 |
| 3.6.2 | I-PCA – path contribution results .....                      | 76 |
| 3.7   | Conclusions.....   | 77 |
| 4     | DIAGNOSTIC TESTING FOR MULTI-LAYERED PARTITIONS.....         | 79 |
| 4.1   | Point connected dual leaf partition .....                    | 80 |
| 4.2   | I-ASCA and I-PCA Measurements.....                           | 81 |
| 4.3   | Structure borne excitation case .....                        | 83 |
| 4.3.1 | Blocked forces.....  | 83 |
| 4.3.2 | Path contributions .....                                     | 88 |
| 4.4   | Airborne excitation case .....                               | 91 |

|       |  |     |
|-------|--|-----|
| 4.5   | Transmission suite tests .....   | 93  |
| 4.5.1 | Construction .....   | 94  |
| 4.5.2 | Second test .....  | 99  |
| 4.6   | Extension to multi-layered partitions .....                            | 111 |
| 4.7   | Pressure validation and flanking.....                                  | 113 |
| 4.8   | Blocked forces.....  | 114 |
| 4.9   | In-situ sound insulation measurement.....                              | 115 |
| 4.10  | Measurement time .....   | 116 |
| 5     | DIAGNOSTIC TESTING FOR MULTI-LAYERED PARTITIONS – DIRECT APPROACH..... | 118 |
| 5.1   | Practical considerations – measurement time .....                      | 119 |
| 5.1.1 | Possible measures.....   | 120 |
| 5.1.2 | The airborne source .....  | 121 |
| 5.2   | Blocked pressure characterisation of airborne sources .....            | 122 |
| 5.2.1 | Blocked pressure measurement – classical definition .....              | 123 |
| 5.2.2 | Blocked pressure measurement – boundary value problem approach .....   | 126 |
| 5.2.3 | Extension to cavity subsystems.....                                    | 128 |
| 5.3   | Transferability of the blocked pressures .....                         | 131 |
| 5.3.1 | A note on definitions.....   | 133 |
| 5.4   | Direct – Airborne Source Contribution Analysis (D-ASCA) .....          | 133 |
| 5.4.1 | Blocked pressure measurement on unbaffled panel .....                  | 137 |
| 5.4.2 | Direct blocked pressure measurement – baffled panels .....             | 141 |
| 5.5   | D-ASCA for multi-layered partition case .....                          | 144 |
| 5.5.1 | Pressure validation.....   | 145 |
| 5.5.2 | Diagnostic contribution .....  | 147 |
| 5.5.3 | Radiated pressure .....  | 148 |
| 5.5.4 | On board validation – vibration response prediction.....               | 153 |
| 5.6   | Conclusions.....   | 154 |
| 6     | COMBINED SOUND INSULATION AND DIAGNOSTIC TESTS .....                   | 157 |
| 6.1   | Airborne sound insulation tests with diagnostic tests .....            | 158 |
| 6.2   | Case study I – double casement window .....                            | 158 |
| 6.2.1 | Airborne sound insulation and diagnostic tests .....                   | 159 |
| 6.2.2 | Diagnostic tests .....   | 160 |
| 6.2.3 | Diagnostic contributions – glazing and frame .....                     | 164 |



---

|       |   |     |
|-------|---|-----|
| 6.2.4 | Diagnostic measurements as a tool for SRI improvement – a case study..... | 168 |
| 6.3   | Case study II – single casement window.....                               | 169 |
| 6.4   | Combined testing – in situ perspective.....                               | 175 |
| 6.4.1 | Source and receiver fields.....   | 175 |
| 6.4.2 | Test structure and flanking.....  | 176 |
| 6.5   | Sound insulation – measurement approaches.....                            | 177 |
| 6.5.1 | Standard sound insulation test with corner measurement.....               | 177 |
| 6.5.2 | Diagonal measurement method.....  | 178 |
| 6.5.3 | FRF based formulation.....  | 179 |
| 6.5.4 | SRI using blocked pressure hypothesis.....                                | 180 |
| 6.6   | Conclusions.....  | 185 |
|       | CONCLUSIONS.....  | 186 |
|       | FURTHER WORK.....   | 193 |
|       | APPENDIX I.....   | 195 |
|       | APPENDIX II.....  | 198 |
|       | APPENDIX III.....   | 202 |
|       | APPENDIX IV.....  | 204 |
|       | APPENDIX V.....   | 207 |
|       | REFERENCES.....   | 209 |

---

# LIST OF FIGURES

---

|  |    |
|--|----|
| Figure 2.1: Paths of airborne and structure borne sound transmission between rooms [22] .....  | 9  |
| Figure 2.2: Irregular spatial distribution of SPL at low frequency room modes in a room of 3 x 4 x 3 m <sup>3</sup> . Left-SPL distribution for 77 Hz tangential mode, right-SPL distribution for 63 Hz axial mode.....  | 11 |
| Figure 2.3: Different regions governing the SRI of a single isotropic panel .....  | 21 |
| Figure 2.4: Source-receiver representation of a dynamic system, source (active component) is coupled to the receiver (passive component) at the source receiver interface (in dashed red), $s_i$ –internal driver/mechanism of the source .....  | 26 |
| Figure 2.5: Active source substructure with velocity $v_{si}$ at interface ‘ $i$ ’. Left –interface is free and interface velocity is the free velocity ( $v_{sf}$ ) of the source, right –interface is blocked and forces acting at the interface are blocked forces ( $f_{bi}$ ) of the sources .....  | 28 |
| Figure 3.1: A single panel between a source and receiver room discretised into patches. For a patch ‘ $j$ ’, the velocity on the patch $v_j$ and the pressure close to the patch $p_j$ are denoted, and the contribution at a receiver point $k$ is $p_{k,j}^c$ where superscript ‘ $c$ ’ denotes contribution .....                                       | 41 |
| Figure 3.2: Interfaces (‘  ’) for structure borne (SB) and airborne (AB) sources coupled to receivers. Left –Structure borne excitation acting at discrete interfaces and right –an airborne excitation acting at a continuous interface.....                           | 44 |
| Figure 3.3: Sound transmission from source DoF $i$ and receiver DoF $j$ represents a single transfer path characterised by its mobility $Y_{ji}$ , while multiple sound transmission paths exist between $i$ and $j$ (in dotted) .....   | 47 |
| Figure 3.4: A source-interface-receiver system (left) with its equivalent representation on right –the blocked forces acting on the receiver through the interface (‘  ’), $f_{bi}$ represents the blocked forces of the source .....                                 | 49 |
| Figure 3.5: System of airborne sound transmission from source to receiving room through a multi-layered partition (on left) and then substructured as a source-interface-receiver system (on right). Source is the source room, partition plus receiving room is the receiver and the interface (in red) is the boundary between source and receiver ..... | 50 |
| Figure 3.6: Approximating an incident sound field on a partition by point forces on discrete patches of the partition (3D view-left graphic). Equivalent force representation of the airborne excitation on partition between rooms (right graphic) .....  | 52 |
| Figure 3.7: A multi-layered partition discretised into patches at the interface (in dashed red). Left –schematic of source contribution of force $f$ (in purple) which diagnoses the radiation (blue arrows)   |    |

|  |    |
|--|----|
| through all patches, superscript 's' denotes source contribution. Right – schematic of path contribution which diagnoses the radiation through individual patch (in purple) under the action of any number of excitations, superscript 'p' denotes path contribution .....   | 53 |
| Figure 3.8: Left graphic –A multi-layered partition installed between a source room and a receiving room with the interface in dashed red. Right graphic – Isolated view of the partition with the interface discretised in 'j' patches. Blue arrows denote the radiation .....  | 54 |
| Figure 3.9: Left – Under the action of 'j' blocked forces, the receiver side pressure predicted as a sum of all source contributions in frequency range $f$ determined by sampling. Right – Under the action of a single blocked force at patch 'n', the pressure measured is a source contribution (with superscript 's') ..... | 56 |
| Figure 3.10: The test setup- the wooden box (top left), Perspex panel (top right), free-field microphones (bottom left), and the assembled box (bottom right) .....  | 59 |
| Figure 3.11: I-ASCA measurement schematic for FRF's (on left) and operational measurements (on right) with an active airborne source-loudspeaker.....  | 60 |
| Figure 3.12: Pressure validation results for a 4x4 measurement grid over the panel comparing the measured and predicted pressure in narrow band (top plot) and one third octave band (bottom plot) in 20-500 Hz range. Frequency axis applies to both plots.....   | 62 |
| Figure 3.13: Representation of FRF (accelerance) measurement in 4 test sessions for 8x8 grid. The hammer is hit at the centre of all patches (X) while response are recorded only at limited accelerometer locations (O) in each test session .....  | 62 |
| Figure 3.14: Reciprocity for randomly chosen nine sets of response-force points on the panel. Bad reciprocity is observed for some data sets indicating wrong measurement data.....  | 63 |
| Figure 3.15: Pressure validation for 8x8 case using poorly measured accelerance FRF's .....  | 64 |
| Figure 3.16: Reciprocity for randomly chosen nine sets of response-force points on the panel for an 8x8 measurement grid .....   | 65 |
| Figure 3.17: Pressure validation results for a 8x8 measurement grid over the panel comparing the measured and predicted pressure in narrow band (top plot) and one third octave band (bottom plot) against grid size/bending wavelength. Frequency axis applies to both plots.....   | 66 |
| Figure 3.18: Panel divided into four regions (left) of equal areas mentioned by color codes (right) .....  | 68 |
| Figure 3.19: Contributions of sources acting on different regions over the panel specified in Figure 3.18 compared to the total pressure .....   | 68 |
| Figure 3.20: Operational measurement phase in PCA. Paths on panel 'B' vibrating with a normal velocity $v'$ (left) characterised as elementary volume velocity sources $Q'$ (in black) radiating into receiver volume R (right) .....  | 70 |

|  |    |
|--|----|
| Figure 3.21: Schematic of direct (left) and reciprocal (right) measurement of the acoustic FRF. PCA employs reciprocal measurement.....  | 71 |
| Figure 3.22: Multi-layered partition (in blue). For reciprocal measurement of acoustic FRF $U_{kj}$ , microphone placement against source side panel A on a path 'j' (in dotted red) is restricted (in red mic) in contrast to accessible placement against receiver side panel B (in black mic) .....                       | 72 |
| Figure 3.23: Left – Under the action of source excitation, the receiver side pressure at 'k' predicted as a sum of all path contributions from the vibrating partition. Right – Under the action of source excitation, the radiation from a single patch 'n' is the path contribution (with superscript 'p') .....           | 74 |
| Figure 3.24: Source and path contributions (in one-third octave bands) for different regions of the panel depicted in Figure 3.18. Source contributions depict the sound transmission globally for a given source while path contributions depict the sound transmission locally .....                                       | 76 |
| Figure 4.1: Point connected dual leaf partition (left). Actual point connection used in the partition (right) .....  | 80 |
| Figure 4.2: The dual leaf partition with a wooden frame assembled on top on the wooden box (in green) representing the receiver cavity .....   | 81 |
| Figure 4.3: Reciprocity between nine sets of response and force locations on the top panel.....  | 82 |
| Figure 4.4: Two different source receiver configurations where the interface is effectively same. Left-the source is not visible and thus the source nature and interface are unknown. Right-the source location and source receiver interface are known. Measurement side refers to the side accessible for measurements .. | 84 |
| Figure 4.5: Blocked forces characterised over different paths of the top panel with magnitude (top plot) and phase (bottom plot) displayed in narrow band .....  | 85 |
| Figure 4.6: Pressure validation results for point connected partition using multiple blocked forces over the partition. This represents to the case when the source location is not known .....  | 86 |
| Figure 4.7: Pressure validation using a single blocked force characterisation of the shaker. This represents the case when the source location is known .....  | 87 |
| Figure 4.8: Path contributions to the sound pressure when the partition is excited by a point structure borne source .....   | 88 |
| Figure 4.9: Estimated effect of removing the Point Connection (PC) contribution from the total pressure in narrow band (top plot) and one-third octave band (bottom plot) for a structure borne excitation on the partition .....  | 90 |
| Figure 4.10: Top plot –Pressure validation for airborne excitation case comparing the measured and predicted sound pressure in the box cavity. Bottom plot –comparing measured pressure against flanking   |    |



|  |     |
|--|-----|
| transmission through box walls to confirm the influence of flanking on the pressure validation results above .....   | 92  |
| Figure 4.11: The transmission suite consisting of the source room (right), receiving room (left) and the mic positions in black in both rooms .....  | 95  |
| Figure 4.12: The aperture in the separating wall between source and receiving rooms prior to the I-ASCA test (left) and on right- the partition (in black) installed in the brick walled aperture with the filler wall structure around it (in blue). The filler wall cavity here is made up of plasterboard stacks..... | 95  |
| Figure 4.13: Sound insulation of the dual leaf partition and filler wall structure measured by ISO 10140 method.....   | 96  |
| Figure 4.14: Schematic for FRF measurements (left) and operational measurements (right) for the I-ASCA test in transmission suite (top view). Red line denotes the interface .....   | 97  |
| Figure 4.15: Reciprocity between nine sets of force-response for randomly chosen paths on the dual leaf partition installed in transmission suite .....  | 97  |
| Figure 4.16: Pressure validation for the I-ASCA test on the dual leaf partition in the transmission suite. Predicted pressure by I-ASCA is compared with the measured pressure in narrow band (top plot) and one-third octave band (bottom plot) .....   | 98  |
| Figure 4.17: (a) Front view from the source room of the test partition installed with the plasterboard partition (b) Construction of the filler wall with the mineral wool in the cavity and the completed construction on the right with microphones in the receiving room.....   | 100 |
| Figure 4.18: ISO 10140 sound insulation of the structure (test partition plus filler wall) measured in the reverberation chambers. Filler wall here is a double layer cavity construction .....  | 101 |
| Figure 4.19: Reciprocity between nine sets of force-response for randomly chosen paths during second test on the dual leaf partition installed in the transmission suite .....   | 102 |
| Figure 4.20: Pressure validation results for airborne excitation case comparing pressure predicted by I-ASCA with the measured pressure in the receiving room in narrow band (top plot) and on-third octave band (bottom plot). Filler wall here is a double layer cavity construction.....                              | 103 |
| Figure 4.21: Top plot-Blocked force on paths in dual leaf partition. Bottom plot-Path contributions measured as per I-PCA method for dual leaf partition under airborne excitation.....  | 104 |
| Figure 4.22: Effect of removing the Point Connection (PC) path contribution from the total pressure in narrow band (top) and one-third octave band (bottom) for an airborne excitation on the partition .....  | 105 |
| Figure 4.23: The point connection configuration used in present test (left) as opposed to Sharp's (right, taken from [72]) which is actually a stud (beam) connected at multiple points to the panels .....  | 107 |

|  |     |
|--|-----|
| Figure 4.24: Sound insulation of the dual leaf partition measured by TMM [144] for no cavity absorption with and without the presence of a single point connection between the panels.....   | 108 |
| Figure 4.25: On-board validation results comparing the predicted and measured acceleration at one reference position (●) on the partition (in grey) in narrow band (top plot) and one-third octave band (bottom plot) .....  | 110 |
| Figure 4.26: A multi-layered partition layout with layers 1-j with structural elements contributing to the pressure at a receiver position denoted by the microphone .....   | 112 |
| Figure 5.1: Reciprocity in the accelerance matrix for transfer accelerances, elements in either shaded region can be measured and be substituted for another .....   | 121 |
| Figure 5.2: Sound transmission between source and receiver room (left) represented by an equivalent source-receiver model (right). $S_i$ is the internal mechanism of the source. '---' represents the source-receiver-interface.....  | 122 |
| Figure 5.3: Representation of the forced vibrations of a system (left) as a resultant of boundary value problems -1) system with active source and blocked interface (middle) and 2) system with inactive source and blocked forces acting at interface (right) .....                  | 127 |
| Figure 5.4: Forced acoustic response of the system (left) as a resultant of two auxiliary problems (middle and right). Quantities in purple denote the source in each problem. '---'is the source-receiver-interface   | 128 |
| Figure 5.5: Airborne sound field in the source room comprising of incident ( $p_i$ ) and reflected ( $p_r$ ) pressures acting on the panel, $Q$ is the volume velocity excitation that represents the internal driver of the source, '---'is the source-receiver-interface .....       | 132 |
| Figure 5.6: D-ASCA methodology schematic showing operational measurements of contact pressures close to the interface ( $p'_c$ ) and pressures in receiver for validation and diagnosis .....  | 134 |
| Figure 5.7: Comparison of measured contact pressure and blocked pressure on dual leaf partition for I-ASCA test described in Section 4.4. Blocked pressure was measured inversely as blocked force/path area. Contact force measured by placing microphones close to the patches ..... | 135 |
| Figure 5.8: Direct and airborne flanking sound incident on the partition (left), magnified view of the top panel showing the source (orange arrows) and source-receiver-interface (- - -) around the top panel (right) .....   | 136 |
| Figure 5.9: An unbaffled panel excited by airborne field on both sides (represented by arrows), '---'is the source-receiver-interface which is present around the panel.....   | 136 |
| Figure 5.10: Measurements on the unbaffled panel (left) as per I-ASCA (left) and D-ASCA (right). The contact pressure is measured above and below the panel as seen on right graphic.....  | 137 |

|   |     |
|---|-----|
| Figure 5.11: On-board validation showing comparison of measured and predicted acceleration response using inversely measured blocked pressure and directly measurement contact pressure in narrow band (top plot) and third octave band (bottom plot) .....   | 138 |
| Figure 5.12: Blocked pressure (measured inversely) and contact pressure (measured directly) comparison over three paths of the unbaffled panel in narrow band (in left column) and one-third octave band (in right column) .....  | 139 |
| Figure 5.13: Blocked Pressure (BP, measured inversely, in red) compared to net Radiated Pressure (RP, in black) at three different paths in narrow band .....   | 140 |
| Figure 5.14: Discretisation (left, in green) on the single panel with the accelerometers placed on paths for I-ASCA measurements, and contact pressure measurements with a microphone close to the paths (right) .....  | 142 |
| Figure 5.15: Pressure validation results for inverse method (blocked forces) and direct method (contact forces) comparing the predicted pressure and measured pressure in narrow band (top plot) and one-third octave band (bottom plot) .....  | 142 |
| Figure 5.16: Comparison between Blocked pressure and Contact pressure for four randomly chosen paths of the baffled single leaf panel under airborne excitation in narrow band (top row) and one-third octave bands (bottom row) in 63-630 Hz .....   | 143 |
| Figure 5.17: Contact pressure measurements by a microphone array close to the paths of the dual leaf partition installed in the transmission suite .....  | 145 |
| Figure 5.18: Pressure validation results for dual leaf partition using direct blocked pressure measurement in narrow bands (top) and one-third octave bands (bottom) till 1kHz .....  | 146 |
| Figure 5.19: Comparing the total pressure with and without the contribution of source acting on point connection path in narrow band (top plot) and one-third octave band (bottom plot) .....   | 148 |
| Figure 5.20: Measurement of radiated pressure at $k$ -first phase is the acoustic FRF with response position $k$ (denoted by $\mathbf{x}$ ) and the volume velocity sources positions (denoted by $\mathbf{o}$ ) .....  | 151 |
| Figure 5.21: Comparison between total contact pressure, radiated pressure and blocked pressure at a single patch in narrow band (top) and one-third octave bands (middle) and convergence of the radiated pressure using the modal model (bottom plot). $\mathbf{f_e}$ represents the Eigen frequencies ..... | 152 |
| Figure 5.22: On board validation results for velocity prediction using directly measured blocked pressure in narrow bands (top plots) and third octave bands (bottom plot) .....  | 154 |
| Figure 6.1: Double casement test window with the frame around the edges and in the centre along the height of the window .....  | 159 |

|   |     |
|---|-----|
| Figure 6.2: Sound Insulation (SI) of the double casement window measured as per ISO 10140 tests displayed in one-third octave bands from 100-5000 Hz .....  | 160 |
| Figure 6.3: Discretisation on the glazing and frame elements for diagnostic measurements.....   | 161 |
| Figure 6.4: Pressure validation results for D-ASCA test on the double casement window at 6 receiver positions –comparing the predicted pressure (in blue) to measured pressure (in red) in narrow band from 30-1000 Hz .....  | 162 |
| Figure 6.5: Averaged receiving room SPL predicted by D-ASCA (in blue) compared to measured pressure (in red) in one-third octave bands from 60-1000 Hz .....  | 163 |
| Figure 6.6: Comparison between total contact pressure, radiated pressure and blocked pressure at a single patch in narrow band (top) and one-third octave bands (bottom plot) in 0-800 Hz.....  | 164 |
| Figure 6.7: Left –Dashed orange line highlights the boundary separating the frame and glazing in the window. Right –expanded cross sectional view along the depth of the window showing gaskets/seals (in red circles) lined between the frames and glazing.....                    | 166 |
| Figure 6.8: Upper plot- Glazing contribution (in blue) compared to Frame contribution (in orange) averaged for six receiver positions displayed in one-third octave bands in 60-1000 Hz. Lower plot-Difference between the glazing and frame contributions in 60-1000 Hz range..... | 167 |
| Figure 6.9: The single casement window chosen for diagnostic testing with the frame (in white) at the edges and the glazing in between. The discretisation markings can also be seen .....  | 170 |
| Figure 6.10: Pressure validation for the D-ASCA methodology applied to the casement window shown in Figure 6.9.....   | 171 |
| Figure 6.11: Comparison of contact pressure, upper limit of radiated pressure ( $p_{rad}$ ) at two source DoF in narrow band (left) and the one-third octave bands (right).....   | 172 |
| Figure 6.12: Comparison of contact pressure, upper limit of radiated pressure ( $p_{rad}$ ) and the radiated pressure calculated from modal model ( $p_{rad,modal}$ ) at one source DoF in narrow band (left) and the one-third octave bands (right).....                           | 173 |
| Figure 6.13: Estimated path contributions of glazing and frame elements of the single casement window in one-third octave bands from 50-800 Hz .....  | 174 |
| Figure 6.14: Comparison between the SRI measured using ISO 10140 method and using blocked pressures (Eq. 6.6-6.11) for the double casement window.....  | 183 |
| Figure 6.15: Comparison between the SRI measured using ISO 10140 method and using blocked pressures (Eq. 6.6-6.11) for the single casement window .....   | 184 |

---

# ABBREVIATIONS

---

SRI – Sound Reduction Index

$R_W$  – Single number rating for airborne sound insulation

SPL – Sound Pressure Level

RT – Reverberation Time

iTPA – In-situ Transfer Path Analysis

TPA – Transfer Path Analysis

LTI – Linear Time Invariant

DoF – Degree(s) of Freedom

FRF – Frequency Response Function

SNR – Signal to Noise Ratio

I-ASCA – Inverse Airborne Source Contribution Analysis

I-PCA – Inverse Path Contribution Analysis

D-ASCA – Direct Airborne Source Contribution Analysis

---

# SYMBOLS

---

Symbols and formulations are by the most part given in frequency domain, unless otherwise specified. Throughout the thesis, bold letters (capital or lower case) denote a matrix or vector. Italic letters denote a matrix/vector element or a single value on its own. The following symbols have been used extensively in the thesis. Symbols used only in passing are not included.

|                      |                  |                       |                   |
|----------------------|------------------|-----------------------|-------------------|
| <b>Y</b>             | Mobility         | <b>A</b>              | Accelerance       |
| <b>Z</b>             | Impedance        | <b>H</b>              | Vibroacoustic FRF |
| <b>a</b>             | acceleration     | <b>v</b>              | velocity          |
| <i>p</i>             | Sound pressure   | <b>f<sub>bl</sub></b> | Blocked forces    |
| <i>p<sub>b</sub></i> | Blocked pressure | <i>V</i>              | Voltage           |
| <i>dS</i>            | Path area        | <i>Q</i>              | Volume velocity   |

---

# 1

## INTRODUCTION

---

Urbanisation of the modern world has integrated humans with different utility systems such as infrastructure, machines, transport, telecommunication, etc. with which we interact and partly rely for survival. Over the years, as the urban environment became denser in terms of population, the needs of the population were met by a proportionate growth in infrastructure development, innovation in machine systems and rapid expansion of transport systems. This has led to a surge in residential spaces, offices and commercial centres being built in close vicinity of the transport systems.

The most apparent and distinct representation of our environment is visual; we see and observe the different systems around us. However, the environment is also perceived in an acoustical sense, as we can hear. In such an environment, humans are constantly exposed to sounds from all the different urban systems that form an integral part of living in an urban environment. The perception of sound can be positive (harmonious/pleasant/refreshing, etc.) or negative (disturbing/noisy/painful, etc.) depending on the type of sounds and their levels, exposure. As such, the acoustic environment can directly affect human comfort [1]. Acoustic comfort means having the right level and quality of noise to use the space as intended [2].

The type of noise experienced in such a complex environment comes from varied sources. Transport systems give rise to road noise, rail noise and aircraft noise, which are a major source of outdoor noise that is experienced in built environments. Noises from construction activity, electrical units, compressor/pump systems, industrial activity, etc. comprise the other sources of outdoor noise. Rural environments are also not completely immune to these noise sources-transportation noise is a big problem. Industrial operations and wind

turbines may also present as noise sources. However, it is not only the outdoor noise that the building is exposed to. Indoor noise in houses and workplaces are usually in the form of speech, communication, impact noises from indoor human activity, footfall noise, and appliance noise from vacuum cleaners, washing machines, dishwashers, refrigerators, TV, sound systems, HVAC noise, etc. As a result, the urban environment often manifests as a 'noisy' combination of various sounds from outdoor and indoor noise sources simultaneously.

The effect of living in noisy environments is well known and researched. Human comfort in residential spaces and workplaces can be affected adversely when exposed to such noise on a continual basis [3-5]. Studies have shown that the conditions such as pain, annoyance, discomfort may persist as well as concentration and work productivity can be adversely affected [6-8]. The damaging effects of such noisy environments can be severe, for example on people working in industrial units with constant high noise levels from machinery and heavy equipment [9]. Use of adequate soundproofing and noise control measures is therefore justifiable in noisy environments to avoid acoustic discomfort. As such, the different noise control measures when installed in residential and non-residential developments are typically intended to reduce the noise levels.

For dwellings and residential spaces, office spaces, ill effects of a noisy environment can be minimised by reducing the sound levels inside the building space from the outside. One way of achieving low noise levels is to insulate the space from outdoor noise. In buildings, building elements such as walls, windows, doors, ceilings, etc. shield the occupants from outdoor environment and provide the insulation from outdoor noise. Likewise, indoor noise sources may be designed for quieter operation and absorption measures may be introduced for lower indoor noise. A typical example of this is using fabric carpets to reduce the footfall noise on a bare floor.

To choose the appropriate noise control measures for a given scenario, it is then essential to have a metric of the sound insulation/absorption performance of building elements. Based



on this intention, it is a standard practice to measure the sound insulation/absorption properties of such building elements in view of designing silent spaces. By measuring the sound insulation properties, the amount of the sound reduction provided by the element to the outdoor/indoor noise could be assessed. Ideally, the sound insulation of each element can be measured for each specific noise case. Due to the vast number of noise sources with different noise spectra, measuring sound insulation against every noise source may be tedious or impractical. A better way would be to have a classification of noise source and a generalised sound insulation metric. This can be done by classifying the noise sources in different categories.

To do this, one has to look at the mechanism of sound source generation. Typically, noise will be created by the dynamic interaction of structures or the interaction between a structure(s) and a fluid (for ex. air, water). The noise sources in everyday life are generated by these mechanisms. In acoustic terms, the noise created by interaction between two structures is classed as 'Structure borne' noise and the noise created by interaction between a structure and a fluid is classed as 'Airborne' noise.

---

## 1.1 Structure borne noise

---

Structure borne noise is created by the dynamic interaction of solid structures. One of the structures acts as an active source and usually applies a dynamic force/moment (or a combination of both) to a passive structure. This dynamic interaction between the two structures results in sound radiation for either/both structures which is then classed as a structure borne noise. In buildings, structure borne noise is typically caused by impact from footfall, appliance noise if they are coupled to the walls or ceilings, etc. For example, the impact on a bare floor excites the floor into vibrations which results in the floor radiating sound in the room below.

---

## 1.2 Airborne noise

---

Airborne noise is created by the dynamic interaction of a structure and a fluid (air). The active source structure excites the air and radiates sound. For example, a loudspeaker operating in a room excites the air volume and a sound field is created. This noise can be classed as an airborne noise. Other examples of these airborne noise sources can include electrical appliances such as cooling fans, vacuum cleaners, washing machines etc.

Of particular interest for the scope of this study is the airborne noise at low frequencies. Low frequency noise has been reported to cause annoyance and health effects on humans on prolonged exposure [10-11]. Examples of such noise include aircraft noise, loud party music [12]. In buildings, structure borne noise at low frequencies is typically caused by impact from heavy sources (such as dropping heavy weights/medicine balls in gyms, home appliances, etc.) and is radiated through floors [13].

---

## 1.3 Sound insulation

---

Typically, living spaces such as rooms are exposed to myriad of structure borne and airborne noise and sounds. In such case, appropriate measures are installed or built in to reduce the noise levels inside the room for acoustic comfort of the occupants. Building elements, such as wall partitions, closed windows, and doors offer such reduction by insulating the room from extraneous airborne sounds. This property is the airborne sound insulation of the structure. To achieve the required degree of sound insulation, which may be different depending on the severity of the noise problem, it is first essential to quantify the sound insulation of a structure which are commonly measured by standard methods. In built constructions, the airborne sound insulation is measured for walls, windows, doors, etc. while the impact (structure borne) sound insulation is usually determined for floors (with or without coverings).

### 1.3.1 Airborne sound insulation measurement

The airborne sound insulation is quantified by the Sound Reduction Index (SRI)  $R$ . Mathematically, the SRI can be written as,

$$R = 10 \log_{10} \left( \frac{W_1}{W_2} \right) \quad (1.1)$$

where,  $W_1$  is the sound power incident on the partition and  $W_2$  is the sound power transmitted by the building element to an enclosing room or free field. In practice, it is not possible to measure the incident sound power falling on a reflective partition directly using an intensity probe. It may be directly measurable only if the surface is non-reflecting or if diffuse field assumptions can be made. A simpler indirect approach is thus used in practice which also forms the basis of the standard ISO 10140 method [15].

Consider the partition separating two rooms. An airborne sound field is created in one of the rooms (the source room) by means of an airborne source. In operational conditions, the airborne sound transmission from the source room to the receiver room is then governed by the sound insulation or the SRI of the partition which is measured as,

$$R = L_1 - L_2 + 10 \log_{10} \left( \frac{S}{A} \right) \quad (1.2)$$

$L_1$  and  $L_2$  are the spatially averaged Sound Pressure Level (SPL) values measured for source and receiver rooms respectively, 'S' is the partition area, and 'A' is the absorption area of the receiving room. The values of SRI can be specified for octave or one-third octave band centre frequencies from 100-5000 Hz. A brief derivation of the Eq. (1.2) is provided in the next chapter. Alternatively, sound intensity based method (ISO 15186 [16]) is also used for the SRI measurement which will be discussed later. For field conditions, ISO 16283-1 [17] method is used to measure the sound insulation.

A single number rating ( $R_w$ ) is also obtained from the sound insulation curve by following guidelines mentioned in ISO 717 [18]. Such single rating enables one to compare and choose an appropriate partition in line with the requirements of sound reduction. However, it is impossible to assess the spectrum values of sound insulation from a single value. Also, at low frequencies, it has been shown that single number ratings may not be a valid descriptor of the sound insulation if the mitigation of annoyance [19-20] is also considered.

At the core of the standard methods (Eq. 1.2), lies a diffuse field assumption which states that in steady state operational conditions, the sound field in a room can be considered to be perfectly diffuse. The term 'diffuse' implies that the SPL's are uniform throughout the room. However, it has been shown that this assumption is not valid at low frequencies [21]. Therefore, there are uncertainties in the low frequency SRI values. A more detailed discussion on the diffuse field assumptions will be presented in Chapter 2. Another important assumption or requirement while using Eq. (1.2) is that the sound between the source and receiver room is transferred through the partition under test only and there is minimal or no leakage and flanking.

---

## 1.4 Motivations

---

With the standard methods of airborne sound insulation measurement, a single number rating is specified which is indicative of a frequency averaged sound insulation of the partition. This single number rating however does not tell anything about how sound is transferred spatially through a structure, or how different elements in the structure contribute to the sound transfer (or towards the sound insulation).

A case can be made for why such information may be useful. In building partitions, the sound transmission through different elements such as ribs, studs, point connections, etc. or different paths will be different. By a diagnostic method, if the weak elements of sound insulation can be identified, then appropriate structural modification measures may be introduced to improve the sound insulation of the structure, and/or optimising designs to

further the sound insulation of the structure. Additionally, the diagnostic information can be used as a complement to the SRI values. This would quantify how different elements in the partition contribute to the sound insulation on a frequency-by-frequency basis. Thus the R&D potential for such a method can be impactful.

Generally, diagnostic methods are well developed for the structure borne noise problems but their application to airborne noise transmission problems is fairly unexplored. The question then arises is whether a diagnostic method can be developed for the problem of airborne sound transmission through building partition. To answer that question, a comprehensive literature review is carried out to assess the structure borne diagnostic methods, whether such diagnostic methods can be adapted for airborne noise cases and the challenges that can arise for airborne cases. Then, in view of the potential advantages of a diagnostic method discussed above as well as the research questions stemming from structure borne diagnostic methods to airborne diagnostic problems, the work presented in this thesis will deal with the problem of diagnosing the sound transmission through building partitions in-situ. A relevant and thorough literature review will now be presented in the next chapter which will pave the way of developing a suitable diagnostic method for airborne sound transmission through the partition locally. Additionally, structured and quantifiable aims and objectives for the work will be formulated.

---

# 2

## LITERATURE SURVEY

---

*In the previous chapter, the topic of airborne sound transmission through building partitions was introduced through the viewpoint of noise, acoustic comfort, annoyance, etc. in residential and non-residential spaces. The work presented in this thesis will deal with the problem of diagnosing the airborne sound transfer spatially through building elements and the measurement methods. It is then appropriate to explore the scientific work related to this topic. This chapter will therefore look into the relevant literature dealing with the history of airborne sound insulation, prediction and measurement methods for measuring sound insulation, and discuss potential methods to diagnose the airborne sound transmission through a building partition.*

---

### 2.1 Sound transmission through building elements

---

In the context of airborne sound transfer in buildings, the most common case of airborne sound transmission into a room can be studied. The airborne sound transfer to a room can occur from adjoining rooms or from outside environment (outdoor noise). This sound transmission can occur through a multitude of paths such as partition walls, windows, doors, etc. and through any openings in windows, clearances around the door, slits in walls, etc. (see Figure 2.1). These structural elements present themselves as a barrier to the sound coming in the room, and thus offer a degree of the sound insulation. It was therefore paramount to quantify the sound insulation performance of each such building element and select the appropriate elements for noise control. This paved the way for

research into airborne sound insulation and theories describing the airborne sound transfer through building elements.

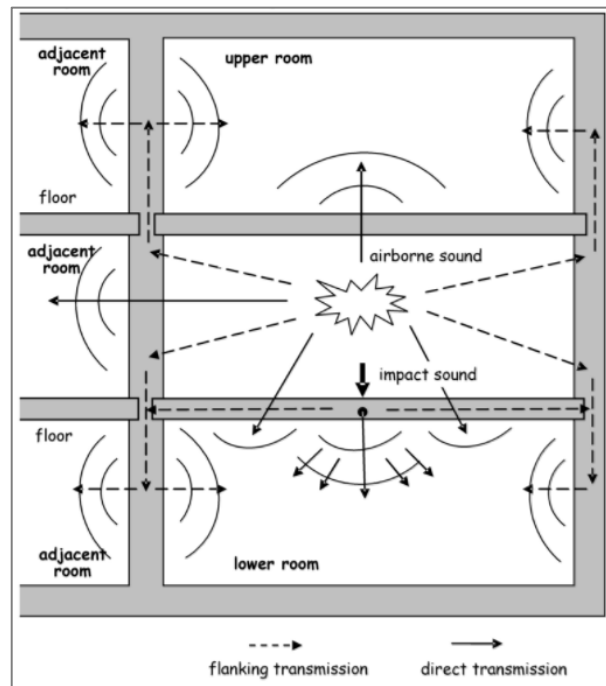


Figure 2.1: Paths of airborne and structure borne sound transmission between rooms [22]

Let us consider the case of a partition wall between two rooms –source and receiving room. When an airborne sound field is incident on the partition from the source room, the partition reflects part of the sound back to the source room and transmits part of the sound to the receiving room. Then the sound insulation of the partition can be described in terms of an input-output relation, which is the ratio of incident to transmitted sound energy by the partition. To measure the sound insulation, an airborne sound transmission model had to be formulated.

The earliest and simplest sound transmission models were defined for infinite partitions surrounded by free fields. In a free field, no reflecting boundaries are present except the partition. The free field is simply described using a plane wave model [23] for a source located far away from the building element. However, in practice for partitions bounding rooms, the sound field on either/both sides is of a reverberant type than a free field type. In a reverberant field, the sound field comprises of a direct field from an airborne source plus the reflections from the boundaries of the room. In case of a room, the sidewalls, floor and

ceiling all constitute a reflective surface that make the sound field reverberant. In such case, a free field model would not be adequate to describe the sound insulation.

For describing the sound insulation to a reverberant sound, a model describing the sound field in a reverberant volume/room was required. Sabine outlined the 'Theory of reverberation' [24], which provided a simplistic model for the reverberant sound field in rooms. The model assumes a diffuse sound field in rooms. The diffuse field assumption postulates the following as outlined by Buckingham [25],

- 1) 'Duration of audibility of the residual sound is nearly the same in all parts of the room'.
- 2) 'Duration of audibility is nearly independent of the position of the source'.
- 3) 'Efficiency of an absorbent in reducing the duration of residual sound is nearly independent of its position'.

In these assumptions, the duration of audibility refers to the time the sound is decayed to a non-audible level. The implication of the first assumption is that the sound field is perfectly diffuse and the Sound Pressure Level (SPL) is ideally same throughout the volume of the room. Only then, the decay rates can be same through the room. Ideally, this also means that the net sound intensity at a point due to sound waves arriving from all directions would be zero. The second assumption implies that the source position does not affect the diffuse field in the room. The implication of the final assumption is that the sound field acting on a surface is similar at any position of the room. A detailed discussion on these assumptions can be found in Davis [26].

Buckingham made a specific mention about isolated modes where the diffuse field assumption will not hold strictly valid. This refers to the low frequency region where a few modes will shape the sound field in a room rendering the field irregular and non-uniform SPL distribution in the room volume. Such irregular sound fields cannot be accepted under the 'diffuse field' definition, as they would violate the three basic properties of an ideal diffuse field mentioned above. Figure 2.2 illustrates this concept.



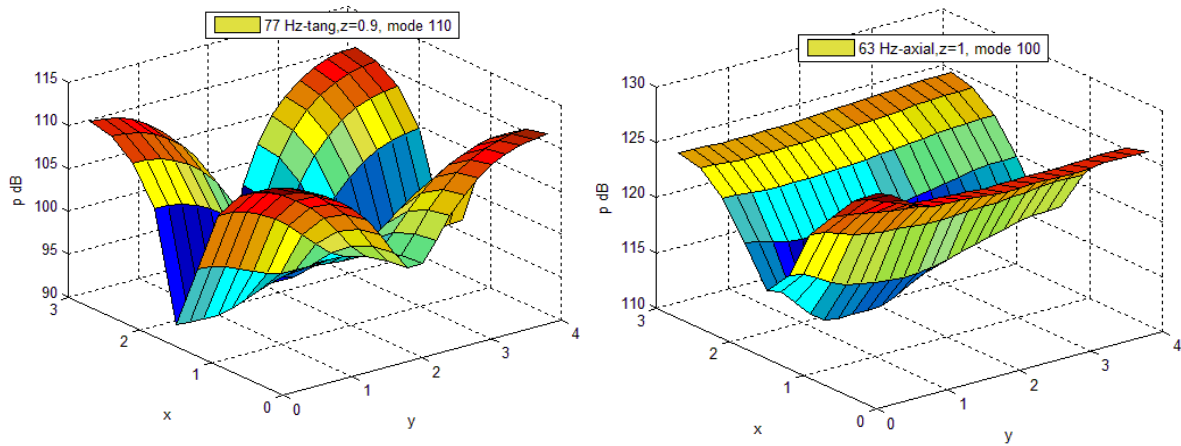


Figure 2.2: Irregular spatial distribution of SPL at low frequency room modes in a room of 3 x 4 x 3 m<sup>3</sup>. Left-SPL distribution for 77 Hz tangential mode, right-SPL distribution for 63 Hz axial mode

### 2.1.1 Measuring airborne sound insulation

Mathematically, the airborne sound insulation or the SRI, which was defined as the ratio of incident sound power on the partition to the sound power transmitted by the partition (Chapter 10 in [23]), as also mentioned in Eq. (1.1). In practice, direct application of Eq. (1.1) is difficult. This is because the direct measurement of incident sound power on a reflective surface is very difficult. Note that the transmitted sound power can be measured by intensity probe however cannot be used for measuring the incident sound power as it would measure the net intensity (incident minus the reflected sound intensity). Therefore, alternate measurement approaches were required to measure the sound powers and the SRI. To solve this problem, based on the reverberation theory and assuming a diffuse field, Buckingham [25] and Davis [27] formulated practical measurement models for SRI measurement (Eq. 1.2).

Eq. (1.2) can be derived from Eq. (1.1), where the sound powers can be measured indirectly using diffuse field SPL's around the partition. To apply Eq. (1.2) in practice, the partition is installed between two reverberant rooms, the source rooms and the receiver room. The source room is the room where an active airborne source excites the partition into vibrations. The vibrations of the partition then transmit sound to the receiver room.

Under steady state conditions, assuming diffuse field in the source room, the incident intensity falling on unit area can be measured from the spatially averaged sound pressure as equal to  $\frac{p_1^2}{4\rho_0 c_0}$  [28]. The incident sound power on the partition is then the intensity falling on the partition area.

$$W_1 = \frac{p_1^2}{4\rho_0 c_0} S \quad (2.1)$$

where,  $p_1$  is the spatially averaged sound pressure in the source room,  $\rho_0$  is the air density,  $c_0$  is the speed of sound in air and  $S$  is the partition area. In the receiving room, under steady state the sound power radiated by the partition should be equal to the sound power absorbed by the receiving room. The energy absorbed by the receiving room will depend on the absorption coefficient of the walls ' $\alpha$ ' which when combined with the surface area is the total absorption area of the room. In other words, the radiated or transmitted sound power is measured from the diffuse field sound intensity and absorption area in the receiving room as,

$$W_2 = \frac{p_2^2}{4\rho_0 c_0} A \quad (2.2)$$

where,  $p_2$  is the spatially averaged sound pressure in the receiving room and ' $A$ ' is the absorption area of the receiving room. By making use of Eq. (1.1, 2.1-2.2), we get,

$$R = L_1 - L_2 + 10 \log_{10} \left( \frac{S}{A} \right) \quad (2.3)$$

In Eq. (2.4), the absorption area ' $A$ ' can be written as,

$$A = 0.161 \left( \frac{V}{T_{60}} \right) \quad (2.4)$$

The absorption area of the receiving room can be calculated as per Eq. (2.4) if the Reverberation Time (RT, mathematically denoted by  $T_{60}$ ) and receiving room volume ( $V$ ) are measured. RT can be measured by the Interrupted noise method [29] where the sound source is stopped from a steady state operating condition in the receiving room. The time

for the sound field to decay by 60 dB is then the RT. RT can also be measured by backward integration on the impulse response of the receiving room [30]. The advantage of Eq. (2.4) is that the SRI can be easily measured by pressure measurements in both rooms, which is more convenient than measuring power. This formulation also forms the basis for the current standards for laboratory measurement of airborne sound insulation [15]. Standard methods for field measurement of airborne sound insulation [17] employ similar technique but with some additional measurements, which will be discussed later.

The SRI measurement based on Eq. (2.3) is in principle a pressure-based method as SPL measurements are used. Alternatively, a sound intensity based method is also available as per ISO 15186 standard [16] to measure the SRI. In the intensity-based method, the incident sound power is measured indirectly similar to the pressure-based method using SPL measurements. The transmitted sound power however is calculated directly by measuring the transmitted sound intensity in the receiving room using a sound intensity probe. ISO 9614 [31] specifies the guidelines of sound intensity measurement from radiating surfaces. The SRI is calculated as per Eq. (2.5).

$$R_I = L_{p,1} - 6 - \left[ L_{I,n} + 10 \log_{10} \left( \frac{S_m}{S} \right) \right] \quad (2.5)$$

' $R_I$ ' is the intensity sound reduction index, ' $L_{I,n}$ ' is the normal sound intensity level, ' $S_m$ ' is the total area of measurement surface(s) and ' $S$ ' is the area of test specimen under test. Note that the measurement of transmitted sound power here is different to the ISO 10140 approach where the transmitted sound power is calculated indirectly from the diffuse field sound intensity absorbed by the receiving room. Thus we do not see the absorption area term in Eq. (2.5).

As the receiving room is reverberant, additional care has to be taken to minimise the interference of the intensity travelling back towards the partition due to reflections in the receiving room. For this purpose, ISO 15186 specifies use of absorbers at low frequencies against the back wall of the receiving room. However, this might be practically difficult to install due to wavelength considerations at low frequencies, which would mean that a thick

layer of absorption material is required. In addition, a sound intensity measurement is shown to be prone to nearfield errors [32], calibration [33] and phase mismatch errors [34] which may corrupt the measurements. As a result, the pressure-based method is more widely practiced for laboratory measurements of SRI and certification ( $R_w$ ). Halliwell et al. [35] proposed that the Intensity method could be better suited for finding the sound power transmitted by individual elements such as doors, windows, etc. in the receiving room. However, for complex geometries, such as a ribbed or corrugated structure, incorrect sampling may induce errors in the SRI measurement.

---

### 2.1.2 Implication of diffuse field assumption

---

As the standard tests have been derived from the theory of reverberation, there is an underlying diffuse sound field assumption in the tests as well. In practice, this assumption holds fairly well only at mid-high frequencies above the Schroeder frequency [36] but is not necessarily respected at low frequencies. The Schroeder frequency is the frequency above which the modal density in the source and receiving volumes is high enough to warrant a near diffuse sound field.

At low frequencies, the sound field is formed from the contribution of a few modes. This makes the distribution of SPL highly irregular throughout the room volume with regions of high SPL mostly around the room corners and regions of low SPL around the centre of the room (see Figure 2.2 for clarity). In other words, the sound field is not diffuse and the diffuse sound field assumption in the standard SRI measurement procedure is violated. Therefore, the source room energy estimated using SPL measurements in centre region of the room could be vastly inaccurate and, carries an inherent uncertainty due to high standard deviation arising from the non-diffuseness of the sound field.

The variation in low frequency sound insulation is also reported with some of the earliest experimental findings. Cremer [37] postulated the ‘Mass law’ that showed that the sound transmission loss is dependent on the mass impedance of the panel below its critical frequency. However, Utley [38] pointed out that there is a discrepancy between the sound

transmission of a single leaf panel characterized by mass law and his experimental evaluations. He compared the results from different transmission suites and concluded that the discrepancy is due to some room effects relevant to the test facility used. Then Mulholland [39] concluded that the resonant room modes at low frequencies are directly responsible for this variation in low frequency sound insulation values. Towards, high frequency end deviations to the mass law were also observed in-situ however that was confirmed as the coincidence effect in panels by Sewell [40]. Additionally at the low frequency end below the fundamental resonance of the panel, the mass law is not satisfied as the sound insulation is controlled by the stiffness of the panel at sub fundamental resonance frequencies.

Ideally, it seems that, to calculate the source room energy at low frequencies, the SPL averaging should be done over as many points as possible in the whole volume of the room. Although, this can be simulated with computing capabilities, it may not be possible to employ such extensive measurement in field or laboratory conditions. Therefore, by employing a few measurement positions, an uncertainty is associated with the SRI values.

---

### 2.1.3 Quantifying uncertainty in SRI

---

ISO 12999 [41] states that the uncertainty associated with a measurement is highly dependent on the standard deviation of the measurement. With a high standard deviation, it would be difficult to define a fixed value to a measurement parameter with sufficient confidence. Due to the diffuse field assumption, the SPL's within the room exhibit a high standard deviation. In qualitative terms, this deviation arises due the non-diffuseness of the sound field because if the field were to be diffuse, the SPL's would be same and the deviation would be ideally minimal. Eq. (2.3) can be written with the standard deviation as Eq. (2.6) where ' $\delta$ ' terms represent the standard deviation associated with the respective measurement. If these deviations are high then the SRI takes a range of values, which makes it difficult to quantify the correct SRI.

$$R \pm \delta R = (L_1 \pm \delta L_1) - (L_2 \pm \delta L_2) + 10 \log_{10} \left( \frac{S}{A \pm \delta A} \right) \quad (2.6)$$

In standard measurement tests of SRI, the SPL measurements are repeated for fixed number of times and each time a mean SPL is determined. The standard deviation is then also referred to as the repeatability. The repeatability is thus a measure of the uncertainty of the repeat SPL measurements. The lower is the standard deviation of the measurement, the better is the repeatability and vice versa.

The reproducibility of the SRI measurement is also affected adversely in the low frequency region. Reproducibility is the measure of uncertainty of SRI measurement in different test facilities. The low frequency SRI is influenced by the room modes, and different test labs have different modal frequencies due to difference in dimensions. This adds uncertainty to the low frequency SRI measurement due to testing in different facilities. Round robin tests [42] are routinely conducted between different labs to assess the repeatability and reproducibility of the sound insulation tests.

Unlike the pressure based method, the intensity method does not depend on a diffuse field assumption for transmitted power calculation. In practice, it was thus found that the Intensity method has better repeatability than the Pressure based method when the reverberation error caused by reflected sound intensity in the receiving room was less [38].

---

## 2.2 Literature survey on SRI measurement of building elements

---

The SRI is intended to be an independent property of the partition installed in a transmission suite; but the diffuse field assumption introduces uncertainties at low frequencies as previously mentioned. A number of studies have been undertaken in past to either improve the reliability of the pressure based method and some have focused on alternative measurement techniques. A review of such methods is presented below.

---

### 2.2.1 Experimental techniques – improving repeatability

---

At low frequencies, there is a pressure maximum at room corners, and the standard methods do not consider these positions for estimating the mean SPL of the room. To obtain a reliable estimate of the mean SPL, one could therefore include a corner position in the measurement. A look into the existing literature shows that a good amount of work has been done to assess the influence of corner measurement position on the repeatability SRI. Studies have been performed at different sites in different conditions to justify the need of improving the current standard methods at low frequencies. A technical report [43] dating back to 1997 compared different existing standards of the time to test the repeatability and reproducibility of mean SPL at low frequencies. It was proposed that for better repeatability a corner point should be included in the measurement and should be chosen carefully as the sound fields are quite unsymmetrical. For the measurement of SRI, Pedersen et al. [44] proposes use of intensity method for finding the transmitted intensity in the receiving room and covering the walls with absorption material. In source room, he proposed inclusion of a corner measurement position to find the sound power level, which showed improvement in the repeatability. For dwellings less than volume of 50m<sup>3</sup>, Hopkins and Turner [21] proposed introducing corner and central positions in the room, which show good repeatability than the current ISO standards. Hoffmeyer and Jakobsen [45] measured sound insulation of facades in Danish dwellings and inclusion of corner measurements gives significantly different results (up to 10 dB level difference) compared to level difference at low frequencies calculated using centre positions of the room. This shows how the corner positions can especially affect the SRI measurement at low frequencies. In a nutshell, inclusion of corner measurement points for estimating mean SPL has seemed to be an acceptable solution for obtaining better repeatability in the low frequency range. It should be noted that although the corner position measurement is based on modal considerations, the overall mean SPL measurement does not get rid of the diffuse field assumption. Regarding reproducibility, Dijckmans et al. [46] found that the intensity based method ranks better than pressure based methods.

The sound insulation standard also requires measurement of equivalent absorption area, which depends on RT. As the RT measurements are also sampled similar to mean SPL measurements, there is some degree of uncertainty attached to them at low frequencies. Not much study has been performed on improving repeatability of RT measurements. Masovic [47] shows that the RT measurements are influenced by the signal to noise ratio and individual modes at low frequencies. He proposes using exponential sine sweeps for determination of RT with improved repeatability at low frequencies. Recently, Prato et al. [48] adopted a modal reverberation time approach at low frequencies where the sound field is non-diffuse. At such low frequencies, measuring RT at room mode frequencies showed lesser standard deviations than the RT measured using standard approaches. However, the effect of using a modal RT term on the SRI is not explicitly given.

---

### 2.2.2 Alternative methods towards SRI measurement

---

Alongside the methods discussed earlier which look at improving the standard procedures, other independent methods were also developed. Measurements of impulse responses have been studied to calculate the SRI. Such methods [49-51] employ determining the impulse responses in the source and receiving volume and the SRI is given as a function of the ratio of incident to transmitted intensities, which can be found out by integrating their respective impulse responses over a finite period. In the source room, the incident intensity can be separated from the reflected intensity by windowing and time of flight techniques. Tricaud [49] was first to measure the sound insulation of a partition using impulse techniques. At the time, he called it the difference between the impulse noise levels in both rooms as the sound insulation however; this did not take into account the RT measurement. The ISO 18233 [52] method based on the same principle specifies these impulse measurement techniques for the measurement of level difference between the source and receiving room. However, measurement of SRI is not explicitly mentioned and it can be seen that this is precisely because the RT measurement is not undertaken which is required for SRI measurement according to standard method. Venegas et al. [53] tested the ISO 18233 method by measuring the acoustic transfer functions for source and receiver rooms. It was



found that the method predicts the level difference very similar to the conventional measurement of SPL difference however, repeatability issues still existed at low frequencies and accuracy of the method was not discussed for bad signal to noise ratios especially in field conditions. Satoh et al [54] found that using a swept sine signal for 10 minutes as the impulse source predicted the level difference closely to the standard method and worked for even negative signal to noise ratios. Therefore, the impulse technique could offer an alternative technique to measure the level difference between source and receiver rooms however, it is important to choose the right source otherwise poor signal to noise ratios will affect the measurement and add to the SRI uncertainty.

Some methods in literature have outlined novel ways to measure the transmitted power. Duarte et al. [55] developed the 'Peak Envelope' method, which can be used for measuring the transmitted sound power at single modes in the low frequency region. The method was derived on the basis of single mode assumption in the receiver room. Therefore, the method is limited to frequencies where single modes exist, typically the low frequency region. As this method is not based on a diffuse field assumption, it was proposed that the power measured here would be better estimate of the true sound power at low frequencies. A similar approach may be applied to the source room however; the power measured then would be a resultant of the incident and reflected powers. Roozen et al. [56] used laser vibrometry to measure the radiated sound power from the velocity response of the panel at different points. This method is a semi-analytical semi-experimental technique as the velocity response is processed using the Rayleigh integral [57] analytically to measure the transmitted sound power. If the source room energy can be measured by SPL measurements, then in principle this approach can provide the sound insulation. Other semi-experimental approaches [58-60] can be found in the literature for prediction of airborne sound insulation. A disadvantage here is that such approaches depend partly on theoretical models and data, which may not be always applicable. Recently, Prato et al. [61] presented a modal sound insulation as a descriptor of the sound insulation at low frequencies but that is not exactly comparable to SRI because the descriptor is dependent on the room modes whereas SRI is independent of room properties by definition.

### 2.2.3 Prediction methods

---

Although the majority of the sound insulation measurements follow the standard approach, the prediction models are far more vast and diverse. The SRI measurement itself is based on a diffuse field model. Therefore, in principle, alternative SRI measurement approaches may be possible based on the different prediction models.

The most commonly used model is the wavenumber model of Cremer, which was used to describe sound transmission through infinite single leaf partition. Notable studies [37, 62-64] laid the foundation for analytical solutions to the sound transmission through cavity backed plate to calculate the SRI. Modal models have also been developed which express the sound field as a resultant of modes and can be used to describe the sound insulation [65, 66]. Statistical Energy Analysis (SEA) methods have also been commonly used for prediction however their accuracy is dependent on the modal density of the structure which means these methods are not accurate at low frequencies where the modal density is not high. A good review of SEA is presented in Chapter 4 of [67]. It is not possible to mention the numerous prediction models here but a good review of the different prediction approaches can be found in Hongisto [68] and more recently by Mak and Wang [69].

---

## 2.3 Factors influencing SRI of a partition

---

As seen in earlier sections, the standard measurement of SRI is influenced by diffuse field assumptions at low frequencies. The uncertainty arising due to this factor was also discussed. An important motivation of the current work is diagnosing the effect of various elements in the partition. Different structural elements (or construction) of a partition also affects the SRI. While we aim to diagnose these elements in-situ, theoretical studies have looked at the topic of how SRI can be affected by partition construction and composition. Therefore, a review of such factors specific to the partition is worth reviewing.

### 2.3.1 Mass effects

Early studies on sound insulation prediction indicate an interest in relationship of mass with sound insulation. Cremer had outlined the mass law for infinite panels, which postulated a theoretical 6 dB increase in sound insulation for every doubling of the mass. However, for finite panels in addition to mass law, the sound transmission is dependent on the stiffness at low frequencies (below fundamental resonance of the panel). At higher frequencies above coincidence frequency, the transmission is dependent on damping [70, 71]. This is shown for a simple case of a single layer wall in Figure 2.3.

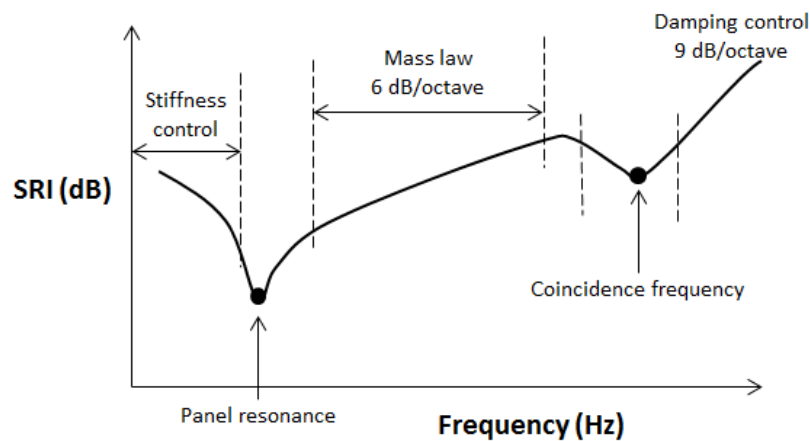


Figure 2.3: Different regions governing the SRI of a single isotropic panel

However, if a layer of the same mass is added to the original panel separated by a cavity with absorptive material, then the SRI increase is more than 5 dB in most regions [72]. For multi-layered partitions, the study also showed that mass law governs only a small part of the SRI behaviour particularly in the lower frequency region. In addition, if a single layered panel is corrugated in along one dimension, then the SRI changes [73]. This shows that the partition construction can be changed to achieve the desired insulation.

### 2.3.2 Source factors

The SRI of the partition is calculated and measured for a diffuse field excitation. Thus, any deviation from the diffuse field is bound to affect the SRI. Many prediction

approaches [72, 74-75] in the past have assumed a field incidence for predicting the sound insulation of a partition. Field incidence assumes equal distribution of incident waves for angles ranging from 0-90 degrees. However, on comparison with the measured sound insulation, Kang et al [76] found differences due to the field incidence assumption. This indicates that a field incidence is not observed in practice and that by changing the field, the sound insulation changes. This is not surprising because the forced transmission of the partition is affected by sound incidence at different angles as shown by Guy [77], with sound insulation being the weakest at grazing incidence. Other studies [78-79] also show the dependence of SRI on incidence angle. Brutel-Vuilmet et al. [80] demonstrated an experimental study on measuring SRI for different incidence of plane waves. The authors report differences to the order of 15 dB in the mid frequency range for angles ranging from 0-80 degrees. This shows that the SRI is dependent on the type of source field. Therefore, for field conditions where the source field may not be diffuse, the SRI measured in diffuse field laboratory conditions will not be representative of the actual sound reduction. This again highlights the requirement of an in-situ sound insulation measurement, which is not based on a diffuse field assumption.

---

### 2.3.3 Structure borne transmission and flanking

---

Typically, for building elements, the airborne sound insulation is measured which is an inherent property of the partition. To measure the SRI, only direct airborne transmission through the partition between the source and receiving room must take place. However, in practice, structure borne sources may be present in the form of a physical source coupled to the partition or it may be present in terms of structure borne flanking from other building elements. The latter is much likely to be present in building partitions. The structure borne flanking may alter the response of the structure and affect the total transmission into the receiving room. Thus, the measured sound insulation may no longer be qualified as an SRI, as the insulation results will contain contributions from flanking.

The effect of flanking on the sound insulation performance is also documented. Hopkins [81] through an experimental study showed that the flanking transmission is one of the main factors that limit the airborne sound insulation that can be achieved by beam and block floors in building constructions. Clasen and Langer [82] performed a finite element modelling study to show that the presence of a flanking wall results in increased transmission through the partition. Therefore, although partitions are rated for airborne sound, any secondary flanking transmission, the perceived sound insulation that is experienced will be different and less than the rated value. While the standard methods specify ways to measure the flanking sound transmission it involves reinforcing the test element with more sound insulation such that it can be assumed that the transmission is now through flanking paths only. This can become a trial and error approach and may not be always suitable for field conditions where it is not always feasible. This points out a need for a measurement method to diagnose the sound transfer contributions from different sources –airborne and structure borne.

---

#### 2.3.4 Effect of structural elements

---

In practice, multi-layered partitions comprise of structural elements between the panels such as studs, ribs, resilient couplings between panels, etc. Such structural elements are installed between the panels of the partition to provide support for lateral loads. However, such structural elements often act as a sound bridge between the panels, resulting in increased sound transmission through them. Sharp [72] developed a prediction model to calculate the SRI of multi-layered panels with rigid studs. The results showed that the SRI decreases when studs are introduced in the partition. Similar conclusions were derived for prediction models for multi-layered partitions with ribs and frames, which connect the panels [83]. Even with safety elements, for example using a firestop between panels, Craik et al. [84] showed that the SRI of the partition decreased. Stani et al. [85] investigated the effect of cavity absorption on the SRI of multi-layered cavity constructions. With absorbing materials of increasing resistivity, the SRI improvements were observed.

Wang et al [86] outlined a review of the existing prediction models for transmission through partition walls with studs, and showed the angle dependent transmission through studs. The influence of stud spacing on the SRI was also discussed. Poblet-Puig et al. [87] outlined an analytical-FE model to model the sound transmission through steel studs that support the partition. The effect of the stud thickness on the sound reduction of the partition was calculated. It was found that increase in stud thickness increases the sound reduction at higher frequencies as increasing the thickness provided increase effective damping for the vibration transmission. On the other side, Bradley et al. [88] found that the change in stud size and spacing in multi-layered partitions had the largest effect on the SRI in the low frequency region (near the primary structural resonance of the partition). Therefore, as per the theoretical studies, the stud size and spacing can have a significant effect on the sound insulation of the partition.

Regarding experimental investigations, Muellner et al. [89] found that the horizontal spacing of fixing screws caused a change in SRI above 200 Hz. He also changed the profile of the metal stud and found significant changes in the sound transmission. Roozen et al. [90] used advanced scanning laser vibrometry to measure the SRI of a multi-layered partition and found that in addition to the number of screws used to fasten panels to studs, the amount of tightening also has a significant effect on the SRI. It was found that increased tightening the SRI decreased. Overall, these studies highlight the introducing structural elements in the partition affects the SRI significantly.

In conclusion, a number of studies highlight the effect of structural elements based on theoretical modelling. For experimental studies, in most cases, the effect on SRI was assessed by comparing a SRI of test partition with SRI of reference partition (without the structural elements). For example, the effect of adding point connections to the partition was discussed in reference to the case of a partition with no point connections [72]. In practice, such a process would be tedious if the diagnosis of sound transmission through structural elements is desired. Additionally if one were to take the partition apart and install it again by removing the structural elements, an uncertainty will be introduced due to workmanship factors. Therefore, it is important to formulate an in-situ method that allows

for diagnosing the sound transfer through such structural element separately. This would allow for measuring the sound transmission through each element separately and help in identifying the elements that affect the SRI adversely.

The source also affects the partition SRI but usually the source cannot be changed or there is no control over the source, for ex. traffic noise incident on a window. However, the sound transmission through the partition may be altered in principle by structural modifications. If the diagnostic information is considered with the SRI then the weak elements may be identified which can be modified in a R&D process.

Currently, there are no research studies outlining an in-situ method for diagnosing the sound transfer contributions of structural elements in a building partition to an airborne excitation. Similar problems exist in the machinery and automotive industry where the diagnosis of structure-borne noise is required. To tackle these problems, experimental methods were formulated to measure the input-output relationships of a MIMO (Multiple Input Multiple Output) dynamic system and the transmission of each input to each output. Most of such methods are part of the umbrella term ‘Transfer Path Analysis’ (TPA) which will be discussed in the next section.

---

## 2.4 Transfer Path Analysis (TPA)

---

TPA methods were traditionally developed to diagnose the sound transmission from the source to a receiver structure through the interface (see Figure 2.4). The interface here refers to the coupling points/junction between the source and receiver. In the early 1970’s the earliest TPA methods were formulated to diagnose the noise transmission in ships. Ten Wolde et al. [91] formulated vibro-acoustical reciprocity based techniques for quantifying the contributions of different structure borne sources in ships to the underwater noise. In his later work [92], he published a comprehensive review of different reciprocity functions that are applicable to a Linear, Time Invariant (LTI) system which could be potentially used for noise transmission measurement. Verheij [93] formulated a reciprocity based measurement for diagnosing the structure borne source contributions through resilient

mountings. Later he also formulated an inverse method for source characterisation [94]. Both the reciprocity and inverse methods were used for characterising the source in each problem. To this date, most of the TPA methods in practice, either use a reciprocity based method or an inverse measurement based method for source characterisation.

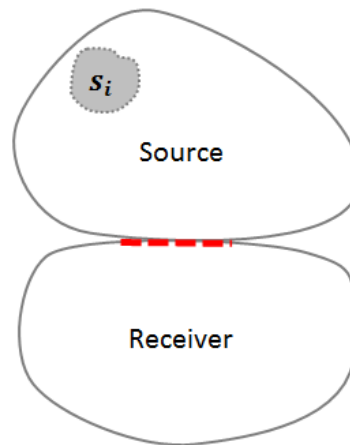


Figure 2.4: Source-receiver representation of a dynamic system, source (active component) is coupled to the receiver (passive component) at the source receiver interface (in dashed red),  $s_i$  – internal driver/mechanism of the source

---

### 2.4.1 Source Characterisation

---

Source characterisation lies at the heart of the TPA method where the contribution of the source to a passive receiver system is desired. As discussed earlier, the characterisation techniques either employ a reciprocity method or an inverse method. Depending on the type of source-structure borne or airborne and ease of measurement, either method may be suitable. A review of the existing source characterisation techniques is given below for the type of each source which will be followed by the challenges for an airborne noise problem.

---

### 2.4.2 Structure borne sources

---

Structure borne sources (for example, motors, pumps, compressors, engines, etc.) are very common in machinery and automobiles. Thus, a large part of the TPA work has been dedicated to the structure borne source characterisation and sound transmission



problem through paths. Some of the early work by Ten Wolde and Verheij referenced in Section 2.4 was based on diagnosing structure borne sound transmission through ships.

In source characterisation, the source quantity should describe the action of the source on a passive receiver. The other criterion for a source characterisation is that it should be ideally a property of the source and independent of the receiver. This would mean the source characteristic quantity is transferable to different receiver for diagnosing the sound transmission. Two quantities satisfy this criterion, namely the free velocity of the source and the blocked force of the source. The source mobility is also an independent property of the receiver however used rarely to describe the source activity.

**Free velocity** –The free velocity of a source is the velocity of the source at the coupling points when the source is operational under free-free boundary conditions, i.e. when no receiver is coupled to the source.

**Blocked force** –The blocked force of the source on the other hand is the force that the source applies to a blocked receiver. A blocked receiver is a rigid receiver compared to the source and is not excited into vibrations when coupled with an operational source. Figure 2.5 illustrates the concept.

Thus, the free velocity or the blocked forces can be measured for an independent characterisation of the source. However, it turns out that these measurements are often not practical if one implements the scenarios illustrated in Figure 2.5.

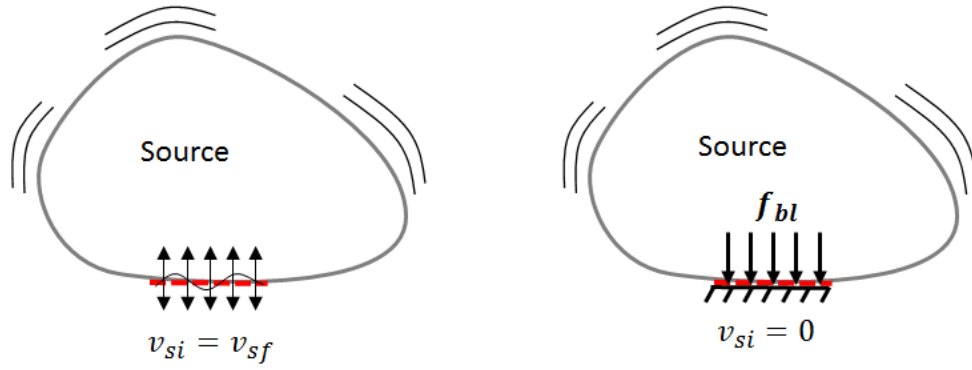


Figure 2.5: Active source substructure with velocity  $v_{si}$  at interface 'i'. Left –interface is free and interface velocity is the free velocity ( $v_{sf}$ ) of the source, right –interface is blocked and forces acting at the interface are blocked forces ( $f_{bl}$ ) of the sources

The free velocity of a source can be measured if the source is operated under a free-free boundary condition uncoupled from any receivers. Usually this would require hanging the source from resilient ropes or cables and then operating the source. However, this method is not very suitable as one has to remove the physical source from an assembly which can be highly impractical especially for large sources. This increases the measurement time. The blocked force similarly could be measured if the source is coupled to a rigid receiver whose mechanical impedance is very high than the source impedance. Some scenarios have been investigated namely the 'Reception plate' method [95] where the source is coupled to a really massive reception plate and the forces then obtained are the blocked forces. However, some in-situ approaches to source characterisation were also developed which are discussed here.

In the characterisation of structure borne sources by force quantity, indirect force determination methods were developed in the late 20<sup>th</sup> century. Blau et al. [96] presented a review of the inverse method of force measurement. Linden et al. [97] presented an experimental case of the same method. In this method, the source is first disconnected from the receiver and the receiver mobility is measured. Then the source is connected to the receiver and the operational velocities at the source receiver interface are measured. The forces measured by this approach are the contact forces and they are not independent of the source structure [98] however they could be used to rank the different sound transmission paths. This approach formed the 'Classical TPA' technique.

Verheij et al. [99] outlined a pseudo force method based on inverse measurement where the source was characterised by a number of correlated point forces over the source. Unlike the contact forces, which are determined at the interface, the pseudo forces could be determined for any positions of choice on the source structure. In theory, an infinite set of pseudo forces could exist for the structure borne source and was also shown for the case study of a pump considered by the authors. Janssens et al. [100] presented multiple case studies on the pseudo forces methodology to characterise different structure borne sources but also highlighted the need for regularisation techniques such as ‘Singular Value Decomposition’ (SVD) [101] to obtain reasonable predictions of receiver response. In case of airborne excitation this methodology would not be feasible as it would be practically difficult to determine point forces on the source which is the air volume. This is because the measurement techniques involve structural FRF measurements (mobility) which is not feasible for fluids where acoustic or vibroacoustic FRF’s are specified. In other study, Janssens et al. [102] also outlined an equivalent forces methodology, which is rather used to characterise the transmission through a single path. The pseudo force and equivalent force characterisations are not independent. Additionally, as one can choose random locations on the source for characterisation, one cannot really assure that all Degree of Freedom (DoF) are accounted for. For the case of airborne excitations, the source is air, thereby making it more important to select the appropriate locations for characterisation and a force characterisation may not be feasible as the source essentially is a pressure field rather than a set of forces. However, if we consider the pressure acting on a surface, then using Classical TPA, the airborne excitation could be in principle characterised at the surface. However, one cannot remove source (air) from the structure for measurements as required by Classical TPA techniques.

Elliott et al. [103] first proposed an in-situ technique for measurement of blocked forces of a structure borne source. This made it possible to characterise the source independently of the receiver structure [104]. An advantage of such characterisation is that it can be done in-situ without removing the source physically from the source receiver assembly, unlike classical TPA techniques. This method came to be known as the Blocked force TPA or iTPA

(in-situ TPA). This would be especially useful for the case of airborne excitations where the source is air and cannot be removed from the receiver (partition) for measurements. Therefore, it is worthwhile to explore the application of iTPA for case of airborne sound transmission through building partitions. It may then be in principle possible to measure the contributions of sources through different paths (elements) in a multi-layered partition.

---

### 2.4.3 Power based quantities

---

Some studies have focused on power based quantities to characterise the source and describe the transmission from source to receiver. Mondot et al. [105] outlined the concept of a source descriptor and a coupling function to describe the active power transmission from a source to a receiver. The source descriptor is a power quantity that characterised the source and can be measured from the free velocity of the source and the source mobility thus requiring the source to be uncoupled from the receiver. The study was analytically validated for the case of power transmission from a single source point to single receiver point. More power based quantities such as the characteristic power and mirror power established by Moorhouse [106] can be found in literature. Such power-based characterisations may be useful to rank different structure borne sources in the same way as airborne sources can be ranked by their airborne sound power. However, diagnosing the contributions of multiple sources/paths may be difficult using such techniques. For diagnosing the contributions, the Frequency Response Functions (FRF's) will have to be referenced to a power excitation (as the source descriptor is a power quantity) which is unconventional: FRF's are typically defined for a force or moment excitation for structure borne sources not for a power excitation. Therefore using a power-based characterisation for case of airborne excitations as well may not be suitable if we want to diagnose the sound transmission through various paths in a partition.

#### 2.4.4 Airborne source characterisation

Airborne sources can be usually characterised by their radiated sound power [107]. Such characterisation is often useful to rank different airborne sources. In TPA however, it may be difficult to use airborne sound power to quantify the airborne sound transmission through various paths. One prominent difficulty that was discussed in the previous section is that FRF is defined for a force or volume velocity excitation while a FRF is not available for a power excitation. Therefore, alternate source characterisation may be useful for the application of TPA methods. Verheij et al. [94] and Ten Wolde [91] have quantified the airborne source by equivalent volume velocity source. Usually a complex source cannot be substituted by a single volume velocity source. In such cases, the source can be defined as an equivalent of correlated or uncorrelated monopoles. This can be visualised by different areas on the source mimicking a set of equivalent volume velocity sources which can be written as,

$$Q_n = v'_n dS_n \quad (2.7)$$

where,  $Q_n$  is the volume velocity of the radiating surface 'n' with area  $dS_n$  on the airborne source. This kind of methodology is common when the airborne noise radiated by a physical source has to be quantified. In vehicles, the exhaust source is often characterised by an equivalent volume velocity excitation. Such characterisation may seem feasible at low frequencies and for simple structures. At high frequencies, the challenge arises of describing the source by a large number of monopoles. Also for the diagnostic part, FRF's will be required which imposes the requirement of a calibrated volume velocity source working at all frequencies. The commercially available volume velocity sources are bigger in size which may impose some limitation on the measurement due to space restrictions. Therefore, the volume velocity characterisation although possible does not seem to be the best option for an in-situ methodology.

The other option that may be feasible is using the independent source descriptors used for structure borne sources. As seen in the previous section, the independent source

characteristic quantities for a structure borne source are its free velocity and the blocked force acting at the interface. The free velocity of the air can be measured if the air can be disconnected from the receiver (the partition) and its velocity at the interface measured but this is practically impossible. If we look at the blocked force characterisation, it is usually easy for structure borne sound sources which are solid in nature. However, an airborne source excitation acts through a fluid onto a structure (the partition). Here, the air is effectively the source which applies a dynamic pressure on the panel (receiver). In such cases, due to the nature of the excitation, the source may be characterised by some pressure quantity. A challenge here is to characterise a pressure excitation by a blocked force quantity. This seems difficult as the quantities are not coherent in units (N and N/m<sup>2</sup>). One option is that a blocked pressure characterisation be devised for airborne sources similar to a blocked force characterisation of a structure borne source. Conceptually, this blocked pressure can be said to be the pressure that the airborne source applies on a blocked structure.

In practice a blocked pressure characterisation has not been explored extensively. Smith [108] outlined the concept of blocked pressure and its relation to the total pressure acting at the interface. According to Smith, the total pressure acting on the source receiver interface can be written as the sum of the blocked pressure and a radiated pressure term. Fahy [109] uses blocked pressure term in the vibroacoustic FRF measurement process, as the pressure on a surface due to a volume velocity source operating in the receiver structure. Bobrovnitskii et al. [110] outlined a general theory for the blocked pressure characterisation of airborne sources. The blocked pressure of the source was derived to be the pressure difference across a virtual interface in air surrounding the source. The study was validated for an analytical case of airborne sound transmission. Later Pavic et al. [111] characterised an airborne source by the blocked pressure on a virtual interface and the source impedance on discrete patches/areas on the source receiver interface. This concept is called as the 'Patch Impedance' concept. An analytical case study was used for validating the method and measurement implication were discussed for the same. In our case, the blocked pressure can be defined at the interface (at the face of the partition), similar to how

blocked force can be defined at the interface between the source and receiver structure. However, a measurement methodology will have to be developed for the same which is not clearly defined or available in the literature as most studies are of theoretical nature.

---

#### 2.4.5 TPA – diagnostic contributions

---

Once a source is characterised it can be combined with the FRF's to get a contribution of the source at the receiver. This is the basic aim of most TPA methods to measure the contribution of various sources. Some variants of the TPA also are developed which do not require the source to be characterised. Such methods have been developed so that the contributions can be obtained from operational data in case it is not possible to characterise the source. Magrans [112] outlined a method for calculating the sound transmission through different paths. The Advanced Transfer Path Analysis (ATPA) method [113] was developed based on this study. ATPA uses transmissibility data instead of FRF's to obtain the path contributions and thus source characterisation is not required in this method. Zaiferopolus [114] presented an experimental study comparing iTPA and ATPA and showed that while the operational response on the receiver can be predicted reasonably, the contributions obtained from both methods are not exactly same. This is because the ATPA provides path contributions while the iTPA provides the source contributions. An Operational TPA (OPA) [115] method has also been developed which takes into account only the operational data between the source locations (input) and receiver locations (output) through use of transmissibility. Although this can be completely implemented in operational conditions, one significant drawback that may present is the cross talk between different paths (especially when they are correlated) that is not accounted by the method. A discussion on this can be seen in [116]. Other variants of TPA such as OPAX [117] and GTDT [118] can also be found.

In principle, these methods can be applied to a steady state LTI system comprising of an active (source) and a passive component (receiver). Most of the examples however available in literature are applications of TPA in vehicles or structure borne sources. We will now

looks into some experimental attempts that have been made to measure the sound transmission through building partitions.

---

## 2.5 Diagnostic methods in building acoustics

---

If we consider the sound transmission through a multi-layered partition, then the sound transfer through different structural components in the partition could be different. This was looked into in Section 2.3.4. A simple sound intensity test could be performed where the sound powers radiated by areas in the partition can be measured. However in reverberant conditions, the measurement of radiated sound power by intensity methods can be erroneous at low frequencies due to strong modal effects. In such cases, special requirements specified by ISO 15186 must be met, particularly the presence of absorption on the back wall of the receiving room. Another error that may be present is the nearfield error. In addition, the sound intensity, which is measured from transmitted pressure and velocity, is not a diagnostic characteristic because the transmitted pressure is contributed by the whole partition rather than the element/path in concern. Roozen et al [90] have used laser vibrometry to assess the change in radiated power from a partition with respect to number of screws used to fasten studs as well as screw tightness. Schevenels et al [119] performed an experimental study to calculate the structure borne sound power injected into the receiving room by a floor. The source by characterised by its contact forces and a reasonable estimate of the contributions could be obtained only after regularisation of the data. Geebelen et al. [120] experimentally investigated the relation between the standardised impact noise level in a receiving room radiated by a partition and its airborne sound insulation as originally derived by Cremer. The relationship is valid above critical frequency of the structure where the radiation efficiency is assumed to be unity. The reciprocity relation at the base of this theory was tested experimentally on a floating floor consisting of a single sound bridge. The authors attributed the deviation in the measured values of reciprocity relation from the ideal value of  $4\pi$  is due to the presence of a sound bridge. Therefore the effect of sound bridge on the reciprocity relation was examined rather than the effect on the actual sound transfer. Thus, the method does not provide an in-situ



diagnosis of sound transfer contributions but proposes to diagnose the physical presence of structural links in the partition. Reciprocity method has been used by Squicciarini et al. [121] to measure the radiation efficiency of single panels but do not provide any sound transmission characteristics of the structure. Acoustic cameras which are traditionally used for source localisation have also been used in rooms but their application is so far demonstrated to localise leaks in the building structure [122]. On the other hand, diagnosis of sound transmission through different structural elements in the partition has not been studied explicitly however their application range is limited in frequency and can be inaccurate in reverberant rooms [123].

Panel noise contribution analysis (PNCA) methods are common to the vehicle acoustics design for diagnosing the sound transfer through various panels for noise control measures and a plethora of publications based on this method can be found here [124]. In principle PNCA can be also applied to diagnose the sound transfer through partitions but no study has been done on this yet. PNCA is similar to the reciprocity-based method of Ten Wolde et al. and Verheij et al. The same concept was used in the 90s under the name of Acoustic Source Quantification (ASQ) method [125].

---

### 2.5.1 Objectives of study

---

As discussed in Section 2.3 extensively, the SRI of a building partition can be affected by several parameters. The structural elements of the partition affect the SRI of the partition and theoretical and experimental studies have shown that. However, it remains to be seen how the in-situ determination of the sound transmission through different elements can be done. Such an in-situ method would allow ranking of the elements according to their sound pressure contributions. If the sound transmission can be measured spatially for all such paths, then the weak sound insulation elements can be identified. Therefore the work in this thesis will be based on formulating the diagnosis of airborne sound transfer through building partitions. The following will be the objectives,

- 1) To formulate a methodology for characterising the airborne excitation on partitions. An appropriate inverse technique will be used to characterise the pressure on the panel surface (or sub areas) in-situ.
- 2) To diagnose the sound transfer through different elements and areas in the partition based on their contributions to the receiver pressure.
- 3) To present a combined measurement application for characterising the partition but also providing diagnostic information as a complement to SRI measurement. This would showcase how the diagnostic information (spatial sound transfer) can be analysed with the SRI (relating to frequency based sound transfer).
- 4) To investigate an alternative method for SRI measurement.

---

## 2.6 Discussion

---

The sound transmission through building partitions has been discussed with an emphasis on the measurement of low frequency sound insulation. The limitation of the current ISO standards for sound insulation at low frequencies has been highlighted as a result of the underlying diffuse sound field assumption. This assumption causes uncertainty in SPL, RT measurements and eventually in the SRI calculations. This uncertainty has been attributed to the room resonant effects at low frequencies which make the sound field irregular; the highest SPL is observed at the corners of the room and low SPL around the centre of the room. Apart from the influence of the test method, a number of factors including construction, material properties, flanking, and structural elements was discussed. The multi-layered partitions are most commonly used in built constructions and typically the panels are supported by structural elements inside the cavity. These elements add to the sound transfer to the receiver room leading to weaker sound insulation. In extreme cases, this may lead to noise issues. Therefore the diagnosis of sound transmission through such elements is important. With the standard airborne sound insulation measurement, such diagnosis is impossible and therefore this forms a valid research question which will be

explored in the context on this thesis. TPA methods will be used to devise a methodology to characterise the airborne excitation and sound pressure contributions of different paths in the partition. Such diagnostic is proposed to be useful in redesign process of the partition to improve its sound insulation.

---

# 3

## DIAGNOSIS OF AIRBORNE SOUND TRANSMISSION – TPA METHODS

---

*In the previous chapter, a literature review relevant to the topic of the study was presented and the aims of the work were formulated. In this chapter, the problem of in-situ diagnosis of airborne sound transfer through building partitions will be addressed. A suitable diagnostic descriptor will be introduced which quantifies the sound transfer through the partition elements. Additionally, a novel TPA application for source characterisation and measurement of the diagnostic descriptor would be formulated. The techniques will be validated for the case of airborne sound transmission through a single leaf panel.*

---

### 3.1 Diagnosis of airborne sound insulation

---

In the previous chapter, the concept of sound insulation<sup>1</sup> was discussed in reference to building elements, which is usually measured by standard methods to give the SRI. A single number rating ( $R_w$ ) is also obtained by comparing the SRI curve and a reference

---

<sup>1</sup> Here onwards, sound insulation refers to airborne sound insulation unless stated otherwise

curve. The SRI and  $R_w$  are typically measured for laboratory conditions in the frequency range of 100-5000 Hz typically. Thus, it can be said that the SRI specifies the frequency dependence of sound insulation.

Although the standard tests are convenient to measure the sound insulation of the global structure, it does not provide any information on how the different elements in the partition contributed to the sound transmission (or insulation). It is important to note that the sound transmission and insulation are complimentary to each other –when the transmission is high, the insulation is low and vice versa. Thus, the spatial dependence of sound transfer through the partition cannot be established using the standard methods.

In the literature review (Section 2.3.4), different studies notably by Sharp [72] and SEA [67] were mentioned which showed how the partition construction, especially the structural connections affected the sound insulation. This analysis was mostly based on prediction models. Experimental investigations were based on measuring the SRI of multi-layered partitions with and without the presence of structural connections. However, an in-situ measurement method to diagnose the sound transfer through these connections locally in a building partition has not been explored yet. Therefore, neither the standard techniques nor existing literature studies have shown to be capable in providing the diagnostic information in-situ.

As an example, for multi-layered partitions the sound transfer occurs through different elements such as point connections/ribs/resilient elements in the cavity that connect the leaves of the partition. In such cases, from SRI or  $R_w$ , it is impossible to know how much sound is transferred through the different structural elements that are incorporated in the partition construction. If the sound transfer through these elements can be diagnosed, it would provide a spatial dependence of sound transfer through the partition. This has potential to identify the weak elements of sound insulation in the partition. It may then be helpful to complement the diagnostic information with the SRI values to assess which elements affect the sound insulation adversely. In short, while the SRI specifies the frequency dependence of sound insulation, the diagnostic information would specify the

spatial dependency of the sound transfer. For the latter part, a diagnostic descriptor would be suitable to quantify the sound transmission spatially through different regions and structural connections in the partition.

---

## 3.2 Diagnostic descriptor

---

Consider a simple case of a single layer partition installed between a source and receiver room as shown in Figure 3.1 (generalised multi-layered case will be discussed later). When a partition is excited by an airborne source, it is set up into a vibrations and sound is radiated by the partition into the receiver volume. While, the SRI can be conveniently measured which represents the frequency dependence of sound insulation, the diagnostic descriptor will be a representative of the spatial dependence of the sound transfer.

To examine the spatial dependence, it is suitable to first discretise the partition into discrete areas (patches) such that each patch contributes to the radiated sound. The total contribution of all such patches would be in principle equal to the total sound radiated by the partition. Similar approaches have been adopted [111,126-128] where a partition is discretised in small radiating areas (referred to as patches) to predict the vibroacoustic response of a coupled system (air-partition-air). To maintain consistency, we will also use the term patch to refer the discretised regions/areas on the partition. It is then clear that diagnosing the contribution of the patch to the total sound transfer (for instance see  $p_{j,k}^c$  in Figure 3.1-right graphic) is then the subject of the study presented here. This means that a suitable diagnostic descriptor is the sound pressure contribution of each patch. It is important to note that such discretisation will impose a frequency limit of vibroacoustic prediction. This will be discussed in more detail later.

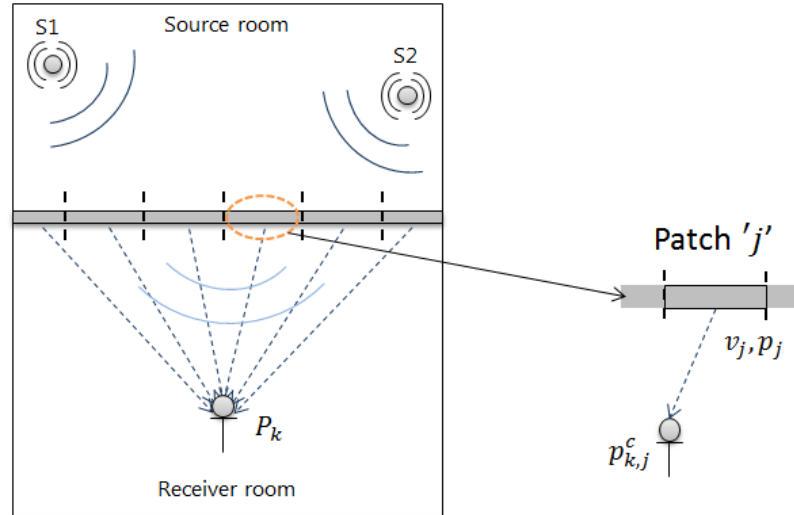


Figure 3.1: A single panel between a source and receiver room discretised into patches. For a patch 'j', the velocity on the patch  $v_j$  and the pressure close to the patch  $p_j$  are denoted, and the contribution at a receiver point  $k$  is  $p_{k,j}^c$  where superscript 'c' denotes contribution

As discussed earlier, the pressure contribution of each patch would be an adequate diagnostic descriptor of each patch. However, for a patch, different quantities like the sound intensity, velocity, or FRF's could be easily measured. Therefore, before proceeding to measure the contributions of the patches, it is sensible to have a quick review of directly measurable vibroacoustic properties to see if they qualify as a diagnostic descriptor of the patch.

### 3.2.1 Transmitted pressure and velocity

For a partition excited by an airborne source, one can readily measure the transmitted pressure close to each patch and the normal velocity. The transmitted pressure can be simply measured by positioning a mic close to each patch on the receiver side and the normal velocity of each patch in bending can be measured by placing an accelerometer over each patch or with a laser vibrometer. The transmitted pressure measured near individual patches may seem a good candidate as a diagnostic property however this pressure is a result of sound radiation from all the patches. Also, in presence of airborne flanking, this pressure will have contributions from the flanking. Hence, transmitted pressure alone does

not qualify as an independent diagnostic property of the patch. Likewise, by measuring the velocity (vibrational property) any information on the sound transmission (acoustic property) cannot be deduced. In addition, the net velocity of a patch is a result of direct airborne excitation and the vibration transmission from surrounding patches as it is coupled to other patches. Thus, the net velocity does not qualify as a diagnostic property of the patch.

The transmitted pressures can be combined with the velocities, and integrated over the partition area to give the transmitted sound power. Again, this transmitted power is a property of the whole partition, rather than a diagnostic feature of the individual patch in consideration. The transmitted power (or intensities) from each patch can also be measured but as discussed earlier, the pressure is not an independent property of the patch. Then the sound intensity of the patch also cannot be qualified as an independent property.

---

### 3.2.2 Vibroacoustic FRF

---

The vibroacoustic FRF or vibroacoustic transfer function defines the pressure in a fluid medium due to unit force excitation on a structure surrounding the fluid (Pa/N). In our case, this FRF can be defined between the patch and receiver point as approximately equivalent to exciting the patch centre and measuring the receiver pressure. In this way, the vibroacoustic FRF can be defined independently for each patch and receiver position, and may qualify as a diagnostic feature. For diagnostics, this would mean measuring the receiver pressure under the operational excitation on the patch. This is nothing but the contribution of the source acting on the patch. To measure this, it is first important to characterise the source.

Traditionally, source characterisation and diagnostic analysis is done using TPA methods commonly for structure borne noise problems (see Section 2.4). Therefore, it is worthwhile to investigate if such techniques could be adapted to the problem of diagnosing airborne sound transfer and the pressure contributions. The following sections will first introduce the concept of TPA methods for structure borne problems and then discuss the challenges



for adapting the approach to an airborne problem followed by a novel application for airborne problems.

---

### 3.3 Diagnostic analysis – TPA

---

In the automotive industry, an important step in the vibroacoustic design of the vehicle is diagnosing the contributions of individual structure borne and airborne sources to the sound and vibration generated in the vehicle interiors. Based on these source contributions, it is easier to identify the dominant sources. These source contributions are traditionally measured by the application of TPA methods.

By the application of TPA techniques, the source is first characterised and then its contribution at a receiver position can be diagnosed. Several variants of the TPA method were mentioned in Section 2.4 which could potentially be applied for such diagnosis. For our study, the iTPA method is particularly of interest as it allows for the in-situ characterisation of the source as well as in-situ diagnosis of source contributions. Here we will outline the steps that are followed in the structure borne iTPA process.

---

#### 3.3.1 Source-interface-receiver model

---

In applying the iTPA method at first, the system is discretised into a source-interface-receiver model, also shown in Figure 3.2. The following definitions are global to the context of the thesis,

Source: The source is the active subsystem of the dynamic system. In operational conditions, it applies forces/moments/pressures (or a combination of these) on the receiver. For airborne excitations the source will be a pressure quantity.

Receiver: The receiver is the passive subsystem of the dynamic system. Under operational conditions, the source excites the receiver into vibration and/or acoustic response(s). The receiver can be a structure or an acoustic medium or a combination of both.

**Interface:** The interface also sometimes referred as the source receiver interface is the common boundary between the source and receiver. It is the boundary where the source is connected to the receiver and the source acts on the receiver through this interface.

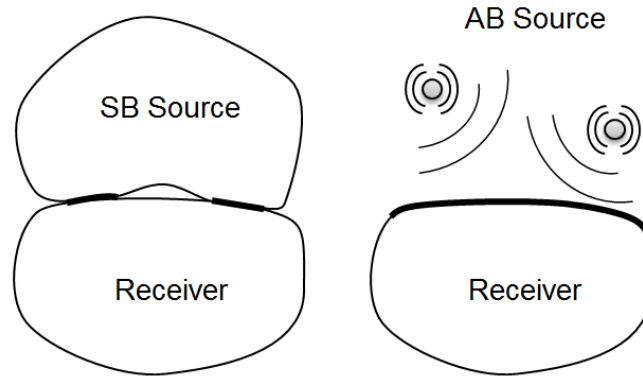


Figure 3.2: Interfaces ('—') for structure borne (SB) and airborne (AB) sources coupled to receivers. Left –Structure borne excitation acting at discrete interfaces and right –an airborne excitation acting at a continuous interface

Such modelling of a dynamic system into a source receiver system is also called as 'Dynamic Substructuring' [129]. The importance of such modelling lies in the fact that any dynamic system can be modelled as a source-interface-receiver problem. For structure borne sources, in practice, the interface is usually discrete owing to finite structural connections between source and receiver (Figure 3.2). For example, this can be a structural joint/engine mount between the engine and the vehicle body in the case of structure borne excitation. For the case of airborne excitation, the interface is continuous (Figure 3.2) as air is not localised to discrete sections of the interface (it spreads rather evenly). This will pose a challenge as iTPA traditionally deals with discrete interfaces.

### 3.3.1.1 Symbols and conventions

Here we will define a standard symbol and convention for every vibrational/acoustic parameter and FRF to be used within the context of this thesis. Table 3.1 below outlines the symbols for the common measurement parameters of vibroacoustic systems that will be used throughout the thesis.

Table 3.1: Common measurement parameters and designations

| Parameter   | Velocity | Acceleration | Force | Pressure | Volume velocity | Voltage |
|-------------|----------|--------------|-------|----------|-----------------|---------|
| Designation | $v$      | $a$          | $f$   | $p$      | $Q$             | $V$     |

Likewise, FRF's can be measured on the independent substructure or the coupled assembly. An FRF is an independent characteristic of an LTI system. These FRF functions in simplest terms are input-output functions that define the output response at the point due to unit excitation at a point in the system. A FRF ' $X_{ij}$ ' denotes the value of the measured FRF ' $X$ ' as the response at point ' $i$ ' due to the excitation at point ' $j$ '. Some of the FRF's can in turn be categorised as point and transfer FRF's. Point FRF specifies that the response and excitation points are same while the transfer FRF specifies that the response and excitation points are different. An FRF can be measured directly or reciprocally using the principle of reciprocity. Table 3.2 denotes the standard conventions for different FRF's for structural and acoustic systems as well as their direct and reciprocal measurements.

Table 3.2: FRF's with designated symbols, direct and reciprocal measurement

| FRF quantity      | Designation                                  | Direct measurement | Reciprocal measurement |
|-------------------|--|--------------------|------------------------|
| Mobility          | $Y_{ij} = \frac{v_i}{f_j} = \frac{v_j}{f_i}$ |                    |                        |
| Accelerance       | $A_{ij} = \frac{a_i}{f_j} = \frac{a_j}{f_i}$ |                    |                        |
| Vibroacoustic FRF | $H_{ij} = \frac{p_i}{f_j} = \frac{v_j}{Q_i}$ |                    |                        |
| Acoustic FRF      | $U_{ij} = \frac{p_i}{Q_j} = \frac{p_j}{Q_i}$ |                    |                        |

### 3.3.2 FRF measurements

Once the system is substructured, the first measurement phase is appropriately defining and measuring its FRF's. These FRF's measured quantify the input-output relationship between a source and receiver DoF. In TPA, each set of such source and receiver DoF is designated as a 'transfer path'.

However the term transfer path used here is global in definition, i.e. it specifies the transmission through the global structure (or through all physical paths between the source and receiver DoF). The transfer path FRF thus helps in characterising the contribution of the source DoF at the receiver DoF through all physical sound transmission paths in the structure (see [130]). To illustrate this (see Figure 3.3), the sound transmission between the source and receiver DoF ( $i$  and  $j$ ) as per TPA constitutes a transfer path, which is characterised by a FRF. In reality, the transmission from DoF  $i$  to DoF  $j$  occurs through multiple sound transmission paths. Thus, the term transfer path is only used in the context

of defining the sound transmission between two points and is not to be confused with the physical paths of sound transmission that exist between two points.

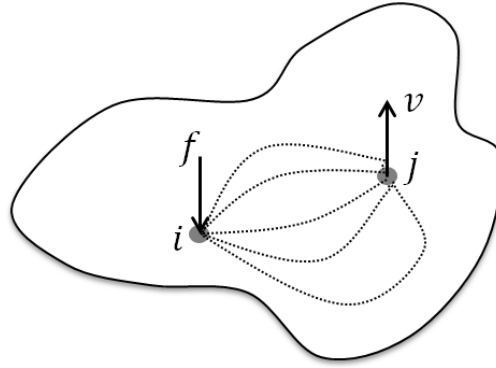


Figure 3.3: Sound transmission from source DoF  $i$  and receiver DoF  $j$  represents a single transfer path characterised by its mobility  $Y_{ji}$ , while multiple sound transmission paths exist between  $i$  and  $j$  (in dotted)

In classical TPA approaches, the FRF's are measured at the interface by removing the source physically or detaching it from the assembly. However, in iTPA, the source is not required to be removed for FRF measurements. Thus, in iTPA, the FRF's are measured at the interface of the coupled source receiver assembly. As the source is not operational for the FRF measurements, this phase is also referred as the 'passive' phase. Usually, for structure borne diagnosis, the structural FRF's (mobility or accelerance) are measured between the interface and receiver DoF sets.

In the context of this work, we are dealing with an airborne excitation where air is effectively the source. In a practical test with airborne excitation, removing/detaching the air (source) from the receiver would be almost impossible for most cases. In such case, the practical advantage of iTPA technique is self-evident, which would allow for the air (source) coupled to the receiver for FRF measurements.

---

### 3.3.3 Operational measurements

---

The second measurement step of iTPA involves activating the source in operation and measuring the steady state operational responses at the interface. Hence it is also called

as the 'active' phase of measurement. Additional remote positions on the receiver can also be accounted for operational measurements for validating the methodology (the corresponding FRF's for those positions will also have to be measured). For steady state conditions, all operational measurements are averaged for a certain time length enough to obtain a good coherence. If all the responses cannot be measured in one single test, it is always a good practice to reference them (like [131]) to a suitable reference parameter. This helps in maintaining the phase relationship between different measurement sessions.

---

### 3.3.4 Source characterisation and diagnostic contributions

---

Once both measurement phases are completed, the next step is characterising the source and diagnosing its contributions at the receiver DoF. In iTPA, the structure borne source is characterised by combining the FRF's of the coupled assembly and operational measurements following an inverse formulation as,

$$\{\mathbf{f}_{bl}\} = [\mathbf{Y}]^{-1} \cdot \{\mathbf{v}'\} \quad (3.1)$$

$$\{\mathbf{f}_{bl}\} = [\mathbf{Z}] \cdot \{\mathbf{v}'\} \quad (3.2)$$

In this thesis, bold letters in curly brackets denotes a vector while bold letters in square brackets denotes a matrix. Then, in Eq. (3.1-3.2)<sup>2</sup>, ' $\mathbf{Y}$ ' is the measured mobility matrix of the coupled source receiver assembly at the interface, ' $\mathbf{Z}$ ' is the impedance matrix of the coupled system as the source is connected for FRF measurements, ' $\mathbf{v}'$ ' are the operational velocities on the interface and/or remote locations and ' $\mathbf{f}_{bl}$ ' are the blocked forces of the source acting at the interface.

The blocked forces obtained characterise the structure borne source independently of the receiver structure. Figure 3.4 shows an equivalent representation of the source receiver assembly by blocked forces acting at the interface (and the receiver). It has been shown that the response of the system under the action of the source can be modelled by the action of blocked forces on the interface [103, 133].

---

<sup>2</sup> A derivation of this formulation is provided in APPENDIX I

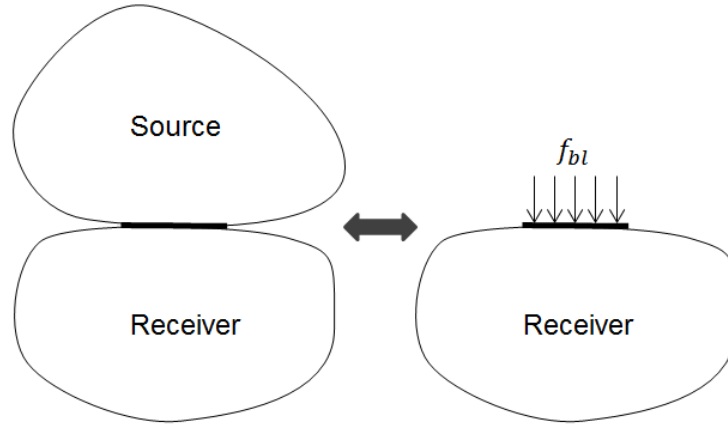


Figure 3.4: A source-interface-receiver system (left) with its equivalent representation on right – the blocked forces acting on the receiver through the interface ('—'),  $f_{bl}$  represents the blocked forces of the source

Thus, the blocked forces are then combined with structural FRF's to predict the vibrational response of the receiver (acoustic response can also be predicted if combined with vibroacoustic FRF vector).

$$v_r = \{\mathbf{Y}_r\}\{\mathbf{f}_{bl}\} \quad (3.3)$$

In Eq. (3.3),  $v_r$  is the predicted response at remote point 'r' and  $\mathbf{Y}_r$  represents the transfer mobility vector from the interface to point 'r'. Any number of structure borne sources can be characterised independently by iTPA. The source contribution for a source 'n' can be found by combining its blocked forces with the corresponding FRF's to a receiver position as,

$$v_{r,n}^s = \{\mathbf{Y}_{rn}\}\{\mathbf{f}_{bl,n}\} \quad (3.4)$$

where, the superscript 's' indicates that it is a source contribution and not the operational velocity (which has contributions from all sources).

---

### 3.3.5 Application of iTPA to airborne problems

---

As the iTPA method has been successfully applied for diagnosis of structure borne problems [104], the question arises whether it can be applied to the problem of diagnosing airborne sound transmission through building elements. To investigate this, consider a

coupled source room-partition-receiver room system as shown in Figure 3.5 (left). The source room hosts an active airborne source which excites the partition and the partition in turn radiates sound to the receiving room.

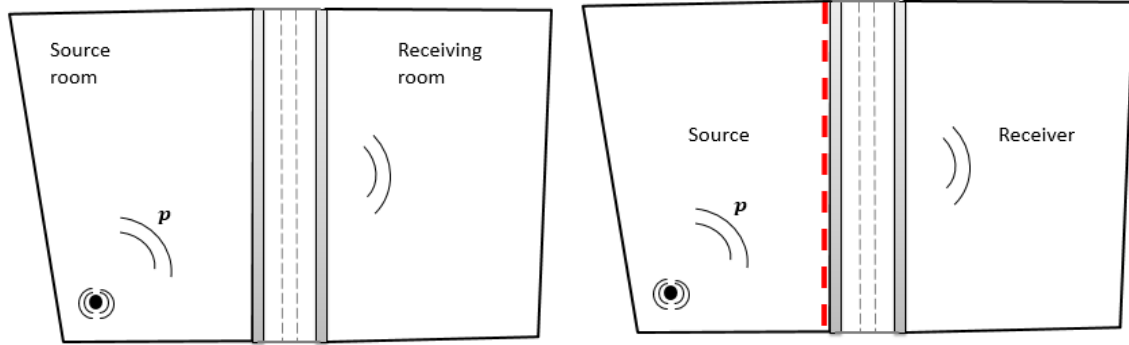


Figure 3.5: System of airborne sound transmission from source to receiving room through a multi-layered partition (on left) and then substructured as a source-interface-receiver system (on right). Source is the source room, partition plus receiving room is the receiver and the interface (in red) is the boundary between source and receiver

To apply iTPA, we can substructure the system as a coupled source-interface-receiver system. Following the definitions outlined in Section 3.3.1, we can identify the airborne excitation acting on the partition as the source and the partition plus the receiving room as the receiver. The interface thus lies at the common boundary between the source room and the partition. The substructured system is also shown in Figure 3.5 (right). Then to apply the structure borne iTPA in this case, the following challenges are present:

- 1) For airborne excitation, the nature of the source is a pressure excitation acting on a continuous interface as opposed to a force/moment excitation acting on discrete interface usual of structure borne sources. In the case of discrete/finite interfaces, the DoF to be accounted in measurement are finite. For an airborne excitation on a partition, like in a reverberant field, an infinite number of pressure waves are incident at all possible angles all along the interface. In such case, the DoF to be accounted for the source will therefore be infinite and impossible to implement practically.



- 2) For structure borne sources (force excitations), the FRF measurements are defined for force excitations (e.g.  $\text{mobility} = \frac{\text{velocity}}{\text{force}}$ ) which can be conducted easily using an impact hammer. For airborne excitation (pressures), these FRF's would be incompatible as they are not defined for pressure excitations. Also, it would be difficult to apply a localised pressure excitation at infinite number of source DoF on the interface to measure an FRF for pressure excitation.
- 3) With structure borne iTPA method, the source contributions i.e. the contribution of discrete sources at a receiver position can be quantified. For the airborne case, as the source is continuous (see Figure 3.2), it is difficult to conceptualise and measure source contributions (as the sources are not discrete). Also, the source contribution represents the sound transmission globally through the structure while we are interested in the local/spatial transmission.

To overcome these practical difficulties, an alternate way of classifying the problem had to be deduced. As the iTPA application has been successfully used on discrete interfaces, we can introduce sampling/discretisation of the continuous interface in ways similar to done in numerical methods. The continuous interface can be first discretised into patches of finite areas and the source can be defined at discrete patches. This would mean that the pressure acting on a continuous interface could be approximated by equivalent point forces acting on discrete patches as shown in Figure 3.6.

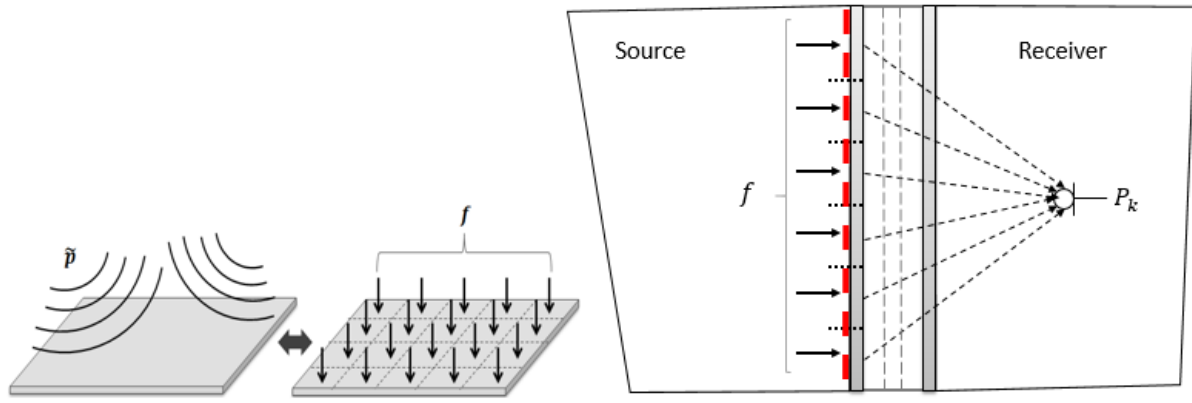


Figure 3.6: Approximating an incident sound field on a partition by point forces on discrete patches of the partition (3D view-left graphic). Equivalent force representation of the airborne excitation on partition between rooms (right graphic)

A force representation of the airborne excitation has two advantages. Firstly, the DoF that need to be accounted for the source characterisation will be finite which allows for the method to be practical. Secondly, for the interface, FRF measurements (like mobility, accelerance, vibroacoustic FRF) can be undertaken as the excitation is now represented by forces. Additionally, the airborne source (pressure excitation) can be characterised by its blocked force (which is typically a structure borne source characteristic) similar to iTPA. For the airborne excitation, the blocked forces per patch area would also represent the blocked pressure on the partition.

An important condition while employing discretisation is that the vibro-acoustic response of the coupled system under such an equivalent source remains the same. The discretisation/sampling of the source and the structure will obviously impose a limit on the frequency range of application in which this response can be predicted with acceptable accuracy. Therefore a sampling criterion will be derived later in conjunction with experimental results to be presented in later sections.

#### 3.3.5.1 Transfer paths and contributions for airborne excitation

In structure borne iTPA, the transfer path which is quantified by an FRF specifies the global sound transfer from a source DoF to a receiver DoF (see Section 3.3.2). Similarly, for an airborne excitation, the term transfer path corresponds to the sound transmission

between a source (force on a patch) and the receiver point (in cavity) through all the physical paths in the structure. For building partitions, if a single point force acts on a patch, the whole partition vibrates and radiates into the receiver volume. This means all the patches contribute to the sound even if the excitation is on a single patch. Then, as per iTPA if the source contributions are diagnosed, they would represent the sound transfer through all paths (see Figure 3.7, left).

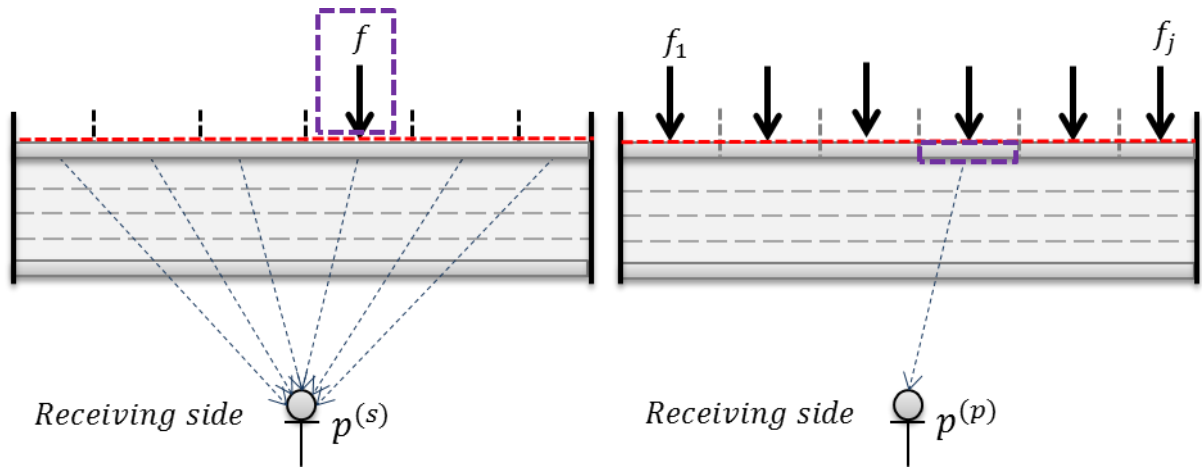


Figure 3.7: A multi-layered partition discretised into patches at the interface (in dashed red). Left – schematic of source contribution of force  $f$  (in purple) which diagnoses the radiation (blue arrows) through all patches, superscript 's' denotes source contribution. Right – schematic of path contribution which diagnoses the radiation through individual patch (in purple) under the action of any number of excitations, superscript 'p' denotes path contribution

However, we are also interested in the sound transfer through individual paths (patches), i.e. the path contribution (see Figure 3.7, right). Such path contributions would show how the sound transfer occurs spatially through the partition under any excitation and potentially help in identifying any weak elements of sound insulation. Accordingly, a methodology for diagnosing both source and path contributions will be presented in the following sections. Also, as all the patches represent a sound transmission path regardless of excitation, they will also be referred as paths.

### 3.4 Airborne source contribution analysis –Methodology

As seen in the Section 3.3.5, it is possible to apply iTPA for airborne source characterisation by employing discretisation at the source receiver interface. Now we will outline the practical methodology of this application. Consider a multi-layered partition with ' $l$ ' internal layers/elements installed between a source and receiver room as shown in Figure 3.8. The partition is treated as a 'black box' so that the internal details are arbitrary provided the interface to the source can be suitably discretised. Thus, the method is suitable for dealing with multi-layered or ribbed partitions.

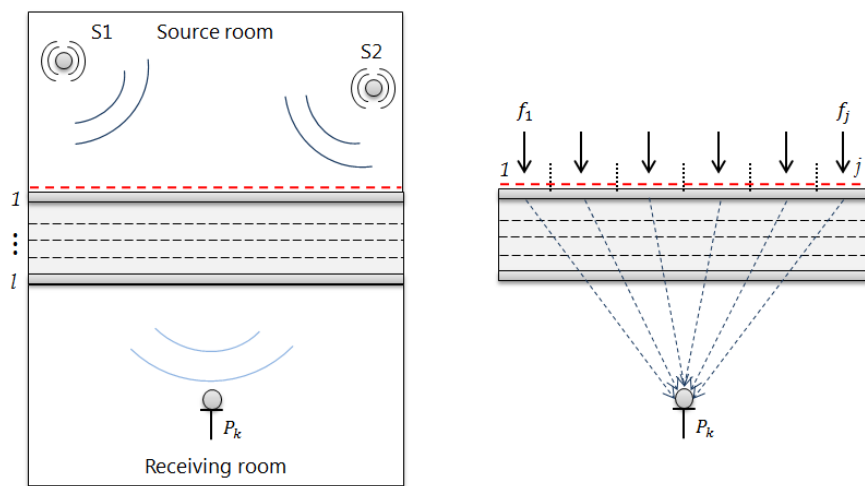


Figure 3.8: Left graphic –A multi-layered partition installed between a source room and a receiving room with the interface in dashed red. Right graphic – Isolated view of the partition with the interface discretised in ' $j$ ' patches. Blue arrows denote the radiation

The interface can then be discretised into ' $j$ ' number of patches. Once we have a discretised interface, the iTPA methodology can be applied. Accordingly, the first phase of measurement is the FRF measurement which is the passive phase. It is assumed here that the structural FRF between different patches (averaged response on patch/ point force on patch) can be represented by the measurement at the centre points of those patches. Such FRF's have also been referred to as the Patch Transfer Function (PTF) before and their validity has been demonstrated below a certain frequency limit determined by a sampling criterion [128, 133]. The FRF measurement can be performed by impacting a patch with a

force hammer and capturing the responses at all patches by use of accelerometers. These measured acceleration functions form the acceleration matrix  $[\mathbf{A}]$ .

$$[\mathbf{A}]_{ixj} = \begin{bmatrix} a_1/f_1 & \cdots & a_1/f_j \\ \vdots & \ddots & \vdots \\ a_i/f_1 & \cdots & a_i/f_j \end{bmatrix} \quad (3.5)$$

To improve the quality of blocked force measurement, the system can be overdetermined where number of response positions ( $i$ ) is greater than number of force locations ( $j$ ). Simultaneously, the vibroacoustic FRF's can also be measured which relate the pressure at receiver points inside the receiving room due to an impact force applied on all patches individually ( $Pa/N$ ). The resulting vibroacoustic FRF matrix can be formed as,

$$[\mathbf{H}]_{kxj} = \begin{bmatrix} p_1/f_1 & \cdots & p_1/f_j \\ \vdots & \ddots & \vdots \\ p_k/f_1 & \cdots & p_k/f_j \end{bmatrix} \quad (3.6)$$

$[\mathbf{H}]$  represents the vibroacoustic FRF matrix measured for ' $k$ ' points in the receiving room. The second measurement phase is the 'Active'/operational test, because the active source excites the system and operational acceleration responses are measured on the patches and pressures inside the receiving cavity for validation.

$$\{\mathbf{a}'\} = \begin{Bmatrix} a'_1 \\ \vdots \\ a'_i \end{Bmatrix}, \{\mathbf{p}'\} = \begin{Bmatrix} p'_1 \\ \vdots \\ p'_k \end{Bmatrix} \quad (3.7)$$

The apostrophe (') indicates the measurements were performed for operational conditions. With the operational accelerations over the paths measured, the blocked forces can then be calculated as

$$\{\mathbf{f}_{bl}\} = [\mathbf{A}]^{-1}\{\mathbf{a}'\} \quad (3.8)$$

' $\mathbf{f}_{bl}$ ' represent the blocked forces on the patches which characterises the discretised airborne excitation. This is an interesting case where an acoustic sound field is mapped on the partition by measuring its vibrational characteristics. Again, the blocked forces will only be valid in a frequency range  $\mathbf{f}: [0 \ f_{max}]$  Hz, where ' $f_{max}$ ' is the maximum frequency of

prediction that can be determined by a sampling criterion (derived in later sections). The contribution of a blocked force ' $f_{bl,n}$ ' at a point ' $k$ ' in receiving volume (i.e. the source contribution) can be measured as,

$$p_{k,n}^s(\mathbf{f}) = H_{k,n} \cdot f_{bl,n} \quad (3.9)$$

where, the superscript 's' denotes that the pressure is a source contribution and not the total pressure. For brevity, the bracketed term  $\mathbf{f}$  will be excluded in further equations and the contributions implicitly represent the prediction in this frequency range.

Similarly the total pressure at the receiver point can be represented as a sum of  $1 - j$  source contributions. The individual or total source contributions will represent the sound transmission through all paths which is depicted in Figure 3.9 below.

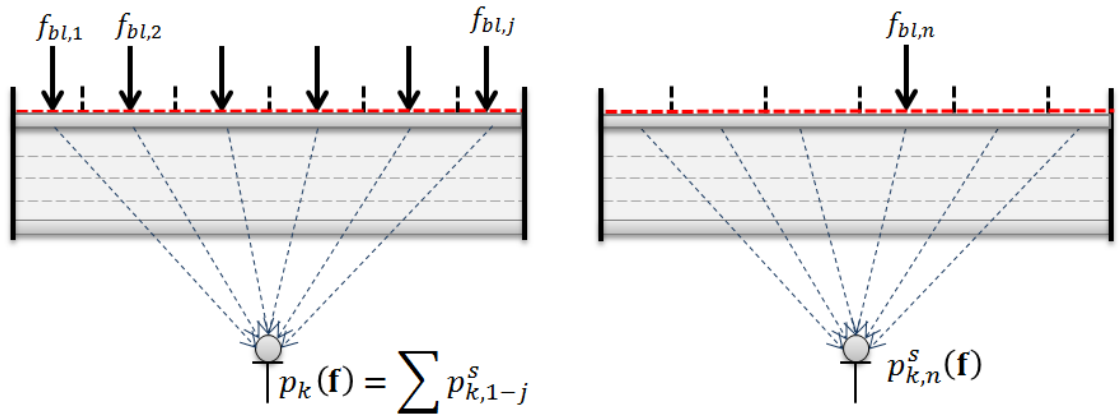


Figure 3.9: Left – Under the action of ' $j$ ' blocked forces, the receiver side pressure predicted as a sum of all source contributions in frequency range  $\mathbf{f}$  determined by sampling. Right – Under the action of a single blocked force at patch ' $n$ ', the pressure measured is a source contribution (with superscript 's')

As the source characteristics and source contributions are measured by an inverse process, the methodology will be denoted by the abbreviation I-ASCA (Inverse Airborne Source Contribution Analysis).

---

### 3.4.1 Validation of I-ASCA methodology

---

Before we apply the I-ASCA methodology for measuring source contributions, it is necessary to validate the methodology with a verified technique. iTPA is usually validated by predicting the remote vibrational response on the receiver using the respective FRF's and blocked forces[134, 135] (see Eq. (3.4)). Likewise, for I-ASCA where the receiver response is acoustic, a pressure response can be predicted by combining the vibroacoustic FRF's and the blocked forces over each patch. This can be written as,

$$p_{p,k} = \{\mathbf{H}_k\}\{\mathbf{f}_{bl}\} \quad (3.10)$$

In Eq. (3.10),  $p_{p,k}$  is the predicted pressure at the validation point ' $k$ ', and  $\{\mathbf{H}_k\}$  represents the vibroacoustic FRF vector measured at the validation point. If it is assumed that the sound transmission takes place solely through the partition and any flanking transmission is minimal, then this predicted pressure can be compared with the measured pressure. If the prediction is equal to the measured pressure then the methodology can be considered to be validated. This is called as the 'Pressure Validation' test.

In practice, the accuracy of a pressure validation will depend on the quality of the measurement data such as blocked forces, FRF's, etc. Additionally, such prediction will not be valid outside the frequency range determined by the sampling criterion which will be discussed now.

---

### 3.4.2 Sampling considerations

---

I-ASCA methodology employs sampling of the structure (into patches) as well as the source excitation (as equivalent point forces). As such, the discretisation imposes a frequency limit under which the vibroacoustic response of the coupled system can be predicted. In other words, the grid size will be determined by maximum frequency of the prediction. Discretisation is commonly employed by Finite Element Analysis (FEA) methods, where a sampling criterion of grid size  $x \leq \lambda/6$  is used, where  $\lambda$  represents the structural

wavelength in vibration. The grid size ' $x$ ' represents the smallest dimension in the grid. As we are discretising the excitation as well as the structure, the longitudinal wavelength in air ( $\lambda_a$ ) or bending wavelength in the structure ( $\lambda_b$ ) will determine the grid size. For building partitions, below the critical frequency ( $\lambda_b < \lambda_a$ ) the sampling criterion will be based on  $\lambda_b$  whereas for supercritical frequencies ( $\lambda_b > \lambda_a$ ), the sampling criterion will be based on  $\lambda_a$ . However, there are some basic differences between FEA based discretisation and a patch based discretisation. In FEA methods, the nodes are coupled between domains while in current case, patches (much larger than nodes) are directly coupled. Also the discretisation is only limited to the source receiver interface as opposed to FEA where complete fluid and structural domains are discretised. Therefore it is possible that a strict FEA based criterion ( $x \leq \lambda/6$ ) would not be necessary.

A quick look at the literature shows that although a FEA based criterion can be sufficient, it is not always necessary in the case of coupling patches for predicting vibroacoustic response of structures coupled to air domains. The theoretical studies in [128, 133] conclusively show that for such cases, a patch size criteria of  $x \leq \lambda_b/2$  is sufficient to predict the radiation till  $f(\lambda_b)$  Hz, where  $\lambda_b$  is the bending wavelength of the structure at frequency  $f$ . In fact, the use of patch based coupling is touted as an advantage over FEA methods in that the coarser discretisation criteria can be used without sacrificing the accuracy and also provides computational time benefits.

For a sampling criterion of  $x \leq \lambda_b/2$ , the maximum wavelength that can be accurately represented is  $\lambda_{b,max} = 2x$  m and accordingly the maximum frequency of prediction is  $f_{max} = f(\lambda_b = 2x)$ . In wavenumber terms, the criterion can also be determined as  $k_b x \leq \pi$ , where  $k_b = 2\pi/\lambda_b$  is the bending wavenumber. For a structure coupled to a heavier fluid (e.g. water), the patch size criteria changes [136]. To verify the validity of this sampling criterion, we will now compare the prediction made by I-ASCA for different grid size with grid size/bending wavelength for a test structure.



### 3.5 I-ASCA: Test setup and measurements

As an initial test, the I-ASCA methodology was applied for the diagnosis of airborne sound transfer through a cavity backed panel. The primary aim was to predict the total sound transfer inside the cavity through the panel and measure the diagnostic source contributions. The test setup is shown in Figure 3.10. A massive hollow wooden box was chosen to represent the receiving cavity. The massive walls of the box (thickness 65 mm) were intended to prevent any airborne flanking transmission.

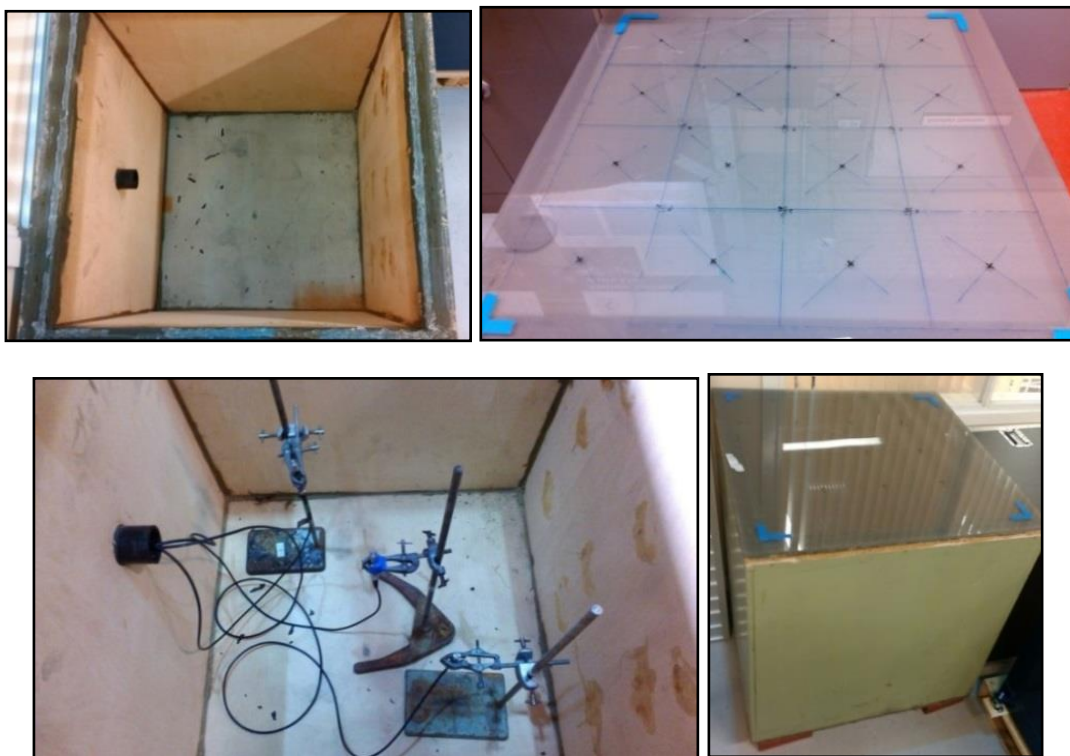


Figure 3.10: The test setup- the wooden box (top left), Perspex panel (top right), free-field microphones (bottom left), and the assembled box (bottom right)

A single leaf Perspex panel, ( $91 \times 91 \times .96 \text{ cm}^3$ ) was assembled on top of the box. The material properties were measured and the results are provided in APPENDIX II. The panel is acoustically compliant compared to the walls and represents the strongest path of sound transfer compared to the walls. Silicone sealant was used between the panel and box edges to minimise any structural flanking transmission from the walls to the panel. An important assumption in this test was that all the sound transmission into the cavity takes place

through the top panel. Thus, the I-ASCA measurements were applied to the panel only. It is still important to note that however thick and hard the cavity walls are, some airborne flanking transmission was expected through them, especially at low frequencies.

Throughout the tests presented in this thesis, the record length of the measurement was 5.12 s which is greater than the mechanical and acoustical reverberation times of the systems tested above 100 Hz. This follows from Roozen et al. [137] which specifies that the record length of the measurement should be equal to or greater than the reverberation time to obtain a truly coherent measurement. For operational measurements, the measurement time was chosen to be above 60 s always unless specified. In the 60 s measurement time, windows of record length 5.12 s were averaged with a 75% overlap ratio between adjacent windows.

For FRF measurements, the panel was first discretised in three different grid configurations, and each was tested independently. The grid sizes tested were 3x3 (9 paths), 4x4 (16 paths), and 8x8 (64 paths). Accelerometers were then placed at every path position on the panel surface and Type MCE 212 (free field) microphones were used inside the box. With impact testing on the panel, the accelerances and vibroacoustic FRF's were measured to populate the respective FRF matrices from Eq. (3.5) and Eq. (3.6). The measurement schematic is shown in Figure 3.11 below.

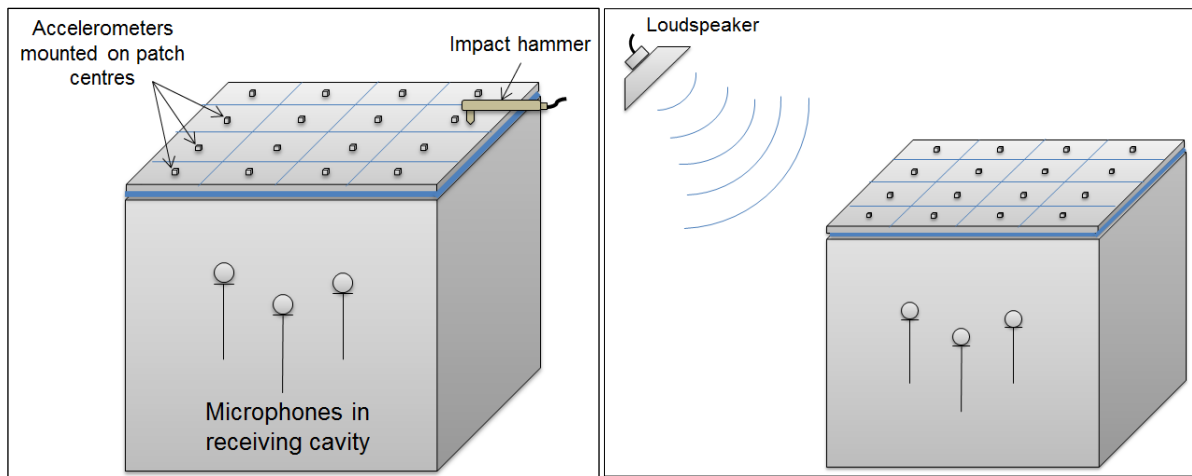


Figure 3.11: I-ASCA measurement schematic for FRF's (on left) and operational measurements (on right) with an active airborne source-loudspeaker

For the operational phase, a loudspeaker was used with a pink noise excitation driven through a B&K noise generator. A pink noise excitation has constant energy in third octave bands and easy to analyse. The airborne sound from the loudspeaker excites the panel which transmits sound in the cavity. The operational accelerations and pressures were measured with respect to the driving voltage of the noise generator which ensures that the signals are synchronous.

Next using Eq. (3.8), the blocked forces were calculated inversely and the pressure at the validation point was also predicted as per Eq. (3.10). These predicted pressures were then compared with the measured pressures for pressure validation test.

---

### 3.5.1 I-ASCA – pressure validation results

---

For grid sizes of 3x3 and 4x4 on the interface, sufficient accelerometers were available so the test could be completed in one test session. Figure 3.12 shows the pressure validation for a 4x4 measurement grid on the panel for frequency range 20-500 Hz. The prediction is not good except in the regions of 20-60 Hz and 160-300 Hz (within 2.5 dB). The grid size for this case was 19.8 cm x 19.8 cm. One could also see that the prediction after  $(\frac{x}{\lambda_b} > .5)$  generally worsens. To analyse the convergence of the  $\lambda_b/2$  criterion, a finer grid size (8x8) was tested next.

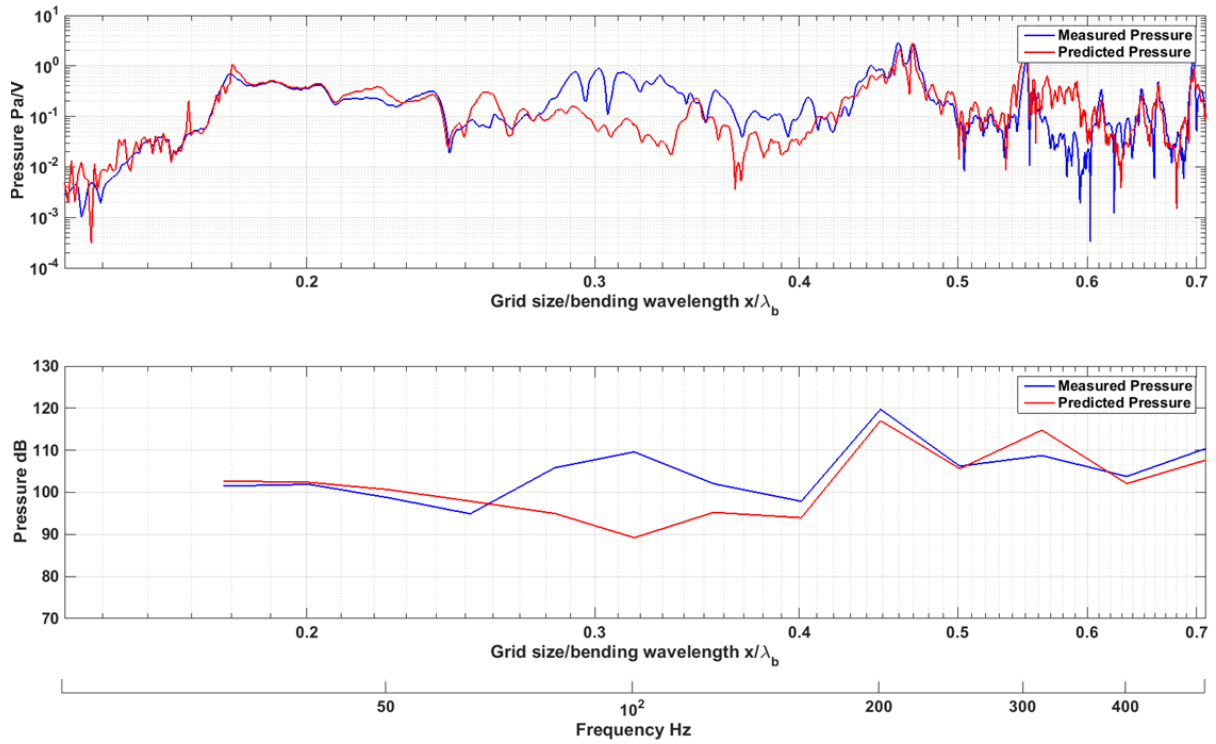


Figure 3.12: Pressure validation results for a 4x4 measurement grid over the panel comparing the measured and predicted pressure in narrow band (top plot) and one third octave band (bottom plot) in 20-500 Hz range. Frequency axis applies to both plots

For the 8x8 test, the total numbers of paths amount to 64 with size 9.87 x 9.87 cm<sup>2</sup>. As only 16 accelerometers were available, the test was divided into four sessions each covering accelerance measurement for 16 paths. Each session provides a measurement of FRF's with 64 force and 16 points over the panel. Therefore, three more runs on different quarters of the panel were carried out to finally obtain an accelerance matrix for 64 paths. This process is illustrated in Figure 3.13.

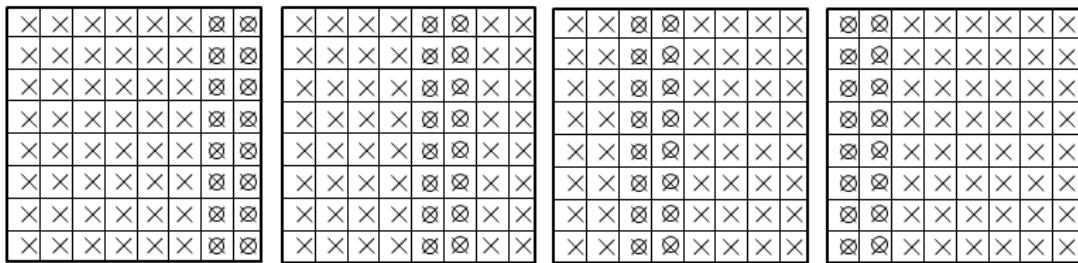


Figure 3.13: Representation of FRF (accelerance) measurement in 4 test sessions for 8x8 grid. The hammer is hit at the centre of all patches (X) while response are recorded only at limited accelerometer locations (O) in each test session

With limited number of accelerometers, the FRF measurement time for an 8x8 grid is enormous. The measurement time also increases due to measurement of vibroacoustic transfer functions. To check the quality of measurement data, the accelerance data can be checked for reciprocity. This basically means comparing  $A_{ij}$  and  $A_{ji}$  elements from the accelerance matrix  $A$ . Ideally they should be equal which would indicate the good quality of measured data. For the first trial of the 8x8 measurement grid, Figure 3.14 shows the reciprocity plots for randomly chosen nine sets of response and force points. It can be seen that the comparison was not good which indicated the FRF's were not measured correctly. This was also evident from the pressure validation test for this case (Figure 3.15).

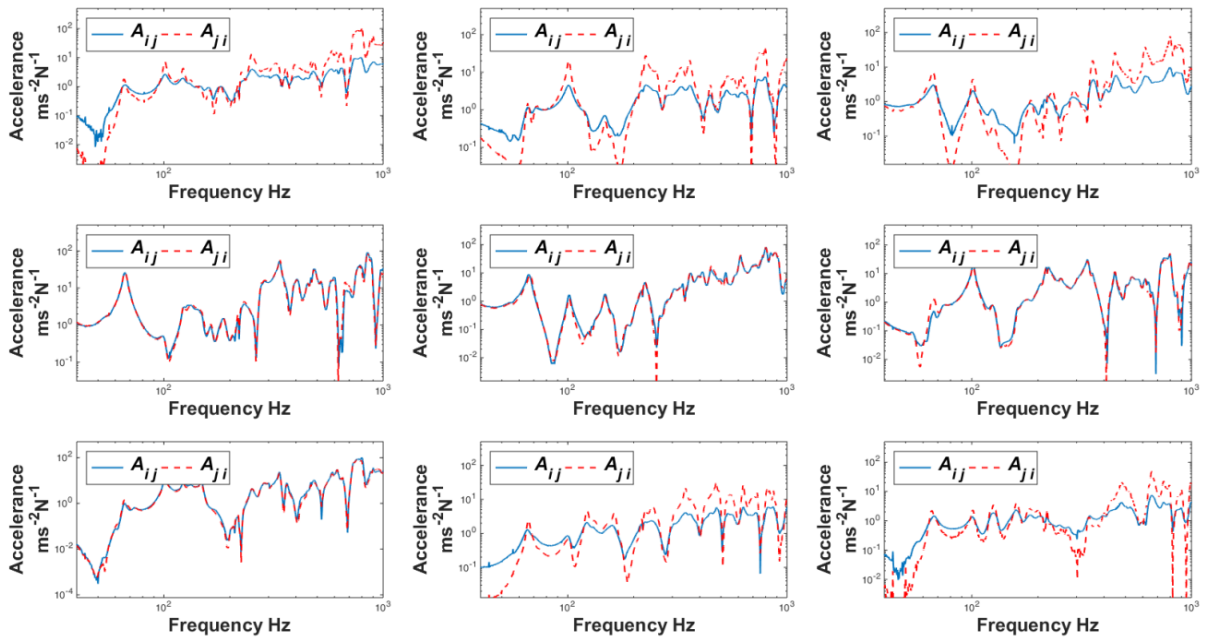


Figure 3.14: Reciprocity for randomly chosen nine sets of response-force points on the panel.

Bad reciprocity is observed for some data sets indicating wrong measurement data

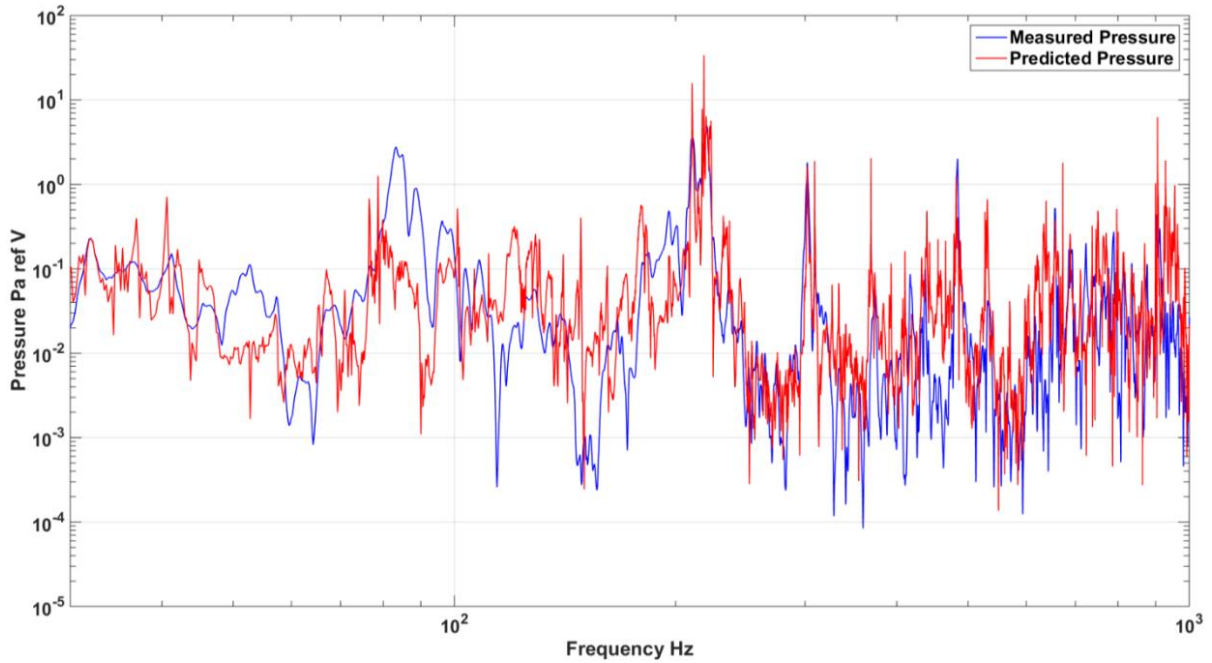


Figure 3.15: Pressure validation for 8x8 case using poorly measured accelerance FRF's

In Figure 3.15, it can be seen that the predicted pressure does not match well with the measured pressure. The predicted pressure spectrum also consists of sharp peaks which are indicative of inversion errors in the accelerance matrix inversion. Such inversion errors are observed when the measured data is corrupted with noise or if the data measured is incorrect. Regularisation techniques namely Singular Value Decomposition (SVD) and Tikhonov regularisation [138] were applied but it still did not improve the pressure validation. Such techniques are useful to remove noise from data but when the data is incorrect then such techniques do not work. The only solution in such case is to measure the FRF's carefully in a new test. Thus a second test was conducted for an 8x8 grid case and the data was measured carefully with utmost attention to impact testing. Coherences were checked meticulously to ensure there are no noisy artefacts in the averaged FRF's. Figure 3.16 shows the reciprocity plots for the new test. It shows the reciprocity between the FRF's is far better (compared to Figure 3.14) which means correct data has been used.

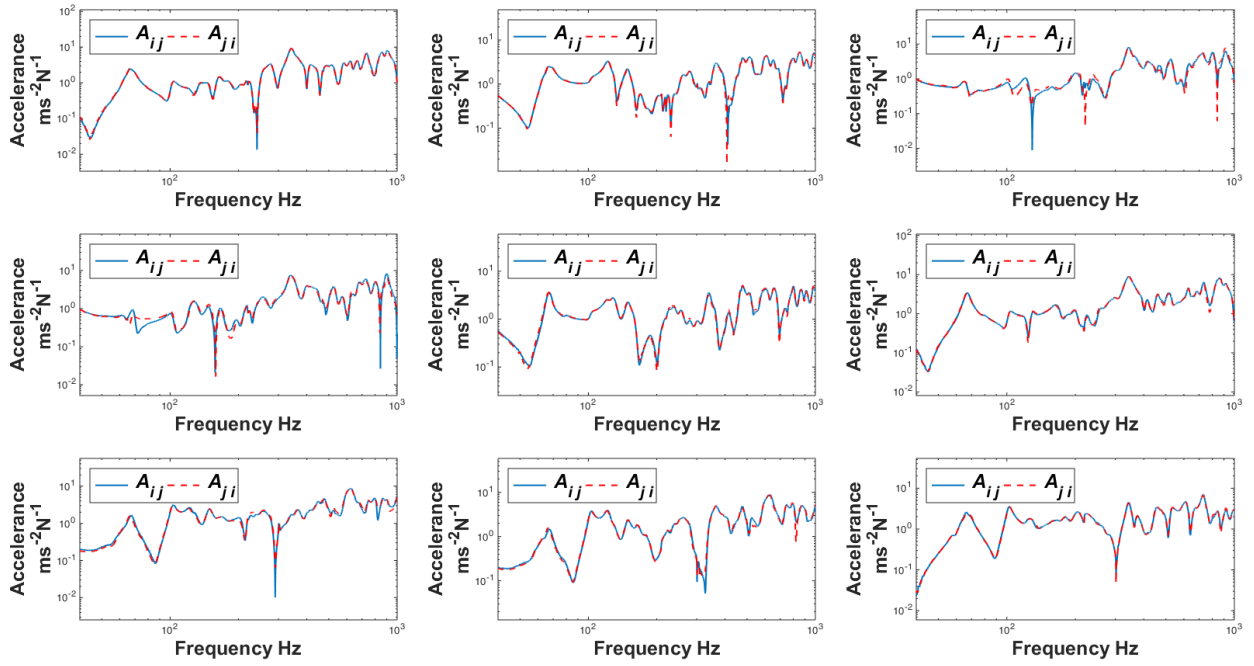


Figure 3.16: Reciprocity for randomly chosen nine sets of response-force points on the panel for an 8x8 measurement grid

Accordingly the pressure validation obtained from this data is much better than the first trial of 8x8 case (Figure 3.17). Note that the validation results for the 8x8 grid are obtained by inverting a 64x64 accelerance matrix without any regularisation which shows the value of a good measurement.



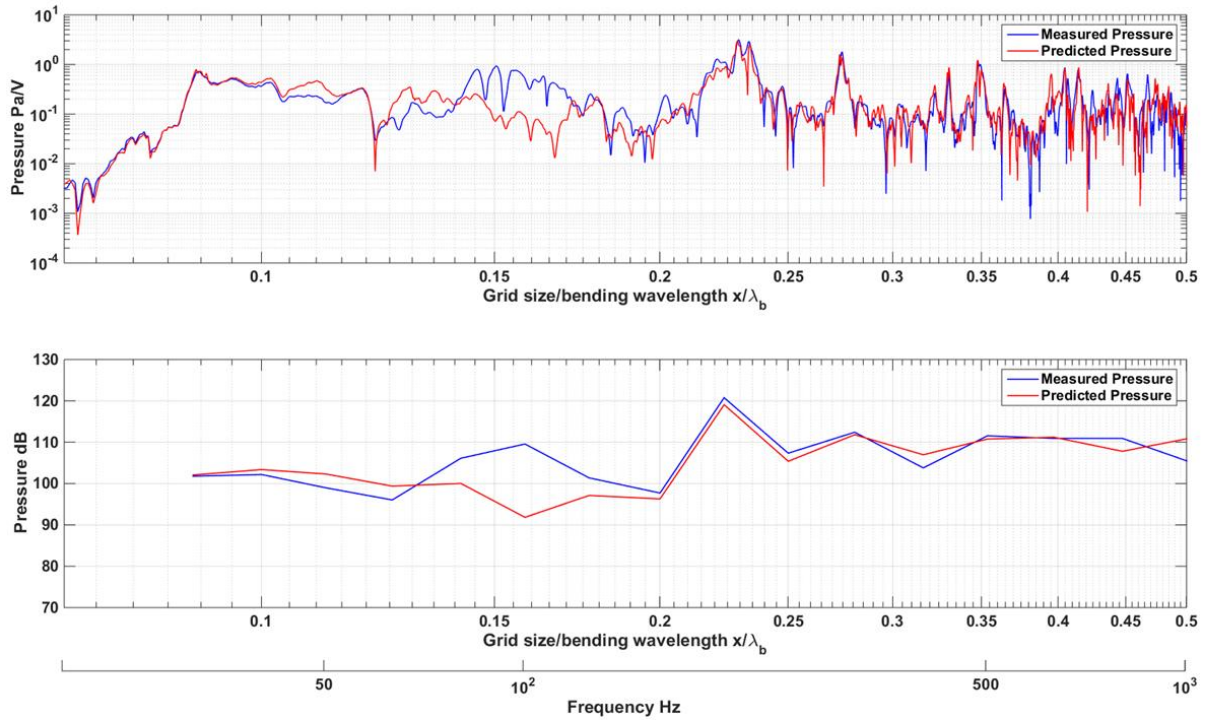


Figure 3.17: Pressure validation results for a 8x8 measurement grid over the panel comparing the measured and predicted pressure in narrow band (top plot) and one third octave band (bottom plot) against grid size/bending wavelength. Frequency axis applies to both plots

The results from Figure 3.17 show that the prediction from 20-950 Hz is within 3.5 dB of the measured pressure except in the low frequency region (70-120) Hz. Again it is interesting to see that the smallest grid dimension of 9.87 cm is half the bending wavelength at 999 Hz. In the 1 kHz band, some inversion errors are present which is why the deviation from measured pressure goes above 3.5 dB in excess of 950 Hz. But overall the prediction thus generally follows the  $\lambda_b/2$  criterion similar to studies [128, 133] that employ patch based measurements for vibro-acoustic prediction.

In the low frequency region where the prediction is off by more than 20 dB, the following reasons for the discrepancy can be considered,

- i. The prediction made using I-ASCA is representative of the sound transmission through the panel only as the measurements were limited to the panel. In practice, some transmission was expected through the box walls (at fundamental resonances)



as well which is not accounted for in this prediction but is accounted in the measured pressure.

- ii. The narrow band spectrum here does not show any peaks which are characteristic of inverse errors and the condition number of the accelerance matrix was also confirmed low ( $<100$ ) in this region. Therefore, the possibility of inversion errors can be rejected.

In lieu of the two factors discussed above, the difference between measured and the prediction amounts to the flanking transmission through box walls. If the sound transmission through the test panel can be blocked then the measured pressure would entirely consist of the sound transmission through the walls. Such exercise was carried out for a different structure and the results are presented in the next chapter. Also, if the test were to be conducted in a transmission suite, such flanking issues would not ideally exist. To confirm this behaviour, tests in a transmission suite will be outlined in next chapter.

In conclusion, the I-ASCA has been applied on a single leaf panel and validated (except in a small low frequency region) and discretisation followed according to a  $\lambda_b/2$  criterion seems to be sufficient to predict the acoustic radiation from the panel. This is better than a  $\lambda_b/6$  criterion which is used in FEA discretisation from a measurement time perspective.

---

### 3.5.2 I-ASCA – source contribution results

---

After the pressure validation, the source contributions were measured as per Eq. (3.9). The source contributions for different areas on the panel (colour coded in Figure 3.18) are shown in Figure 3.19.

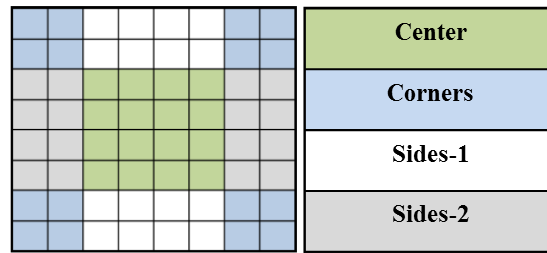


Figure 3.18: Panel divided into four regions (left) of equal areas mentioned by color codes (right)

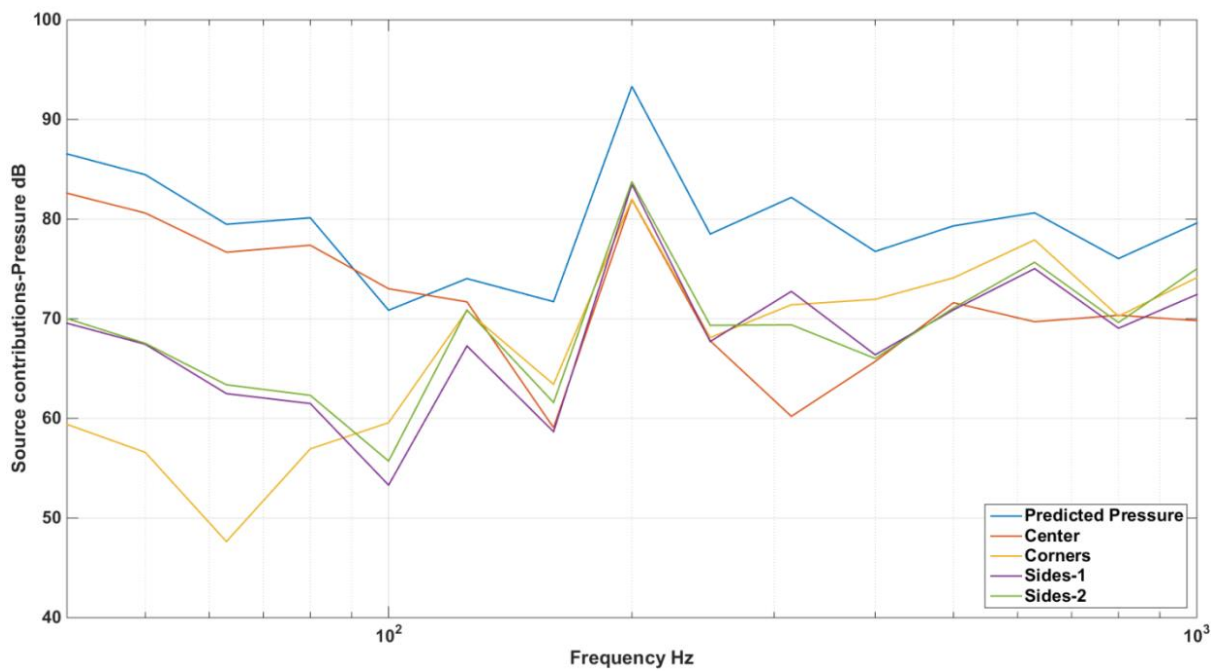


Figure 3.19: Contributions of sources acting on different regions over the panel specified in Figure 3.18 compared to the total pressure

Figure 3.19 shows the source contributions for excitations acting on localised regions of the panel specified in Figure 3.18 with respect to the total predicted pressure. The source contributions below 100 Hz indicate that the sources acting in the centre region contribute dominantly to the sound transfer. Usually, at such low frequencies the sound transfer is dominated by the fundamental resonances in the panel (31, 61 Hz, etc.) which have a high displacement in and around the centre of the panel. Therefore, the sources acting in the centre region will be more effective in exciting this resonance in the panel than the sources acting towards the edges/corners where displacements are minimal around the fundamental frequency. The peak in 200 Hz band is due to the first axial mode of the cavity

(216 Hz) in the direction bounded by the panel and the bottom of the box. Thus, any excitation on the panel will excite this cavity mode which is why we see different source regions contributing equally at this mode.

As we go high in the frequency range, the transmission is dominated by corner regions followed by edge regions. In this range the wavelength is small and the radiation from adjacent quarter wave areas cancels but the radiation from corners and patches which are separated from each other sufficiently in terms of wavelength does not cancel [139]. This is also termed sometimes as the air sloshing effect where the air just sloshes between the adjacent quarter wave areas on the centre of the panel and no net radiation occurs. This shows that the contributions obtained here are broadly consistent with the expected physical behaviour of the panel. In conclusion, the I-ASCA methodology has been formulated and validated for airborne sound transmission through a cavity backed panel. The next step is to diagnose the path contributions, which would allow us to quantify the sound transfer locally through various regions.

---

## 3.6 Path contribution analysis

---

In the previous sections (3.4, 3.5), the I-ASCA method was formulated where the contribution of discrete sources can be quantified. As discussed earlier the source contribution represents the sound transfer from all patches under the action of an individual source DoF to the receiver DoF (see Figure 3.9). The path contribution in turn is the contribution from an individual patch under the all source DoF (see Figure 3.7). Thus, the source contribution is not equivalent to the path contribution because we are looking at the radiation from an individual patch rather than all patches.

In I-ASCA, to quantify the source contribution, the excitation on each path had to be characterised first by the blocked forces. Therefore, following the same principle, to measure the path contribution, the path has to be characterised first. In operational conditions, each path vibrates with an operational velocity under the action of the airborne source. Therefore each path area with a vibrating velocity could be characterised as an

equivalent volume velocity source. Cremer [33] has also used this principle to model the vibration of the panel as a combination of elementary volume velocity radiators. The basic principle is that a vibrating panel can be discretised into areas, and each vibrating area can be characterised as a volume velocity source (see Figure 3.20 for illustration). Cremer used such representation to solve the airborne sound transmission problem theoretically. In our study, we can use the same principle for in-situ characterisation of vibrating paths as equivalent volume velocity sources.

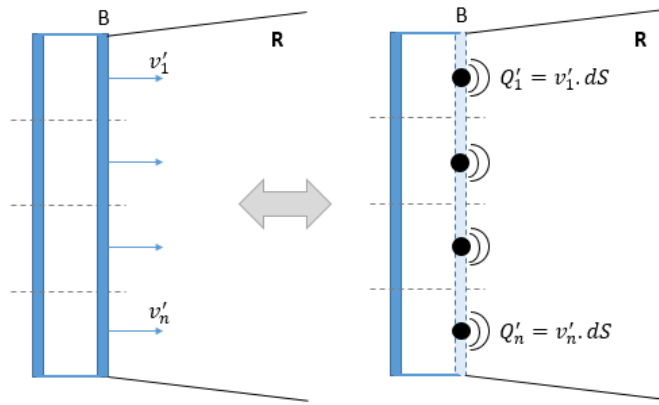


Figure 3.20: Operational measurement phase in PCA. Paths on panel 'B' vibrating with a normal velocity  $v'$  (left) characterised as elementary volume velocity sources  $Q'$  (in black) radiating into receiver volume R (right)

For a path 'n' of vibrating with a velocity  $v'_n$ , its equivalent volume velocity can be written as,

$$Q'_n = v'_n \cdot dS_n \quad (3.11)$$

In Eq. (3.11),  $Q'_n$  is the operational volume velocity of path 'n' and  $dS_n$  is the path area. In the context of vehicles, the contribution of body panels to the receiver sound under airborne excitation has been diagnosed based on such volume velocity characterisation. This was first called as 'Airborne Source Quantification' (ASQ) [125]. Later panel contribution analysis methods were developed on the basis on ASQ. Such methods have been predominantly applied in vehicles to diagnose the contributions of different panels to the interior cabin sound.

Following the methodology of I-ASCA, the next step after characterisation is the combining the characteristic quantity with the FRF relating the path vibration to the receiver point. In

acoustic domain, the pressure at a point 'j' due to a volume velocity source 'Q' can be related by the acoustic FRF ( $p/Q$ ) which is also referred to as the acoustic impedance. In our problem, the volume velocity sources are located at the panel paths. Then, to measure the acoustic FRF, a volume velocity source will need to be placed close to each panel path (direct measurement), which may not be convenient. Instead, this FRF can be measured reciprocally instead where a volume velocity source is placed at the receiver position and microphones are placed close to the paths which is more convenient. Such reciprocal measurement of the acoustic FRF has been employed in most versions of panel contribution analysis methods. Figure 3.21 illustrates this concept.

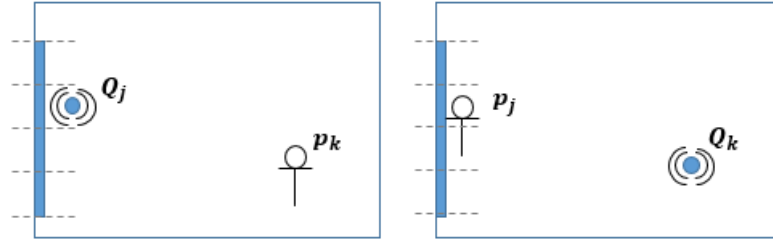


Figure 3.21: Schematic of direct (left) and reciprocal (right) measurement of the acoustic FRF.

PCA employs reciprocal measurement

Once the path is characterised and the acoustic FRF's are measured, the total pressure at a receiver point 'k' can be written as a summation of contribution from all the paths (i.e. volume velocity sources) as,

$$p_k = \left\{ \frac{p_k}{Q_1} \quad \dots \quad \frac{p_k}{Q_n} \right\} \begin{Bmatrix} Q'_1 \\ \vdots \\ Q'_n \end{Bmatrix} = \{ U_{k1} \quad \dots \quad U_{kn} \} \begin{Bmatrix} v'_1 \\ \vdots \\ v'_n \end{Bmatrix} dS \quad (3.12)$$

In the Eq. 3.12, ' $U_{ij}$ ' is the acoustic FRF for the pressure at point 'i' due to a volume velocity excitation at point 'j'. The individual path contribution for a path 'n' is then measured as,

$$p_{kn}^c = U_{kn} Q'_n \quad (3.13)$$

This is the general methodology of panel contribution methods that has been demonstrated and validated for diagnosing contributions of vehicle panels to interior sound. This analysis can similarly be applied to diagnose the path contributions in multi-layered partitions used

in buildings. To do this, the velocities on each path as well as the acoustic FRF's are required. For building partitions, the FRF measurement would only be possible for the panels facing the receiver volume. Diagnosing the path contributions of the panel facing the source side would be impossible as there is no room to place microphones next to that panel for acoustic FRF measurement (see Figure 3.22). In that case, this method will be limited to only diagnosing the path contributions of the receiver side panel.

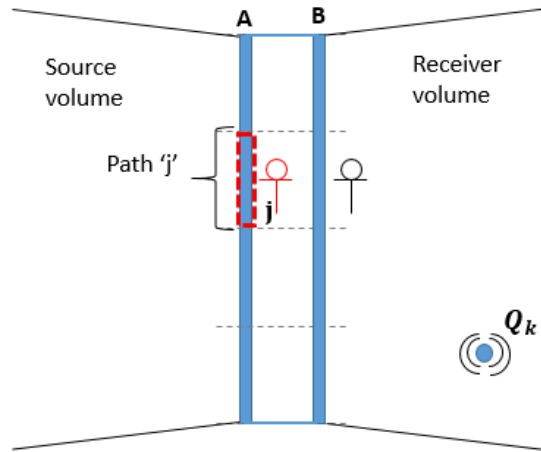


Figure 3.22: Multi-layered partition (in blue). For reciprocal measurement of acoustic FRF  $U_{kj}$ , microphone placement against source side panel A on a path 'j' (in dotted red) is restricted (in red mic) in contrast to accessible placement against receiver side panel B (in black mic)

However, it may also be important to diagnose the path contributions of the source side panel in a multi-layered partition. To do this, an alternative way of measuring the acoustic FRF's will have to be devised. The following section will present an alternate methodology for measuring the acoustic FRF's inversely and the path contributions for the source side panel, where conventional acoustic FRF measurements cannot be conducted in-situ. Accordingly, the method will be referred by the abbreviation I-PCA (Inverse Path Contribution Analysis).

### 3.6.1 I-PCA – methodology

Consider a multi-layered partition discretised into 'j' paths (patches) on the source side panel of Figure 3.8. In operational conditions, the velocities on each path can be easily

measured and the volume velocity can be found as per Eq. (3.11). Under PCA methodology, the total pressure at point 'k' in the receiver volume for this source '1' can be written as,

$$p_k = \{U_{11} \quad \dots \quad U_{1n}\} \begin{Bmatrix} v'_1 \\ \vdots \\ v'_n \end{Bmatrix} dS \quad (3.14)$$

where,  $dS$  is the patch area. To maintain phase between all the operational quantities, the operational responses  $v$  and  $p$  can be referenced to the source. The source can be airborne (loudspeaker) or structure borne (shaker or impact hammer). In the case of an impact hammer hit at patch '1', the operational quantities can be referenced to the force  $f_1$  and Eq. (3.14) can be written as,

$$\frac{p_k}{f_1} = \{U_{k1} \quad \dots \quad U_{kn}\} \begin{Bmatrix} \frac{v'_1}{f_1} \\ \vdots \\ \frac{v'_n}{f_1} \end{Bmatrix} dS \quad (3.15)$$

The ' $v_1/f_1$ ' quantity is nothing but the mobility of the patch '1' for a source acting on patch '1'. Similarly the quantity ' $p_k/f_1$ ' is the vibroacoustic FRF ' $H_{k1}$ '. The above Eq. (3.15) can now be concisely written as,

$$H_{k1} = \{U_{k1} \quad \dots \quad U_{kn}\} \begin{Bmatrix} Y_{11} \\ \vdots \\ Y_{n1} \end{Bmatrix} dS \quad (3.16)$$

In the same way, the hammer can now be hit on every patch centre position from 1 to n, and the mobilities and vibroacoustic FRF's that are measured can be written in a matrix formulation as below,

$$\{H_{k,1} \quad \dots \quad H_{k,n}\} = \{U_{k,1} \quad \dots \quad U_{k,n}\} \begin{bmatrix} Y_{11} & \dots & Y_{1n} \\ \vdots & \ddots & \vdots \\ Y_{n1} & \dots & Y_{nn} \end{bmatrix} dS \quad (3.17)$$

$$\therefore \{\mathbf{H}\} = \{\mathbf{U}\}[\mathbf{Y}]dS = \frac{1}{j\omega} \{\mathbf{U}\}[\mathbf{A}]dS$$

Note that for each excitation, only the velocity and pressure responses change while the acoustic FRF's remains the same. This is because the acoustic FRF is an invariant property of vibroacoustic system. Post-multiplying by the inverse of the accelerance matrix and dividing by  $dS$  on both sides of Eq. (3.17), we get,

$$\frac{j\omega}{dS} \{\mathbf{H}\} [\mathbf{A}]^{-1} = \{\mathbf{U}\} \quad (3.18)$$

Thus the acoustic FRF vector can be measured inversely from accelerance and vibroacoustic FRF's. Therefore the first step of I-PCA is measuring the accelerances and vibroacoustic FRF's similar to I-ASCA methodology outlined in Section 3.4 and utilising Eq. (3.18) to get the acoustic FRF's.

Next, for the operational phase, the airborne source can be activated and the operational accelerations and pressures can be measured as per Eq. (3.7). The FRF and the operational measurements together constitute the I-PCA measurement phase. Then the path contribution of interest can then be measured as per Eq. (3.13) which represents the radiation from a single patch under the given airborne excitation. Likewise, the total pressure at a receiver point can be represented as a sum of all such path contributions under the airborne excitation as shown below.

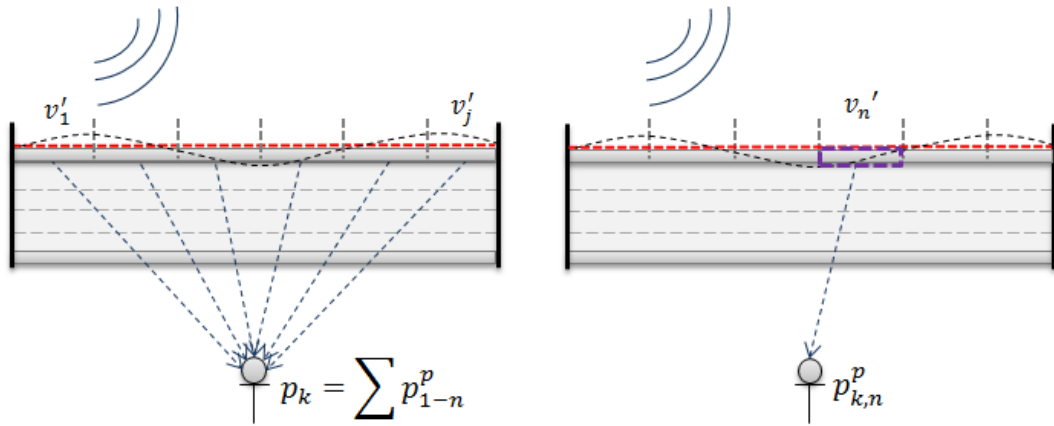


Figure 3.23: Left – Under the action of source excitation, the receiver side pressure at ‘ $k$ ’ predicted as a sum of all path contributions from the vibrating partition. Right – Under the action of source excitation, the radiation from a single patch ‘ $n$ ’ is the path contribution (with superscript ‘ $p$ ’)



### 3.6.1.1 I-PCA validation

To validate the I-PCA methodology outlined in previous section, a pressure validation test can be conducted where the total pressure at a validation point ' $k$ ' can be written as a sum of contributions from all the patches characterised as equivalent volume velocity sources. The pressure predicted in this case would be,

$$p_{p,k} = \{\mathbf{U}_k\}\{\mathbf{Q}'\} = \{\mathbf{U}_k\}\{\mathbf{v}'\}dS = \frac{1}{j\omega} \{\mathbf{U}_k\}\{\mathbf{a}'\}dS \quad (3.19)$$

If the predicted pressure is equal to the measured pressure then the methodology can be said to be valid in the frequency range  $\mathbf{f}$ . This would also confirm the validity of the inversely measured acoustic FRF's. We can also see that by substituting Eq. (3.18) into Eq. (3.19), we get,

$$p_{p,k} = \frac{1}{j\omega} \frac{j\omega}{dS} \{\mathbf{H}_k\}[\mathbf{A}]^{-1}\{\mathbf{a}'\}dS = \{\mathbf{H}_k\}[\mathbf{A}]^{-1}\{\mathbf{a}'\} = \{\mathbf{H}_k\}\{\mathbf{f}_{bl}\} \quad (3.20)$$

Thus using the I-PCA methodology, we have reached a result (Eq. 3.20) which has been proven and validated in Section 3.5. This result is also not surprising as the total receiver pressure can be conceptualised to be either a sum of source contributions or sum of path contributions. The result also provides confidence in the I-PCA methodology to predict the airborne sound transfer through the partition and diagnose the path contributions. These path contributions would allow us to diagnose the sound transfer locally/spatially through the partition. Using these contributions, the weak regions of sound insulation can be diagnosed as regions of high path contribution.

We can also see that, using the same measurements from I-ASCA, we can measure the acoustic FRF's (Eq. 3.18) and path contributions (Eq. 3.13), without performing a single extra measurement. This proves the versatility of the analysis in that both source and path contributions can be obtained from a single set of data with the same accuracy. Additionally, this analysis presents a novel measurement approach for acoustic FRF's where a direct

measurement cannot be performed due to space restrictions so the path contributions can be measured for source side panels as well.

### 3.6.2 I-PCA – path contribution results

To test the I-PCA methodology, the case of single leaf panel (8x8 grid size) from Section 3.5 was considered. Using the FRF measurements from I-ASCA methodology, the acoustic FRF's were first determined as per Eq. (3.18) for all 64 paths. The pressure validation for the case would yield to the exact same result as Figure 3.17 and hence is not repeated here. The path contributions were of more interest here as they represent the diagnostic property of the panel paths. These were measured for the regions described in Figure 3.18. The total path contribution from each region was measured and was compared to the source contributions as shown in Figure 3.24.

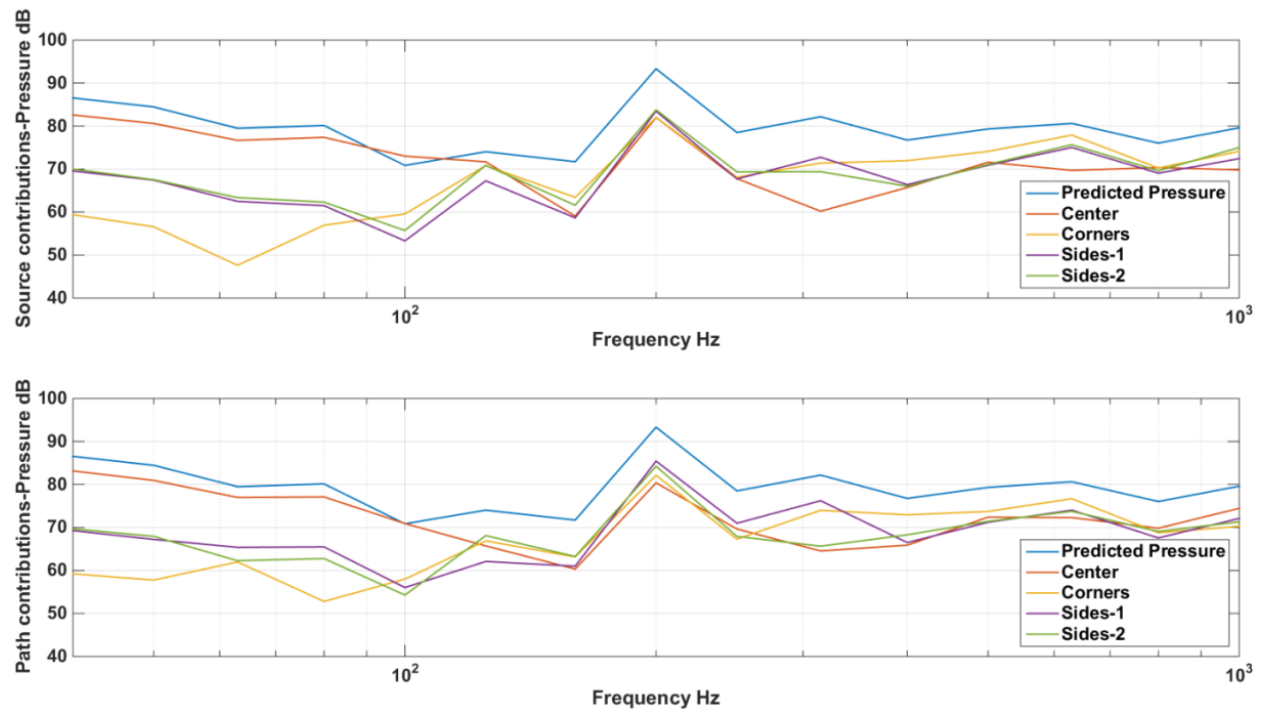


Figure 3.24: Source and path contributions (in one-third octave bands) for different regions of the panel depicted in Figure 3.18. Source contributions depict the sound transmission globally for a given source while path contributions depict the sound transmission locally

For path contributions, it is interesting to see that at low frequencies up to 100 Hz, the majority of sound is transmitted by the centre region of the panel. This is due to the fundamental resonance of the panel at which the sound transfer is usually dominant. As we go higher up the frequency range, the sound transfer through the corners and sides become more significant due to reasons discussed in Section 3.5.2. Thus at each frequency, a ranking of different regions could be established based on their contributions to the cavity pressure. It can be also seen that the source contributions and path contributions for the respective regions in the single leaf panel follow a similar trend, although there are differences observed in some frequency regions. One possible reason for the source and path contributions being similar is that the panel under test is a single leaf homogenous, isotropic panel with a simplified geometry. However the path and source contributions for a multi-layered partition may not be similar like the case for a single leaf partition especially due to inhomogeneity in its construction (e.g. presence of structural connections). These results overall help to illustrate the potential for diagnostic analysis of airborne sound transmission in measuring the spatial dependence of sound transfer (or insulation). It would be particularly useful to now apply such analysis to a multi-layered building partition to diagnose the airborne sound transmission by measuring the source and path contributions.

---

## 3.7 Conclusions

---

The chapter presented the concept of the diagnostic descriptor which would describe the contributions to the receiver sound pressure. While the SRI quantifies the frequency dependence of sound insulation, the premise of the diagnostic descriptor was to quantify the spatial dependence of the sound transfer in-situ. It was found that the iTPA method is used to diagnose structure borne source contributions in-situ. Next, the challenges for applying iTPA to an airborne case were discussed. To overcome these challenges, discretisation/sampling was employed at the interface by which the continuous pressure excitation was represented by set of equivalent point forces acting on discrete patches. Accordingly, I-ASCA methodology was outlined which inversely characterises the airborne source by discrete blocked forces. To validate the methodology, a diagnostic case

study of airborne sound transfer through a cavity backed panel was considered. The accuracy of prediction up to 1 kHz was found to be within 3 dB. From the maximum frequency of prediction, the grid size and the bending wavelength in the structure, a  $x \leq \lambda_b/2$  sampling criterion was devised which was found to be the same as being employed by analytical studies employing patch based discretisation. From the blocked forces measured, the source contributions were measured. This quantifies the contributions of a local excitation to the cavity pressure through the global partition. However, to diagnose the path contributions, an I-PCA methodology was developed. This method allows for novel inverse measurement of the acoustic FRF's which can then be applied for measuring the path contributions. The path contributions were measured for the single panel case which shows the potential of the method in identifying the weak regions of sound insulation in different frequency regions. In conclusion, the I-ASCA and I-PCA methodologies allow us to measure the source and path contribution of partitions and provide useful diagnostic information about the paths. In the following chapters, the application of these methods will be explored for the cases of multi-layered partitions.

---

# 4

## DIAGNOSTIC TESTING FOR MULTI-LAYERED PARTITIONS

---

*In the previous chapter, a novel iTPA application for diagnosing the airborne sound transfer through building partitions was formulated. Two versions of the method, namely I-ASCA, which provides the source contributions, and I-PCA, which provides the path (patch) contributions, were outlined. Later, a case of cavity backed panel excited by an airborne source was presented and the source contributions and path contributions were diagnosed. The path contributions provided the spatial dependence of the sound transfer through the partition area. The accuracy of the methods was dependent on the discretisation of the continuous interface (the number of paths considered). Having tested the application on a single leaf panel, it was of interest to apply these methods for diagnosing the airborne sound transfer through a multi-layered partition. It is intended to diagnose the sound transmission through different structural elements in the multi-layered partition. This chapter will present the application of I-ASCA and I-PCA methods on a point connected dual leaf partition.*

## 4.1 Point connected dual leaf partition

To study the application of the diagnostic tests on a realistic multi-layered partition, a dual leaf partition was chosen as a case study. It comprises of two panels/leaves separated by a cavity. To construct a dual leaf partition, two Perspex panels were used. The two panels represented the two leaves of a dual leaf partition. Next, a wooden frame was constructed and the two panels were attached on either sides of the frame as shown in Figure 4.1.

When the frame was fixed with the two panels, an air cavity is created between the panels due to the depth of the frame. Traditionally cavity absorption would be used to increase the sound insulation of multi-layered partitions and usually a mineral wool infill is used. As such, mineral wool was added to cavity of the dual leaf partition. This makes the partition a close representation of actual multi-layered partitions used in buildings. A point connection made from iron was also added between the top and bottom leaves. The point connection was about 1.4 cm in diameter. Fig. 4.1 shows the point connected partition.

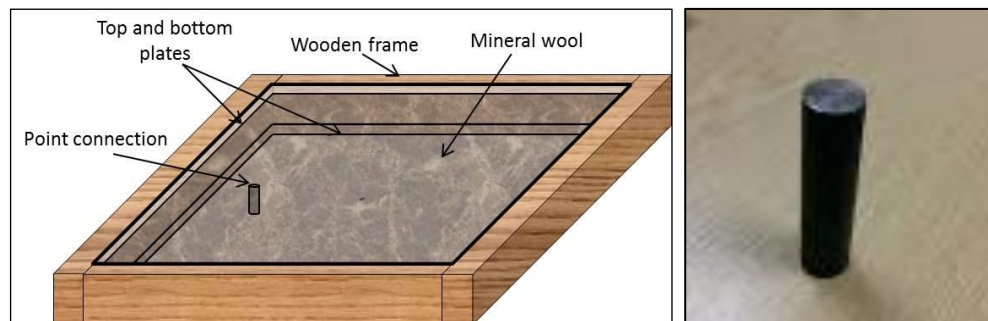


Figure 4.1: Point connected dual leaf partition (left). Actual point connection used in the partition (right)

The point connection creates an inhomogeneity in the construction but most importantly, it acts as a sound bridge between the top and bottom leaf. The sound bridge represents a direct path of sound transfer from the top leaf to the bottom leaf and the receiver cavity. As such, the point connection path may provide higher sound transmission into the receiver cavity compared to other paths at certain frequencies. Some theoretical studies (see Section 2.3.4) have also attributed the effect of point connections in the partition to a direct

increase in total sound transfer and decrease in sound insulation in specific frequency regions.

With the measurement approaches outlined in Chapter 3, it should be in principle, possible to quantify the contributions of the point connection path. Thus, the addition of the point connection was strategic to showcase the application of I-ASCA and I-PCA approaches for diagnosing a possibly strong sound transmission path (the point connection) in comparison to other paths of the dual leaf partition. Also, as the grid size has been kept the same as a single panel for 8x8 grid ( $9.87 \times 9.87 \text{ cm}^2$ ), the maximum frequency limit of application would be 1 kHz according to the tested  $\lambda_b/2$  criterion. It should be possible to see the effect of point connection in this frequency range otherwise the discretisation will have to be refined to a finer grid. The complete dual leaf construction was then installed on top of the wooden box, which represents a receiver cavity. The complete setup is shown in Figure 4.2.

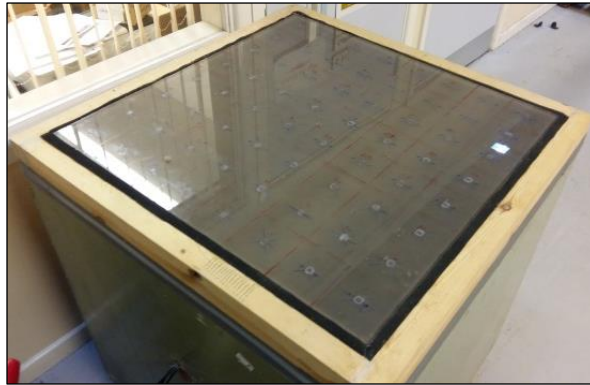


Figure 4.2: The dual leaf partition with a wooden frame assembled on top on the wooden box (in green) representing the receiver cavity

---

## 4.2 I-ASCA and I-PCA Measurements

---

Following the measurement methodologies for I-ASCA and I-PCA tests, at first, the top panel was discretised in an 8x8 grid resulting in 64 sound transmission paths. Any medium below the top panel including the partition cavity, bottom panel and the receiver cavity are inaccessible. Thus, the measurements are to be conducted on the top panel. In a

setup where both panels are accessible for measurements for example, in a transmission suite, diagnosis of the top and bottom panel paths would be possible.

After discretisation on the top panel, accelerance was measured at the interface (or between paths) by impact testing. A force hammer and ICP accelerometers were used for the purpose. This had to be measured in parts as described in Figure 3.8. During the setup, three mics were placed along the solid diagonal of the receiver cavity. This allowed for the measurement of the vibroacoustic FRF for all paths to these points in the receiver cavity. The reciprocity of the accelerance measurement is presented in Figure 4.3 for random set of response and force locations. The good reciprocity provides confidence in the quality of FRF measurements and that they represent the LTI system under test.

For the operational test, it was of interest to diagnose the paths for structure borne and airborne sound transmission. At first, a structure borne excitation was considered. A structure borne excitation can be diagnosed with I-ASCA as the method is not limited to airborne sources. In principle, the I-ASCA method for a structure borne source reduces to iTPA. As long as a source can be represented by blocked forces, the I-ASCA method is applicable.

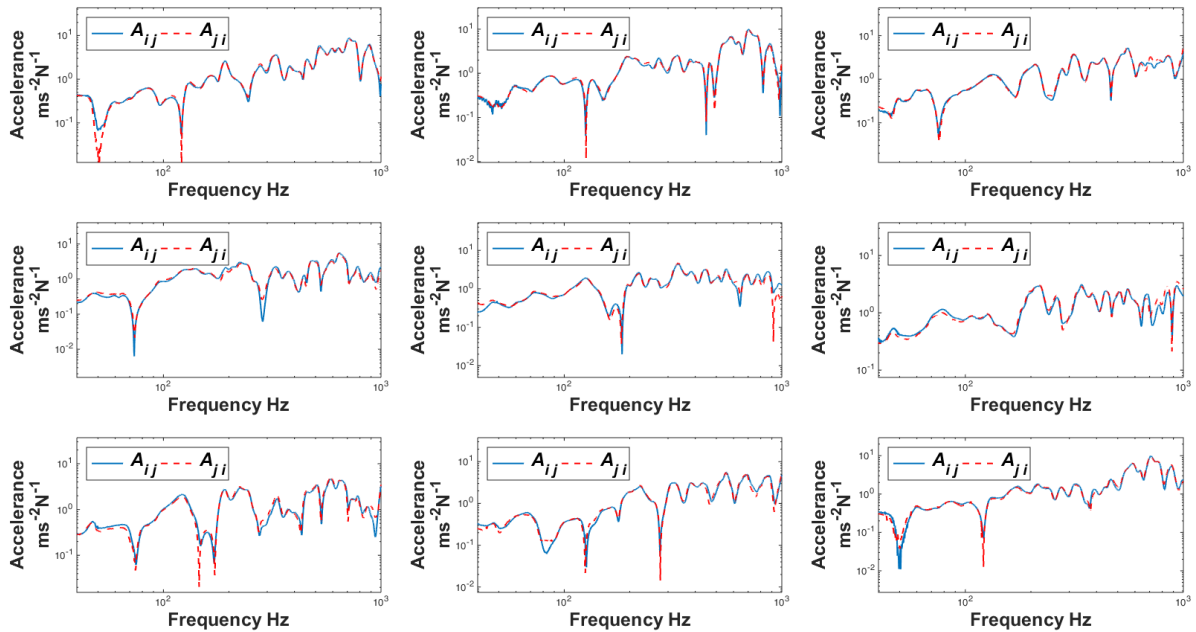


Figure 4.3: Reciprocity between nine sets of response and force locations on the top panel



---

## 4.3 Structure borne excitation case

---

For a structure borne excitation, a shaker equipped with a stinger was attached on the top panel. Note that the shaker was attached at a different location to the point connection path location. The shaker was then driven with a pink noise, which simulates a structure borne excitation on the partition. The stinger that forces the top panel is a thin stiff wire. Thus, the excitation is rather a point excitation than a surface excitation. Under operational conditions, the accelerations were measured on the partition paths and pressures were measured at receiver points inside the cavity for validation. The operational accelerations and pressures were again normalised to the driving voltage of the shaker to maintain a phase reference between different measurements.

---

### 4.3.1 Blocked forces

---

According to the blocked force theory, the blocked forces are always determined at the source receiver interface. In the case of airborne excitation, the source excitation is present all over the panel that results in a continuous interface (which coincides with the top panel surface). Accordingly, by employing the I-ASCA method for an airborne excitation, the blocked forces are determined over the panel surface (see Section 3.4).

In the case of a structure borne excitation such as the shaker, the nature of the source is a point excitation where the stinger is attached to the top panel. Therefore, the interface here is a point rather than a continuous surface. For this case, the source can be characterised by a single blocked force at the point interface conveniently using the iTPA approach.

However, if the source location is not visible, (see Figure 4.4 for illustration), then the nature of source and interface is not identifiable. The source could be a point excitation, a multiple point excitation or an airborne excitation, which acts all over the partition.

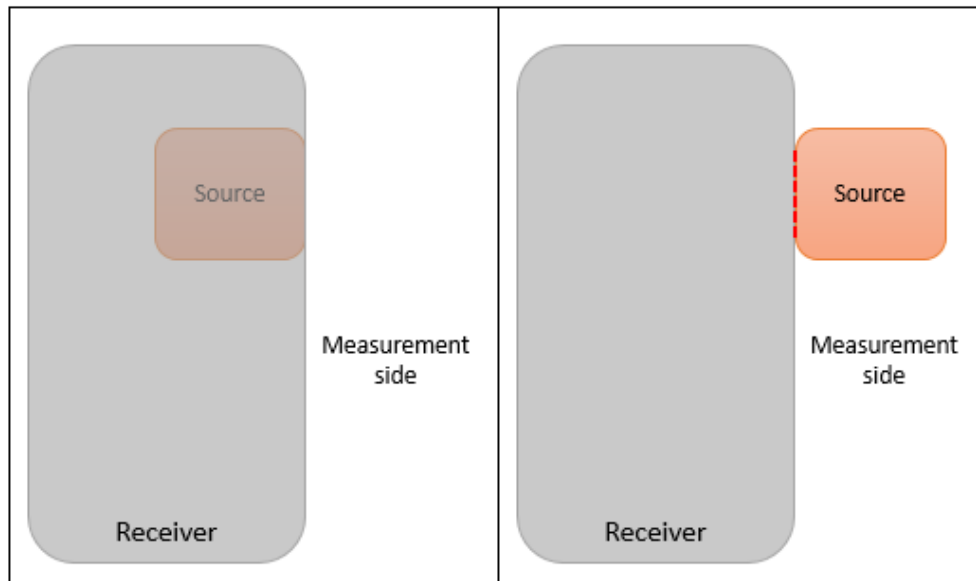


Figure 4.4: Two different source receiver configurations where the interface is effectively same. Left-the source is not visible and thus the source nature and interface are unknown. Right-the source location and source receiver interface are known. Measurement side refers to the side accessible for measurements

To characterise the source for such case, it is best to measure the blocked forces over all the partition to ensure that no source DoF are neglected. It is then expected that if the blocked forces all over the partition can be measured, then the blocked force at the source location(s) would show up dominant, and at other locations where the external force is zero the blocked forces would be minimal (ideally zero). If that is true, then by comparing the blocked forces, it may be possible to localise the source. To investigate this, the I-ASCA approach could be used which allows us to consider a continuous interface and measure blocked forces on all of the partition.

Using Eq. (3.8), the blocked forces for all paths were measured for the structure borne excitation case. Note that we are measuring blocked forces for all paths assuming the nature and location of source is unknown. These blocked forces then characterise an imaginary source, which acts all over the paths and produce the same vibration and acoustic response in the receiver similar to the structure borne excitation. These blocked forces are compared in Figure 4.5.

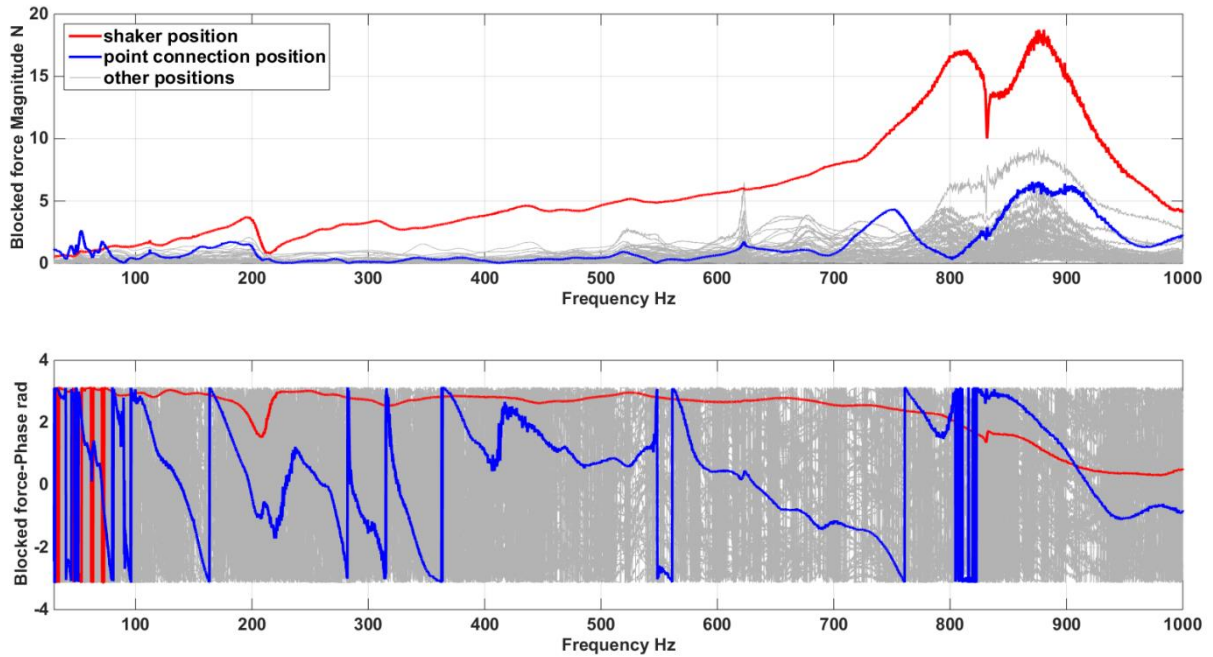


Figure 4.5: Blocked forces characterised over different paths of the top panel with magnitude (top plot) and phase (bottom plot) displayed in narrow band

Figure 4.5 shows that the blocked force at the shaker location is most dominant in the frequency range up to 1 kHz. This provides confidence in our assumption that the dominant blocked force location(s) might be used to identify the source location. This presents an interesting potential of the I-ASCA technique in identifying the source location when the source is a point excitation. Additional tests may be required to confirm this conclusion for multipoint excitations. As the inputs (accelerances and operational accelerations) for blocked force calculations are obtained purely from measurements, this technique may offer a better alternative for source localisation than other approaches, which use computational methods [140].

A key criterion that must be fulfilled for substituting the shaker (point excitation) by an imaginary source (multiple blocked forces over partition) is that the imaginary source must produce an identical vibration and acoustic field in the receiver. To validate this, the blocked forces were used to predict the receiver cavity pressure as per Eq. (3.10). The results are shown in Figure 4.6.

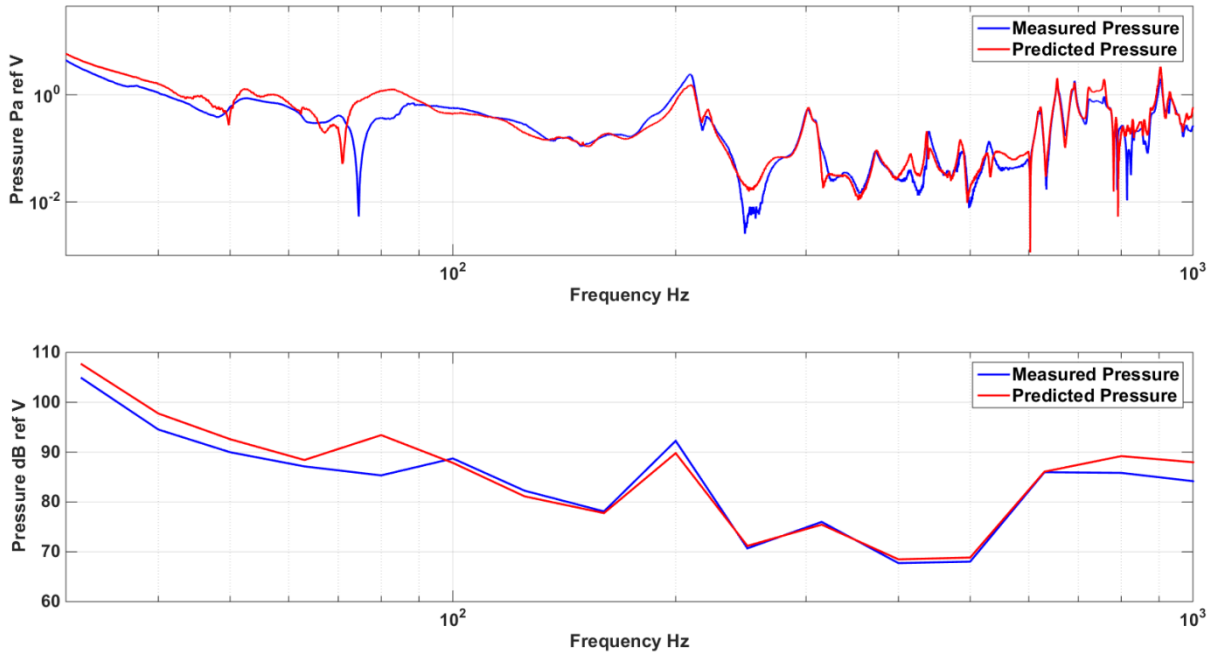


Figure 4.6: Pressure validation results for point connected partition using multiple blocked forces over the partition. This represents to the case when the source location is not known

The results for the pressure validation in Figure 4.6 show that the agreement between the predicted and measured pressure in the range 100 Hz-1 kHz is within 3.5 dB. At low frequencies, around 70-80 Hz the prediction is not good due to noise issues and measurement errors in vibroacoustic FRF. The noise issues result from strong anti-resonances below 80 Hz which is also visible in Figure 4.6 (top plot). Also at such low frequencies, for FRF measurement, a hard tip of hammer is not ideal; a soft tip has better SNR. Above 1 kHz, the prediction worsens due to sampling limitations. The sampling criterion  $\lambda_b/2$  imposes a 1 kHz limit on the frequency range of application with the grid size of  $9.87 \times 9.87 \text{ cm}^2$ . Above 1 kHz the grid size does not obey the criterion and thus the grid size is not sufficient to characterise blocked forces in this frequency range. Finally, these results validate the imaginary source obtained by application of I-ASCA for a structure borne excitation case. This shows the potential of the I-ASCA in situations where the source receiver interface is unknown.

If we consider the case where the source location and nature is known, the interface is then identifiable and the blocked force characterisation in that case is limited to this interface. For the shaker, which is a point excitation, we know that the interface is also a point.

Therefore, a single blocked force characterisation for the shaker excitation should suffice. This blocked force can be calculated as the product of inverse of the measured point accelerance and operational acceleration at the interface. This could be overdetermined by using the following equation,

$$f_{bl,shaker} = \begin{bmatrix} A_{1s} \\ \vdots \\ A_{ns} \end{bmatrix}^+ \begin{Bmatrix} a'_1 \\ \vdots \\ a'_n \end{Bmatrix} \quad (4.1)$$

In Eq. (4.1),  $A_{ns}$  represents the acceleration at a remote receiver point 'n' due to force at 's'. Using this equation the blocked force can be found and the receiver pressure at a point 'k' can be predicted as,

$$p_k = f_{bl,shaker} \cdot H_{k,shaker} \quad (4.2)$$

The pressures were predicted for the receiver cavity and the pressure validation results are shown in Figure 4.7. The agreement between the predicted and measured pressure is within 4 dB in the range 100 Hz-1 kHz. This also shows that the blocked forces of a structure borne source can be used to predict its acoustic response in the receiver cavity. Incidentally, this prediction is also the source contribution as a single blocked force represents the source.

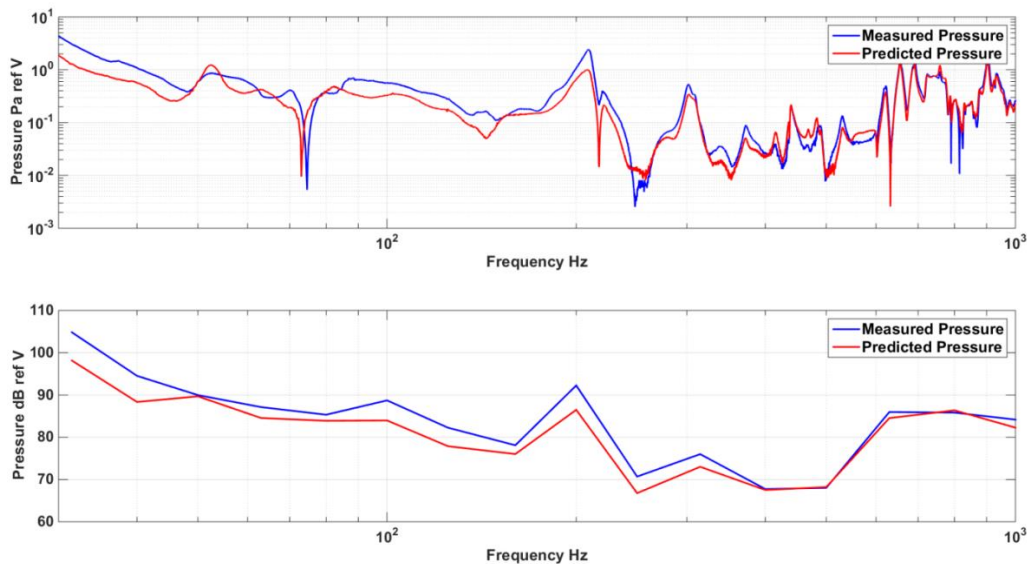


Figure 4.7: Pressure validation using a single blocked force characterisation of the shaker. This represents the case when the source location is known

### 4.3.2 Path contributions

For the structure borne excitation case discussed in Section 4.3, the source was a point excitation and accordingly was characterised by a single blocked force. Therefore, only one source contribution exists which is also equal to the predicted pressure. However, even though only one source acts on the partition, the complete partition vibrates. This means that all the panel paths contribute to the receiver pressure. Thus, even though there is a single source contribution, multiple path contributions exist to the receiver pressure. These path contributions can be simply measured as per the I-PCA methodology described in Section 3.6. On applying the methodology to the measured FRF and operational data, the acoustic FRF's and the path contributions were measured for the top panel paths. The path contributions are plotted in Figure 4.8. Of particular interest is the path contribution of the point connection to check if it acts as a sound bridge and provides a dominant contribution compared to other paths.

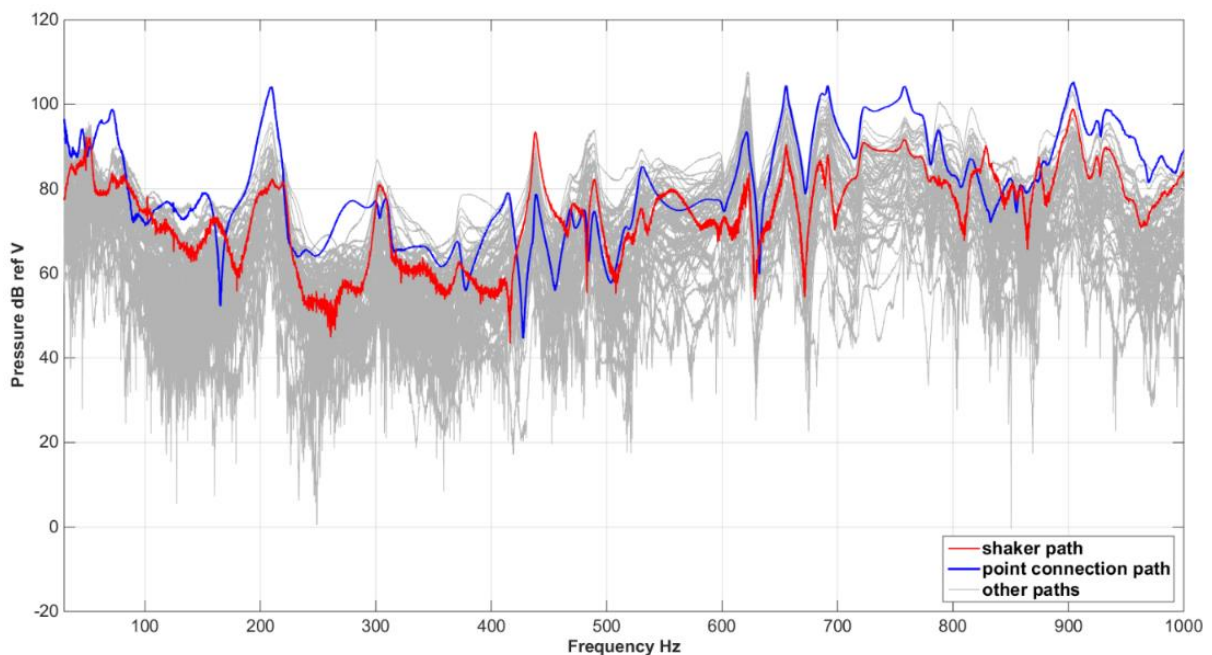


Figure 4.8: Path contributions to the sound pressure when the partition is excited by a point structure borne source

Figure 4.8 shows the path contributions to the sound pressure. The first observation from these results is that even though there is one source contributing to the sound pressure in

the cavity, the sound transfer occurs through multiple paths as each path has a finite (non-zero) contribution. Another observation is that the shaker path (where the source is located) contribution is not the most dominant throughout the frequency range. This is interesting because it proves that the path that is forced is not always the path that radiates the highest sound pressure. Another interesting observation is that the contribution of the point connection path is most dominant towards the high frequency end (above 630 Hz) even though there is no external force acting on this path. This highlights the role of the point connection as a sound bridge (a strong sound transmission path). It also ranks above the shaker path in most frequency ranges as far as path contribution is concerned. This shows that a strong source on a path does not necessarily correspond to a strong path contribution. It is also interesting to see that in a few frequency regions neither the shaker nor the point connection path has the highest contribution. Overall, the path contributions allow us to diagnose and rank different paths compared to the source contribution for a structure borne excitation case.

To assess the effect of the point connection on the partition's radiation, one can easily subtract the path contribution of the point connection from the total contribution of the partition. This would provide a close estimate of the receiver response in absence of a point connection.

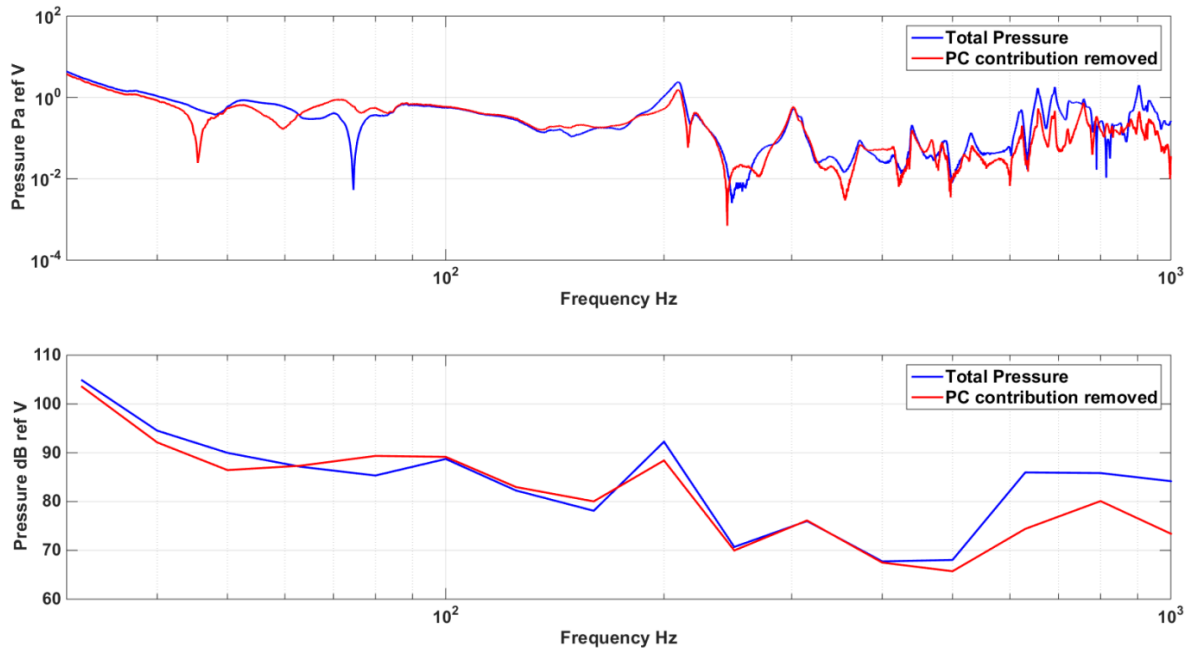


Figure 4.9: Estimated effect of removing the Point Connection (PC) contribution from the total pressure in narrow band (top plot) and one-third octave band (bottom plot) for a structure borne excitation on the partition

Figure 4.9 shows the effect of removing the contribution of the point connection path from the total pressure. A significant effect can be seen in the receiver pressure at high frequencies (above 600 Hz) for this case. This also aligns well with the theoretical observations (Section 2.3.4) that predict the effect of sound bridging elements at high frequencies. At some frequencies (80 Hz band) the pressure seems to be increased but that is due to the noise in total pressure as can be seen in narrow band. Additionally, the pressure is a sum of all the path contributions. So it is entirely possible that the remaining contributions add constructively (in phase) causing a slight increase in the pressure spectrum when the point connection contribution is removed. Finally, this example demonstrates the potential of I-ASCA and I-PCA method in diagnosing structure borne sound transfer through a multi-layered partition and measuring source and path contributions respectively.



---

## 4.4 Airborne excitation case

---

Having investigated and validated the accuracy of the method with structure borne excitation in the previous Section 4.3, the application of the diagnostic methods will now be presented for an airborne excitation on the dual leaf partition. For this case, the setup from Figure 4.2 was used. To simulate an airborne excitation on the partition, a loudspeaker driven by pink noise was used. The loudspeaker was placed roughly 6-7 m apart and 1 m elevation from the partition surface. Following the I-ASCA methodology in Section 3.6, the FRF and operational measurements were performed and the predicted pressure was calculated for receiver points in the cavity. The results of the pressure validation are shown in Figure 4.10 (top plot).

As can be seen from the pressure validation results (Figure 4.10, top plot), the predicted pressure was much lower than the measured pressure, around 10 dB lower in most frequency regions. Two reasons were considered for this mismatching –1) there are inversion errors in the calculation of blocked forces or 2) there is considerable flanking through the walls of the box which shows up as the higher measured pressure. The first reason can be dispelled as the same FRF data (accelerance and vibroacoustic FRF's) have been used for calculating the predicted pressure in structure borne excitation case, which provides a good pressure validation (Figure 4.6).

Considering flanking, if the box walls are acoustically more compliant (or weak in sound insulation) than the dual leaf partition, then the dominant sound transfer inside the cavity will be through the walls (i.e. airborne flanking). This could be true considering that the dual leaf partition is thicker, and acoustically more rigid compared to single leaf walls of the box. To verify this, the flanking transmission i.e. the sound transfer through the walls had to be measured. To do this, the sound transfer through the partition has to be blocked such that any sound transfer to the receiver cavity then occurs only through the walls (flanking paths). Accordingly, the partition was blocked by placing nine layers of plasterboard sheets over it, effectively blocking the sound transfer through the partition when the airborne

excitation is on. Without changing the source, the receiver cavity pressure was again measured under operational conditions. The measured pressure then corresponds to the flanking sound transmission as the partition path is blocked. Figure 4.10(bottom plot) compares this flanking transmission with the measured pressure (when the partition is not blocked).

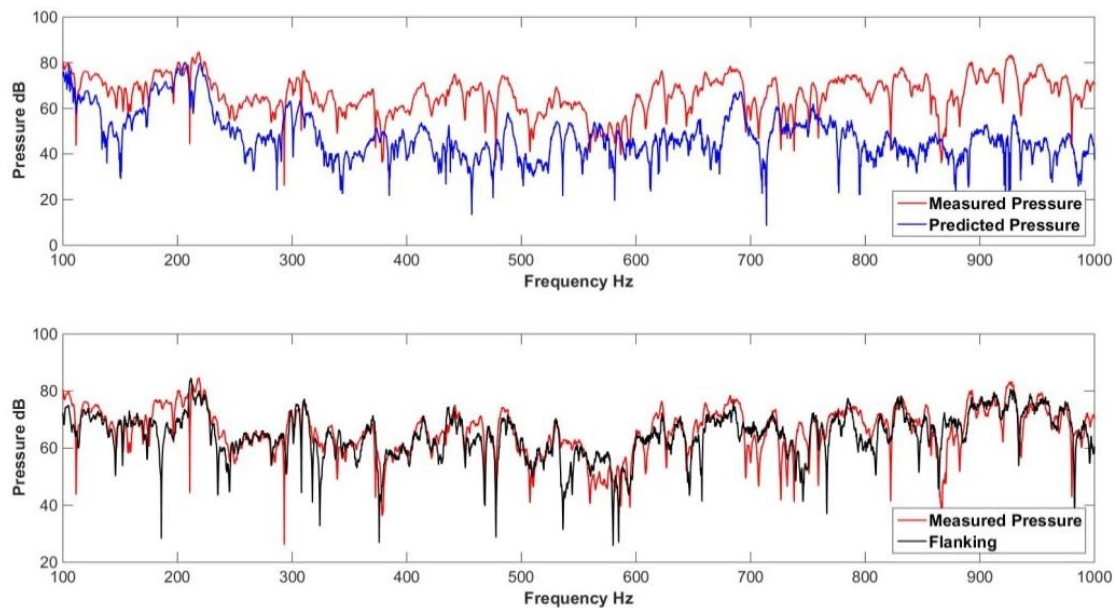


Figure 4.10: Top plot –Pressure validation for airborne excitation case comparing the measured and predicted sound pressure in the box cavity. Bottom plot –comparing measured pressure against flanking transmission through box walls to confirm the influence of flanking on the pressure validation results above

Figure 4.10 (bottom plot) clearly shows that the flanking transmission (when sound transfer is through the box walls only) and the measured pressure are similar. This means that flanking was responsible for majority of the sound transmission inside the cavity for this case. This finding is also supplemented by the fact that the predicted sound transfer through the partition as per the I-ASCA methodology is, mostly less than 10 dB to the measured pressure (Fig. 4.10, top plot). Therefore, between the two paths of sound transfer inside the cavity (the partition and the walls), the walls are the dominant path. It is also important to note that subtracting the flanking contribution from the measured pressure would not provide the correct sound transfer contribution of the partition in this case, as the predicted pressure is 10 dB lower than the measured pressure. This means that the partition

contribution is simply not accounted in the total measured pressure as per the 10 dB rule. The 10 dB rule states that if two sound pressures ( $L_1, L_2, L_1 > L_2$ ) are added, then the total sound pressure will be equal to  $L_1$  if  $L_1 \geq L_2 + 10$ . This finding also supports the observations regarding flanking for the single panel case in Figure 3.17 at low frequencies where the pressure validation was not good. The results here show conclusively the transmission in this low frequency region must have been through the walls.

Hence, in this case, the I-ASCA method enables us to conclude that the sound transfer to the receiver cavity is predominantly through the flanking paths and that flanking has to be minimal if a good pressure validation is desired. Another thing to note is that one can always calculate the source and path contributions even for this case, by using on-board validation as a test of validity of the blocked forces. The on-board validation would allow one to identify the frequency range in which the measured blocked forces are valid. This would also provide additional confidence in predicting the airborne transmission through the partition in presence of flanking. The contributions can then be measured but the diagnosis is more meaningful when the flanking is minimal. This just ensures that there are no weak flanking paths to be diagnosed.

---

## 4.5 Transmission suite tests

---

From previous attempts of I-ASCA test on the partition with a box assembly, it was clear that there was significant airborne flanking through the box single leaf walls. This led to an unsuccessful pressure validation. To obtain a successful validation of the I-ASCA method for dual leaf partition case, the flanking should be minimal or negligible. This is due to the assumption of pressure validation test, which states that the sound transfer only occurs through the partition. An attempt was made to reinforce the box walls with layers of plasterboard however; it did not provide any significant reduction in flanking transmission. Therefore, it was essential to install the partition in an assembly where any airborne or structural flanking transmission is negligible compared to the direct airborne sound transfer through the partition.

A similar requirement has to be met when the airborne sound insulation of partitions is measured. In a typical sound insulation test, the airborne sound transfer from a source room to a receiving room has to be predominantly if not completely through the partition and the flanking (airborne and structure borne) has to be minimal. The source and receiving rooms are usually hard walled reverberation chambers and isolated from each other to prevent flanking transmission. The separating walls from the source and receiver rooms are decoupled from each other (by using a porous/resilient infill) to minimise structural flanking from source to receiver rooms. The partition when installed in the separating wall aperture then represents the dominant path of sound transfer between the rooms. Under test conditions, when a source is operational in the source room, the dominant airborne sound transfer occurs through the partition. Therefore, such a facility was ideal to test the applicability of I-ASCA and I-PCA methods on the dual leaf partition after the box tests. Accordingly, for further tests, the dual leaf partition was installed in the transmission suite at University of Salford.

---

#### 4.5.1 Construction

---

This transmission suite at the University of Salford is a test facility that meets the requirements of the ISO standard specifications for measuring airborne sound insulation, impact sound insulation, and sound absorption of building elements. It comprises of two reverberation chambers – the source room and the receiving room with a separating wall between them. These rooms are isolated from each other such that any sound transfer from the source to the receiving room only occurs through the partition installed in the aperture of the separating wall. The facility is supported on springs and resilient elements to isolate the chambers from ground borne vibration. For these test chambers, the separating wall has a  $R_w$  value of about 70 dB. Figure 4.11 shows the transmission suite.

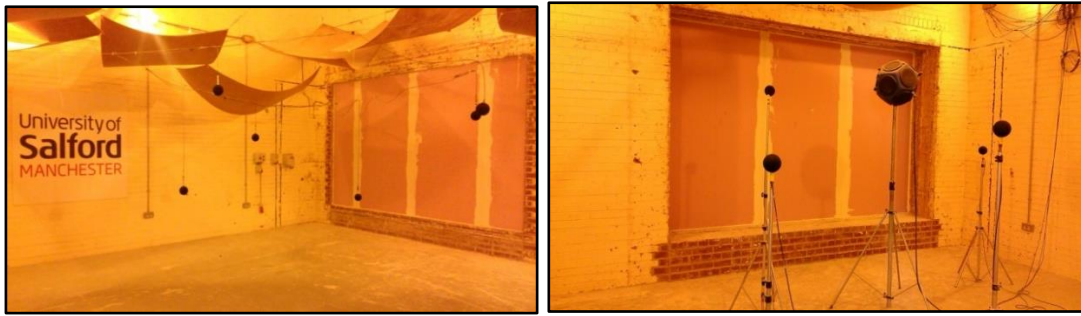


Figure 4.11: The transmission suite consisting of the source room (right), receiving room (left) and the mic positions in black in both rooms

For the I-ASCA test, the dual leaf partition was first installed in the separating wall aperture between the source and receiving rooms. The aperture size in the separating wall was  $1250 \times 1500 \text{ mm}^2$  (Figure 4.12-left graphic) and the partition size was smaller ( $910 \times 910 \text{ mm}^2$ ). Therefore, after placing the partition in the aperture, a filler wall had to be constructed in the remaining aperture space. In the first attempt of the I-ASCA here, the filler wall was entirely built with plasterboard stacks. Next, a single layer facing wall was put up in front and behind of the plasterboard stacks. It was intended that the filler wall would provide insulation to any flanking transmission. The complete construction is depicted in Figure 4.12-right graphic.

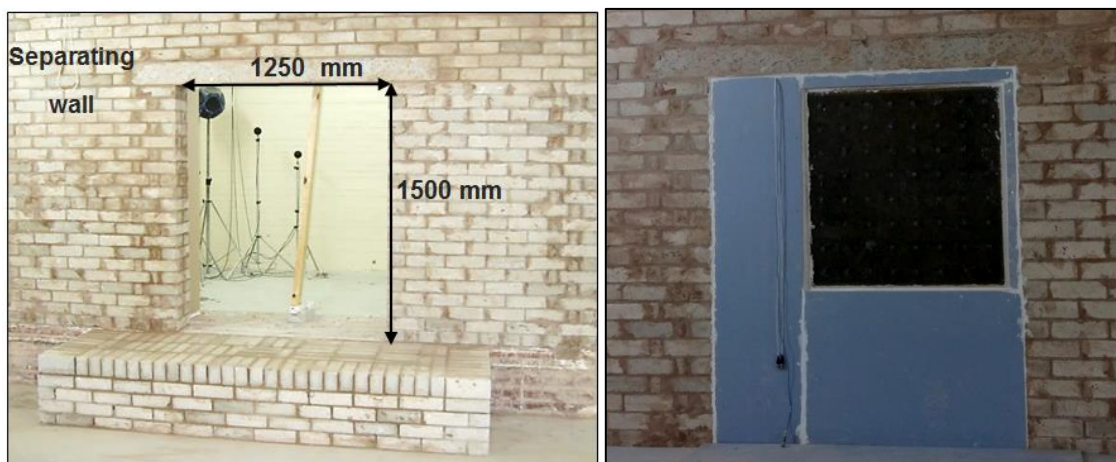


Figure 4.12: The aperture in the separating wall between source and receiving rooms prior to the I-ASCA test (left) and on right- the partition (in black) installed in the brick walled aperture with the filler wall structure around it (in blue). The filler wall cavity here is made up of plasterboard stacks

One of the motivations of the diagnostic tests was that the diagnostic results could be potentially used as a complement to the standard sound insulation tests. Therefore, the tests in the transmission suite provided a good opportunity to perform the combined sound insulation and I-ASCA tests on the test structure in a controlled environment. At first the sound insulation of the construction was measured by ISO 10140 standard test. Figure 4.13 shows the measured sound insulation of the test structure.

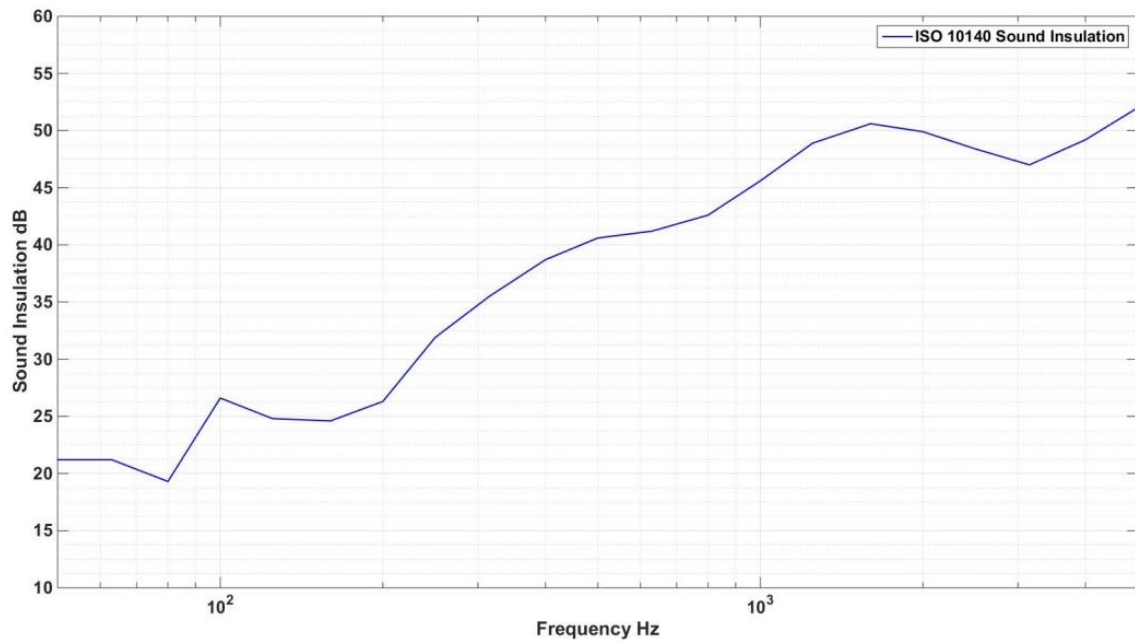


Figure 4.13: Sound insulation of the dual leaf partition and filler wall structure measured by ISO 10140 method

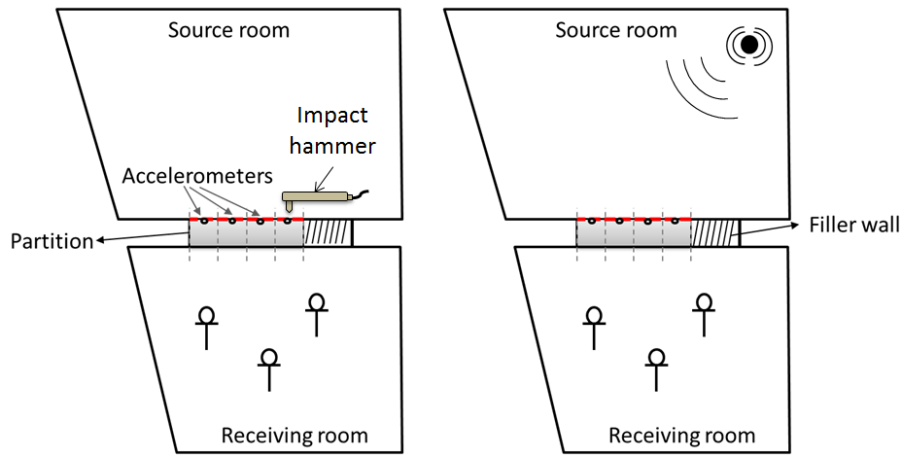


Figure 4.14: Schematic for FRF measurements (left) and operational measurements (right) for the I-ASCA test in transmission suite (top view). Red line denotes the interface

Next, the I-ASCA tests had to be performed (see measurement schematic in Figure 4.14). The grid discretisation from previous tests was kept the same to yield a total of 64 sound transmission paths. Next, the acceleration measurement was performed in parts to yield an accelerance matrix 'A' as per Eq. (3.5). The validity of these measurements was checked by performing a reciprocity check on the cross diagonal elements of the accelerance matrix. A few plots of reciprocity for nine sets of force-response for randomly chosen paths are shown in Figure 4.15.

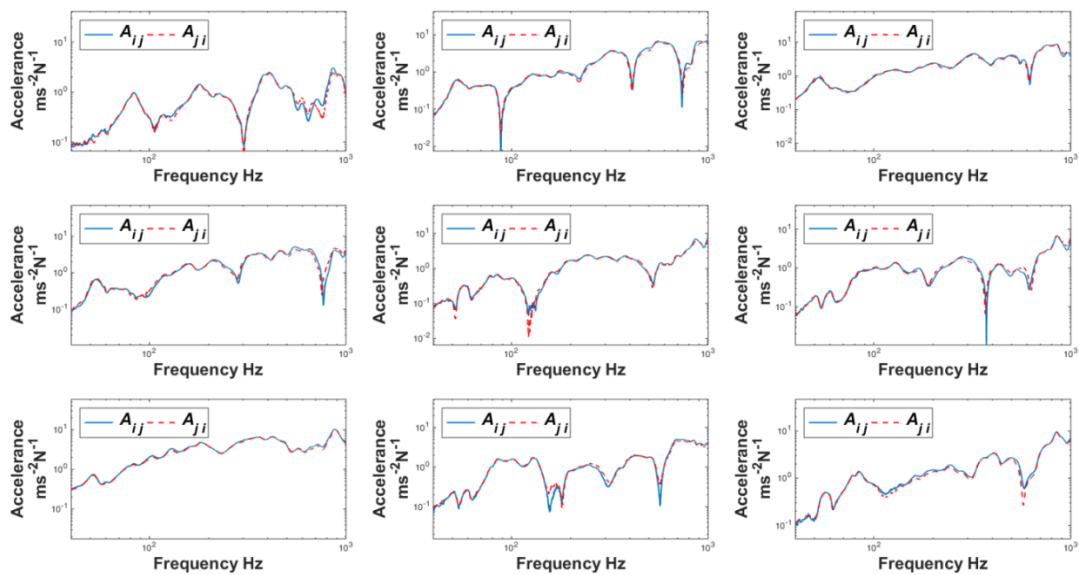


Figure 4.15: Reciprocity between nine sets of force-response for randomly chosen paths on the dual leaf partition installed in transmission suite

At the same time of performing the FRF measurements, the vibroacoustic FRF's had to be measured. For this, three microphones were placed in the receiving room and the FRF's were measured for these positions. In the operational test, a loudspeaker was placed facing the corner of the source room. Placing the loudspeaker in the corner position allows the excitation of all the source room modes under operational conditions. When driven with a pink noise excitation, all the modes are excited and due to hard walls and diffusing elements a near diffuse field is created in the room above the Schroeder frequency [141]. Thus, the sound transfer of the partition could be studied for a diffuse field excitation. With the loudspeaker operational, the accelerations of the paths and the pressures at receiver room positions were measured. All operational measurements were referenced to the driving voltage of the loudspeaker to maintain the phase between different measurement sessions. Following Eq. (3.5-3.8) the blocked forces were calculated and the sound pressure radiated by the partition was predicted (Eq. 3.10). Figure 4.16 shows the pressure validation results.

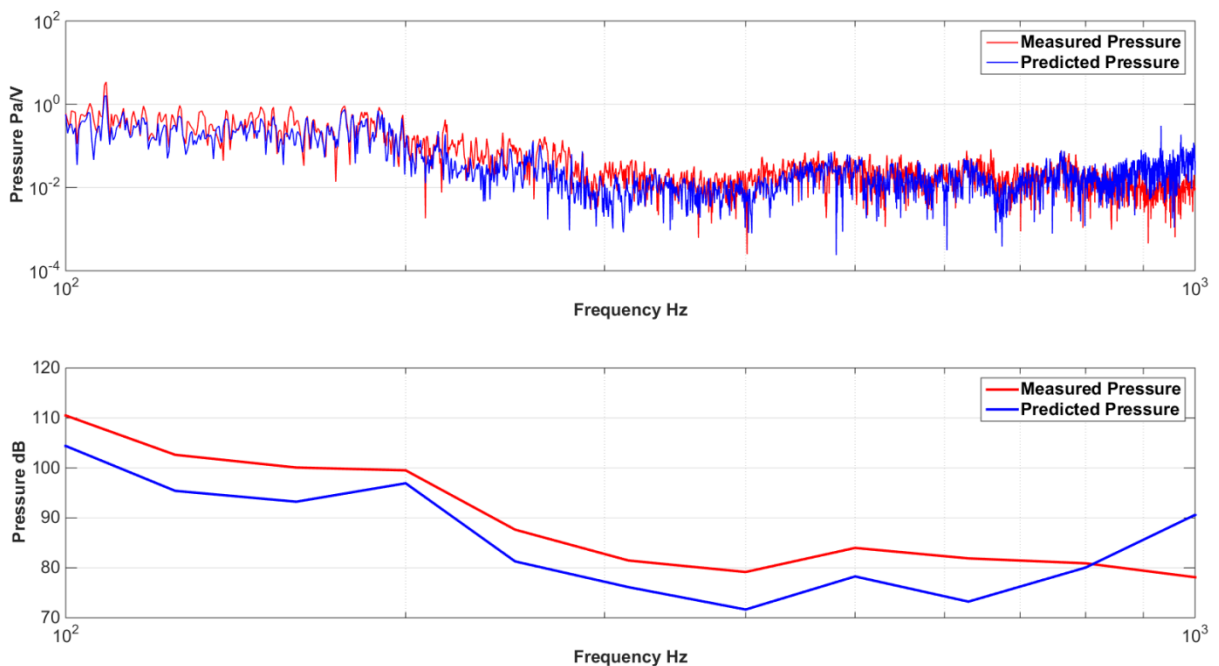


Figure 4.16: Pressure validation for the I-ASCA test on the dual leaf partition in the transmission suite. Predicted pressure by I-ASCA is compared with the measured pressure in narrow band (top plot) and one-third octave band (bottom plot)



From Figure 4.16, it was observed that the predicted pressure was lower than the measured pressure, about 4-5 dB lower till 800 Hz. Again, the possible reasons of this mismatching considered were the blocked forces or flanking. The accelerance matrix showed good reciprocity and the operational data was referenced to the excitation voltage to prevent any phase mismatching between different measurement sessions. Thus, the first the blocked force calculated should be correct as their accuracy depends on correct FRF and operational measurement on all paths. In addition, the predicted pressure does not show any peculiar inverse error peaks (except above 800 Hz). Regarding flanking, some transmission through the filler wall was expected as it was attached to the frame of the dual leaf partition (structure borne flanking). In addition, some airborne flanking was also expected at low frequencies through the filler wall. To avoid this flanking transmission from the filler wall, the filler wall has to be rated higher for sound insulation than the test partition as well as acoustically isolated from the frame of the partition. Thus, with these observations a second test was again set up to reduce the flanking transmission.

---

#### 4.5.2 Second test

---

In the previous attempt of testing I-ASCA on the partition in the transmission suite, we found that the filler wall made of plasterboard did not offer good sound insulation and acted as a flanking path. The requirement for the filler wall was thus to provide minimal or ideally no flanking transmission at all frequencies compared to the partition under test. For this, the following two steps were taken.

- 1) The filler wall was constructed as a dual leaf cavity partition with mineral wool inside the cavity. A dual leaf cavity construction with cavity absorption offers higher sound insulation than a single layer cavity of the same thickness. Each leaf of the partition consisted of two joint layers of 15mm plasterboard sheets. The cavity depth was 20 cm filled completely with mineral wool.
- 2) The sound insulation of the partition under test was reduced by removing the mineral wool from the cavity. This reduces the sound insulation of the partition

compared to the filler wall, as we want all the sound to be transferred through the partition only.

The combined effect of these two changes is that the dominant sound transfer occurs through the partition and flanking is negligible so that I-ASCA can be validated. The test partition installed with the surrounding filler wall is shown in Figure 4.17.



Figure 4.17: (a) Front view from the source room of the test partition installed with the plasterboard partition



Figure 4.17: (b) Construction of the filler wall with the mineral wool in the cavity and the completed construction on the right with microphones in the receiving room

An acoustic sealant was applied at all edges to seal any air gaps or leaks. Additionally, care was taken that the plasterboard from the filler wall is not coupled strongly with the frame of the partition by using resilient linings at the junctions.

#### 4.5.2.1 Airborne sound insulation

At first, the airborne sound insulation of the combined structure was measured according to ISO 10140 standard procedures in the transmission suite. The results of the test are shown in Figure 4.18. The sound insulation is of the combined structure –the test partition and the plasterboard partition. It can be seen that there are pronounced dips in the sound insulation curve at 80, 160, 250 and 500 Hz centre frequencies. The dips represent increased sound transmission to the receiving room at those frequencies. The structures that can contribute to this sound are the partition and the filler wall. On close examination, it can be suspected that these dips are a result of the lateral resonances of the cavity which show up as the mineral wool was removed from the partition cavity. Using I-ASCA, the sound transfer from the partition can be measured and it can be assessed for certain if the dips are caused by the sound transmission through the test partition.

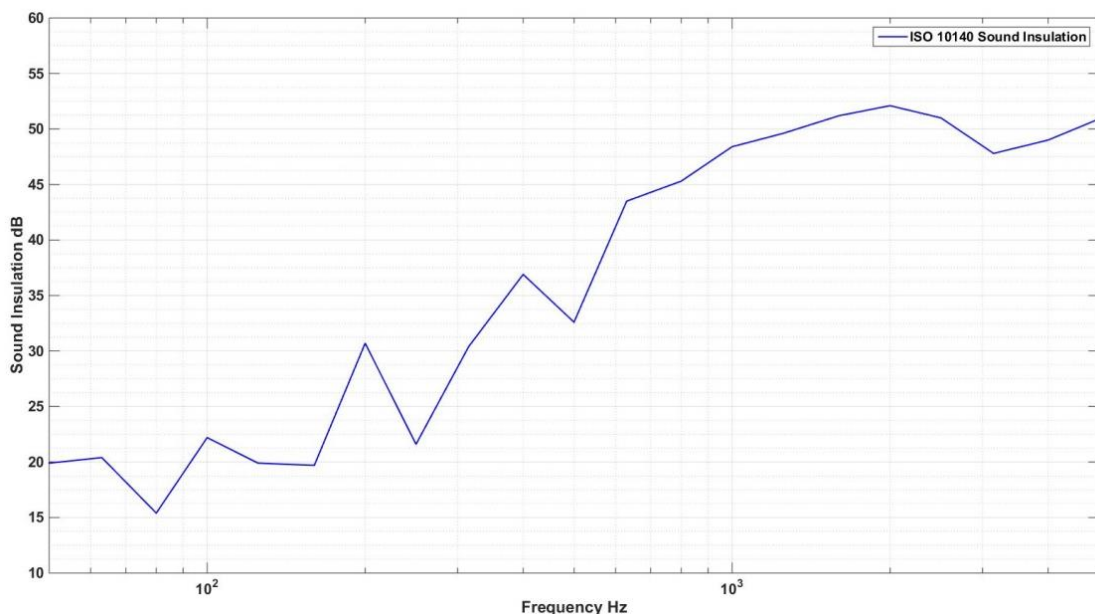


Figure 4.18: ISO 10140 sound insulation of the structure (test partition plus filler wall) measured in the reverberation chambers. Filler wall here is a double layer cavity construction

### 4.5.2.2 I-ASCA – Measurements and validation

Keeping the discretisation the same as the previous test, acceleration measurement was performed for 64 paths. Simultaneously the vibroacoustic FRF's (Pressure/Force) were measured for three pressure positions in the receiving room. A few sets of accelerances are shown in Figure 4.19, which highlight good reciprocity. Some deviations at low frequencies in a few sets of accelerances were reduced by averaging the transfer FRF's of the acceleration matrix.

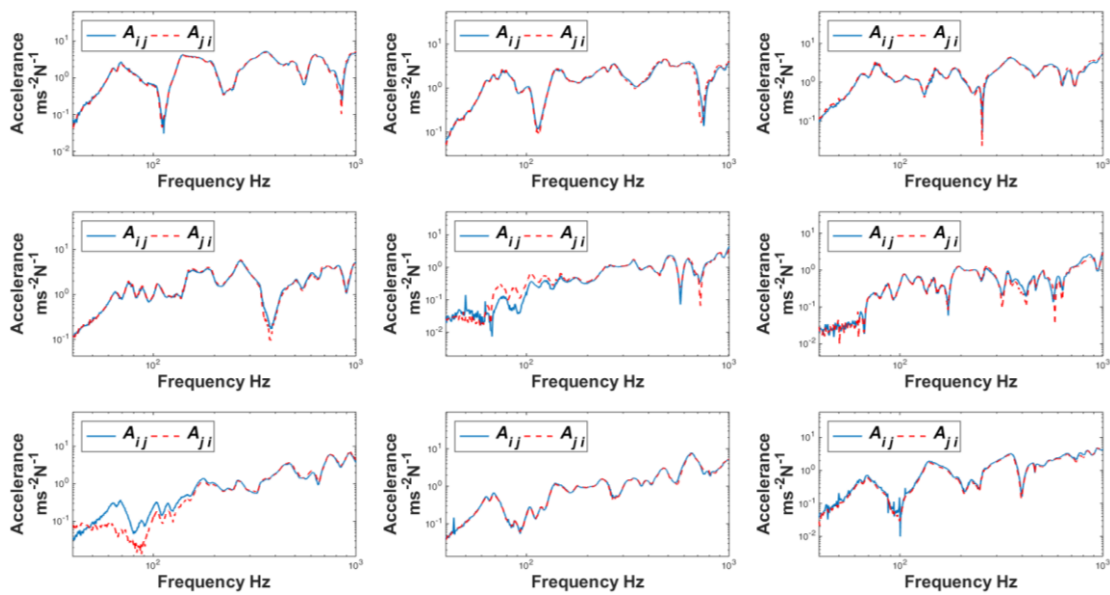


Figure 4.19: Reciprocity between nine sets of force-response for randomly chosen paths during second test on the dual leaf partition installed in the transmission suite

For the operational measurement, a loudspeaker exciting the room with pink noise was used. The accelerations were measured at all the 64 points and a reference point on the partition for an on-board validation. The operational pressures in the receiving room were also measured for comparison with predicted pressures. Following Eq. (3.8-3.10), the predicted pressure was calculated for pressure validation. Figure 4.20 shows the pressure validation results.

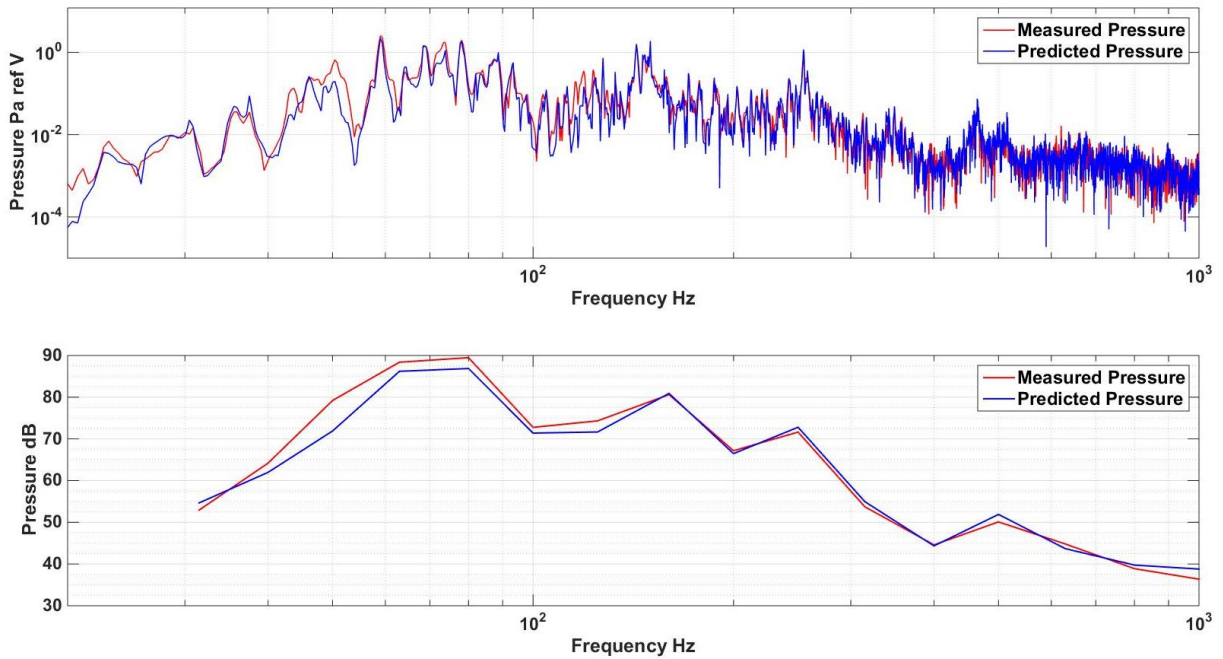


Figure 4.20: Pressure validation results for airborne excitation case comparing pressure predicted by I-ASCA with the measured pressure in the receiving room in narrow band (top plot) and on-third octave band (bottom plot). Filler wall here is a double layer cavity construction

Figure 4.20 shows that the prediction obtained from I-ASCA method matches well (within 2 dB) with the measured pressure from 100 Hz-1 kHz which is the typical range of building acoustics measurements. The dips in the sound insulation curve (Figure 4.18) can now be attributed to the transmission through the test partition. At frequencies lower than 100 Hz, the measured pressure is slightly higher than the predicted pressure. Possible reasons for this are errors in blocked force calculation, airborne flanking transmission through the filler wall (possibly due to its fundamental resonance). To confirm these, the validity of blocked forces in this region can be checked by an on-board validation test to be discussed in next section. From the on-board validation it can be assessed whether the error is due to blocked force calculation or airborne flanking. Also, at such low frequencies the vibroacoustic FRF measurement is slightly erroneous as the measurement time was less than RT of the room as well as poor SNR is observed due to usage of hard tip of hammer. However for the range of building acoustics applications (which is typically above 100 Hz), the prediction is within 2 dB. Thus the I-ASCA method was finally validated for the case of dual leaf partition. It is

also evident from this study that for a successful pressure validation, having minimal flanking transmission is paramount.

#### 4.5.2.3 I-PCA results

Once the method was validated, the path contributions can be measured which diagnose the sound transmission through paths in-situ. Following I-PCA methodology, the acoustic FRF's for the 64 paths were calculated following Eq. (3.18). Using Eq. (3.12), the path contributions were also calculated which are plotted in Figure 4.21 (bottom plot). It should be noted that the contributions in grey represent individual contributions from the acoustic paths. The blocked forces on each path are also plotted (top plot). It can be seen that on an individual patch by patch basis, the path contribution of the point connection dominates for most frequency ranges above 100 Hz compared to the 'individual' path contributions for this particular case.

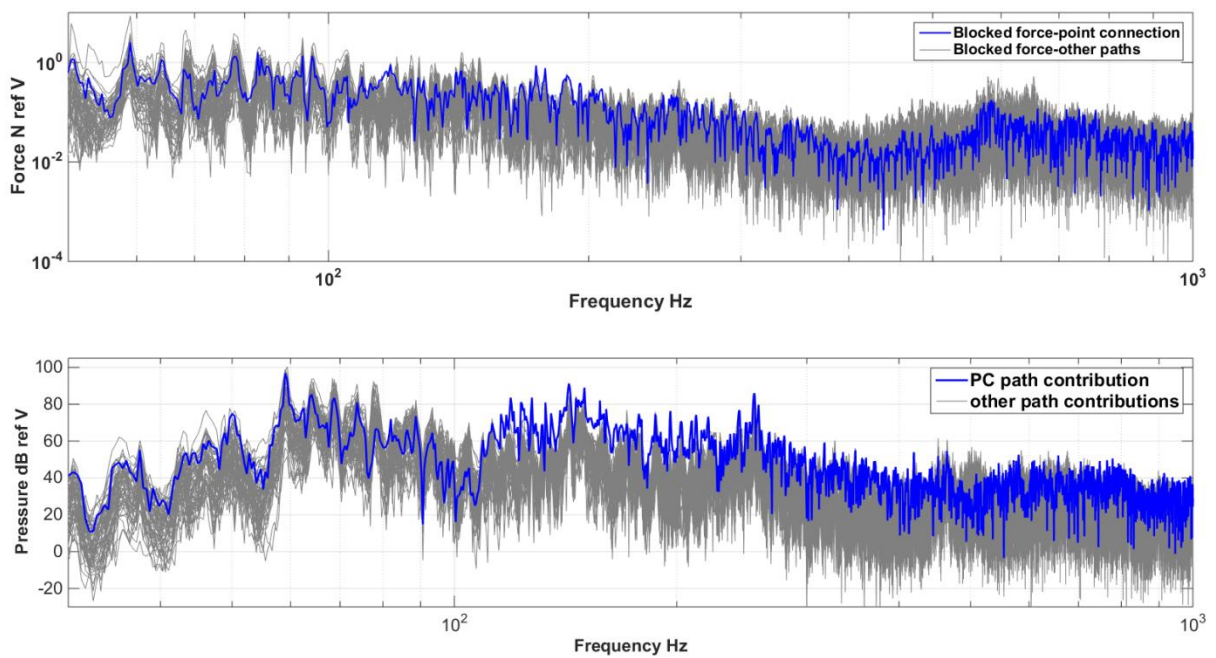


Figure 4.21: Top plot-Blocked force on paths in dual leaf partition. Bottom plot-Path contributions measured as per I-PCA method for dual leaf partition under airborne excitation

To assess if the contribution is significant compared to the 'total' acoustic path contribution through the cavity, the contribution of a single point connection can be compared to the total contribution from multiple acoustic paths through the cavity. To do this, the



contribution of the point connection can be removed from the total prediction to estimate the sound transfer through the partition in absence of the point connection. This would show if addition of a single point connection has a significant and larger effect on the sound radiation compared to the transmission through all acoustic paths. Figure 4.22 shows the effect of removing the point connection path contribution from the total pressure up to 1 kHz.

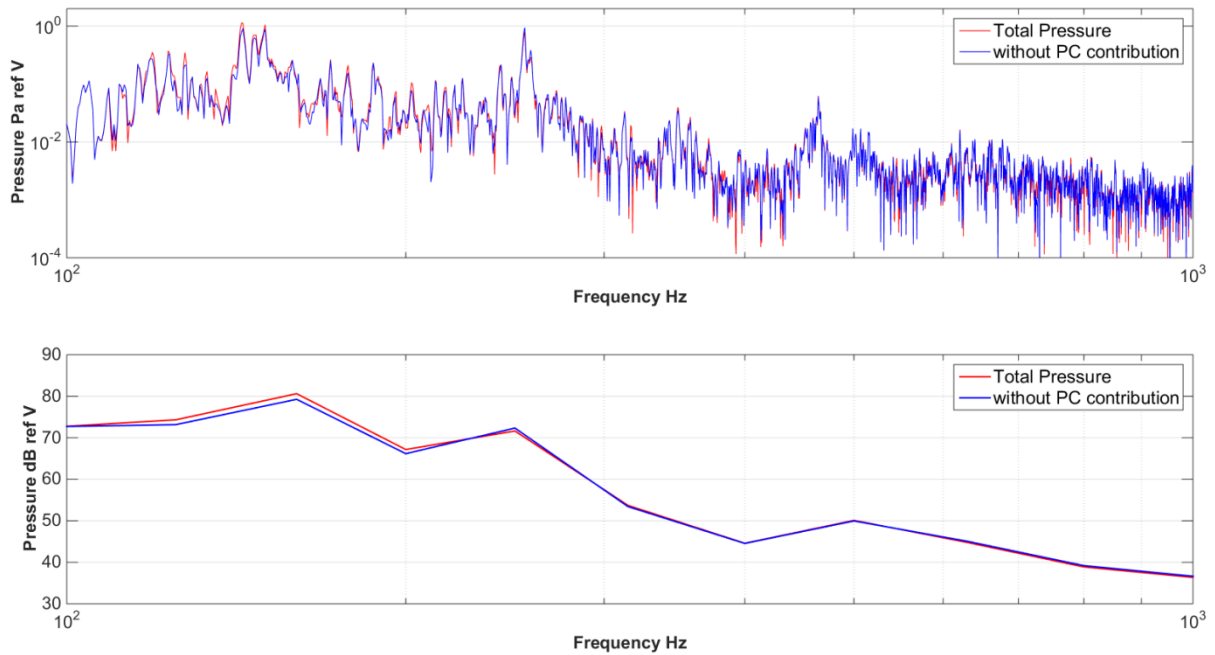


Figure 4.22: Effect of removing the Point Connection (PC) path contribution from the total pressure in narrow band (top) and one-third octave band (bottom) for an airborne excitation on the partition

Figure 4.22 shows that removing the contribution of the point connection has no significant effect in this case and that the total radiation through the all acoustic paths (compared to single structural path) is more dominant. This is in contrast to the structure borne case (Section 4.3.2) where the point connection affects the total pressure at high frequencies. This can be explained as follows.

- i. In structure borne excitation case, there was only one dominant source on the shaker path and the cavity was filled with acoustic absorption. The cavity absorption effectively limits the sound transmission through all the acoustic paths. In such case the structural path (which is not blocked) is dominant and its effect on the global

radiation can be seen (Figure 4.9). In the case of airborne excitation, it is important to recall that the cavity absorption was removed. This means that the sound transmission through multiple acoustic paths will not be limited and thus comparable to the transmission through a single structural path which can also be seen in Figure 4.22 (bottom plot).

- ii. Compared to the structure borne case, where only one source was present, in the airborne excitation case the source is acting on all paths (structural and acoustic). Therefore each path has direct excitation acting on it and the contribution will be significant.
- iii. The tested partition had only one structural path-point connection (surface area  $0.0000785 \text{ m}^2$ ) compared to the acoustic paths (surface area  $0.624 \text{ m}^2$ ). In practice, multiple studs (generally line connection) are used in dual leaf partitions with cavity absorption in the cavity. In those cases, the total structural path contribution is usually dominant and its effect on the global radiation is significant. Therefore, in such case if I-PCA is applied, it is much more likely that a significant effect would be observed when the path contributions of all point connections are removed from the total pressure.

To measure the path contribution of the point connection above 1 kHz, a finer discretisation is needed on the partition. The required grid sizes could be determined from the sampling criterion (see APPENDIX II).

#### 4.5.2.4 Theoretical analysis

To further provide confidence in the result from Figure 4.22, a theoretical analysis may be performed to assess the effect of point connection on the radiation from the partition. In the literature, the effect of structural connections on sound insulation is provided. For double walls with sound bridges (studs), Sharp's model [72] is commonly used. However, the point connection configuration discussed by Sharp and the current study are very different (see Figure 4.23). Perhaps the most important difference is that Sharp's model assumes the cavity to be fully absorbent, which is a limitation as pointed by



Hongisto [68]. As the model assumes completely absorbent cavity, Sharp's model would not account for the sound transmission through the cavity/airborne paths between the two panels (which is important to calculate in our case where the cavity is empty) and is thus not appropriate to be used here as a cross check.

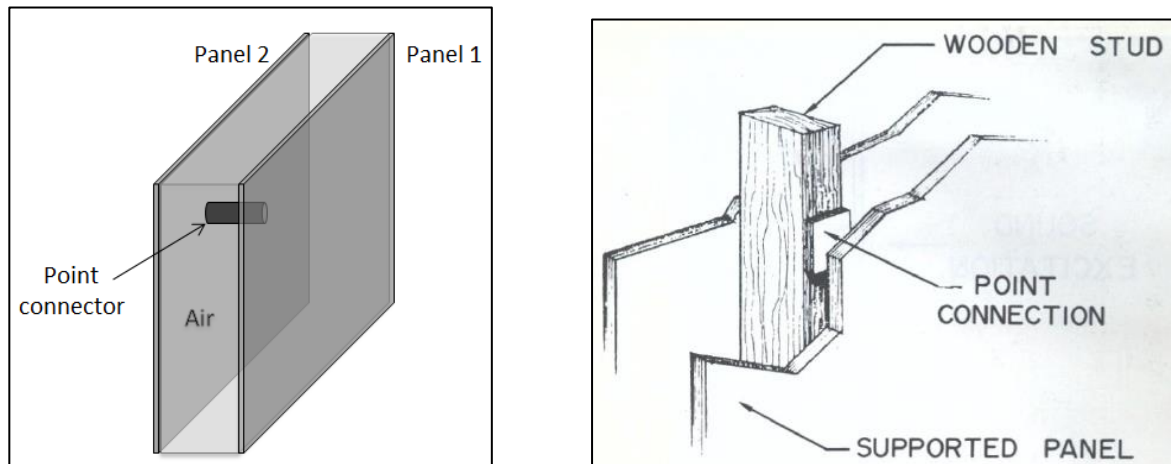


Figure 4.23: The point connection configuration used in present test (left) as opposed to Sharp's (right, taken from [72]) which is actually a stud (beam) connected at multiple points to the panels

Another option is to apply SEA to assess the structural connection effect on the sound insulation. The SEA model developed by Craik and Smith [142] is the most relevant model for the present case of double wall and predicts sound transmission in presence of point/line connected studs (not point connectors) but the work states that the transmission through the cavity cannot be predicted correctly using the theory and works well only when cavity absorption is added. Additionally for small cavity depths (50 mm), the air in the cavity behaves as a stiffness element below the first cross cavity mode (above 3 kHz in this case). Incorporating this effect in SEA model is not very accurate using current SEA approaches and loss factors for the air spring reported in literature are not so accurate [67]. Overall, an SEA model is also not appropriate here as it would lead to uncertainties in prediction. Another commonly used approach is a Transfer Matrix Model (TMM) to predict the sound insulation. Using TMM, the transmission through the double leaf partition in the absence of cavity absorption can be modelled which would be suitable in our case. Therefore a very recent model by Massaglia from 2017 [143] was used for this purpose. The theory can

model the sound insulation in presence of point connectors used in the study. To apply this model, the material properties of the panels used in the study were measured. The measurement details for determination of the material properties are provided in Appendix II. Using this model, the sound insulation of two configurations (with and without point connection) of the dual leaf partition was measured. The results are shown in Figure 4.24.

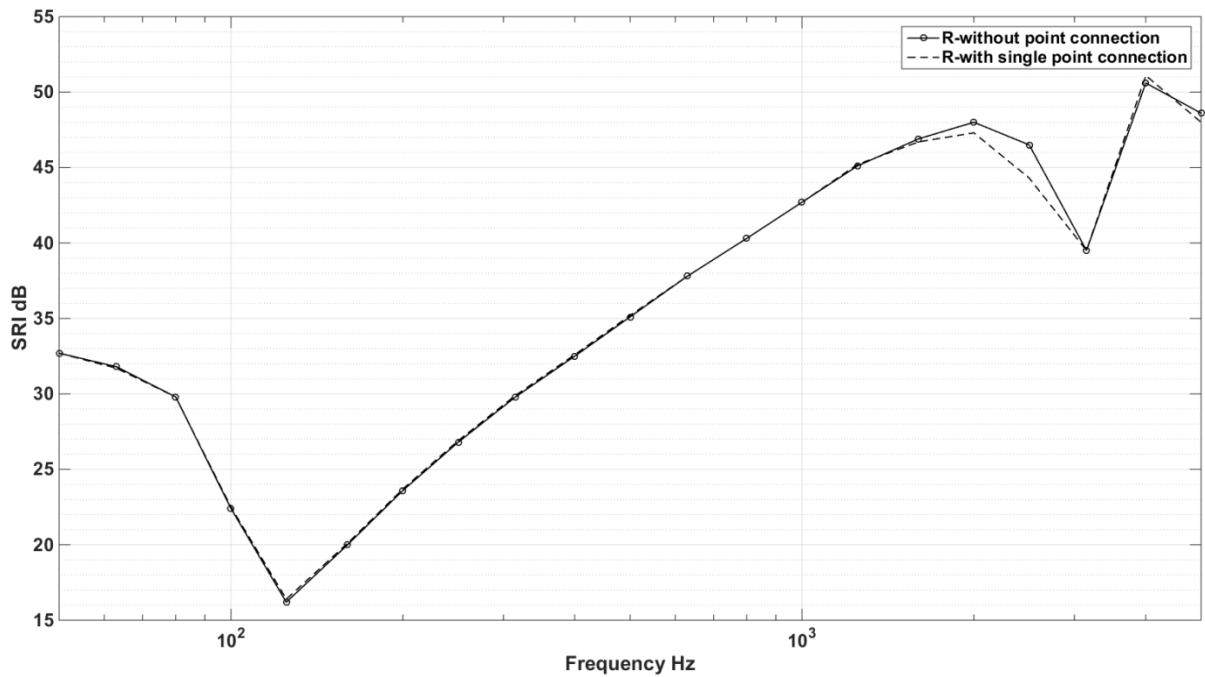


Figure 4.24: Sound insulation of the dual leaf partition measured by TMM [144] for no cavity absorption with and without the presence of a single point connection between the panels

The results from the model tend to show that the effect of the single point connection is not significant on the sound insulation of this particular dual leaf structure below 1 kHz. There are some differences in transmission in the range 1.6-3.15 kHz which was outside the test range of I-ASCA for the grid size chosen in this particular case. One limitation of the model used here is that it does not account for the lateral modes in the partition cavity but only modes perpendicular to the panel. However that would not be a problem as presence of lateral modes only increases the sound transmission through the acoustic paths. In other words, this would not change the structural path contribution. Then not accounting for the lateral modes should not be a problem. It should be noted that the model does include the

cavity modes perpendicular to the panels. In total, it can be concluded that the results obtained from Figure 4.22 are valid and provide confidence in the following findings

- i. The sound transmission through the structural path (point connection) is dominant if they are compared to an individual acoustic path contribution in the 110-350 Hz and 750-1000 Hz ranges (see Figure 4.21).
- ii. The total sound transmission through all the acoustic paths combined dominates that through the single structural path. This shows why removing the single point connection would not have any significant effect on the total sound transmission through the global structure.
- iii. The findings are only valid in the tested range till 1 kHz as it can be seen through Figure 4.24 that there is some effect of the point connection on the sound insulation above 1.6 kHz. To test in this range, the test can be conducted with finer grid size.

These findings are interesting because it shows that although the structural path contribution may be dominant when compared to an individual acoustic path contribution, it may not affect the total sound radiation through the structure because that is determined by how the total structural path contribution compares with the total acoustic path contributions (which was higher due to empty cavity). This case study thus demonstrates the application of I-ASCA and I-PCA on a dual leaf partition for airborne excitation. It also shows the potential of the method in measuring the individual structural and acoustic path contributions to the receiver pressure and identify if the structural path contribution affects the total sound transmission through the structure.

#### 4.5.2.5 On-board validation

The blocked forces obtained from I-ASCA can be in principle also used to predict the vibration response in the panel. To do this, an on-board validation test was used where reference point acceleration on the receiver can be predicted as,

$$a'_{ref} = \{\mathbf{A}_{ref,1-n}\}_{1 \times n} \{\mathbf{f}_b\}_{n \times 1} \quad (4.3)$$

In Eq. (4.3),  $a'_{ref}$  is the reference point acceleration, which can be compared to the measured acceleration at the same point. The results of the on-board validation are shown in Figure 4.25.

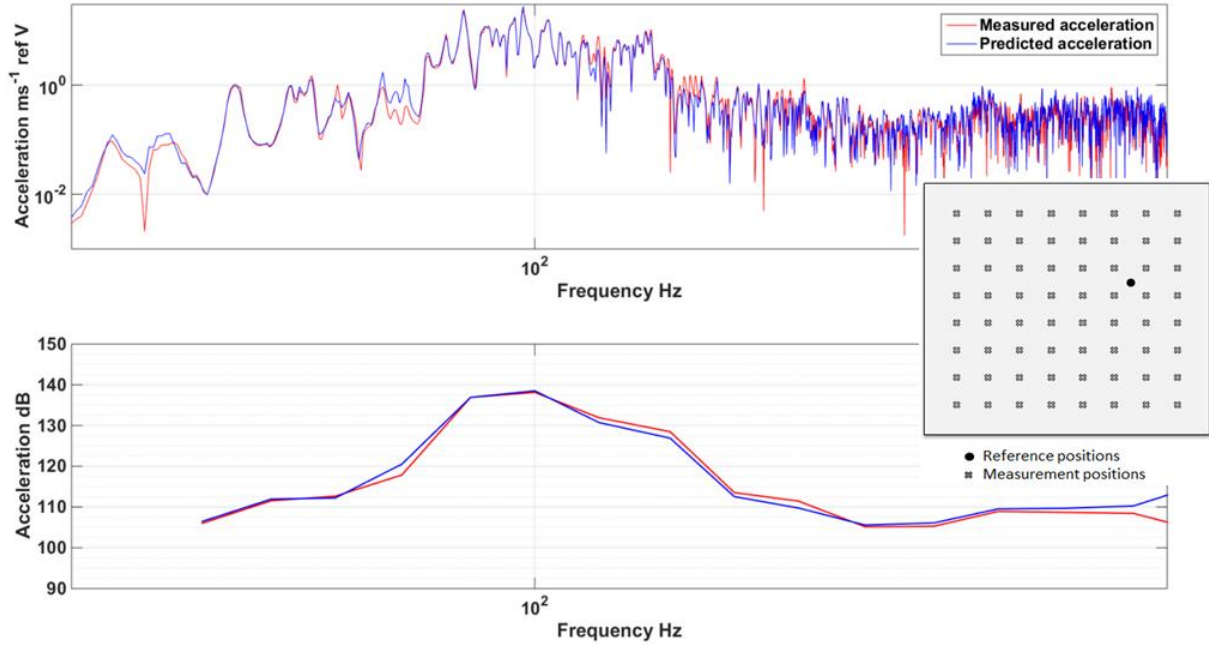


Figure 4.25: On-board validation results comparing the predicted and measured acceleration at one reference position (●) on the partition (in grey) in narrow band (top plot) and one-third octave band (bottom plot)

Figure 4.25 shows that the predicted acceleration at reference position matches well (within 2.5 dB) with the measured acceleration in the frequency range 31.5-900 Hz. The results highlight the applicability of the I-ASCA for predicting the vibration response of a system under an airborne excitation. Therefore, the I-ASCA technique is versatile in predicting the acoustic as well the vibratory response in the receiver. It can also be seen that the blocked forces predict the vibration response really well (within 0.5 dB) in the low frequency region (below 100 Hz, except in 63 Hz band). As such this provides confidence that the blocked force measured in this frequency region. Then in Figure 4.20, the differences between the measured and predicted pressure below 100 Hz could be attributed to either poor measurement of the vibroacoustic FRF's and/or airborne flanking through the filler wall. This concludes the application of I-ASCA and I-PCA methods for a special case of multi-layered partition i.e. a double layered partition.

The application of the diagnostic methods is thus demonstrated for the case of point connected dual leaf partition for structure-borne and airborne cases. For the airborne case, the diagnostic contributions of acoustic paths and structural paths were measured and compared, and the structural path contribution did not significantly affect the total sound transfer through the partition in the measured frequency range. To further exploit the full potential of the diagnostic method, it is suitable to apply the methods on a structure where the path(s) under diagnosis have a significant path contributions compared to the total sound transfer. Further tests with multiple point connections were planned but due to limited availability of the transmission suite at the time, they were not performed. However, more tests were conducted on different structures later with prominent path contributions which show how the diagnostic potential of the method could be fully exploited. These cases will be outlined in Chapter 6 where they will be discussed along with SRI measurements to highlight how the diagnostic results can complement the SRI. Also for partitions with more layers, the methodology can be applied, which is explained in the following section.

---

## 4.6 Extension to multi-layered partitions

---

The measurement of diagnostic source and path contributions was presented for the case of a single layer and double layer partition. In principle, the methodologies can be applied towards measurement of such diagnostic contributions in triple (or more) layered partitions as well.

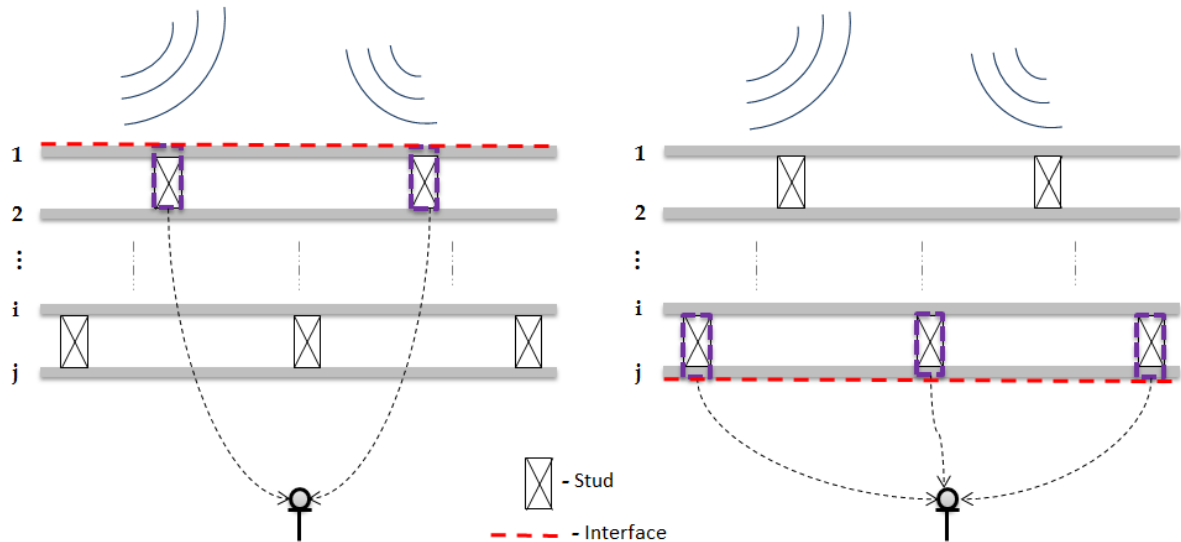


Figure 4.26: A multi-layered partition layout with layers 1-j with structural elements contributing to the pressure at a receiver position denoted by the microphone

Consider the case of the multi-layered partition as shown in Figure 4.26. It is readily evident that the first and the last panel are accessible for measurements and thus the diagnostic techniques can be applied there. The interface (in dashed red) shows the measurement surface for I-ASCA and I-PCA. Then the contributions of the structural paths (where the studs are located-in dashed purple) and acoustic paths can be readily measured and any weak paths can be identified. It can then be estimated how much reduction in the sound transmission can be obtained in absence of a particular structural or acoustic path.

If any weak paths are to be diagnosed on the inside layers, then access to those layers will be required. As with any measurement, the measurement surface should be accessible (physically or optically) otherwise measurements cannot be performed. In such cases to measure the FRF's, the accelerometers can be first placed on the inside layers by removing the outer layers and building outside layers back again. Then the FRF's and blocked forces can be measured remotely using roundtrip methods [134] and reciprocity principles. Although this would be a tedious and invasive process, it is in no way a limitation of the measurement method because for a measurement to be performed, access (partial or full) to the measurement surface is necessary. Following these studies, a brief discussion on the

I-ASCA and I-PCA application is presented with respect to the topics in the following sections.

---

## 4.7 Pressure validation and flanking

---

The pressure validation test is performed to validate the methodology of the I-ASCA in predicting the acoustic response of the partition under consideration. As seen from pressure validation tests for the case of single leaf partition and dual leaf partition (structure borne excitation case), the pressure validation is good while for the pressure validation in airborne sound transfer through the dual leaf partition, flanking transmission was a problem (Figure 4.10, Figure 4.16). Hence, the pressure validation works if the sound transfer takes place through the partition alone, or to say if the flanking transmission is minimal (ideally 10 dB lower than the partition transmission). However, with airborne excitations, where air is effectively the source, it might be practically difficult to stop the flanking transmissions. The case of flanking through the box walls (in Section 4.4) is quite representative of real building installations where flanking paths may exist through other walls or any common doors. On the application of I-ASCA in such cases, one may not be able to obtain a good pressure validation, as the flanking transmission can be dominant. However, this does not imply that the I-ASCA method is incorrect. Two checks should be carried out in such cases. Firstly, if the total pressure is greater than 10 dB as compared to the pressure contribution by the partition predicted by I-ASCA, it means that the partition may be a good insulator but all the sound transfer is through the flanking paths in that particular case, which is still useful information for an acoustician, sound consultant or the architect. Secondly, a bad pressure validation could also mean that there are inversion errors in the calculation of blocked forces owing to bad measurement data. To check this, a structure borne excitation such as a shaker can be used. This permits a controlled excitation of the partition only, with no flanking transmission. A good pressure validation in this case will ensure that the measured accelerance matrix is correct and can be used in measurement of blocked forces in I-ASCA. Using a structure borne excitation is valid as the

methodology and underlying assumptions of the I-ASCA are same, the only change being the source quantity or rather the blocked forces.

One other check that can be performed by using airborne excitation for validating the blocked forces is using an on-board validation test. By using an on-board validation test, the vibrational response of the partition can be predicted as per Eq. (4.3). If the measured and predicted responses are similar, then the blocked forces can be said to be valid. If the blocked forces are valid and measured correctly, the pressure contribution of the partition measured under these blocked forces should be correct. This means that even in the presence of flanking transmission, the acoustic response of the partition may be separated from the total pressure (which includes partition contribution plus flanking). If that is true, then the source and path contributions can also be found in presence of flanking. This indicates an interesting potential or ability of the I-ASCA method to diagnose total airborne sound transmission through the partition and measure the diagnostic contributions even in presence of airborne flanking.

---

## 4.8 Blocked forces

---

The blocked forces measurement for airborne excitation is a tedious process. As a result, accelerance matrix of size 64x64 was measured for our dual leaf partition system. The accuracy of the blocked forces is highly dependent on the inverse of the accelerance matrix. If the FRF's are measured incorrectly or the FRF's are corrupted with noise then the blocked force will suffer from inverse errors. A higher condition number [135] of the matrix may be indicative of that the matrix is ill posed meaning the data is not measured correctly. If the FRF's are measured incorrectly, the whole accelerance matrix is to be measured again and regularisation methods do not work. Use of regularisation methods [101, 144, 145] is more justified if the measurements are corrupted with noise. Both measures can significantly increase the time and effort to get a good prediction of receiver response. Thus, the careful and accurate measurement of FRF's is paramount to the accuracy of blocked forces and source and path contributions.



---

## 4.9 In-situ sound insulation measurement

---

In-situ measurement of sound insulation according to ISO 16283 can be affected by the presence of airborne and structural flanking paths. In such cases, it is ideally desired for the airborne sound transmission to be dominant through the partition only to calculate the correct receiver room sound energy. However flanking contributions may be present in the measured pressure in the receiver room. The amount of flanking is not known and cannot be controlled in most situations. At first instance, this might be achieved by reducing flanking by soundproofing or blocking all the flanking paths such that the sound transfer occurs through the partition alone. Blocking flanking paths is practically difficult especially at low frequencies due to wavelength considerations, besides adding any soundproofing can change the acoustic behaviour of the rooms. The intensity method can also be used to find the transmitted power but requires use of absorbers on the opposite wall at low frequencies which may be quite impractical in most in-situ cases. Therefore, a method by which the sound transfer through the partition can be measured or quantified in-situ without blocking of any flanking paths is desired. In principle, the I-ASCA method allows to diagnose the sound transfer through a partition in presence of airborne flanking paths provided the inversion errors and any structural flanking from surrounding walls to the partition is minimal. If the surrounding walls are massive and rigid, then such structural flanking can be neglected, which is usually the case for real buildings. With careful measurement of FRF data, the inversion errors are minimal. Then the I-ASCA can be employed in such cases to find the blocked forces and the resulting sound transfer through the partition can be deduced. This sound contribution obtained through I-ASCA can be then used to calculate the receiver room energy to be used in the calculation the in-situ sound insulation or SRI of the partition, as it accounts for the sound energy transmitted by the partition alone. Additionally, from I-ASCA measurements, the I-PCA methodology can be applied which provides the path contributions. These path contributions are the diagnostic characteristics of the partition paths and provide the spatial dependence of sound transfer through the

partition. From these contributions the weak sound insulation elements may be identified and be treated to improve the sound insulation of the global structure.

---

## 4.10 Measurement time

---

For airborne excitations of partitions, the source, an incident pressure field can be visualised as a continuum of point forces exciting the partition. In the I-ASCA method, this airborne excitation is approximated by a set of discrete point blocked forces on the partition as can be seen in Figure 3.6. Because of such discretisation, the validity of the I-ASCA methodology is dependent on the number of blocked forces or measurement positions considered over the partition or it can be said that the accuracy of the I-ASCA with frequency is dependent with respect to the incident wavelength. For example, if a lower number of measurement positions were considered (<64) in the current test case (Section 4.5.3), the validity of the method would be limited to frequencies less than 1 kHz. As the calculation of blocked forces involves measurement of FRF's and operational data and subsequent inverse problem, the method tends to be quite time consuming with increasing measurement points. This might be a bigger issue when number of sensors for the FRF measurement is less than the measurement positions in which case one has to do the FRF measurements in parts over the partition. For example, with the case of a dual leaf partition with 8x8 grid, there are 64 measurement points and with 16 acceleration sensors, the measurement is 4 times longer than if 64 sensors were available. With 64 measurement points at spacing of ~10 cm, the accuracy of I-ASCA is limited to 1 kHz in this specific case. This gives an idea about the measurement time needed if one wishes to apply the I-ASCA method at higher frequency region. Unless the blocked forces can be measured directly, the method is quite time consuming. Hence, it would be apt to say that this method is more suitable for R&D purposes to identify the weak paths of sound insulation in specific cases with sound insulation ratings are highly non-representative of the sound transmission through the structure. An interesting example of this would be panels used in vehicle bodies (windows, doorframe, etc.) which could be hard to characterise using standard methods. The sound insulation of such panels is not easy to measure in-situ due to flanking from other

panels. Additionally, unlike building partitions, where the nature of sound insulation curves for typical single leaf and multi-layered partitions is well established, the panels in a vehicle body are complex in shape and construction and their sound insulation/transmission characteristics is not readily known. Therefore, the I-ASCA and I-PCA method would be really useful in such instances to not only predict the total sound transmission through the panel but to also quantify the diagnostic contributions in presence of flanking.

In conclusion, this chapter dealt with the application of I-ASCA and I-PCA methodologies for diagnosing airborne and structure borne sound transfer through a multi-layered partition. For a structure borne point excitation, it was shown that the blocked forces might be used to estimate the source location(s). Using the I-PCA methodology, it was seen that the point connection path overall has the highest contribution in the mid-high frequency region. This shows the potential of the method in diagnosing the different paths of the partition under a structure borne excitation. The paths were again diagnosed for an airborne excitation case and the point connection was again shown to be a dominant sound transmission path. It was observed that airborne flanking has to be minimal for a good pressure validation for airborne excitation case. In presence of flanking, an on-board validation test may be used instead to confirm the validity of the measurements and blocked forces. It was also observed that for airborne excitations, the diagnostic methods might be practical for small sized partitions (like windows) or else the measurement time would be enormous. Therefore, an investigation has to be made for reducing the measurement time of the methods which will be discussed in the next chapter with more case studies.

---

# 5

## DIAGNOSTIC TESTING FOR MULTI-LAYERED PARTITIONS – DIRECT APPROACH

---

*In the previous chapter, the application of the I-ASCA and I-PCA methods was presented a dual leaf partition consisting of a point connection. The diagnosis was performed for a structure borne and airborne excitation on the partition. To avoid airborne flanking issues, the tests were performed in a transmission suite where the SRI and diagnostic properties could be measured. The contributions of the point connection path were measured which highlighted the role of the point connection as dominant sound transmission path (sound bridge). This shows the potential of the methods in diagnosing the sound transmission paths in multi-layered partitions which effectively provides the spatial dependence of sound transfer. In this chapter, a critique of the methodology will be performed with respect to its practical application. Based on this, an investigation will be made into a simplified version of the method and a new methodology will be proposed. Validation of the concept and the application on the dual leaf partition will be presented.*

## 5.1 Practical considerations – measurement time

In I-ASCA, the measurement of blocked forces follows an inverse approach where the FRF measurements are combined with the operational measurements. The measurement process however is a slow and tedious task. If we compare the measurement phases, then the operational phase of acceleration measurement over the paths is quick. However, for the FRF measurement phase, two different FRF's are measured at the interface –the accelerances and vibroacoustic FRF's to the receiver volume positions. The accelerances in turn are measured as point and transfer accelerances. Therefore, for ' $n$ ' paths, there are ' $n$ ' accelerances to be measured for each path giving in total  $n^2$  accelerances. Additionally, there are  $n \times m$  number of vibroacoustic FRF's to be measured for ' $m$ ' microphone positions in the receiver room. Thus, the FRF measurement process is tedious and time consuming.

To illustrate this issue in practical terms, the case of I-ASCA on the dual leaf partition (Section 4.5) is considered. The partition tested in the study was sized .8m x .8m, discretised in an 8x8 grid, which gives 64 paths to be diagnosed. For every path, 64 accelerances had to be measured –hitting at one path (at its centre) with the force hammer and measuring the acceleration simultaneously at all 64 paths. Ideally, 64 vibration sensors were needed and accordingly a data acquisition system that can capture 64 signals at once. However, such capabilities were and are not usually available and hence the accelerance measurement was performed in parts as described in Section 3.5. With 64 paths, and capacity to measure 16 accelerances simultaneously for each path, the measurement time increased fourfold. Additionally, every accelerance measurement was averaged from two to three impact hits. The requirement for such a large number of accelerance functions combined with the limited availability of sensors and manual testing means that the approach is costly in terms of measurement time.

For the dual leaf partition study, an important objective was to diagnose the source and path contributions individually. To measure a source contribution, the blocked force on the path has to be measured. Following an inverse approach (Section 3.5), a single blocked force

cannot be individually measured; all blocked forces have to be measured. This required for FRF and operational measurements over all the paths even though the contribution of one path was of interest. This highlights the limitation of the I-ASCA in not providing a local solution (single source contribution) without measuring the whole structure. Additionally an inverse approach is highly susceptible to inverse errors, which means that the correct measurement of FRF's is critical and the measurement noise should be minimal.

If a common partition size of 3m x 4m were tested by this inverse approach, the measurement time would be enormous. To reduce the measurement time for such case, one possibility is discretising the partition in a coarse grid, however that would seriously restrict the frequency range of application. Therefore, for the method to be practical for real life structures it was required to refine the methodology in consideration with the following points: -

- 1) The method should be faster without sacrificing the grid size (or the frequency limit), and ideally no accelerance measurements are required.
- 2) The method should be able to provide a local solution i.e. the whole structure should not have to be tested for measuring few contributions.

The method should not be prone to inversion errors, possibly a direct approach may be more suitable.

---

### 5.1.1 Possible measures

---

Manual impact testing is the standard or direct test for measuring the accelerances and there is no indirect measurement available. One possible option is to measure accelerances over half of the paths and employ the principle of reciprocity to reduce the number of the transfer accelerances (see Figure 5.1). However, point accelerances still need to be measured for all the paths. Therefore by using the reciprocity principle, the measurement of structural FRF's cannot be skipped completely and no significant time advantage can be gained.

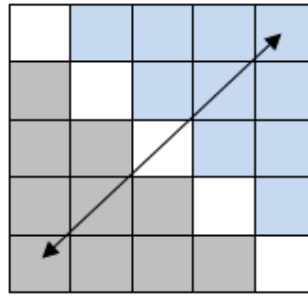


Figure 5.1: Reciprocity in the accelerance matrix for transfer accelerances, elements in either shaded region can be measured and be substituted for another

Another possible option is to exploit the physical symmetry of the structure to measure the FRF's. If the structure is symmetric, then the FRF's measured at symmetric DoF sets should be equal, which could provide further reduction in measurement time. However, in in-situ conditions, the boundary conditions are not guaranteed to be symmetric around the geometry, which makes it harder to exploit symmetry.

As an alternative, a method where accelerances are not required may be suitable from the point of view of time considerations. In the I-ASCA test, the accelerances are only required to find the blocked forces through an inverse approach. Therefore, one has to explore the possibility a direct measurement approach for blocked forces that does not require accelerance measurement. Following a direct approach, there would also be no chance of inverse errors. This would satisfy the requirements for the refinement outlined in previous section.

---

### 5.1.2 The airborne source

---

To examine the possibility of measuring the blocked forces directly, one has to first look at the nature of the source i.e. the airborne excitation. Let us consider a sound transmission scenario through a partition installed between a source room and the receiver room as shown in Figure 5.2. When an airborne source is activated in the source room, a reverberant sound field is established in the source room that forces the partition. Under steady state, the partition then transmits sound to the receiving room.

By modelling this dynamic system as a source receiver system, the pressure field in the source room that acts on the partition forms the source whilst the partition plus the receiving room forms the combined receiver structure. Note that the loudspeaker should be imagined as an internal driving mechanism of the source and not the actual source. A source-receiver-interface exists on the surface of the panel on the source room side.

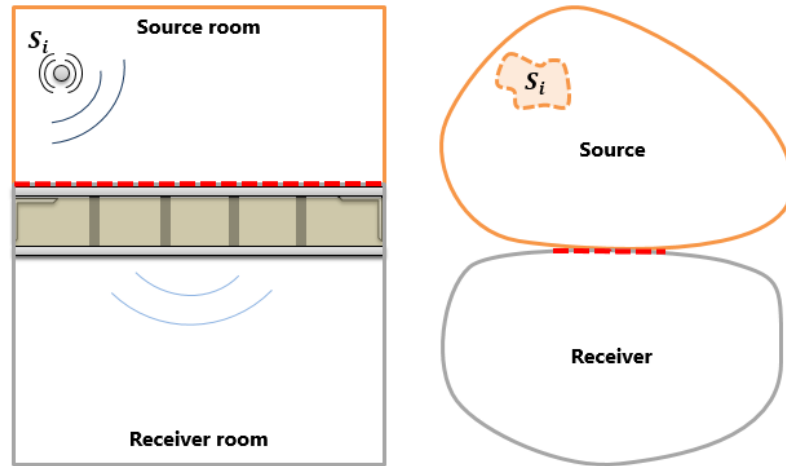


Figure 5.2: Sound transmission between source and receiver room (left) represented by an equivalent source-receiver model (right).  $S_i$  is the internal mechanism of the source. '---' represents the source-receiver-interface

## 5.2 Blocked pressure characterisation of airborne sources

The successful application of I-ASCA method lies in the accurate characterisation of the source quantity. In I-ASCA, a blocked force characterisation was adopted for airborne excitations on discrete paths. As the nature of the source is a pressure excitation, a corresponding characteristic quantity, the 'blocked pressure' can also be used. In definition, the blocked pressure of the airborne excitation is the pressure that it applies on a blocked interface [108]. Other studies in the literature utilise the concept of blocked pressure to describe the airborne field around the vibrating receiver structure [109] and in independent characterisation of airborne sources [110, 111]. If the interface is discretised, then the blocked pressure on a discrete path may be imagined as the blocked force per path area. Thus, the blocked pressure in principle should be measurable by using I-ASCA methodology.



To avoid the time consuming inverse methodology, a direct measurement approach for the blocked pressures seems more suitable. To explore the blocked pressure concept further, existing approaches from literature followed by novel measurement approaches for blocked pressure will be discussed in the following sections.

---

### 5.2.1 Blocked pressure measurement – classical definition

---

As per the classical definition of blocked forces, the forces applied by the source on a rigid (blocked) receiver are the blocked forces. Smith [108] has used this definition in formulating a relationship between the operational pressure acting on the partition and the blocked pressures of the source. These blocked pressures characterise the airborne excitation acting on the receiver. A simple relation between the operational pressure and the blocked pressure was derived in the study, which is given as,

$$p = p_{bl} + p_{rad} \quad (5.1)$$

In Eq. (5.1),  $p$  is the measured pressure at the partition face (or interface) when the source is operational,  $p_{bl}$  is the blocked pressure, and  $p_{rad}$  is the pressure radiated by the partition when the source is off but the partition is vibrating with a velocity field similar to that observed in operational conditions (see APPENDIX III). In the literature [128, 137, 138], a common finding/assumption is that the radiated pressure is usually negligible in practice. If that is true, then the blocked pressure may be approximately measured as the operational/contact pressures. However, an in-depth examination is required to check the validity of this approximation for the case of airborne excitation on partitions. Blocked pressure measurement – contact pressure approach

To formulate a blocked pressure measurement methodology for the case of airborne excitation on building partitions, we will attempt to express the blocked pressures in terms of an impedance formulation in the same way as the blocked forces (Eq. (3.2)). Consider the case from Figure 3.8 where the partition is discretised into ' $j$ ' patches and subjected to airborne excitation. By applying the I-ASCA method, the source field can be characterised by

' $n$ ' blocked forces over ' $n$ ' discrete paths of equal area ' $dS$ '. The blocked forces are then obtained as,

$$f_{bl} = [A]^{-1}a' \quad (5.2)$$

The same blocked forces can also be written as,

$$\{f_{bl}\} = [Y]^{-1}.\{v'\} \quad (5.3)$$

$$\{f_{bl}\} = [Z_c].\{v'\} \quad (5.4)$$

$Z_c$  represents the impedance of the coupled source receiver system at the interface. Like an FRF it also describes the input-output relationship of the system. As the source (air) is not disconnected from the partition during the mobility (or accelerance) measurements, the impedance matrix obtained is a combined impedance of the source (air) and receiver (partition with receiver volume). Hence, the coupled impedance can be broken down into individual impedances of the source (air) and the receiver in this case as,

$$Z_c = Z_p + Z_{air} \quad (5.5)$$

In Eq. (5.5),  $Z_p$  represents the in vacuo impedance of the receiver (partition + receiver room) which could in principle be measured if the source (air) is disconnected from the receiver (partition). It can be recalled that similar exercise is adopted in classical TPA techniques where a structural source can be disconnected from the receiver for the mobility measurements, which on inversion gives the receiver impedance.  $Z_{air}$  represents the mechanical impedance of air at the interface. Eq. (5.5) can now be expanded as,

$$\{f_{bl}\} = [Z_p].\{v'\} + [Z_{air}].\{v'\} \quad (5.6)$$

In classical TPA, when the receiver impedance is combined with the operational responses on the source receiver interface, the forces obtained are the contact forces applied by the active source on contact with the receiver [119, 148]. Then, the first term in Eq. (5.6) corresponds to a case of classical TPA approach where the *in vacuo* receiver impedance is

combined with the operational responses. Hence, it should represent the contact forces ( $f_c$ ) of the airborne excitation on the partition.

$$\therefore \{f_c\} = [Z_p] \cdot \{v'\} \quad (5.7)$$

Hence, Eq. (5.6) can be written as,

$$\{f_{bl}\} = \{f_c\} + [Z_{air}] \cdot \{v'\} \quad (5.8)$$

The  $Z_{air}$  term refers to the mechanical impedance ( $Nm^{-1}s$ ) and not the acoustic impedance ( $Pa.s.m^{-3}$ ). For fluids like air, the acoustic impedance (ratio of pressure at a point in the acoustic volume to the volume velocity of a source exciting the volume) is easy to measure or can be computed by means of FEM/BEM methods, however it is not consistent with the units of mechanical impedance and cannot be used for  $Z_{air}$ .

In building acoustics applications, the mechanical impedance of the partition (solid structure) is far higher than air (fluid), i.e.  $Z_p \gg Z_{air}$ . Therefore, the product  $[Z_{air}] \cdot \{v'\}$  is likely to be negligible in comparison to  $\{f_c\}$ . However, in the case of a very thin and light structure (e.g. a thin membrane/film of plastic), this would not be the case as the mechanical impedances of the air and structure could be comparable. Then, by neglecting the second term of Eq. (5.8), it can be seen that the blocked forces are approximately equal to the contact forces.

$$f_{bl} \approx f_c \quad (5.9)$$

Dividing both sides with the path area ' $dS$ ' we get,

$$p_{bl} \approx p_c \quad (5.10)$$

where,  $p_c$  is the contact pressure. Eq. (5.10) then shows that for the case of airborne excitations, the contact pressures are approximately equal to the blocked pressures. These contact pressures are nothing but the operational pressures that can be measured directly by placing a microphone against each path, and be substituted for blocked pressure. Such

direct approach is then simpler and will be much quicker than a blocked force characterisation, which requires extensive FRF measurements.

As we are approximating the blocked pressures by the operational pressure, this introduces an uncertainty in the blocked pressure measurement. This uncertainty is equal to the difference between exact and approximate blocked pressures. Note that the exact blocked pressures can be obtained on dividing Eq. (5.8) with the path area on both sides, but cannot be measured as  $Z_{air}$  is not known.

Although, we can conveniently use the approximation (Eq. 5.10), a practical determination of the uncertainty is important. Therefore, an alternate derivation of exact blocked pressures will be derived in the next section, which would allow for the practical calculation/measurement of this uncertainty.

---

### 5.2.2 Blocked pressure measurement – boundary value problem approach

---

To derive an exact relationship for blocked pressures, an approach comparing the solution of a forced system to the response under the action of blocked forces can be investigated. Bobrovnitskii [132] outlined a general theorem<sup>3</sup> for the solution to this forced vibration problem, which can be stated as follows,

*“The forced vibrations of the system can be represented in the form of the sum of two components, which are the solutions of two simpler auxiliary boundary-value problems. The first component is the field of vibrations of the isolated (separated or blocked along  $S$ ) subsystems under the effect of preset external forces. The second component represents the forced vibrations of the junction of the subsystems, where the external forces are taken equal to zero and only the reaction forces obtained in solving the first auxiliary problem act at the surface  $S$ .”*

Let us consider ‘a’ and ‘b’ as the two subsystems coupled at an interface ‘S’ (Figure 5.3, left). Let  $\phi_a$  and  $\phi_b$  be the external forces or the sources acting in the subsystems ‘a’ and ‘b’

---

<sup>3</sup> A full derivation of the theorem can be found in APPENDIX IV

respectively, which result in responses  $u$  and  $v$  respectively. The solution for this problem can be broken down as solutions to two simple auxiliary problems as,

$$\begin{aligned} u &= u_0 + u_1 \\ v &= v_0 + v_1 \end{aligned} \quad (5.11)$$

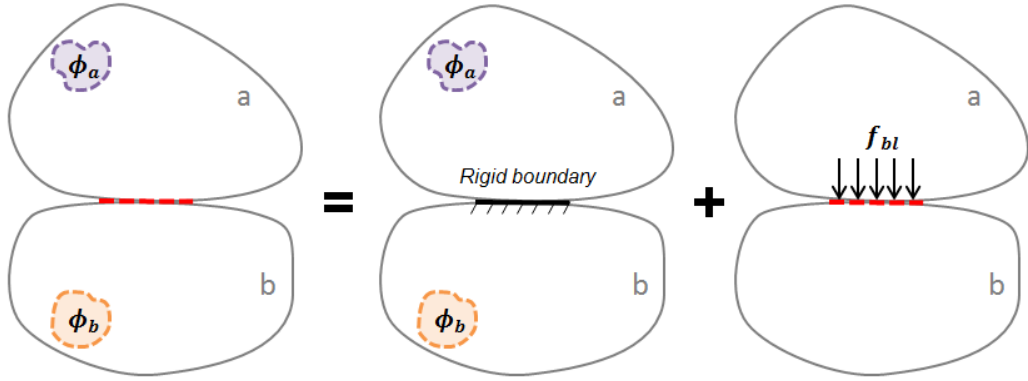


Figure 5.3: Representation of the forced vibrations of a system (left) as a resultant of boundary value problems -1) system with active source and blocked interface (middle) and 2) system with inactive source and blocked forces acting at interface (right)

In Eq. (5.11), responses  $u_0$  and  $v_0$  are solutions to the first problem under the action of external stresses when the interface 'S' is blocked. Responses  $u_1$  and  $v_1$  are the solutions to the second problem when the source is switched off and the blocked forces act at interface 'S'. This theorem can be applied to a source receiver system in TPA analysis, where external stresses (or forces) are only present in the one subsystem (source). In that case, the receiver response can be written as,

$$v = v_0 + v_1 = v_1 \quad (5.12)$$

In Eq. (5.12),  $v_0$  is zero for the receiver as there is no external excitation acting in the receiver when the interface is blocked. Then Eq. (5.12) shows that the response of the receiver under the action of an active source ( $v$ ) is equivalent to the response of the receiver under the sole action of blocked forces acting at interface 'S' ( $v_1$ ). In principle, similar analysis could be applied to acoustic/vibroacoustic systems for the solution of acoustic responses at the interface in terms of the blocked acoustic response (i.e. blocked pressure).

### 5.2.3 Extension to cavity subsystems

Let us now consider the case of two cavity subsystems –Source Room (SR) and Receiving Room (RR) coupled at the interface ‘S’ which lies at the boundary of the partition which radiates sound in the receiver room (see Figure 5.4). An active airborne source (for ex. volume velocity source or loudspeaker) excites a sound field in the source room. Under steady state operational conditions, the sound field in source room excites the partition, which in turn radiates sound to the receiver room. Then, our objective is to find an exact relationship for blocked pressures at the interface ‘S’ following Bobrovnskii’s theorem.

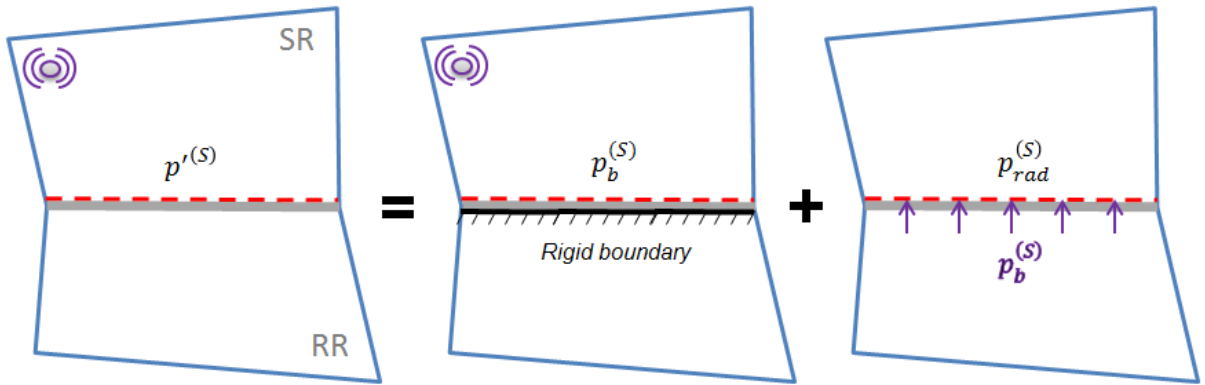


Figure 5.4: Forced acoustic response of the system (left) as a resultant of two auxiliary problems (middle and right). Quantities in purple denote the source in each problem. ‘---’ is the source-receiver-interface

As per the theorem outlined in the previous section, the forced response of the system can be written as a sum of the response when source is active (and the interface is blocked) plus the response under the action of blocked reactions (blocked pressure) acting at the interface ‘S’. As we are dealing with cavity systems with an acoustic excitation, the response of the system can be written in acoustic (pressure) terms. As we are interested in finding the blocked pressure at the interface, we will focus our analysis to the solution at interface ‘S’. Similar to Eq. (5.12), the operational/contact pressure response at ‘S’ can be written as,

$$p(S) = p_0(S) + p_1(S) \quad (5.13)$$

In Eq. (5.13),  $p_0(S)$  and  $p_1(S)$  are the respective solutions to the two auxiliary boundary value problems -1) when the source is active and the interface is blocked, and 2) when the source is inactive and blocked pressures act at 'S'. For the first problem, as the interface is blocked, the pressure observed there would be the blocked pressure. Then Eq. (5.13) can be written as,

$$p = p_b + p_1 \quad (5.14)$$

For brevity, we have omitted the bracket notation (S) and the terms presented in the current analysis are determined at the interface 'S'. Under operational conditions, the operational pressure  $p(S)$  at the interface can be written as,

$$p = p_i + p_r + p_{rad} \quad (5.15)$$

In Eq. (5.15),  $p_i$  and  $p_r$  are the incident and reflected pressures arising from the incident waves and reflected waves from the partition.  $p_{rad}$  is the pressure radiated by the vibrating partition back into the source room under the action of the source field (made up of incident and reflected pressure) and used here for rigor. Note that this  $p_{rad}$  term is same as the radiated pressure term defined in Section 5.2.1. In both cases, it is the pressure radiated by the partition when it vibrates with operational velocity amplitude. In majority of SRI prediction models, this term is not accounted as the acoustic response (radiation) from the partition to the receiving room (not source room) is desired. In addition, studies [128, 137, 138] can be found which neglect this term for partitions excited by airborne sound due to its negligible value.

As discussed in previous Section 5.2.3, the vibration field at the interface (and the partition) under the action of the source is the same as when blocked forces act at the interface. If that is true, then the pressure radiated by the partition (because of vibrations) under the action of source will be same as when the blocked pressures act at the interface. However, the acoustic response of the receiver (partition) when a blocked pressure acts at the interface is  $p_1$  according to Eq. (5.13).

$$\therefore p_1 = p_{rad} \quad (5.16)$$

Eq. (5.13) can then be written as,

$$p = p_b + p_{rad} \quad (5.17)$$

Comparing Eq. (5.15) and Eq. (5.17), at interface 'S' we get,

$$p_i + p_r + p_{rad} = p_b + p_{rad} \quad (5.18)$$

$$\therefore p_b = p_i + p_r$$

Thus, the blocked pressure of the source is the sum of incident and reflected pressure at the interface. Note that this is not the total contact pressure that would be measured in operational condition. We can see that the contact pressure according to Eq. (5.16) would be,

$$p = p_i + p_r + p_{rad} = p_b + p_{rad} \quad (5.19)$$

Interestingly, we have reached a similar formulation as to that derived in Section 5.2.1. This provides confidence in the analysis presented here. As the radiated pressure is a result of the vibration of the partition under the action of source or blocked pressure at the interface, it can be calculated using the I-PCA methodology as,

$$p_{rad} = \{U\}\{v'\}dS = \{f_{bl}\}\{H\} \quad (5.20)$$

Eq. (5.19) is an exact derivation for the blocked pressure measurement if the contact pressure ( $p$ ) and the radiated pressure (Eq. (5.20)) can be measured. If the blocked pressures are approximately measured as the contact pressures, then Eq. (5.20) quantifies the difference between exact and approximate blocked pressures, or in other words the uncertainty of the approximate measurement.

An interesting finding of Eq. (5.18) is that the blocked pressures are the sum of incident and reflected pressures, which also forms the airborne source field. A conceptual way to understand blocked pressures is that it is a reaction pressure (or force) required to stop the



movement of the source at the interface. In our case, if we apply an equal and opposite phased pressure to the incident plus reflected pressure at the interface, the net pressure on the interface (and the partition) will be zero and the response of the partition will be zero (similar to blocked condition,  $p_b = -(p_i + p_r)$ ). This follows from the principle of superposition of pressure sources that implies if two pressure sources equal in magnitude and opposite in phase act on a point/surface, then the net pressure acting at the position will be zero. Thus, we can see that the blocked pressures obtained in Eq. (5.18) stay consistent with the definitions of blocked pressure.

As a final comparison, three different approaches were outlined for blocked pressure measurement, which suggest that the blocked pressures on the interface can be approximated by the contact pressure if one neglects the residual terms ( $p_{rad}$ ). Experimental case studies will be discussed later to discuss the validity of this argument and measurement of radiated pressure.

---

### 5.3 Transferability of the blocked pressures

---

An important property of the blocked forces or pressure is that it is independent of the receiver structure and is proved rightly so for the case of structure borne sources [148, 149]. An additional advantage that is gained by an independent characterisation is that the blocked forces of the structure borne source are transferable. Thus, if one were to physically remove the source and couple it to a different receiver, then the blocked forces would remain same. Here we will examine the transferability of blocked pressures for airborne excitations to different receivers, or in other words, to examine if an airborne source field remains constant with the change in the receiver structure. Consider a panel as shown in Figure 5.5, which responds to a source field consisting of incident and reflected pressures. If we want to have an independent source quantity irrespective of the receiver structure then the physical source field should remain the same.

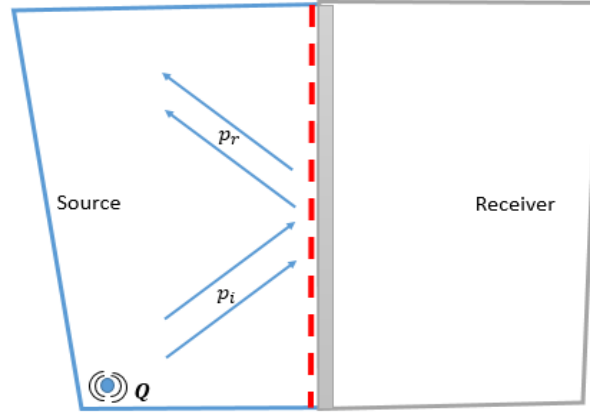


Figure 5.5: Airborne sound field in the source room comprising of incident ( $p_i$ ) and reflected ( $p_r$ ) pressures acting on the panel,  $Q$  is the volume velocity excitation that represents the internal driver of the source, '---' is the source-receiver-interface

Keeping in mind Eq. (5.18) describing the blocked pressure, we examine the following three cases. In each of the cases, the internal source driver location and strength will be unchanged.

- I. For a nearly acoustically transparent panel ( $Z_p \approx Z_{air}$ ), having negligible sound insulation, the reflected pressure is negligible and the total pressure in the source field is then similar to the incident pressure. Therefore,  $p_b \approx p_i$ .
- II. For a panel with finite sound insulation ( $Z_p > Z_{air}$ ), the reflected pressure is not negligible and the total pressure in the source field is then made up of the incident plus the reflected pressure. Therefore,  $p_b = p_i + p_r$  and  $p_r < p_i$ .
- III. For a heavyweight panel, ( $Z_p \gg Z_{air}$ ), which can be considered close to a blocked panel, the sound insulation is very high and the reflected pressure is almost equal to the incident pressure ( $p_i \approx p_r$ ). In this case, the source field is then almost equal to twice the incident pressure. Therefore,  $p_b \approx 2p_i$

Thus, we can see that without changing the driver of the source, the source field was affected by the change in the receiver structure. This is because the source field is made up of the direct field from the driver plus the reverberant field from wall and panel reflections. The direct field practically would remain constant, but the reverberant field changes due to change in the panel (receiver) as each panel reflects differently.

Therefore, it appears that the source (and the blocked pressure) in the airborne excitation case is not exactly transferable to different receiver structures unlike structure borne sources where the receiver does not change the source. Thus, we will have to characterise the airborne source field for each receiver, as the source will not remain the same for different panels. It is also important to note that airborne source characterisation is not the sole objective of the work presented here. We are interested in measuring the diagnostic contributions of partitions and airborne source characterisation is an important step to achieve the same.

---

### 5.3.1 A note on definitions

---

The classical definition of the blocked pressure is the pressure applied by the source on a blocked receiver. Thus according to this definition, the blocked pressure is equal to twice the incident pressure (see case III in previous Section 5.3). In the other two cases, the source driver was unchanged, but by changing the receiver, the blocked pressure did not stay equal to twice the incident pressure. Therefore, the classic definition of blocked pressure is not consistent and may be confusing.

A more consistent way of describing blocked pressures for all the cases above is that it is the pressure that is required to apply at the interface to block the motion of the source ( $p_b = -(p_i + p_r)$ ). When a pressure equal and opposite to the source pressure ( $p_i + p_r$ ) is applied, then the net pressure acting on the interface will be zero and the interface motion will be restricted (similar to blocked condition). According to this definition, the blocked pressures obtained in the three scenarios earlier seem conceptually sound.

---

## 5.4 Direct – Airborne Source Contribution Analysis (D-ASCA)

---

As discussed in Section 5.2.2. and 5.2.3, in the case of building partitions subjected to airborne excitation, the blocked pressure at the interface can be approximated by the contact pressure at the interface. As opposed to I-ASCA where the source is inversely characterised, the source here is characterised directly by measuring contact pressures. In

principle, it would be possible to measure source contributions using the contact pressures. Therefore the new approach will be named as Direct-Airborne Source Contribution Analysis (D-ASCA). The following two measurement phases form the D-ASCA methodology,

- i. FRF measurements – Here, the vibroacoustic FRF's will be measured as per Eq. (3.6) from the interface (patches) to receiving points in the receiver.
- ii. Operational measurements – In this phase, the contact pressures will be measured first  $\{p_c'\}$  which will be used for the blocked pressures (Eq. (5.10)). The pressures at receiver positions will also be measured for validation and diagnosis (see schematic below).

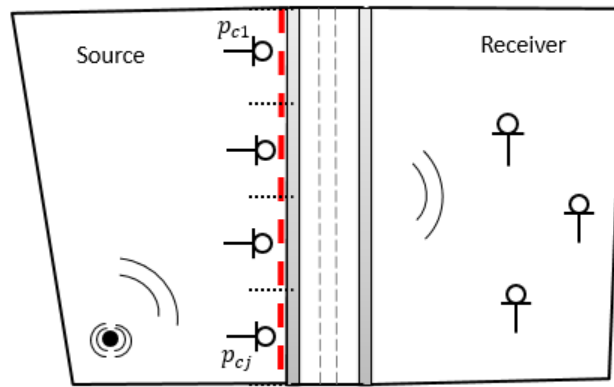


Figure 5.6: D-ASCA methodology schematic showing operational measurements of contact pressures close to the interface ( $p_c$ ) and pressures in receiver for validation and diagnosis

For direct approach, the contact pressures are to be measured on the surface of the panel. Ideally, the microphones should be placed touching the surface however that will cause some loading on the panel. A small clearance between the microphone and panel is therefore desirable. This will cause a phase mismatch error in contact pressure measurement at frequencies where the clearance is comparable to wavelength. This is because the phase of the pressure at the surface and the phase of the pressure at a clearance distance may be different depending on frequency of the wave as well as the incidence angle. However, for small clearances ( $<1$  cm), such error will be negligible except at very high frequencies. Therefore a standard 0.5 – 1 cm clearance has been used for D-ASCA case studies in the current work.

To test the validity of such a direct measurement of source characterisation against an inverse measurement approach the case of dual leaf partition with box assembly (Section 4.4) was chosen. In that test, by applying I-ASCA, the blocked forces were found by the inverse approach. Although the pressure validation was not possible in that case due to the flanking issues, we could still compare the blocked pressure (blocked force/patch area) with the contact pressure.

Thus, microphones were placed close (0.5 cm) to randomly chosen patches on the source side and the steady state pressure was measured. Figure 5.7 shows the contact pressures plotted with the inversely measured blocked pressures on the respective paths for comparison.

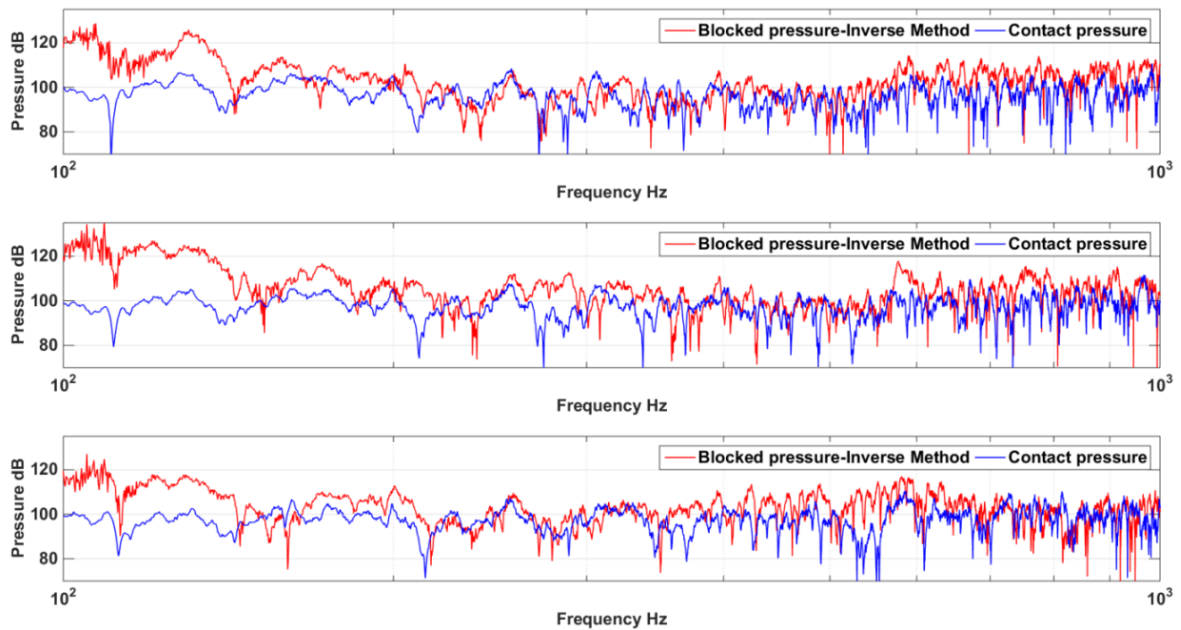


Figure 5.7: Comparison of measured contact pressure and blocked pressure on dual leaf partition for I-ASCA test described in Section 4.4. Blocked pressure was measured inversely as blocked force/path area. Contact force measured by placing microphones close to the patches

From Figure 5.7, it is clear that for this case, the contact pressures measured on the top of the panel did not match with the blocked pressures. A possible reason for this is that the airborne flanking also excited the partition from the bottom. This is equivalent to having the source field and source-receiver-interface around the panel as shown in Figure 5.8 (right).

Then the net contact pressure for such case will be the resultant of the pressures around the interface.

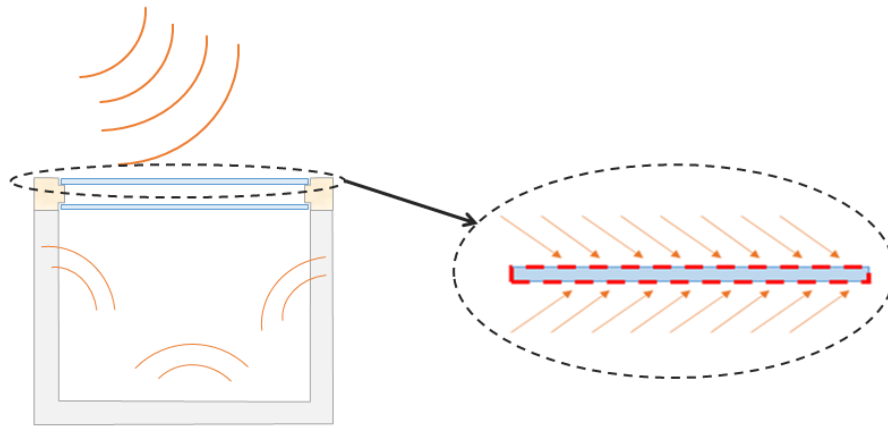


Figure 5.8: Direct and airborne flanking sound incident on the partition (left), magnified view of the top panel showing the source (orange arrows) and source-receiver-interface (---) around the top panel (right)

For the dual leaf partition (Figure 4.2), only one contact pressure component could be measured from the top, the other component (from below the path) was impossible due to inaccessibility. To compare the blocked and contact forces for such case, a similar case had to be examined where the airborne source is present around the panel and all sides around the panel are accessible for contact pressure measurements. An unbaffled panel excited by airborne source formed an ideal test case to verify this. In such a case, the exciting field is present around the panel and all interfaces are accessible for measurements as illustrated in the Figure 5.9 below.

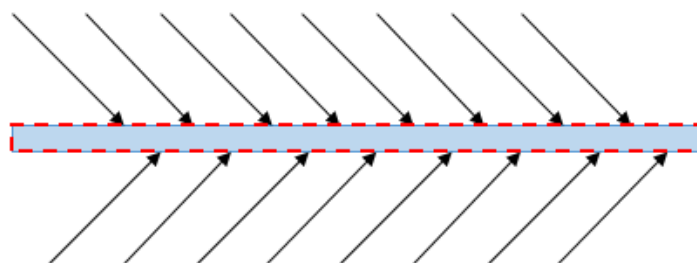


Figure 5.9: An unbaffled panel excited by airborne field on both sides (represented by arrows), '---' is the source-receiver-interface which is present around the panel

### 5.4.1 Blocked pressure measurement on unbaffled panel

The unbaffled panel is a case where airborne excitation (and the interface) exists around the panel (like Figure 5.9). We will now investigate if the net contact pressure closely approximates the blocked pressure (blocked force/path area) for such a case. Notice that this test was performed in complement to the test in previous section to investigate if the contact pressures measured around the path approximate the blocked pressures when the excitation is present on both sides of the panel. The unbaffled panel ( $35 \times 35 \text{ cm}^2$ ) shown in Figure 5.10 was chosen for this purpose. The panel is supported by resilient elements at corners to closely represent free-free mounting conditions. To measure the blocked and contact pressure, the following measurement steps were performed,

- 1) At first, conventional I-ASCA testing was applied to the panel. The panel was discretised in total 25 patches ( $7 \times 7 \text{ cm}^2$  each) and accelerances were measured by impact testing. For operational phase, a loudspeaker driven by pink noise excitation was used as a source, which simulates an airborne excitation around the panel. The measured operational accelerations were referenced to the voltage of the loudspeaker.
- 2) Keeping the loudspeaker unchanged, the contact pressure around all patches was measured. The measurements were performed by placing a microphone close to the surface ( $0.5\text{-}1 \text{ cm}$ ) of each patch.

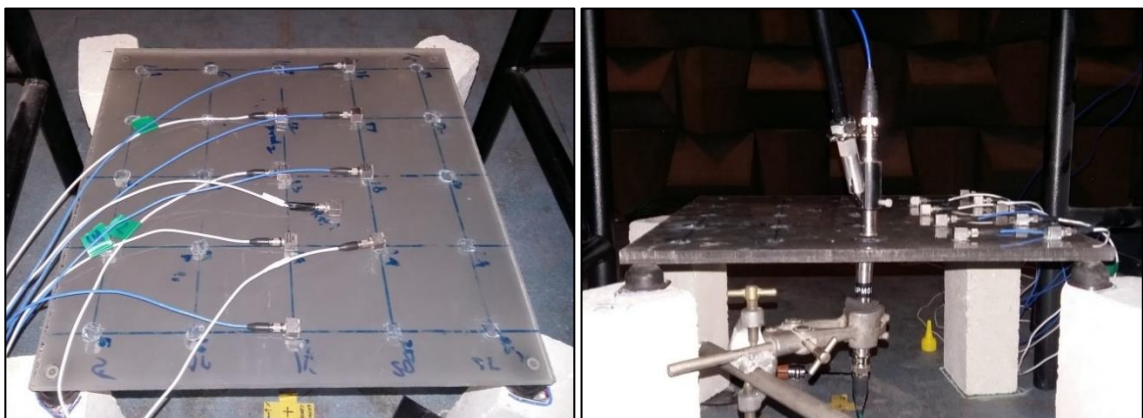


Figure 5.10: Measurements on the unbaffled panel (left) as per I-ASCA (left) and D-ASCA (right).

The contact pressure is measured above and below the panel as seen on right graphic

At first, as per Eq. (3.8) the blocked forces were calculated inversely. The exact blocked pressures for these paths were simply obtained by dividing the blocked forces with the patch area  $dS$ . Next the net contact pressure was measured on each patch as,

$$p_{c,n} = (p_{top,n} - p_{bottom,n}) \quad (5.21)$$

$$f_{c,n} = (p_{top,n} - p_{bottom,n})dS$$

where,  $p_{c,n}$  and  $f_{c,n}$  is the net contact pressure and contact force acting on a patch 'n' as a result of the pressure difference between top of patch ( $p_{top,n}$ ) and on the bottom ( $p_{bottom,n}$ ). Next an on-board validation test (Eq. (4.3)) was used to validate the methods by comparing the measured response at a reference point and the predicted response at the same point. The prediction was made using blocked forces and contact forces and so the force term in the Eq. (4.3) was modified as ( $Force = Pressure \times area$ ). The validation results comparing measured and predicted acceleration at a reference point are shown in Figure 5.11.

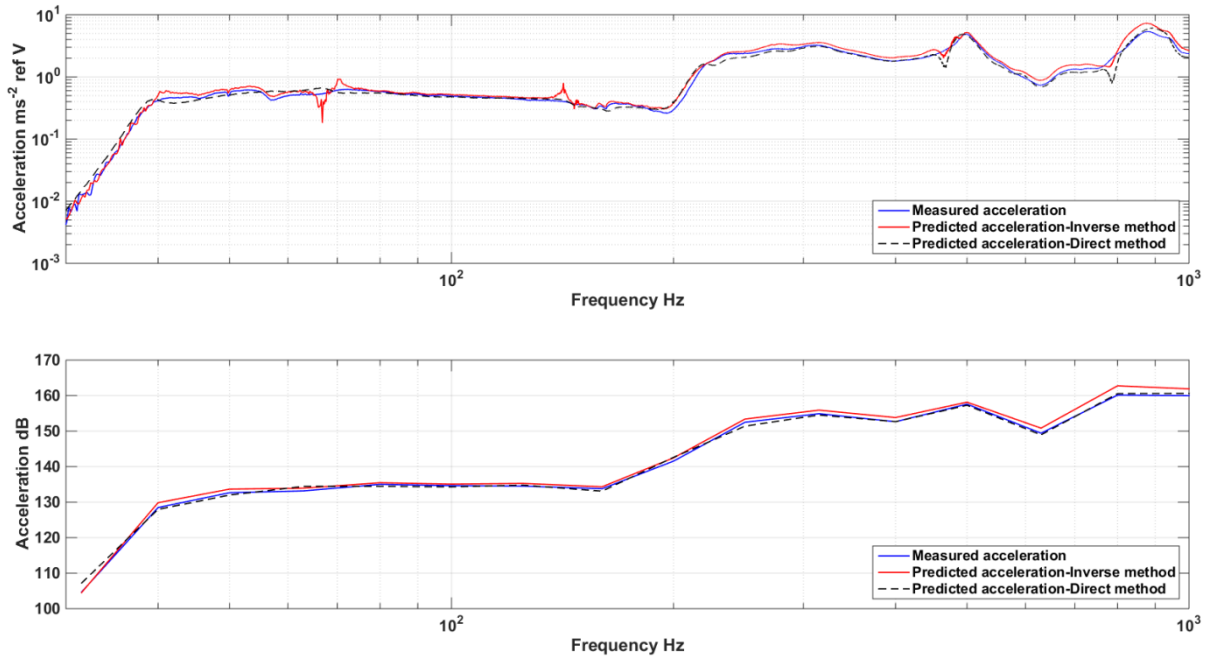


Figure 5.11: On-board validation showing comparison of measured and predicted acceleration response using inversely measured blocked pressure and directly measurement contact pressure in narrow band (top plot) and third octave band (bottom plot)

Figure 5.11 shows excellent prediction for the reference point acceleration, using both blocked pressures (within 2.5 dB) and contact pressures (within 1 dB) above 50 Hz. The



results here are shown till 1000 Hz above which there are some inversion errors in the prediction using blocked pressures (inversely measured) but the contact pressure prediction is within 1 dB till 2500 Hz one-third octave band and does not show any such errors throughout the measured frequency range. This shows the robustness of the contact pressures to predict the response far better than an inverse measurement. The comparison between individual blocked pressure and contact pressure is also made for three random paths on the panel as shown in Figure 5.12.

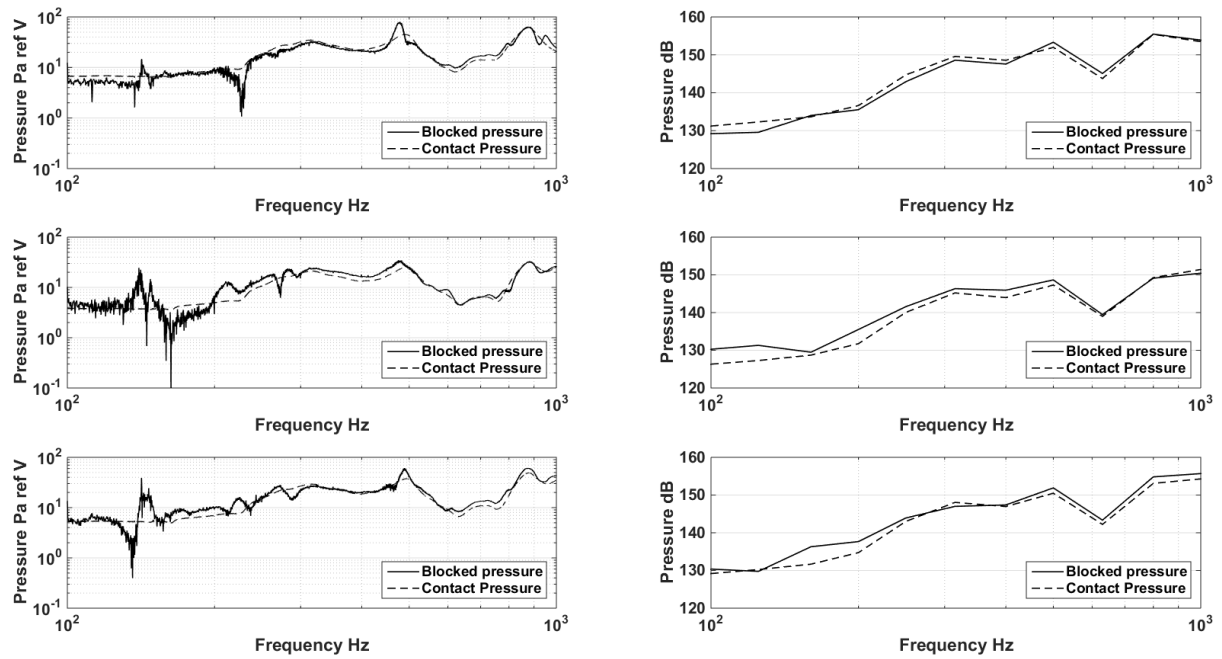


Figure 5.12: Blocked pressure (measured inversely) and contact pressure (measured directly) comparison over three paths of the un baffled panel in narrow band (in left column) and one-third octave band (in right column)

In Figure 5.12, the comparison between the blocked pressure and the contact pressure shows that the prediction above 200 Hz band is generally well (within 2-3 dB). At the low frequency end, the blocked pressure contains some inversion errors and is noisy as can be seen in the narrow band in comparison with the contact pressure which exhibits a smooth spectrum. The contact pressure spectrum is smooth and generally free from noisy artefacts due to better SNR and no inversion errors are present as the measurement is direct. However these results are a good proof to show that for measuring the net contact pressure on a path, the interface should be completely accessible. For the case described in Section

5.4, the interface was not completely accessible, as part of excitation was from cavity side due to flanking (and is inaccessible). This explains the disagreements from Figure 5.7, because the net contact pressure was not measurable.

Next as per Eq. (5.19), we can see that the difference between the blocked pressure and the contact pressure is the radiated pressure. While the radiated pressure is likely to be negligible for the case of building partitions ( $Z_p \gg Z_{air}$ ), the measurements for radiated pressure were conducted for the sake of completeness. The radiated pressure is a result of the vibrations of the panel and can be measured as per Eq. (5.20) using blocked forces and the vibroacoustic FRF's at source DOF. As the blocked forces were measured in this study, the vibroacoustic FRF's were measured for three positions above and below the paths. The results of the radiated pressure in comparison to the blocked pressure are shown in Figure 5.13.

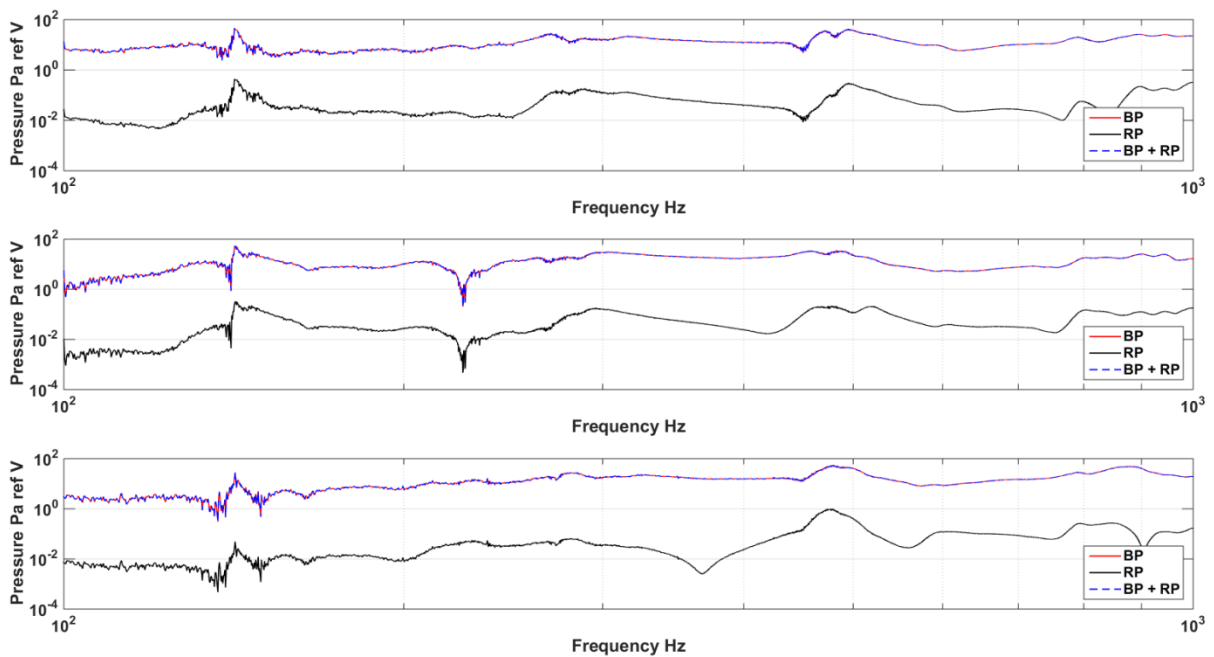


Figure 5.13: Blocked Pressure (BP, measured inversely, in red) compared to net Radiated Pressure (RP, in black) at three different paths in narrow band

Figure 5.13 shows firstly that the radiated pressure is negligible in comparison with the blocked pressure which was expected. Secondly, it shows that the sum of the blocked and the radiated pressure is equal to the blocked pressure (due to the radiated pressure being

negligible). According to Eq. (5.19), this sum is nothing but the contact pressure which can be measured directly. This result along with the results from Figure 5.11 and 5.12 shows that the contact pressure is almost equal to the blocked pressure for cases of building panels or partitions excited by airborne sound.

---

#### 5.4.2 Direct blocked pressure measurement – baffled panels

---

In the previous section, it was shown that for unbaffled panels, the net contact pressure very well approximates the inversely measured blocked pressure. However, unbaffled panels are not representative of actual building constructions. Most of the building partitions have a boundary condition which is either fixed, simply supported or a combination of both. So we now want to confirm the validity of the contact pressure approximation for such partition. To investigate this, a baffled single leaf panel could be tested. This was possible with the box assembly (Figure 5.14). Although, in this case, the panel is just attached at the edges of the box, the case still is a representative of panels in a baffle because in both cases the edge boundaries are supported/fixed. The discretisation of the panel is also shown in Figure 5.14.

At first, using I-ASCA, the blocked forces were measured for 64 paths (8x8 grid). Next, the contact pressure was measured by placing calibrated microphones above the panel. The measurements had to be done on the source side (above the panel) only as the interface exists above the panel (by considering negligible flanking). The contact force was also obtained by combining the contact pressure with the path area.

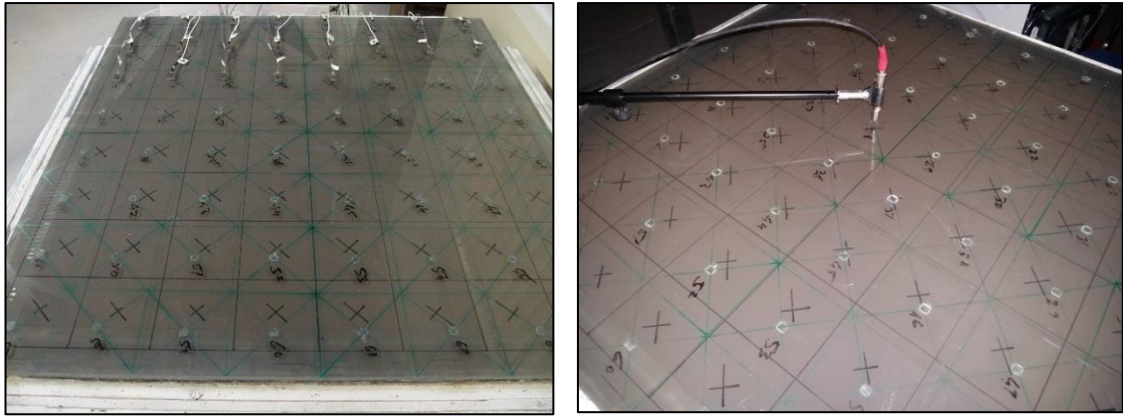


Figure 5.14: Discretisation (left, in green) on the single panel with the accelerometers placed on paths for I-ASCA measurements, and contact pressure measurements with a microphone close to the paths (right)

To test the validity of blocked and contact forces, a pressure validation was performed. The results of the pressure validation are shown in Figure 5.15.

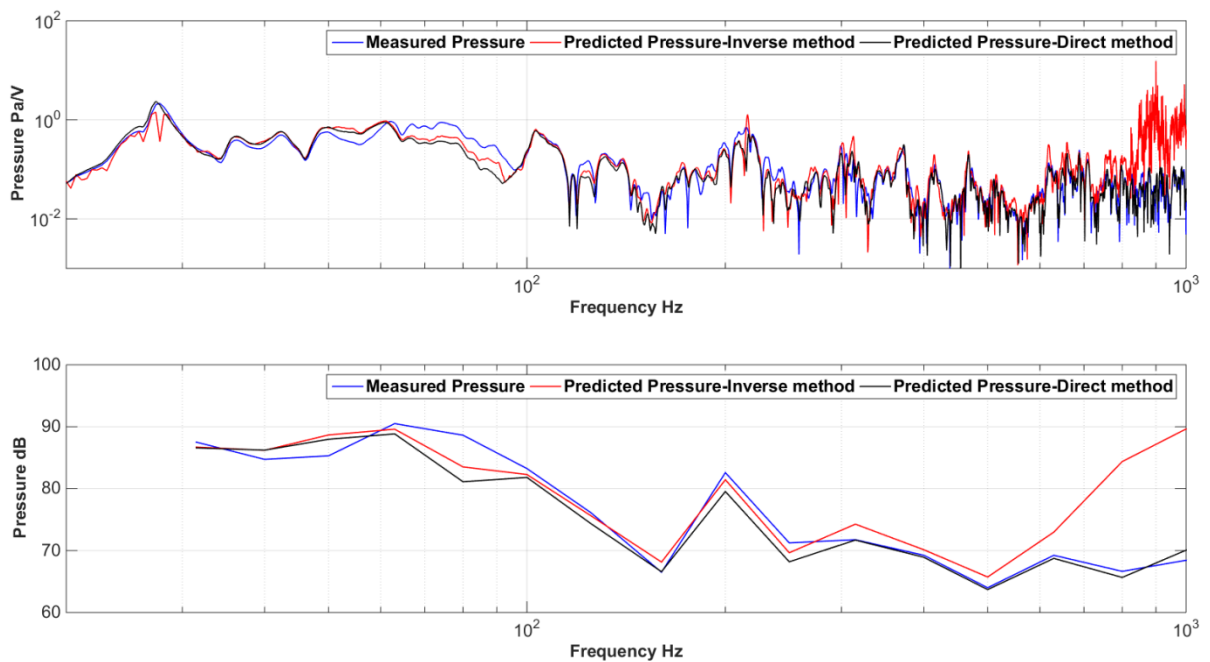


Figure 5.15: Pressure validation results for inverse method (blocked forces) and direct method (contact forces) comparing the predicted pressure and measured pressure in narrow band (top plot) and one-third octave band (bottom plot)

In Figure 5.15, it can be seen that the pressure predicted by inversely measured blocked forces is within 3.6 dB with the measured pressure except in the region ( $>650$  Hz and 63-100 Hz region), where the deviation is higher. The narrow-band spectrum above 650 Hz

exhibits sharp peaks indicating inversion errors. On closer analysis, it was revealed that the condition number of the accelerance matrix in the region was high (order of  $10^3$ ), which indicates the possibility of inverse errors thereby causing the mismatch above 650 Hz. In the region of 63-100 Hz, the mismatch is due to flanking as previously seen with the same box cavity (Section 3.5.1). On the other hand, the prediction from contact forces is within 3 dB of the measured pressure up to about 1000 Hz except in 63-100 Hz region due to flanking. As there is no inversion involved using a direct approach, any inverse errors are out of question.

Therefore, as far as predicting the total airborne sound transfer is concerned, the choice of contact pressures seems favourable than using an inverse approach as the accuracy of prediction is better than inverse approach. Next, we can also compare the blocked pressures measured by inverse and direct approach to see if they match well. A comparison for blocked pressures on four different paths is shown in Figure 5.16.

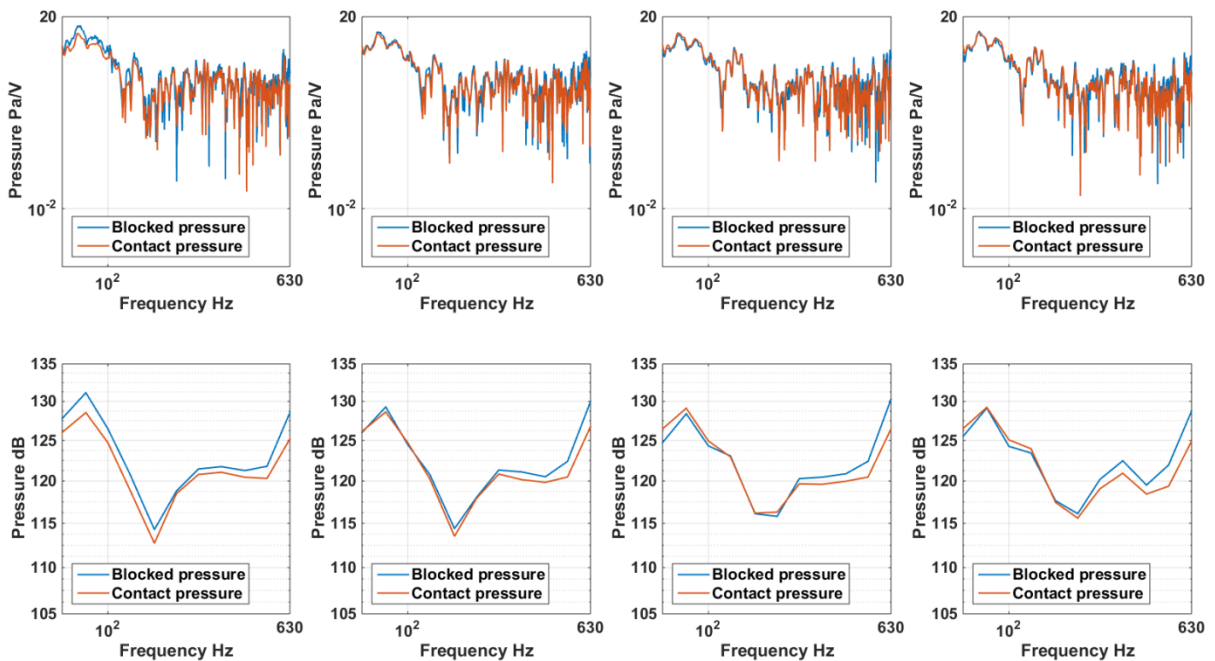


Figure 5.16: Comparison between Blocked pressure and Contact pressure for four randomly chosen paths of the baffled single leaf panel under airborne excitation in narrow band (top row) and one-third octave bands (bottom row) in 63-630 Hz

Figure 5.16 shows that general agreement between the blocked pressures (measured inversely) and the contact pressures (measured directly) is within 3 dB in the range 63-630 Hz. Results above 630 Hz are not shown as the blocked pressure contains inversion errors there. Along with the pressure validation, these results highlight the efficacy of a direct measurement over inverse measurement for source characterisation. It is also clear that using a direct approach removes the possibility of inversion errors. This study shows that for baffled panels, the directly obtained contact pressure may be used to approximate the exact blocked pressures of the source.

---

## 5.5 D-ASCA for multi-layered partition case

---

It is now of interest to test the application of D-ASCA (employing directly measured blocked pressure) for measuring the diagnostic contributions. For this study, the dual leaf construction as shown in Figure 4.17 was tested in the transmission suite.

As the blocked pressures were to be measured directly, the test did not involve any accelerance measurements which are otherwise required for I-ASCA application. Only vibroacoustic FRF measurements were performed so that pressure validation and the diagnostic contributions to the receiver can be measured. Due to the nature of the environment, which is highly reverberant, it was hard to maintain a good coherence between different hits for the vibroacoustic FRF measurements.

For the operational test, a loudspeaker driven with pink noise excitation was used. The loudspeaker was again placed facing the corner of the source room. In steady state, a near diffuse field is created in the source room which acts on the partition. To measure the blocked pressure directly, the contact pressures are required. An array of eight mics was thus constructed with the spacing between mics equal to adjacent path positions (Figure 5.17). The microphone array was placed close to the source side of the partition about 0.5-1 cm from the panel and contact pressures were measured on all the 64 paths. These contact pressures were then used as the approximate blocked pressures on the

partition. The pressure measurements were referenced to the driving voltage of the loudspeaker to make sure the phase is maintained between different measurements.



Figure 5.17: Contact pressure measurements by a microphone array close to the paths of the dual leaf partition installed in the transmission suite

Once all the vibroacoustic FRF's and contact pressure measurements were performed, they were combined for a pressure validation test.

---

### 5.5.1 Pressure validation

---

To validate the I-ASCA methodology using directly measured blocked pressures, the pressure validation approach outlined in I-ASCA can be used. Then the pressure at a point in the receiving volume can be predicted using blocked pressures as,

$$p_{pred,k} = \{\mathbf{p_b}\} \cdot \{\mathbf{H}\} \cdot dS \approx \{\mathbf{p_c}\} \cdot \{\mathbf{H}\} \cdot dS \quad (5.22)$$

In Eq. (5.22),  $p_{pred,k}$  is the predicted pressure,  $\{\mathbf{p_b}\}$  is the vector of the blocked pressures against all path positions measured as the contact pressures  $\{\mathbf{p_c}\}$ ,  $\{\mathbf{H}\}$  is the vector of vibroacoustic FRF measured for each path to receiver point 'k' and  $dS$  is the path area. By employing the pressure validation test, the predicted pressure can be compared with the measured pressure if it can be assumed that all the sound transfer occurs through the

partition. Using Eq. (5.22), the predicted pressure was calculated and then compared with the measured pressure as shown in Figure 5.18.

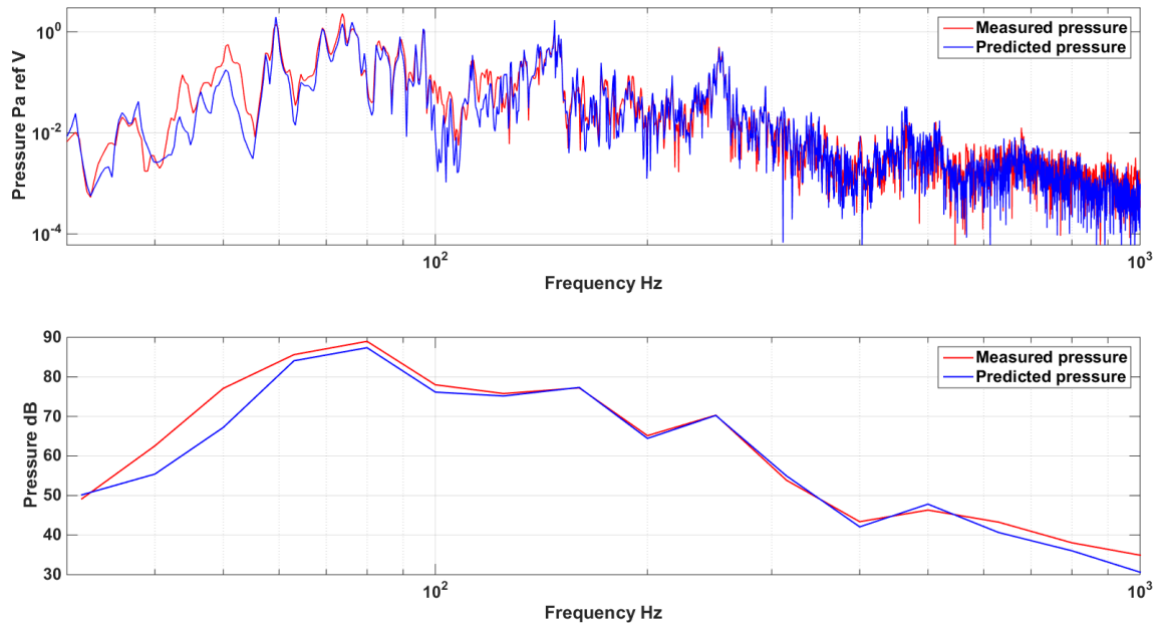


Figure 5.18: Pressure validation results for dual leaf partition using direct blocked pressure measurement in narrow bands (top) and one-third octave bands (bottom) till 1kHz

In Figure 5.18, the predicted pressure using D-ASCA approach is within 3 dB of the measured pressure in the range 63-1000 Hz. The peaks and levels in both spectra match very well which implies that the methodology is validated for a realistic case of a dual leaf partition. In the low frequency region (below 63 Hz band), it can be seen that the deviation of the prediction from the measured pressure is up to 7 dB. A few possible reasons may explain this difference. Firstly, we are using a contact pressure approximation for the blocked pressures and the approximation may not hold well at such low frequencies. This can be explained due to the fact that at low frequencies in the vicinity of the fundamental resonance, the impedance of the structure is low, and the response (velocity) on the partition is high meaning the radiated pressure will be large. Secondly, we assumed that all the sound transfer occurs through the partition; however some sound transmission could still be expected through the filler wall especially at its fundamental structural resonance that could lie in this region. Thirdly, the vibroacoustic FRF's could not be measured accurately in this region due to instrumentation error. The hammer tip is not very efficient



in inputting low frequency energy to the structure and thus the FRF suffers from some errors here. However, for diagnostic and SRI measurement, the region above 100 Hz is usually of interest and the prediction is much better (within 3 dB) in this region.

For frequencies above 1000 Hz, the prediction starts to deviate and fall below the measured pressure. This was expected, as the sampling assumption starts to break down and a finer grid should be tested to improve the frequency range of our pressure validation. However, one interesting implication of a direct measurement is that increasing the grid size and increasing the frequency range of application would be relatively easier as we are measuring the blocked pressures directly instead of an inverse process. This highlights the significant time advantage of D-ASCA over I-ASCA. Overall, this example shows that the blocked pressures (measured as contact pressure) predict the total sound radiation fairly well for the case of a realistic multi-layered partition.

---

### 5.5.2 Diagnostic contribution

---

In the previous Section 5.5.1, the airborne excitation on the dual leaf partition was characterised by blocked pressures, which were measured directly as the contact pressures. After the successful pressure validation, one can now calculate the source contributions. It was of special interest to diagnose the sound transfer through the point connection as it acts as a sound bridge between the two leaves of the partition. In this case, the contact forces (contact pressure  $\times$  area), can be used to obtain the source contributions using Eq. (3.10).

In D-ASCA, the acoustic FRF's cannot be measured as their measurement requires the accelerance FRF's as per Eq. (3.21). Thus, the D-ASCA will be limited to provide only the source contributions. To measure the path contributions directly, an alternative way will have to be devised. However, the influence of the point connection on the total sound transfer may be estimated by removing the source contribution (source on point connection) from the measured receiver pressure. This is shown in Figure 5.19, in the frequency range of 600-900 Hz. The results below 600 Hz were not shown because no significant effect was seen in this region.

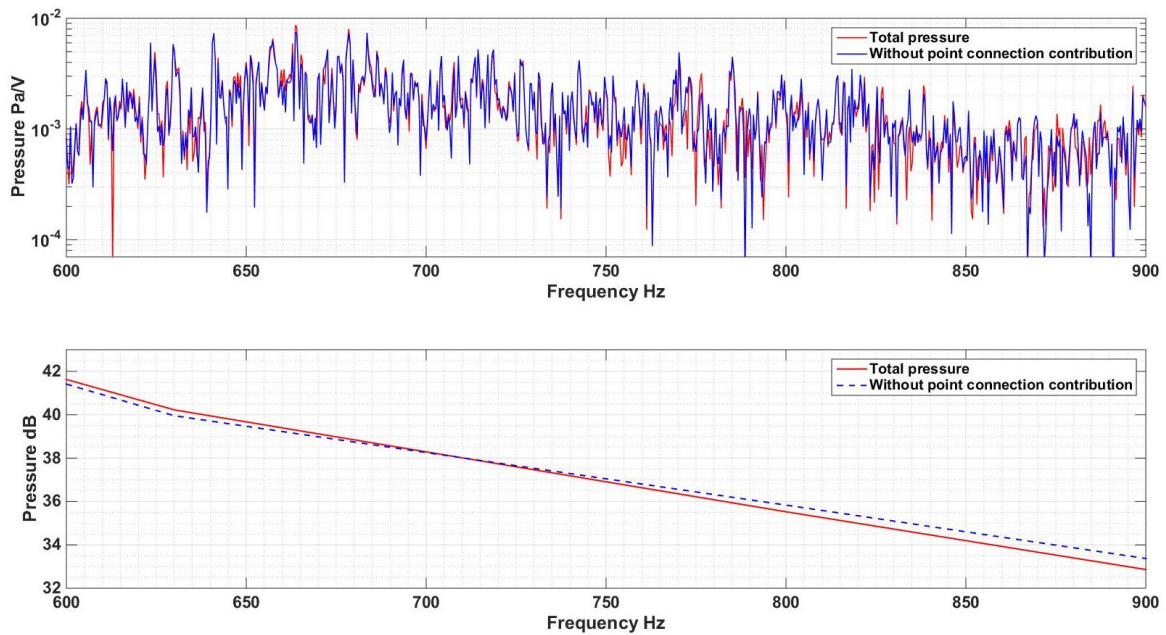


Figure 5.19: Comparing the total pressure with and without the contribution of source acting on point connection path in narrow band (top plot) and one-third octave band (bottom plot)

From Figure 5.19, it is evident that the point connection did not provide any significant contribution to the overall sound transfer through the partition. Differences less than 0.5 dB can be seen in some frequency ranges, which do not indicate a strong influence of the point connection on the sound transfer through the partition. Above 900 Hz, the point connection may become a path of strong path for sound transfer and a finer test grid will have to be tested to measure the diagnostic properties in the high frequency range. Next, a measurement methodology will be presented for calculating the radiated pressure term from Eq. (5.20). This accounts for the uncertainty in direct blocked pressure measurement examined for a realistic case.

---

### 5.5.3 Radiated pressure

---

The radiated pressure is the pressure radiated by the partition into the source room under the sole action of the blocked forces/pressures. As the radiated pressure is contributed by the partition under the action of blocked pressures, that means that the radiated pressure can be written as a sum of contributions of blocked pressures acting on the partition similar to Eq. (5.20) as,

$$p_{rad,j} = \{\mathbf{H}_{j,s}\}\{\mathbf{p}_b\}dS = \{\mathbf{U}_{j,s}\}\{\mathbf{v}'\}dS \quad (5.23)$$

In Eq. (5.23),  $p_{rad,j}$  is the radiated pressure at a point 'j' on the interface,  $\{\mathbf{H}_{j,s}\}$  is the vibroacoustic FRF vector defined for pressure at a point 'j' in source room with respect to forces on the partition paths. Therefore if the blocked pressures and vibroacoustic FRF's can be measured the radiated pressure can be calculated using Eq. (5.23). However, by using a direct approach the exact blocked pressures are not known.

Alternatively, the radiated pressure can also be calculated using the second relation of Eq. (5.23) if the acoustic FRF's  $\{\mathbf{U}_{j,s}\}$  can be measured. This describes the radiated pressure as a sum of pressures contributed by paths, which act as elementary volume velocity radiators ( $Q'_n = v'_n dS$ ). To apply Eq. (5.23), the operational velocities were measured on all paths. The acoustic FRF however, is not known and to measure this, volume velocity source will be required. However, at the time, a volume velocity excitation was not available so the measurement could not be conducted.

Another possibility here to calculate the acoustic FRF analytical (Rayleigh integral [57]) or numerical methods (BEM/FEM [150]). The second relation of the Eq. (5.23) is actually is discretised version of the Rayleigh integral where  $\{\mathbf{U}_{j,s}\}$  vector encapsulates the Green's function terms from discrete sources 'S' to a receiver point 'j'. As the measurement was conducted in a room, an analytical modal model could be used to calculate the acoustic FRF's  $\{\mathbf{U}_{j,s}\}$ .

To apply the modal model in our case we assume that the non-rectangular room can be approximated by a rectangular volume. The source room in actual measurement is not exactly rectangular as the walls in one dimension are not parallel. The modal frequencies of a non-rectangular room are not the same for a rectangular room but studies have shown that for small angles between opposite walls the Eigen frequencies of rectangular and non-rectangular rooms can be similar [151]. To validate this for our case where the perturbation angle is  $8.8^\circ$  (see APPENDIX V), the Eigen frequencies were calculated using analytical model (for rectangular rooms [152]) and using FEM model (for non-rectangular rooms).

APPENDIX V outlines the comparison which shows that the predicted Eigen frequencies for the rectangular and non-rectangular room were similar for this case and provides confidence in using a rectangular room model approximation. For cavities where walls in all direction (x, y and z) are not parallel, the application of room model would not be accurate.

In non-rectangular rooms, the modes that are excited are mostly oblique as opposed to rectangular rooms where all axial, tangential and oblique modes are excited. Therefore, the prediction from a modal model (with large number of oblique modes at high frequencies) will be more accurate than at low frequencies for our non-rectangular room. Towards the higher frequency bands, where more oblique modes are excited, the radiated pressure predicted by a modal model should ideally converge to the actual radiated pressure that could be measured in practice.

Also as the radiated pressure is likely to be negligible for solid building partitions, we are just interested in estimating it for the sake of completeness. This justifies the use of a modal model in our case to estimate if the radiated pressure is negligible compared to the contact pressure even though the rooms are non-rectangular.

According to a modal model, the acoustic FRF in a rectangular room between a source point 'S' and receiver point 'j' can be written as a summation of modes [152] as,

$$\frac{p_j}{Q_s} = i\omega\rho c^2 \frac{\cos\left(\frac{n_x\pi x_i}{L_x}\right) \cos\left(\frac{n_y\pi y_j}{L_y}\right) \cos\left(\frac{n_z\pi z_j}{L_z}\right) \cos\left(\frac{n_x\pi x_s}{L_x}\right) \cos\left(\frac{n_y\pi y_s}{L_y}\right) \cos\left(\frac{n_z\pi z_s}{L_z}\right)}{(\omega^2 - \omega_n^2 - j\eta\omega_n^2)K_n} \quad (5.24)$$

In Eq. (5.25),  $(x_j, y_j, z_j)$  are the co-ordinates of position 'j',  $(x_s, y_s, z_s)$  are the co-ordinates of the volume velocity source position 'S',  $\omega$  and  $\omega_n$  are the forcing and eigen frequency of the room respectively with dimensions  $L_x, L_y$  and  $L_z$ .  $n_x, n_y$  and  $n_z$  are the mode numbers for the eigen frequencies and  $K_n$  is a normalising factor. Using a modal model is convenient to calculate this FRF as we do not have to perform measurements with an actual volume velocity source.

Now consider the situation below where a discretised partition is mounted in a separating wall facing the source room. Then, to calculate the radiated pressure at a point 'k', the

acoustic FRF is to be calculated at 'k' with volume velocity excitation positions coinciding with paths on the interface S.



Figure 5.20: Measurement of radiated pressure at k –first phase is the acoustic FRF with response position k (denoted by  $\mathbf{x}$ ) and the volume velocity sources positions (denoted by  $\mathbf{o}$ )

In the present case study of the dual leaf partition to measure the radiated pressure according to Eq. (5.23), at first all the operational velocities of the paths were measured. Then, using the modal model of Eq. (5.24), 64 acoustic FRF's (as there are 64 paths) were calculated for a response position 'j'. The loss factor in the calculation was determined from the measured RT in the source room using the following equation.

$$\eta = \frac{2.2}{fT_{60}} \quad (5.25)$$

In Eq. (5.25),  $\eta$  is the loss factor,  $f$  is the frequency, and  $T_{60}$  is the measured RT. Alternatively, the loss factors can also be determined from the total pressure spectra using the half power method [153]. To cover a frequency range of 1000 Hz, different number of modes were considered in the modal summation. Modes covering 1 kHz, 1.25 kHz, 1.5 kHz and 1.8 kHz range were used in calculations and the deviation between 1.5 kHz and 1.8 kHz series was found to be 0-0.5 dB. The criteria for convergence was decided to be within 1 dB which was satisfied using 106982 modes under 1.8 kHz for the calculation of the radiated pressure up in 0-1 kHz frequency range. Then using Eq. (5.23), the radiated pressure in the source room from the dual leaf partition was calculated. As, the contact pressures were already measured (Section 5.5.1), the exact blocked pressure was also calculated as per Eq. (5.19). The exact blocked pressure, radiated pressure and contact pressure are compared in Figure 5.21 for a single point on the interface.

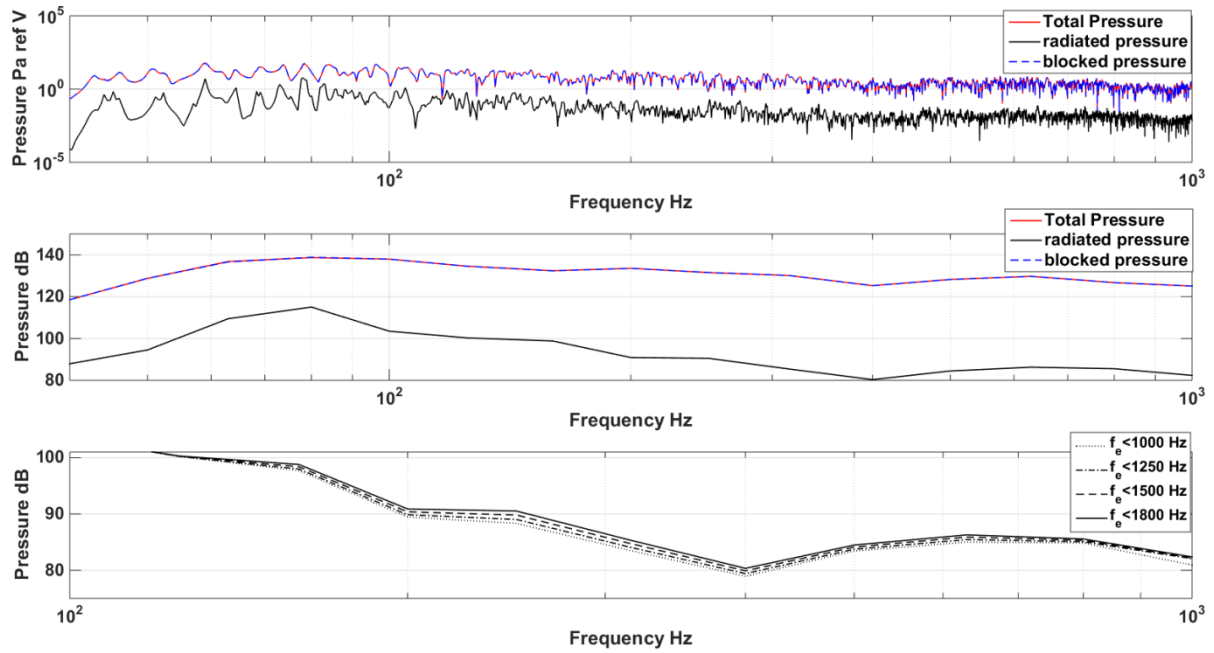


Figure 5.21: Comparison between total contact pressure, radiated pressure and blocked pressure at a single patch in narrow band (top) and one-third octave bands (middle) and convergence of the radiated pressure using the modal model (bottom plot).  $f_e$  represents the Eigen frequencies

From Figure 5.21, it can be clearly seen that the radiated pressure is negligible compared to the contact pressure rendering the contact pressure equal to the blocked pressure. This finding was also validated for several other paths and is in line with the theoretical observations/comments from studies highlighting that the radiated pressure is usually negligible compared to the blocked pressure. This also shows the validity of a modal model in such case for the estimation of the radiated pressure. In general, for practical building acoustics applications where  $Z_p \gg Z_{air}$ , it can be said that the radiated pressure will be negligible in comparison to the contact pressure.

This analysis tends to show that the difference in the low frequency region (Figure 5.18, below 63 Hz) is not be due to the radiated pressure, which makes it more likely the errors in vibroacoustic FRF's below 63 Hz is responsible for the difference.

This analysis thus presents a novel application of the modal model in conjunction with experimental data for predicting the radiation from a building partition on the source side, thereby a semi analytical-semi experimental approach. An advantage of using such an

approach is that a volume velocity source is not required to measure the acoustic FRF but rather a simple room model could be used for this purpose, which should be relatively faster. However, this approach would be only limited to hard walled rectangular rooms as the acoustic FRF is calculated from a modal model, which is only valid for rectangular cavities. For more accurate modelling of acoustic FRF's in non-rectangular cavities, FEM/BEM methods can also be used. Alternatively, it can also be measured if a calibrated volume velocity source is available.

---

#### 5.5.4 On board validation – vibration response prediction

---

For the pressure validation test to be applicable, it is important that the sound transfer occurs through the partition only. However, for in-situ installations other flanking transmission to the receiver room may exist, such as a window or a door separate from the test partition. Such elements will also transmit pressure to the receiving volume and the measured pressure then is a resultant of pressure transmitted by the partition as well as these secondary sources. Then, a pressure validation test may not be applied successfully. Rather in such cases, the on-board validation test can be applied to predict the vibratory response at the interface. This will also confirm if the directly measured blocked pressures are able to predict the vibratory response of the partition. The acceleration on the partition at a point 'k' can be predicted as,

$$a_{pred,k} = \{\mathbf{p}_b\} \cdot \{\mathbf{Y}_{k,i}\} \cdot dS \quad (5.26)$$

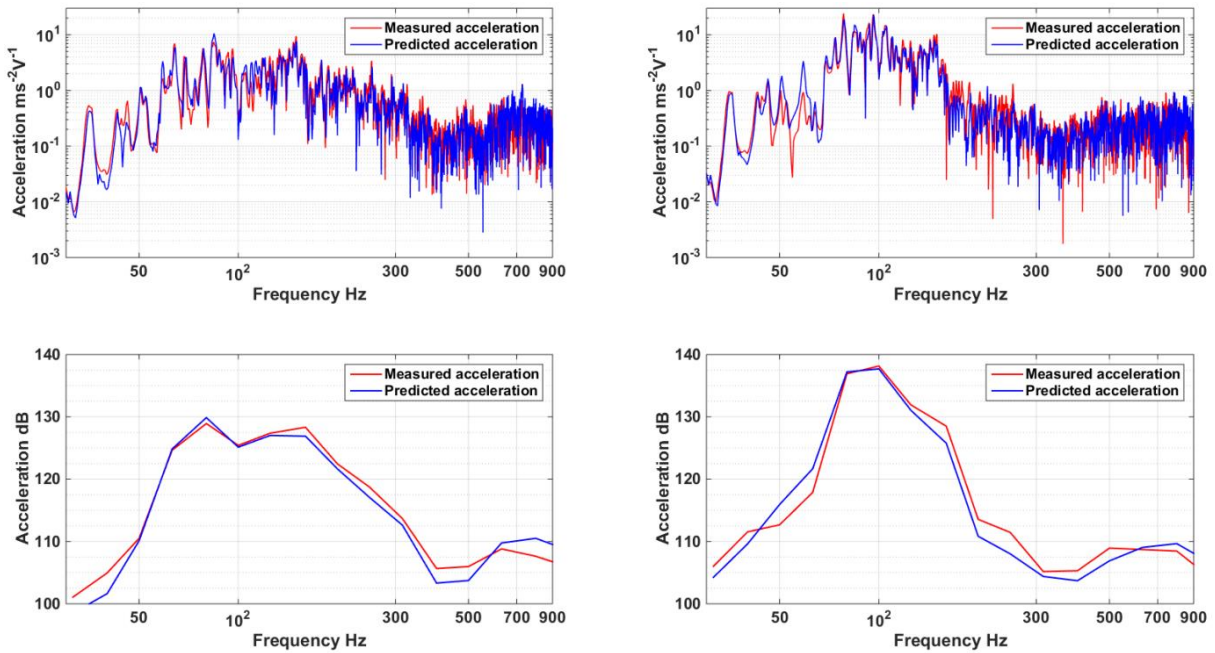


Figure 5.22: On board validation results for velocity prediction using directly measured blocked pressure in narrow bands (top plots) and third octave bands (bottom plot)

Figure 5.22 shows the on-board validation results for two reference points on the partition. The predicted and measured accelerations at the reference points are within 2-3 dB in the region from 50-900 Hz. Again, an interesting implication of the direct blocked pressure measurement is that vibratory response of the panel can be predicted relatively faster than inverse methods like I-ASCA.

## 5.6 Conclusions

The main motivation behind the work presented in this chapter was to develop a faster approach than blocked force based I-ASCA for diagnosing airborne sound transfer through dual leaf partitions separated by a cavity. To achieve this, the direct measurement of blocked forces was considered. Three different approaches were discussed for the direct measurement of blocked pressures (blocked force/path area) which led towards a conclusion that the contact pressure is equal to the blocked pressure and a radiated pressure term. By neglecting the radiated pressure, the blocked pressure can be closely approximated by a direct contact pressure measurement.



The direct blocked pressure measured as contact pressures were studied for cases of unbaffled and baffled partitions. The difference between the contact pressure and blocked pressure is the radiated pressure, which was later estimated to be negligible. The validity of these blocked pressures was determined by using a pressure validation and on board validation test. An important consideration for measuring contact forces is that complete source-receiver-interface of the partition should be accessible as seen for the case of unbaffled partition. In case of airborne flanking, on-board validation may be a better test to validate the blocked pressures.

With this approach, accelerances are not measured and only the vibroacoustic FRF's were measured. As a result, the measurement time of D-ASCA is significantly reduced compared to I-ASCA. D-ASCA does not involve an inversion process, and therefore the inverse errors are avoided. In addition, any local blocked pressures can be measured independently without a global testing of the whole structure. This means that a local source contribution can be measured without measurements on all paths. As accelerances are not measured, accelerometers are not used, and there is no effect of mass loading on the structure otherwise present in conventional I-ASCA.

It was also observed it was difficult to obtain a good coherence in the vibroacoustic FRF measurements as the source and receiving room were highly reverberant. This problem is especially worse at low frequencies where the signal to noise ratio is very low as the hammer does not input much low frequency energy into the structure. These add to measurement errors and the pressure prediction may then be affected. If this measurement can be automated, then measurement errors may be further minimised and the measurement time can be reduced further. Quite favourably, this is possible by measuring the FRF reciprocally using the well-established principle of vibroacoustic reciprocity. Using the principle of vibroacoustic reciprocity, the vibroacoustic FRF can be measured reciprocally as velocity on the partition due to volume velocity excitation in receiver volume (see Table 3.2).

$$\frac{p_k}{f_j} = \frac{v_j}{Q_k} \quad (5.27)$$

If a scanning laser vibrometer is used to measure the velocities on the panels instead of using accelerometers, then the FRF measurement can be fully automated and may be quicker than direct measurements for large partitions. This would make the measurement approach totally non-invasive to the partition under test. It can also be seen that the measurement can be done with a minimum of three microphones (one for measuring contact pressures, one for pressure validation and one as a receiver for diagnostic test) thereby providing some cost advantages.

---

# 6

## COMBINED SOUND INSULATION AND DIAGNOSTIC TESTS

---

*In the previous chapter, a direct approach –the D-ASCA method was outlined for a direct characterisation of airborne excitation. Using a contact pressure approximation for characterisation, the source contributions are measured relatively faster, easier than I-ASCA method thus making the D-ASCA more practical. The path contributions however cannot be obtained. In total, three different diagnostic tests have been outlined and tested, namely I-ASCA, I-PCA and D-ASCA. In conjunction with the SRI which provides the frequency dependence of sound insulation, the diagnostic results were shown to provide information on the spatial dependence. Therefore, it was now of interest to investigate how the diagnostic test results may complement the standard sound insulation test results for an actual product. Additionally a novel formulation for estimating the in-situ sound insulation without diffuse field assumptions will be presented. A key advantage of such an approach would lie in the low frequency sound insulation measurement, which is prone to many uncertainties due to diffuse field assumptions of the standard test methods.*

---

## 6.1 Airborne sound insulation tests with diagnostic tests

---

The sound insulation of a partition is measured by standard methods under laboratory conditions to give the SRI. The SRI provides the frequency dependence of the sound insulation of the partition. However, as mentioned previously, these SRI values (or single number rating  $R_w$ ), do not provide any information on the sound transfer contribution of different paths/elements in the partition which may be important for R&D purposes. With diagnostic tests outlined in Chapter 3 (I-ASCA, I-PCA) and Chapter 5 (D-ASCA), the source and path contributions can be measured. Using this diagnostic data, the weak paths of sound insulation can be identified. If such information is compared with the SRI results, then the weak paths may be identified in specific regions where the partition exhibits low SRI. Thus, the diagnostic tests can run in complement to the standard airborne sound insulation tests under laboratory conditions, which may help in improving the sound insulation of the partition.

---

## 6.2 Case study I – double casement window

---

To perform the diagnostic tests with the SRI tests, a suitable building element had to be chosen. Typically, building elements that are tested for airborne sound insulation are multilayered walls, windows, and doors. For the combined testing, these were the available choices of partitions that could be tested. The diagnostic methods developed in this thesis are measurement intensive and thus practically suitable for smaller test partitions. Windows are usually smaller in size compared to wall partitions which render them quick to test. Additionally, most windows will have distinctive structural elements (frame, glazing, seals). This makes the window an interesting case study where the diagnostic methods could be employed to diagnose the contribution of such distinctive elements.

To test the combined application of standard and diagnostic tests, the double casement window shown in Figure 6.1 was chosen as a case study. The window is a double glazing construction with an air cavity between the two glass panels of the window. A frame is

present around the glazing and in the middle separating the two casements. Thus, there are two prominent sound transmission paths in the construction –the glazing and the frame (transmission through seals is not considered for the current analysis). Given the difference in the structural construction of the frame and glazing, the different material properties and boundary conditions of these two elements, it can then be reasonably assumed that the airborne sound transmission through the frame and glazing will be different. Then the aim of the test was to measure the airborne sound transmission through the frame and glass separately by applying diagnostic methods in-situ. This in turn would help in understanding how each element affects the sound insulation (SRI) in the frequency range of interest.



Figure 6.1: Double casement test window with the frame around the edges and in the centre along the height of the window

---

### 6.2.1 Airborne sound insulation and diagnostic tests

---

At first, the sound insulation of the window had to be measured according to standard methods (ISO 10140). To measure this, the transmission suite test facility described in Section 4.5 was utilised which allows for control over test environment and flanking transmission. Thus the window was installed in the aperture between the source and receiving rooms (Figure 6.1).

The measurement results for the sound insulation are shown in Figure 6.2. Of particular interest is the region below 1 kHz where the sound insulation has dips in low frequencies and then has a gradual increase. Diagnosing the contributions of glazing and frame in this region may be useful to diagnose any weak elements of sound insulation.

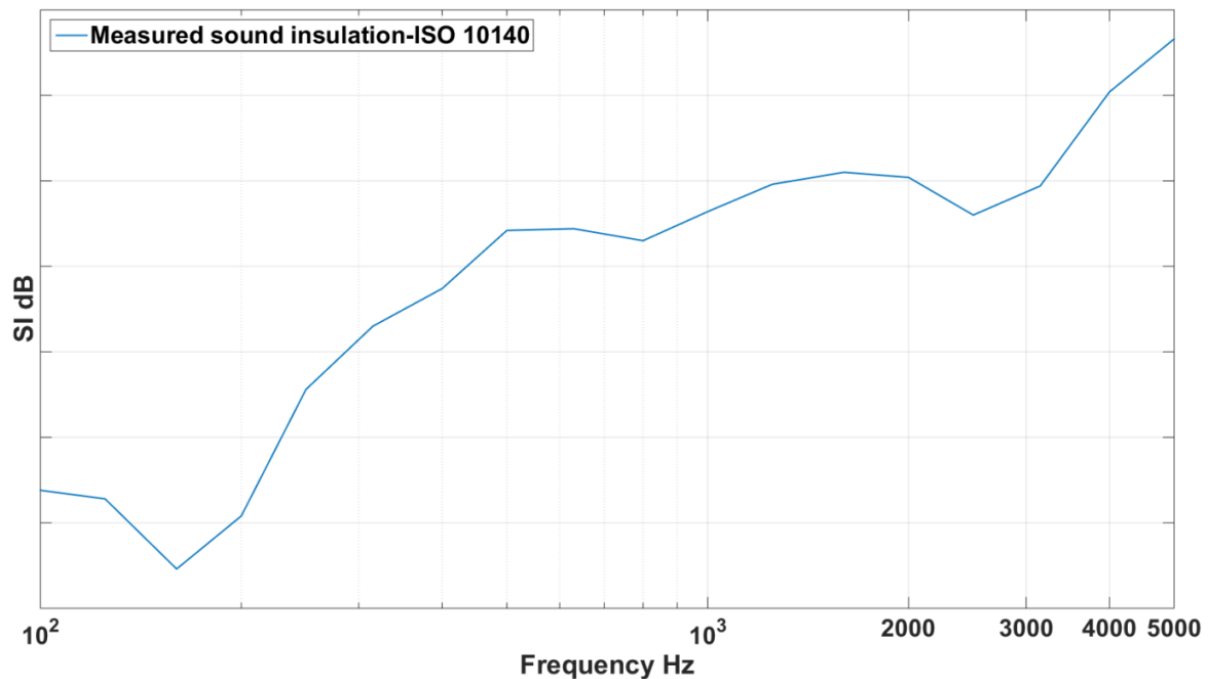


Figure 6.2: Sound Insulation (SI) of the double casement window measured as per ISO 10140 tests displayed in one-third octave bands from 100-5000 Hz

### 6.2.2 Diagnostic tests

After the sound insulation testing, the diagnostic tests had to be performed. As mentioned earlier, the glazing and frame elements present a path for sound transfer from source to receiving room assuming the transmission through seals can be neglected. Thus, the next step was to measure the sound transfer through these elements using diagnostic tests. Then, following the I-ASCA methodology, the first step of the measurement was to discretise the partition in smaller areas. The discretised partition is shown in Figure 6.3.

Due to the different size and dimensions of the glazing and frame as well as test time restrictions, a fine discretisation could not be maintained throughout the window surface. Ultimately, a coarse grid was used on the glazing (15 x 15 cm<sup>2</sup> path area) while the

discretisation on the frame was much finer ( $7.5 \times 9 \text{ cm}^2$  path area). Because the size of the glazing was bigger than the frame, more low order modes would be excited in the glazing. This would mean efficient coupling with lower order room modes and more transmission in the low frequency region through the glazing. At low frequencies the grid size can be coarse as grid size increases with frequency. Thus, using a coarse grid on the glazing and a finer grid on the frame made sense. After the discretisation, the following measurements were conducted according to D-ASCA.



Figure 6.3: Discretisation on the glazing and frame elements for diagnostic measurements

1) Contact pressure measurements –A loudspeaker driven by pink noise excitation was set up in the source room facing the corner. The sound field driven by the loudspeaker simulates the airborne excitation on the window. Under operational conditions, the contact pressures against each path were measured using microphones. The measurements were referenced to the loudspeaker voltage. Each measurement was averaged over 60s containing multiple windows. These contact pressures then approximate the blocked pressures on the window.

2) Vibroacoustic FRF's –Using a force hammer to impact at each path position, the pressures were measured at receiver positions in receiver room. The receiver positions were the same

as the ISO 10140 positions so that the diagnostic results can be averaged over the room volume following standard guidelines.

3) Operational accelerations –The accelerations were also measured on the path positions using accelerometers under operational conditions. The accelerations too were referenced to the driving voltage of the loudspeaker. This was measured to be used in the I-PCA methodology.

Once all the measurements were completed, using the D-ASCA methodology (Eq. (5.22)) the sound transfer through the window in the receiving room was predicted and compared to the measured pressure as a part of the pressure validation. The results of the pressure validation are shown in the Figure 6.4.

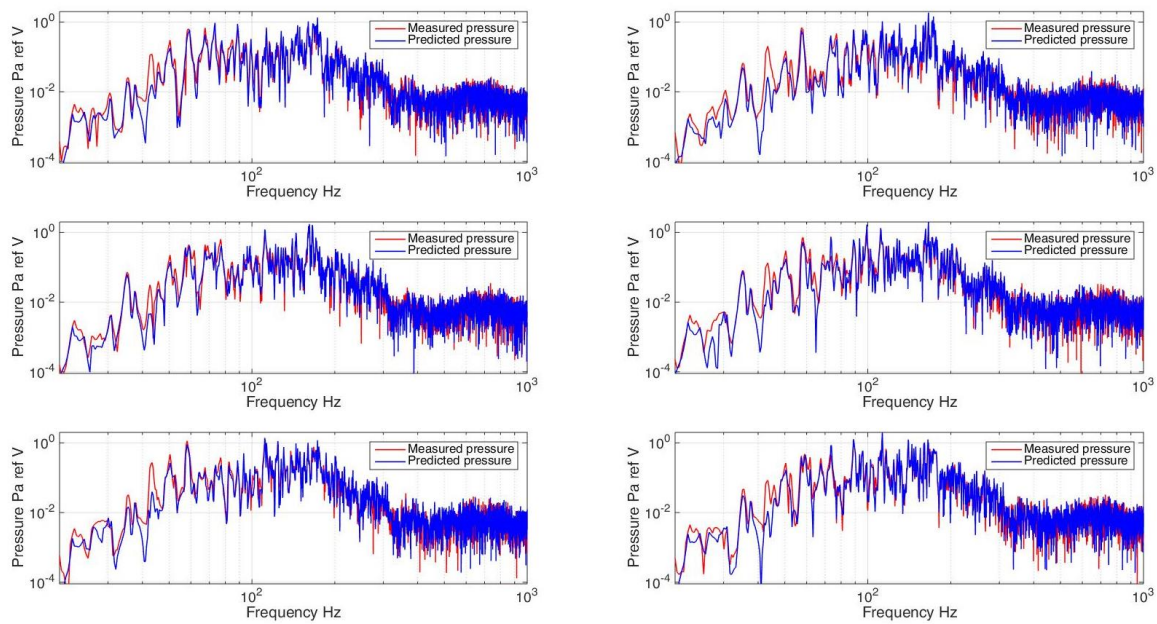


Figure 6.4: Pressure validation results for D-ASCA test on the double casement window at 6 receiver positions –comparing the predicted pressure (in blue) to measured pressure (in red) in narrow band from 30-1000 Hz

The pressure validation results in Figure 6.4 show that the measured and predicted pressure spectrums match well for frequencies above the 60 Hz. The prediction accuracy was quantified in on-third octave bands for the spatially averaged receiving room pressure as shown in Figure 6.5.



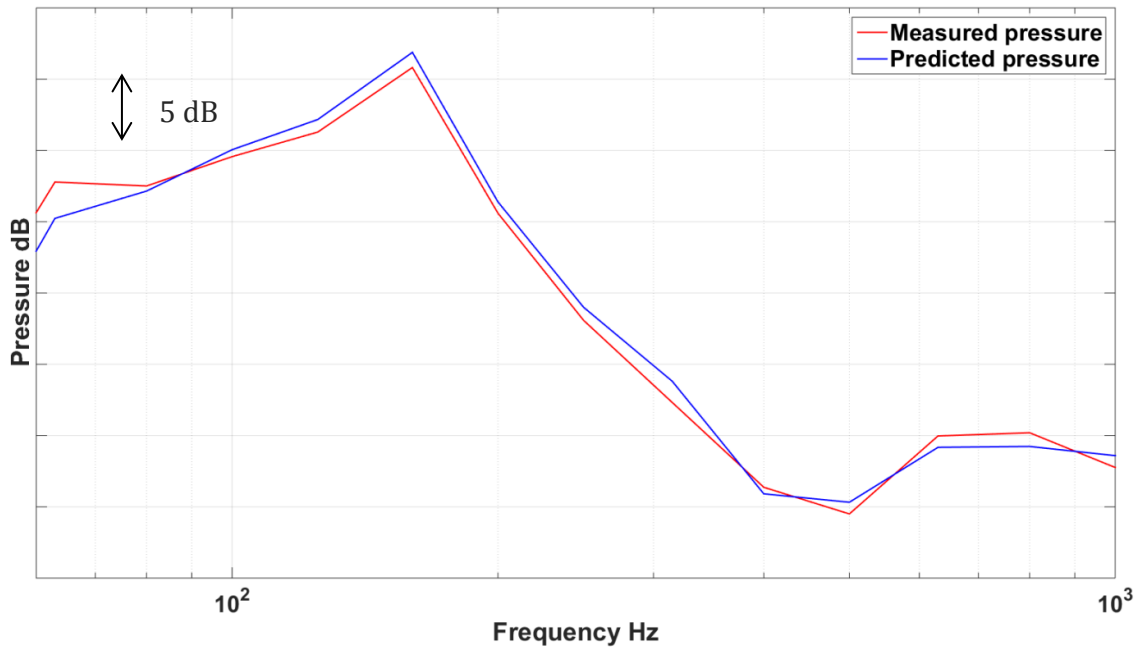


Figure 6.5: Averaged receiving room SPL predicted by D-ASCA (in blue) compared to measured pressure (in red) in one-third octave bands from 60-1000 Hz

An excellent agreement (within 1 dB above 63.5 Hz band) between the predicted and measured SPL for the receiver room in one-third octave bands can be seen. The deviations (2-3 dB) in low frequency band of 63.5 Hz are firstly due to the error in measuring the vibroacoustic FRF's. The hard tip of hammer is not very suitable to impact low frequency force into the structure which results in poor signal to noise ratio at very low frequencies. To overcome this, a softer hammer tip is suitable. This would mean testing the whole structure again with soft hammer tip; however, due to time constraints this test was not done. Also for building acoustics applications the frequency range above 100 Hz is mostly of interest. Secondly, the RT in that band was greater than the length of the time window used for FRF measurement. To obtain an accurate FRF at such low frequency end, it is advisable to use the individual window length greater than the RT [137]. The window length of 5.12 s was therefore not ideal for the FRF measurement below 63.5 Hz band. For building acoustics applications, the frequency range of interest is typically above 100 Hz (but not always), and the prediction above 100 Hz is within 1 dB which shows the potential of the method in predicting the receiver response. Using the methodology described in Section

5.5.3, the radiated pressure was also calculated and the results for radiated pressure compared to the contact pressure on a single patch are shown in Figure 6.6.

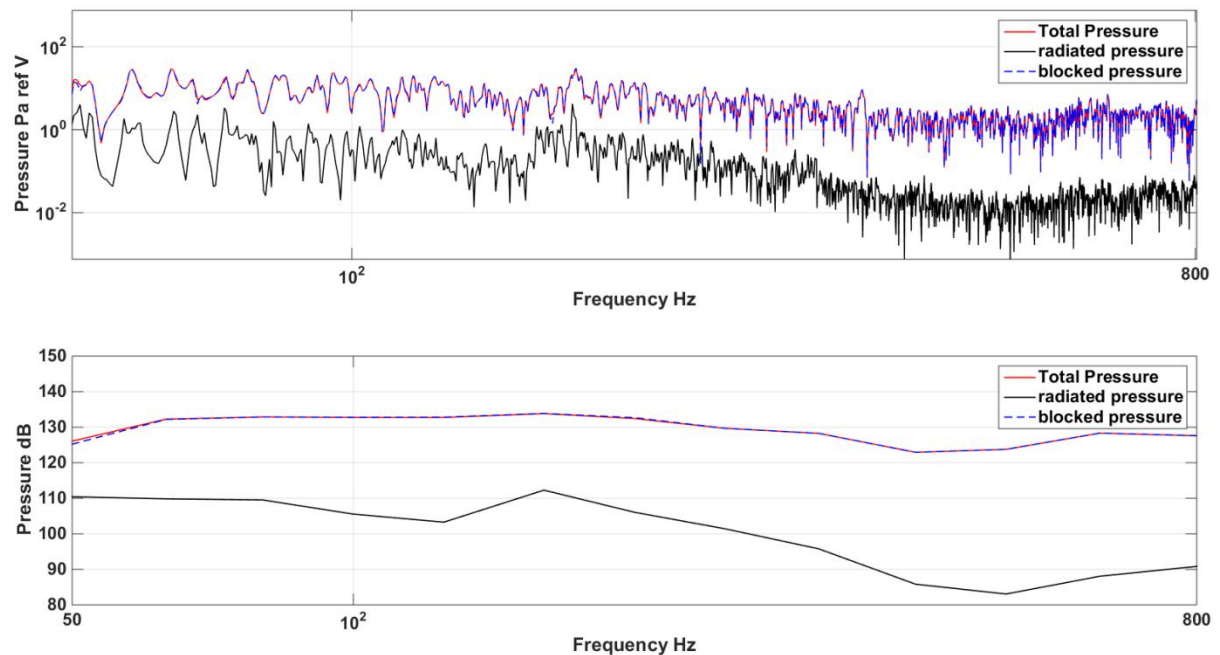


Figure 6.6: Comparison between total contact pressure, radiated pressure and blocked pressure at a single patch in narrow band (top) and one-third octave bands (bottom plot) in 0-800 Hz

Figure 6.6 again shows negligible value of the radiated pressure which means that the contact pressure are equal to the blocked pressure in this measurement case. Therefore, the disagreements in the low frequency (<63 Hz) from Figure 6.5 arising due to contact pressure approximation can be ruled out.

### 6.2.3 Diagnostic contributions – glazing and frame

Once the validity of the method was confirmed by pressure validation tests, the next step was to separate the contributions of glazing and frame elements. As the D-ASCA test was applied in this case, the contributions that can be measured are of the sources (blocked pressures) acting on the frame and glazing paths. However, for diagnosing the sound transfer of each element, the path contributions are important rather than source contributions. This is because the source contributions describe the sound transfer through

the global structure, while path contributions describe the sound transfer locally. The elements can then be ranked if their path contributions are known.

To measure these path contributions the acoustic FRF's ( $U$ ) have to be combined with the operational volume velocities of the paths (see Eq. (3.12)). In our case, the operational volume velocities are known as we have measured the accelerations. But the acoustic FRF's could not be measured under the time frame of the test as it required measurement of the accelerance FRF's as per Eq. (3.18). Therefore, the path contributions could not be measured.

The path contribution is not equal to the source contribution but globally, the total sound transfer can be written as a sum of source contributions which is equal to the sum of path contributions (Eq. (3.20)). If the frame and glazing elements were to act independently of each other (no cross talk or transmission across junctions), then the sum of the source contributions for each element would be equal their path contributions. In the current case, we do not know if that is the case. However, we can consider the following observations.

- 1) The structural impedances of the frame and glazing material in the current case are relatively different due to different material properties, construction (one is more beam-like, other is more plate like). Due to this impedance mismatching, the structural interaction or sound transmission across the boundaries (see Figure 6.6, left-in dashed orange) can be considered minimal or inefficient.
- 2) The boundary/junction where the glazing meets the frame is lined with resilient gasket which acts as a seal (see Figure 6.7, right-in red circles). This means that the frame and glazing are decoupled from each other to a certain extent. This would further provide insulation to any transmission through the boundaries between the elements. At the resonant frequency of the seal, this may not be the case, but it is likely that the resonant frequency lies in the higher frequency region outside the range of test.

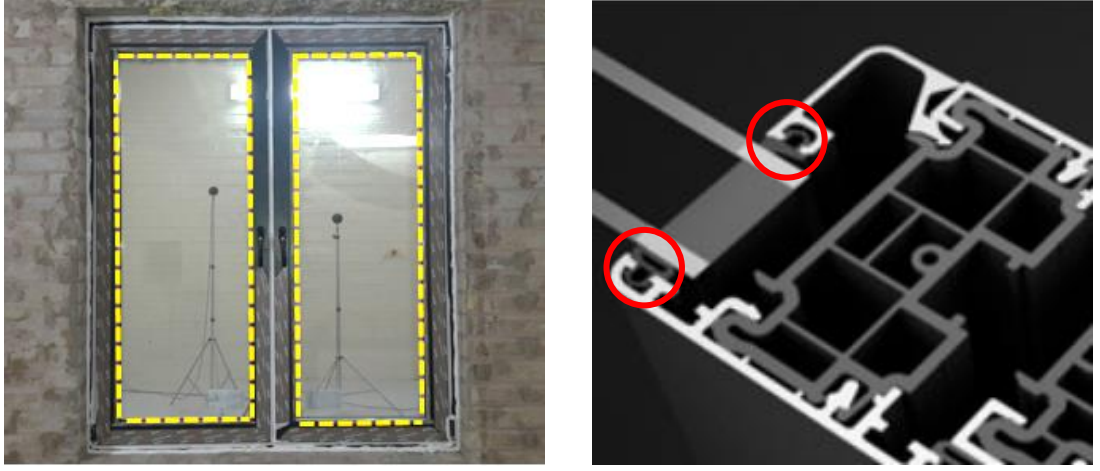


Figure 6.7: Left –Dashed orange line highlights the boundary separating the frame and glazing in the window. Right –expanded cross sectional view along the depth of the window showing gaskets/seals (in red circles) lined between the frames and glazing

Overall, the implication of the two observations outlined above is that the sound transmission across the boundary from one element to the other (i.e. the flanking transmission from one to other) is very less (but not zero). This means that the elements can be treated as acting independently of each other. Exceptions to this assumption are likely to exist, especially in the frequency region of the fundamental resonance of the seal and at low frequencies.

By making use of the above assumption we can say that the sound radiated by each element is predominantly due to the airborne excitation acting on them. In other words, this means that the radiation through each element can be approximated by the sum of source contributions acting on each element. Therefore, similar to Eq. (3.20), we can write,

$$p_G^c = \{\mathbf{U}_{R,G}\}\{\mathbf{v}_G'\}dS_G \approx \{\mathbf{H}_{R,G}\}\{\mathbf{p}_{bl,G}\}dS_G \quad (6.2)$$

$$p_F^c = \{\mathbf{U}_{R,F}\}\{\mathbf{v}_F'\}dS_F \approx \{\mathbf{H}_{R,F}\}\{\mathbf{p}_{bl,F}\}dS_F \quad (6.3)$$

where,  $p_G^c$  and  $p_F^c$  is the total pressure contributed by the glazing 'G' and frame 'F' respectively,  $\{\mathbf{H}_{R,G}\}$  and  $\{\mathbf{H}_{R,F}\}$  are their respective vibroacoustic FRF vectors for 'G' and 'F' at receiver positions 'R',  $[\mathbf{U}_{R,G}]$  and  $[\mathbf{U}_{R,F}]$  are the respective acoustic FRF vectors,  $\{\mathbf{p}_{bl,G}\}$  and

$\{\mathbf{p}_{b,F}\}$  are the blocked pressure vectors for the sources acting on 'G' and 'F' respectively.  $dS_G$  and  $dS_F$  is the path area on glazing and frame respectively.

The advantage of using Eq. (6.2, 6.3) is that one does not need to measure the path contributions using I-PCA technique. Instead, they can be measured as an approximate sum of source contributions for individual elements. Measurement of the source contributions is relatively simple as per D-ASCA technique and therefore use of Eq. (6.2, 6.3) is advantageous in regards to measurement time. Using Eq. (6.2, 6.3), the total path contribution of glazing and frame were calculated for six receiver positions from the source contributions. It is to be noted that the path contributions here are an estimate and not exact contributions. These contributions were spatially averaged and the results are shown in Figure 6.8.

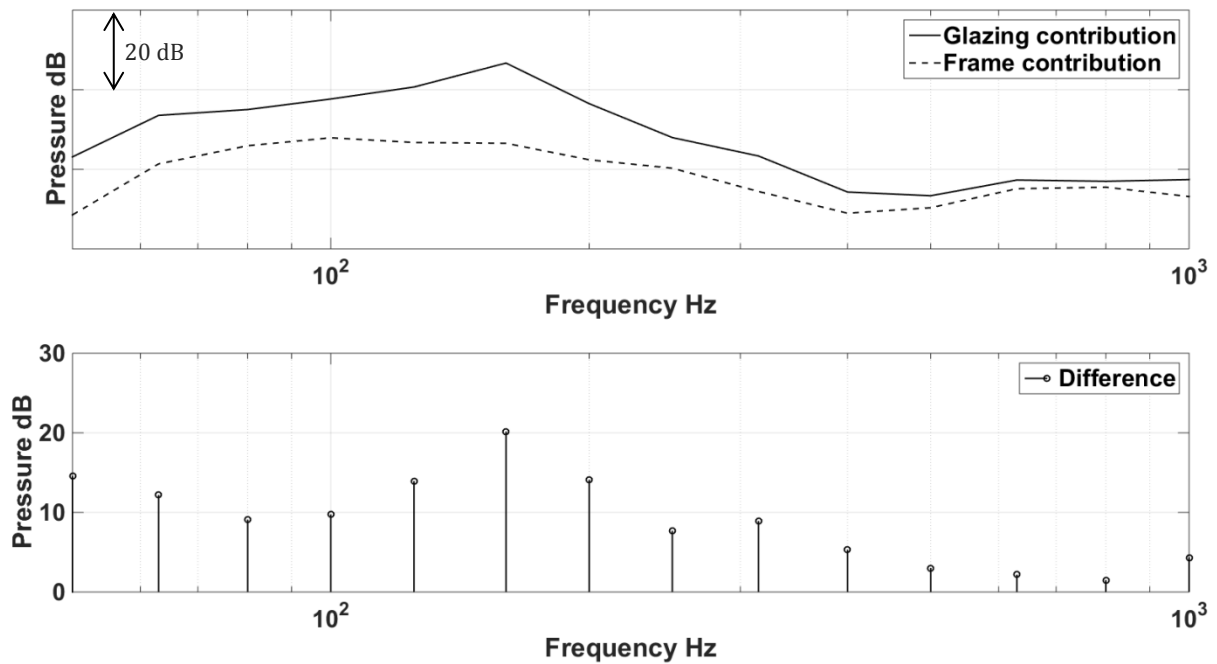


Figure 6.8: Upper plot- Glazing contribution (in blue) compared to Frame contribution (in orange) averaged for six receiver positions displayed in one-third octave bands in 60-1000 Hz.

Lower plot-Difference between the glazing and frame contributions in 60-1000 Hz range

Figure 6.8 shows the potential of the diagnostic tests in separately quantifying the contributions of different elements in a building element. It can be seen that the glazing and frame contributions vary with frequency which is not surprising. Perhaps, the significant finding here is that the glazing is the dominant contributor compared to the frame in the

frequency region up to 1 kHz which qualitatively allows us to rank them. These contributions provide important insights on the sound transfer (or insulation) characteristics of the different elements which are not otherwise measurable by a standard sound insulation testing. The ranking may in turn be used as a guide for sound insulation improvement measures which will be discussed in the next section.

An alternative method that can be employed to measure the sound transfer through both elements is the sound intensity measurement. However, the sound intensity is measured for a radiating area and the pressure used for sound intensity calculation has contributions from the global structure. Thus even though, the sound intensity can be measured it is not purely a property of the element in consideration. Thus, the information obtained from a sound intensity measurement is not adequate for our diagnostic tests.

---

#### 6.2.4 Diagnostic measurements as a tool for SRI improvement – a case study

---

In the previous section, the sound transfer characteristics (or contributions) of the glazing and frame elements were estimated. These contributions are contrary in concept to the sound insulation characteristics. This means that an element with higher contribution (higher sound transfer) provides less sound insulation and vice versa. Therefore, the contributions may be potentially studied to investigate the weak elements of sound insulation in the structure. Any improvement measures may then be introduced at the weak spots to improve the global sound insulation of the structure. Here we discuss one such hypothetical case study in reference to our window example.

At first, the main aim is to detect the weak element of sound insulation. Clearly, the glazing was found to be the dominant sound transfer path, which means it is a weak sound insulation path and could potentially be treated. In the low frequency region (below 400 Hz), the glazing contribution exceeds the frame contribution by overall 10 dB. Then to reduce the glazing contribution in this region, material properties and/or cavity absorption has to be changed. However, the first option would increase the weight of the structure, and the second option would adversely affect the transparency of the glazing. Also in the low

frequency region, by introducing these measures, it may be difficult to obtain an appreciable difference in the sound insulation, as these frequencies are often the hardest to treat.

Between 400-1000 Hz, the sound pressure contributions of the glass and frame are quite comparable (within 4-5 dB of each other). Therefore by modifying the behaviour of any one of these elements, it is quite possible to affect the overall sound insulation of the window in this region. As already discussed above, the treatment measures for glazing are not suitable. Therefore a possible option is to treat the frame. By filling the cavity of the frame with absorption, the sound transfer through the frame may be further reduced. Thus, it may be possible to affect the global sound insulation of the structure.

This study thus demonstrates a possible process to alter/modify the sound insulation characteristics of the structure by making use of the diagnostic contributions. Thus, the potential of diagnostic tests is demonstrated in complement to the standard tests for separating the contributions of different elements of the structure, which may aide in R&D for sound insulation improvement.

In conclusion, Section (6.2) and (6.3) showcase the combined application of diagnostic tests with standard sound insulation tests on a commercial window was demonstrated. Along with the SRI which provides the frequency dependence of sound insulation, the contributions measured from diagnostic tests provide the spatial dependence of sound insulation. The potential of diagnostic testing in identifying weak elements for sound insulation was demonstrated. The results from a combined test can also be exploited for R&D purposes to improve the sound insulation of the structure.

---

### 6.3 Case study II – single casement window

---

The diagnostic tests were also applied to a different window case – a single casement type window as shown in Figure 6.9. Again, it was of interest to diagnose the airborne sound transmission through the frame and the glazing. This case was different than the previous window case as here the glazing is a massive dual panel with cavity structure (mass per unit

area of  $\sim 50\text{-}60 \text{ kg/m}^2$ ) while the frame material is of lightweight PVC type. Therefore it was expected that the frame would have more/similar contribution compared to the glazing.



Figure 6.9: The single casement window chosen for diagnostic testing with the frame (in white) at the edges and the glazing in between. The discretisation markings can also be seen

To apply the diagnostic tests, the frame and the glazing were first discretised into 148 patches. Then, as per D-ASCA methodology, using a loudspeaker driven with pink noise, the contact pressures were measured directly against each patch. Next the vibroacoustic FRF's were measured at microphone locations (same as ISO 10140 locations) in the receiving room. For the FRF measurements, it was difficult to get a high SNR at high frequencies while impacting on glazing. This is because the glazing was very hard and additionally low noise microphones were not available at the time of the test to improve the SNR. The pressure validation was then performed and the pressure was predicted at all six positions in the receiving room. The spatially averaged SPL in the receiving room was also measured and compared with the predicted spatially averaged SPL.



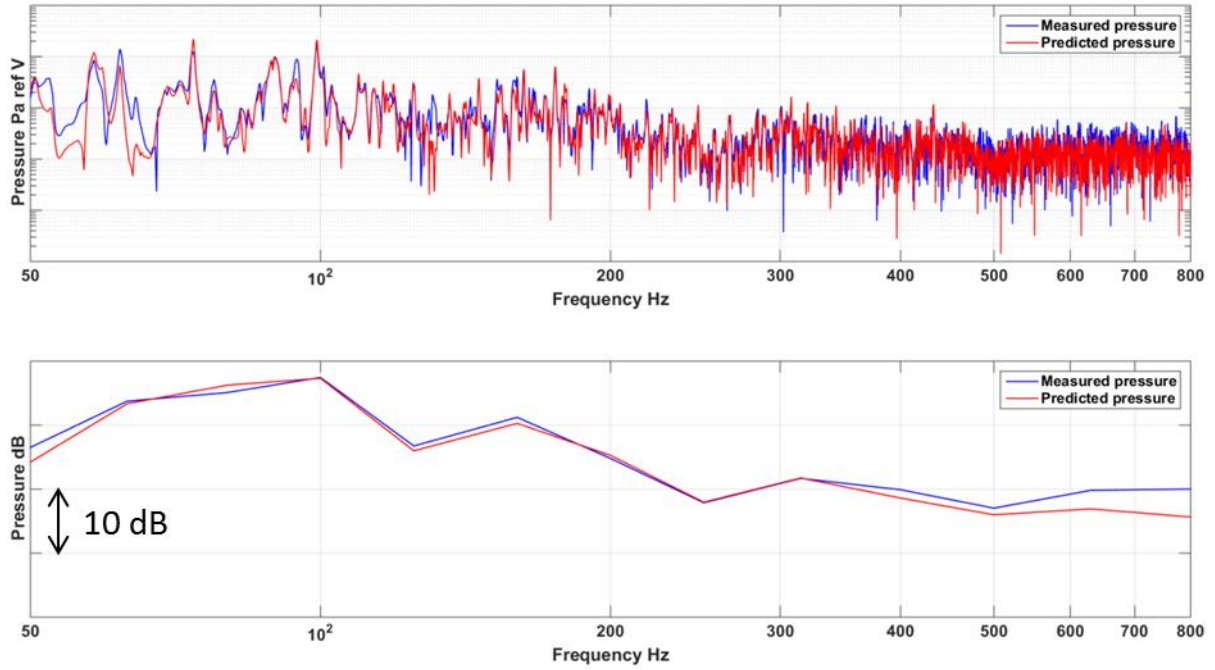


Figure 6.10: Pressure validation for the D-ASCA methodology applied to the casement window shown in Figure 6.9

Figure 6.10 shows that the pressure predicted using D-ASCA is within 1-2 dB in the low frequency region and starting at 600 Hz the deviation starts to increase with a maximum deviation of 4 dB between measured and predicted SPL in 800 Hz third octave band. The cause of this deviation was the poor SNR in FRF measurements as discussed earlier. Therefore, it is advisable to use low noise microphones for the case of heavy structures at least for vibroacoustic FRF measurements. If the contact pressure approximation of blocked pressures is not correct for this case, then that may also explain the deviations. To check this, the radiated pressure could be measured as per Eq. (5.23). Previously a semi-analytical semi-experimental approach was outlined in Section 5.5.3 for measurement of radiated pressure however that requires the velocity distribution to be measured which could add to the measurement time. Instead a higher estimate of radiated pressure can be predicted using contact pressures as,

$$\tilde{p}_{rad} = \{\mathbf{p}_c\}\{\mathbf{H}_{js}\}dS \quad (6.4)$$

where,  $\{\mathbf{H}_{js}\}$  represents the vibroacoustic FRF's measured on the source side at source DoF. As  $p_c \geq p_b$ , the value of radiated pressure predicted by Eq. (6.4) above will be always

greater than the actual radiated pressure ( $\tilde{p}_{rad} > p_{rad}$ ). This value of radiated pressure can be compared to the contact pressure and if this is negligible, then the actual radiated pressure can be guaranteed to be negligible. In accordance with Eq. (6.4), the vibroacoustic FRF's at two locations on the interface were measured and the results are plotted in Figure 6.11.

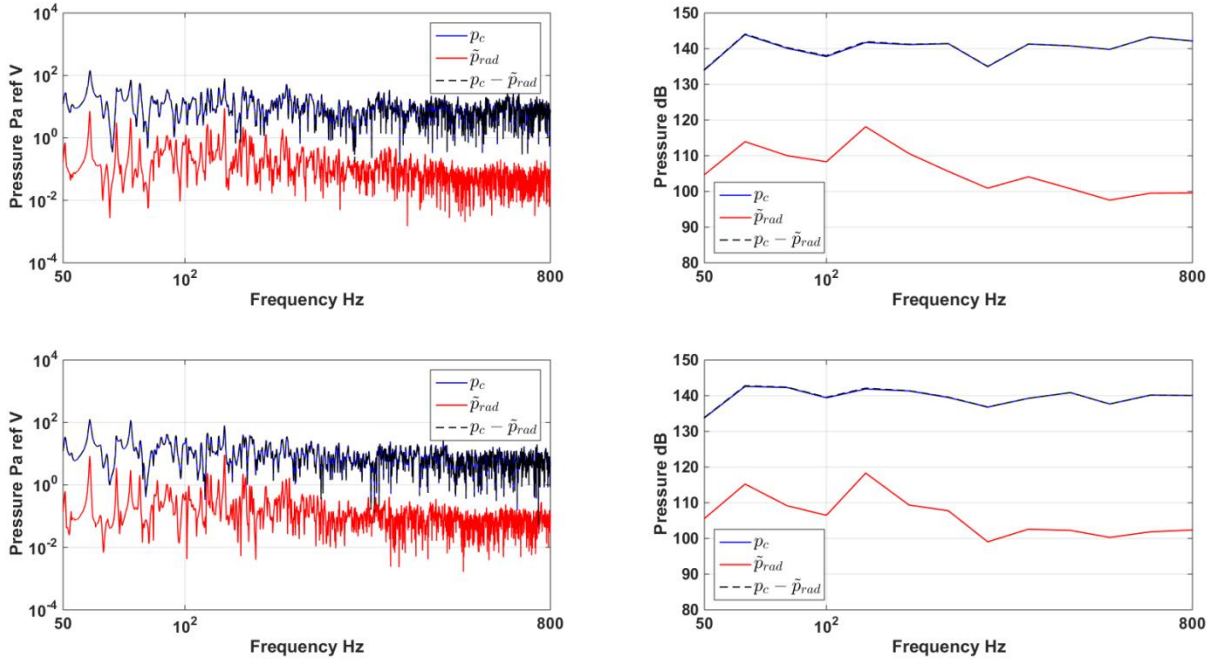


Figure 6.11: Comparison of contact pressure, upper limit of radiated pressure ( $\tilde{p}_{rad}$ ) at two source DoF in narrow band (left) and the one-third octave bands (right)

As can be seen from Figure 6.11, the radiated pressure ( $\tilde{p}_{rad}$ ) is negligible compared to the measured contact pressure which means that the contact pressure is almost equal to the blocked pressure ( $p_c \cong p_b$ ). This result is not surprising as it was earlier discussed in Chapter 5 that the contact pressure will be almost equal to the blocked pressure for cases where  $Z_p \gg Z_{air}$ . The result obtained here thus provides further confidence in the D-ASCA methodology employing a contact pressure approximation. This also shows conclusive proof that the deviations from the pressure validation (Figure 6.9) are not due to the contact pressure approximation. This methodology also serves as a faster and more accurate check for comparing contact and radiated pressures than the approach discussed in Section 5.5.3. It can be also seen that the actual blocked pressures ( $p_b$ ) will follow  $p_c > p_b > p_c - \tilde{p}_{rad}$ .

The radiated pressure was also predicted using the modal model to see how well it compares to the measured estimate of radiated pressure. Using Eq. (5.24), the radiated pressure was calculated at a point on the interface. The comparison with the measured estimate is shown in Figure 6.12

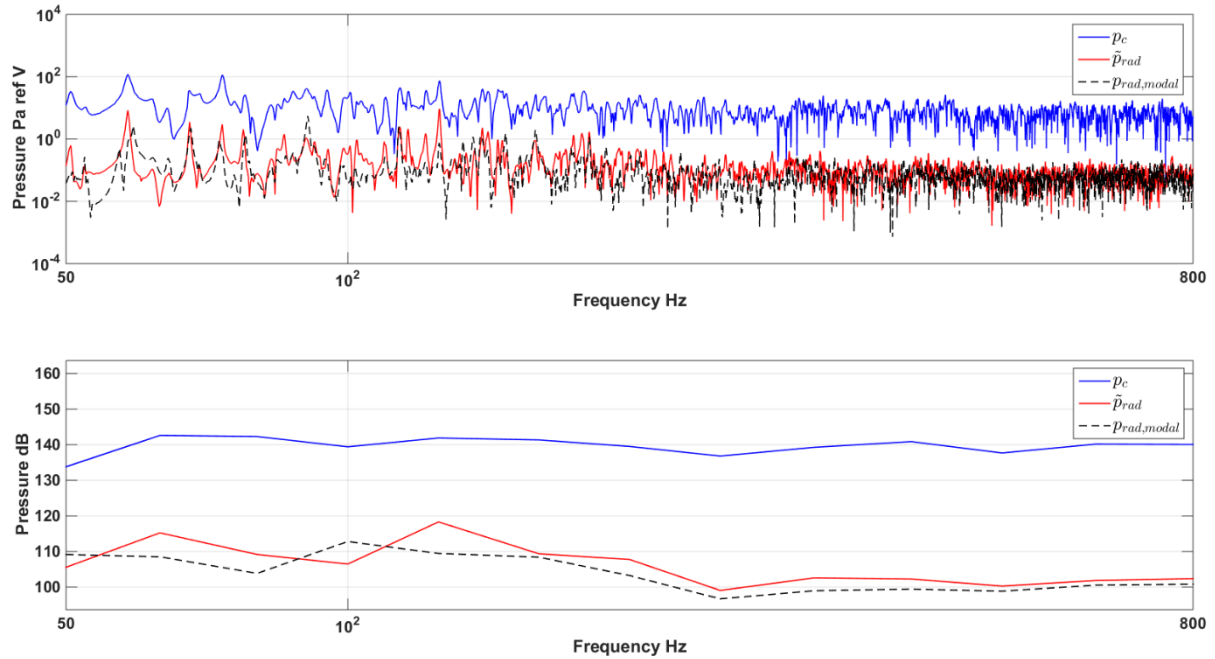


Figure 6.12: Comparison of contact pressure, upper limit of radiated pressure ( $\tilde{p}_{rad}$ ) and the radiated pressure calculated from modal model ( $p_{rad,modal}$ ) at one source DoF in narrow band (left) and the one-third octave bands (right)

Figure 6.12 shows that the comparison between the calculated and the measured radiated pressure is within 7-8 dB at low frequencies and the deviations decrease to about 2-3 dB as we go higher in the frequency range. The most important finding is that again the calculated radiated pressure is negligible compared to the contact pressure. The comparison between the calculated and the measured radiated pressure can be improved by more accurate determination of loss factors ( $\eta$ ) in narrow bands. In the current study these loss factors were calculated in one-third octave bands from RT measurements in the centre of the room. To use the modal model till a frequency of 800 Hz, modes up to 1600 Hz were used in calculation. By using more number of modes would improve the prediction but it also adds to computational costs.

Next, to diagnose the contributions of the frame and the glazing separately, the source contributions were measured. Due to presence of resilient seals between the frame and glazing, the frame and glazing were assumed to be decoupled from each other (similar to the case study I). Then the path contributions were simply estimated as the source contributions for the frame and glazing elements following Eq. (6.2, 6.3). These estimated path contributions are plotted in Figure 6.13

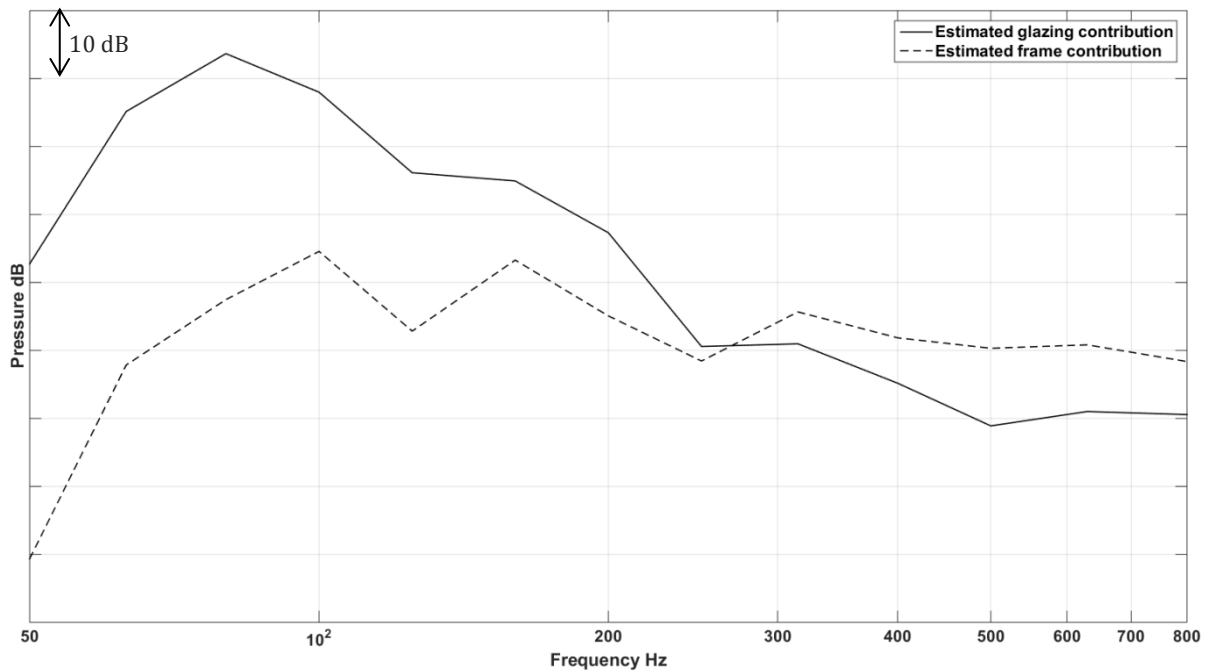


Figure 6.13: Estimated path contributions of glazing and frame elements of the single casement window in one-third octave bands from 50-800 Hz

The path contributions tend to show that at low frequencies (below 220 Hz), the contribution from the glazing is higher than the frame, while above 220 Hz, the frame contribution is higher. Thus we see a cross-over region in 200-300 Hz where the frame contribution overtakes the glazing contribution. As the glazing was a high performance insulator, while the frame is lightweight, the contributions from the frame were expected to be significant. The diagnostic method allows us to check this through in-situ measurements and the frequency regions in which different path contributions dominate.

As the frame contributes more to the receiver SPL above 200 Hz, the superior sound insulation performance of the glazing cannot be fully exploited in practice. Ideally, the frame

contribution should be lower to the glazing in such a case which would improve the sound insulation of the whole window structure. The diagnostic tests thus again show their potential in providing the path contributions and practical insight into SRI improvement based on in-situ measurements.

---

## 6.4 Combined testing – in situ perspective

---

In the previous sections, the combined SRI and diagnostic testing was performed in a laboratory where the test environment (flanking, sound field, background noise, etc.) can be controlled. Such tests in principle could also be applied in in-situ/field conditions. However, for field conditions, the test environment may be different than laboratory conditions which may impose restrictions on testing. In general, the diagnostic tests do not require any special test environments and can thus be applied in-situ provided the source, receiver and interface are defined correctly. On the other hand, the standard sound insulation methodology imposes requirements on the test environment. Therefore, it is important to discuss the implication of such test requirements if the combined application has to be practical for field conditions. In the following sections, a brief overview of such test conditions is presented.

---

### 6.4.1 Source and receiver fields

---

An important requirement of the standard sound insulation tests is that the test environment must be reverberant and the sound field to be diffuse. For diagnostic testing, the type of environment (reverberant, free field) does not restrict the application of the method. So the diagnostic contributions can be measured for any type of source field. If that is true, the diagnostic measurements could be further exploited in measuring the SRI. While ISO 16283 specifies SRI measurement for non-diffuse fields in field situations, it may not be always feasible to apply due to space restrictions (presence of furniture close to mics), or if the field is non-reverberant (for e.g. free field). One possible way to bypass such practical difficulties could be to use the diagnostic data to measure the SRI, as the diagnostic

measurements on source side are performed close to the partition. However, it is not obvious how the diagnostic data could be used for SRI measurement.

---

#### 6.4.2 Test structure and flanking

---

The standard sound insulation methods are specified for building elements such as walls, window, doors, etc. Similar functional elements are also present in non-building installations, for example, a door or window in a car or aircraft body. As the diagnostic tests are not limited to building elements, they can be in principle applied to any dynamic structure. But for such structures, no standard guidelines are available for measuring the sound insulation in-situ.

For sound insulation measurement, it is ideal that the structure borne and airborne flanking is minimal so that the SRI measured is a representative of the direct airborne transfer through the test structure. While the flanking in laboratory conditions is controlled, it may often be present in field conditions. Then, if the flanking is present, the SRI measured will be an apparent SRI which includes contributions of flanking. For diagnostic tests, the flanking transmission does not pose a problem per se, as the flanking transmission can be diagnosed similar to the direct airborne transmission. This ability could be exploited in field SRI measurement where the direct airborne transmission component could be diagnosed and used in a suitable SRI formulation.

The general observation from sections 6.4.1 and 6.4.2 is that while the diagnostic tests can be applied for field conditions, the application of standard tests may be restricted depending on whether the diffuse field conditions are met and whether flanking can be removed or made negligible. However as the diagnostic tests can still be applied in such cases tells that it is worthwhile to attempt SRI measurement using diagnostic data. We will now look into existing approaches for SRI measurement in field conditions before formulating a novel SRI measurement using diagnostic test data.

## 6.5 Sound insulation – measurement approaches

Consider the general case of a partition installed between a source and a receiving room. Mathematically, airborne sound insulation ('R') is then defined as the ratio of sound power incident on the partition ( $W_I$ ) to the sound power transmitted by the partition ( $W_T$ ) which can be further expanded in terms of pressures and velocities as,

$$R = 10 \log_{10} \left( \frac{W_I}{W_T} \right) = 10 \log_{10} \left( \frac{Re(p_I v_I^*)}{Re(p_T v_T^*)} \right) \quad (6.5)$$

In Eq. (6.5),  $p_I, p_T$  are the incident and transmitted pressures respectively while  $v_I, v_T$  are the incident and transmitted velocities respectively,  $Re$  refers to the real part of the sound intensity. However, Eq. (6.5) cannot be applied in due to practical challenges in measuring the incident intensity, incident pressure and incident velocity directly as discussed in Chapter 2. If the sound fields in both rooms can be assumed diffuse, then the sound insulation can be measured by an energy based approach (Eq. (1.2)) however that introduces errors and uncertainties in the low frequency SRI values. For field conditions, the uncertainties can be usually large for small rooms and some alternate approaches have been proposed which will be discussed now.

### 6.5.1 Standard sound insulation test with corner measurement

The uncertainty in low frequency SRI measurement arises due to a high standard deviation in SPL values. This means that the sound field is highly irregular (non-diffuse) in terms of spatial SPL distribution. The physical reason behind this is that at low frequencies, only a few modes contribute to the sound field. For each mode, a maximum SPL exists at the boundary while the SPL's at the centre can be minimal depending on the mode number. With the microphone positions specified by ISO 10140-5 around the centre of the room, the calculated source room energy does not account for the high energy at the room boundaries [154]. As such, the energy level measured then will underrepresent the true

energy level of the room. Then to reduce the uncertainty of SRI measurement at low frequencies, a corner position can be accounted in the measurements.

Multiple experimental studies (see Section 2.2.1) have looked into the measurement of SRI by incorporating a corner SPL measurement position. It was found that such practice reduces the uncertainty of the SRI values in the low frequency range. This corner measurement approach is also formally adopted in the field measurement standard of sound insulation (ISO 16283). The approach is easy to implement as one simply needs to add one more mic position at the corner. However the corner measurement focuses on reducing the uncertainty in the measurements while the diffuse field assumption is still preserved at the core of the method. The equations for measuring SRI (which are derived by diffuse field assumption) remain the same are still included. A corner measurement does not remove the effect of this assumption completely but rather takes into consideration the effect of pressure distribution at isolated modes in the low frequency region.

---

### 6.5.2 Diagonal measurement method

---

The diagonal measurement approach is another modification of the standard method where the room SPL's are calculated by positioning the microphones along the solid diagonal of the room. The diagonal measurement approach derives from the modal model which proves that the average SPL in a room (calculated by considering all positions) is equivalent as the average SPL calculated along the solid diagonal of the room. This approach has been tested and validated experimentally by Moorhouse [155] and Scheoenwald [156]. Again, in this method the equations used to calculate the SRI remain same as the standard method, so the diffuse field assumption is still inherent in the method. However the source room energy calculated from diagonal SPL positions has much less uncertainty at low frequencies. This is because the diagonal measurement is similar to measuring the SPL average at all positions in the room. One disadvantage of this method could be that the number of measurement positions can be higher than conventional ISO positions (6 mics in both rooms) as the solid diagonal of the room is the longest straight-line dimension of the



room. Thus this method could be ideal for small rooms but could become impractical for large rooms. An investigation can be made to refine this measurement approach for optimising the number of microphone positions along the solid diagonal.

Overall Section 6.5.1 and 6.5.2 show the approaches from the literature that have attempted to reduce the low frequency SRI uncertainty that arises due to the diffuse field assumption, but require separate SPL measurements. We will now investigate new approaches that could be applied in-situ for measuring the sound insulation for any structure, under airborne excitations where flanking may be present.

---

### 6.5.3 FRF based formulation

---

In this section, we will investigate if FRF measurements in the room-partition-room system could be used to measure the SRI. An FRF represents the output-input characteristic of a dynamic system i.e. the response of the system to an input source. The SRI also relates the input (in this case, the incident power) to the output (transmitted power) for the partition. FRF measurements do not relate two power quantities as the SRI does. Then, the quantity transmission loss (ratio of the transmitted pressure to the incident pressure) can be considered to find parallels with an FRF measurement.

In theory, the SRI or transmission loss is solely a property of the partition without any influence of the environments (free field or reverberant volume) on either side of the partition. On the other hand, FRF measurements are typically conducted for coupled system of two structures/fluids or a vibroacoustic system. Therefore they are generally not an independent property of a single subsystem such as a partition. For example, the vibroacoustic FRF is a property of the coupled partition-receiving room as the pressure measured in the room will be affected by the receiving room's properties.

For a free field in the receiving room, the vibroacoustic FRF can be used to relate the true pressure transmitted by the partition with respect to a force (or pressure on the partition). However in in-situ conditions, the receiving conditions are hardly of a free field type. Additionally the vibroacoustic FRF does not relate the transmitted pressure to the incident

pressure (which is the transmission loss), but it relates the transmitted pressure to the force (which is equivalent to contact pressure over an area). Therefore, the vibroacoustic FRF is conceptually dissimilar and unsuitable for a SRI measurement. The acoustic FRF is also not compatible with the definition of the transmission loss or SRI and thus cannot be used. In total, an FRF based approach would be unsuitable for measuring SRI in practical room-partition-room scenarios.

---

#### 6.5.4 SRI using blocked pressure hypothesis

---

Some studies (like [44]) take into account the assumption that a simple pressure doubling occurs at the surface of the partition ( $p_c = 2p_{incident}$ ) to measure the SRI. Such pressure doubling implicitly assumes the partition is blocked. Measuring the source room SPL's close to the partition surface has shown to improve SRI repeatability and reproducibility over ISO methods. However, these studies neither prove experimentally that a pressure doubling indeed occurs at the interface nor propose a method to validate this assumption.

By doing a pressure validation and/or measuring the radiated pressure, we can validate if a pressure doubling assumption is valid for a certain test case. For the cases of single and double casement window we can indeed apply a pressure doubling assumption as we performed a pressure validation and measured the radiated pressures. Then, we can formulate a SRI based on a pressure doubling approach.

If the contact pressure is equal to the blocked pressure, then the pressure doubling assumption is valid. For such cases, the sound power incident on a finite structure of area 'S' can be measured for a diffuse field as per [157],

$$W_I = \frac{p_b p_b^*}{8\rho c} S \quad (6.6)$$

In Eq. (6.6), the factor 8 accounts for the pressure doubling. If we have discretised the partition into 'j' number of patches with surface area  $dS$ , then the incident power can be written as a sum of incident power on all discrete patch areas as,

$$W_I = \frac{\sum_j p_{b,j} p_{b,j}^*}{8\rho c} dS \quad (6.7)$$

Although Eq. (6.6) is based on a diffuse field assumption, its use is practically advantageous because,

- i. The formulation employs blocked pressure measurements. This means that a single set of blocked pressure data can be used to measure the diagnostic contributions as well as the incident power which can be used for predicting the SRI.
- ii. Blocked pressures are measured at the room boundaries close to the partition which gives better SNR unlike SPL measurements around the centre of the room in standard methods of SRI measurement. The blocked pressure based approach would therefore be especially suited for low frequencies where a pressure minimum can be observed in the centre of the room but a pressure maximum observed at the boundaries of the room.

The incident sound power level can then be calculated as,

$$L_{W_I} = 10 \log_{10} \left( \frac{W_I}{10^{-12}} \right) \quad (6.8)$$

The transmitted sound power can either be calculated by an intensity approach [16] or indirectly by SPL measurements in receiving room as per ISO 3741. Using ISO 3741, the transmitted sound power level can be measured in one-third octave bands as,

$$L_{W_T} = L_2(f) + 10 \log \left( \frac{A}{A_0} \right) + 4.34 \frac{A}{S_R} + 10 \log \left( 1 + \frac{cS_R}{8Vf} \right) + C_1(f) + C_2(f) - 6 \quad (6.9)$$

where,  $f$  is the centre frequency of one-third octave bands,  $A_0$  is the reference absorption area equal to 1 m<sup>2</sup> and  $S_R$  is the surface area of the receiving room.  $C_1$  and  $C_2$  are the

metrological correction factors whose contribution is well below 1 dB and so can be neglected [56]. The expression can then be simplified to,

$$L_{W_T} = L_2(f) + 10 \log(A) + 4.34 \frac{A}{S_R} + 10 \log\left(1 + \frac{cS}{8Vf}\right) - 6 \quad (6.10)$$

Once both the incident and transmitted sound powers are known, the SRI can be calculated as,

$$R = L_{W_I} - L_{W_T} \text{ dB} \quad (6.11)$$

We will now predict the SRI of the partition using this approach for the single and double casement window case studies. As it was found that the radiated pressure for those cases was negligible, the contact pressure is equal to the blocked pressure or in other words, pressure doubling occurs at the interface. Although it is likely that a pressure doubling occurs on the surface of most building partitions as  $Z_p \gg Z_{air}$ , the novelty in this approach is that one can indeed measure the radiated pressure and assess whether a pressure doubling assumption is correct for a certain test case.

Taking the case of the double casement window, the incident sound power was first measured using Eq. (6.6) and the transmitted sound power was measured using the measured SPL's and absorption area of the receiving room. The SRI was then calculated as per Eq. (6.11) and the results are compared with the SRI measured according to standard ISO 10140 method in Figure 6.12.

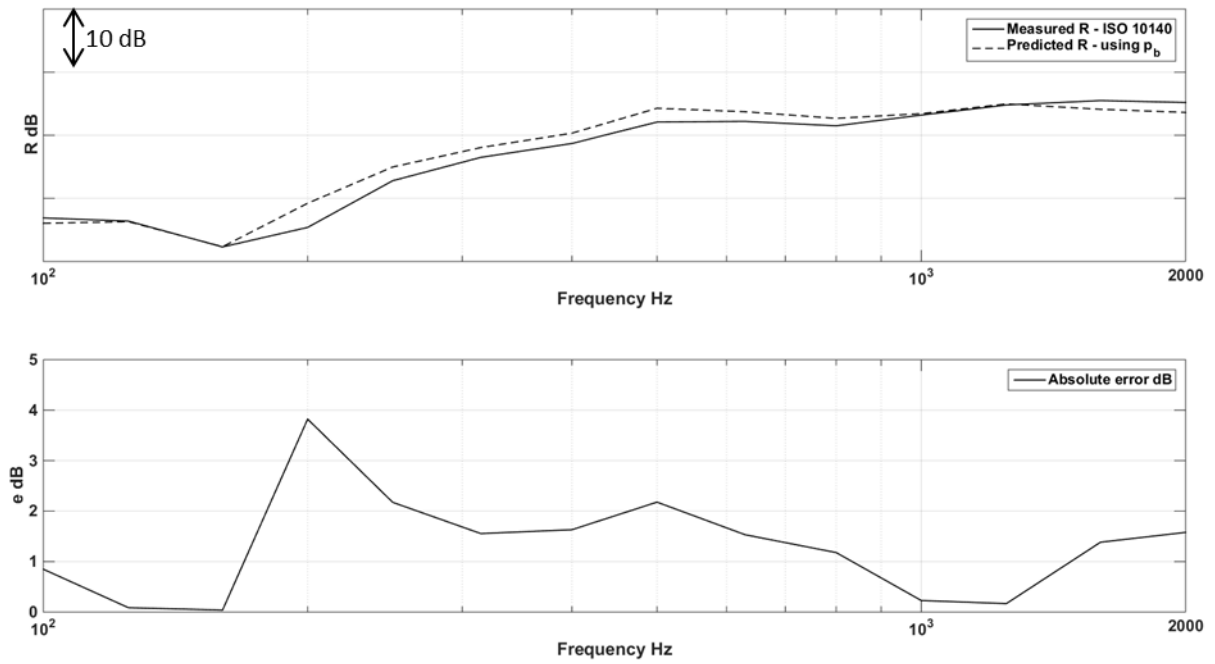


Figure 6.14: Comparison between the SRI measured using ISO 10140 method and using blocked pressures (Eq. 6.6-6.11) for the double casement window

Figure 6.14 shows the SRI of the double casement window predicted using the blocked pressures agrees with the standard measured SRI within 3 dB in general except at 200 Hz where the deviation is 3.9 dB. This was caused due to uncertainty in the absorption area measurements as the RT was not measured and was approximated from other SRI measurements. Nonetheless, the results show the added usability of the diagnostic data in predicting the SRI. Next the SRI was predicted for the single casement window case and the comparison with ISO 10140 results is plotted below.

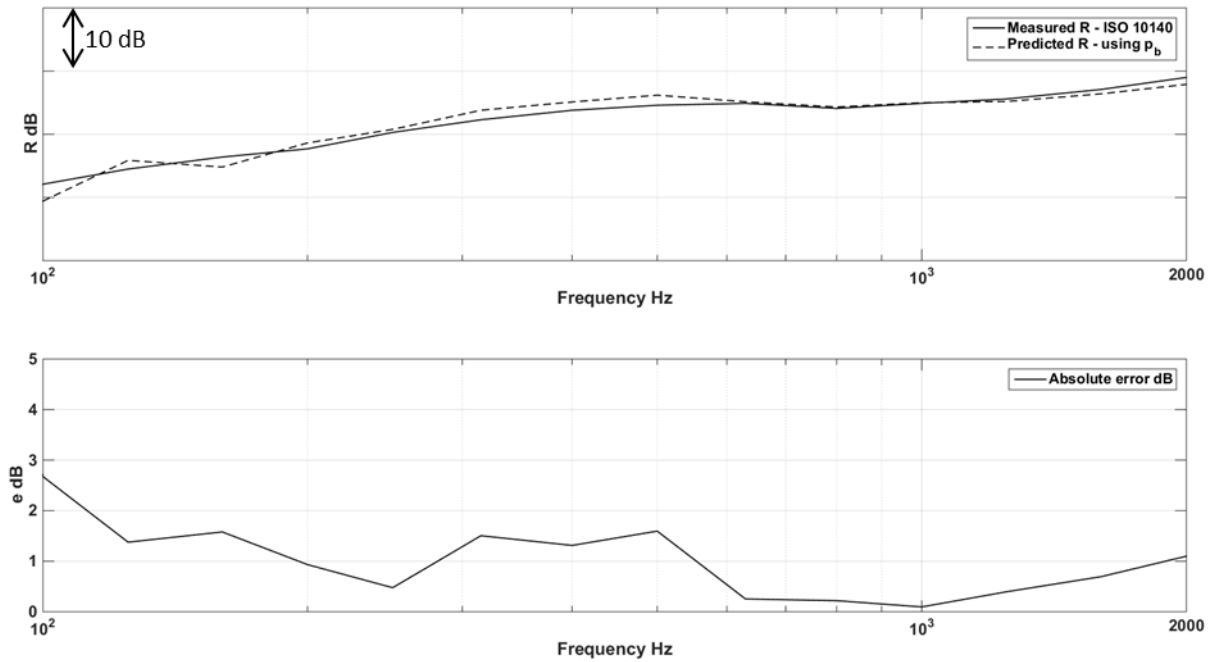


Figure 6.15: Comparison between the SRI measured using ISO 10140 method and using blocked pressures (Eq. 6.6-6.11) for the single casement window

Figure 6.15 shows the predicted SRI using blocked pressures and measured SRI using the ISO 10140 method for the single window casement case agree within 2 dB. The deviation in 100 Hz one-third octave frequency band is slightly higher at 2.7 dB. As the absorption area was measured accurately for this case, the deviations have slightly decreased compared to the double casement window case. Overall, this result provides further confidence in using diagnostic measurements (contact pressures) for SRI prediction. If the receiving room sound power is measured by intensity methods, it would further help in improving the repeatability and reproducibility of SRI measurements.

Although this SRI method is practically advantageous and suitable as blocked pressures (from diagnostic tests) can be used for predicting the SRI, the method is limited to building partitions where pressure doubling occurs. For the case where a pressure doubling may not occur for example, a limp panel/film of a lightweight material ( $Z_p$  comparable to  $Z_{air}$ ), a curtain, etc., a blocked pressure based approach to measure the SRI would not be suitable.

---

## 6.6 Conclusions

---

In summary, the chapter discusses how the diagnostic tests can be complemented with SRI results for realistic partitions. The case of a double and single casement window was discussed. For the case of double casement window, the SRI was first measured which provides the frequency dependence of sound insulation. Next the contributions of the glazing and frame elements were measured. The D-ASCA tests were applied and the source contributions of the glazing and frame were obtained. By making careful assumptions, it was shown that these source contributions would approximate their path contributions. These path contributions provide the spatial dependence of sound insulation in the partition. By comparing the path contributions in various frequency regions, the weak elements of sound insulation were identified. This information may be used for R&D practice to improve its sound insulation performance. Similar test was applied on a single casement window where the contributions of frame and glazing were separately assessed.

To measure the SRI with the diagnostic test, a comparison between different SRI approaches was discussed and new ideas were investigated. Following this, a blocked pressure based SRI approach was found to be suitable where the incident sound power can be measured using blocked pressures. The approach can be applied if a pressure doubling occurs at the partition surface. Using novel measurement approaches for radiated pressure, it can be assessed in-situ if a pressure doubling occurs at the surface. If a pressure doubling can be proved then the incident power can be worked out and SRI can be measured. The approach was applied on both windows and the predicted SRI was compared with the ISO 10140 measurement. It was found that when all the required measurements were performed (like in single window casement case), the error between measured and predicted SRI was within 3 dB. The novelty of the method is that radiated pressure can be measured to assess if a pressure doubling indeed occurs. The potential of the diagnostic tests was thus demonstrated to measure the diagnostic contributions as well as SRI.

---

# CONCLUSIONS

---

The work presented in this thesis concerns with the diagnosis of airborne sound transmission through building partitions. The airborne sound insulation measured as the Sound Reduction Index (SRI) provides the frequency dependence of the sound insulation. However, the spatial dependence of sound transfer i.e. how much sound is transmitted or contributed by different paths in the structure cannot be established using SRI data.

Thus, the motivations of the work formed in part from the inadequacy of the standard tests in diagnosing sound transmission paths as well as the uncertainties in SRI measurement. If the diagnostic contributions can be measured they would be a complement to the sound insulation tests in that both the frequency and spatial dependence of sound transfer (or insulation) can be measured. Additionally, the diagnostic contributions would help to identify the weak sound insulation elements. Accordingly, the objectives of the study were formulated which will be recalled now as,

- 1) To formulate a methodology for characterising the airborne excitation on partitions. An appropriate inverse technique will be used to characterise the pressure on the panel surface (or sub areas) in-situ.
- 2) To measure the sound pressure contributions of different elements and areas in the partition.
- 3) To complement the diagnostic results with standard airborne sound insulation results to provide a complete picture of how different elements affect the sound insulation of the complete structure.
- 4) To investigate a new technique for measuring the low frequency sound insulation of the partition without any diffuse field excitation assumption.

From the literature review, it was found that similar diagnostic problems are encountered by the automotive industry when dealing with structure borne. Transfer Path Analysis



(TPA) methods (particularly the inverse TPA (iTPA)) are used there to diagnose the contributions of the different structure borne sources at a receiver point. To formulate an iTPA approach for diagnosing the airborne noise spatially through the partition the following challenges were encountered.

- i. Source characterisation –Using iTPA, structure borne sources can be characterised in-situ by blocked forces at finite/discrete interface Degree of Freedom (DoF). For airborne excitation (pressure field) where the interface is continuous (infinite interface DoF), in-situ characterisation in practice would be really difficult.
- ii. FRF measurement –For finite interfaces as traditionally observed for structure borne sources, measurement of FRF's is practical and easy. For airborne sources, the interface is continuous which complicates the FRF measurement. Also for pressure excitations, structural FRF's are not compatible.
- iii. Source contributions – The iTPA only provides the source contributions however for an airborne problem diagnosis of path contributions is also essential which was not possible to measure by structure borne iTPA approach.

To avoid such practical difficulties, discretisation was employed to the continuous source excitation and structure at the interface. Accordingly, the system is represented by an equivalent system of point forces acting on discrete patches of the partition (see Figure 3.4). The path contribution of each patch was thus of interest.

A novel methodology Inverse-Airborne Source Contribution Analysis (I-ASCA) was then outlined where the continuous airborne excitation was characterised inversely by the blocked forces on discrete patches. This fulfils the problem from objective (1). The case study of airborne sound transmission through a cavity backed panel was discussed and validated experimentally and the predicted pressure was found to be within 3 dB except in the low frequency region (70-120 Hz) due to airborne flanking issues. For successful application of the pressure validation test it was thus necessary that no/negligible flanking transmission is present.

As the discretisation is employed, the validity of I-ASCA is limited to a certain maximum frequency. By observing the maximum frequency ( $f_{max}$ ) of prediction (within 3 dB of measured response) for the tested cases, a sampling criterion of grid size  $x \leq \lambda_{b,f_{max}}/2$  was determined, where  $\lambda_{b,f_{max}}$  is the bending wavelength at  $f_{max}$ , which was also used in similar theoretical studies in the literature. Above the critical frequency the grid size criterion should be based on the wavelength in air as it is smaller than  $\lambda_b$  in this region. After source characterisation, the source contribution were measured which represents the transmission through all paths under the action of a single blocked force. However, the path contribution which represents the transmission from an individual path under the action of source excitation could not be measured which is a limitation of the I-ASCA methodology.

*In summary, the I-ASCA method characterises the airborne excitation on the partition is by inversely measured blocked forces acting on discrete paths. The accuracy of prediction of total response is within 3 dB and only the source contributions can be measured provided the grid size is less than  $\lambda_b/2$ .*

To measure the path contribution, the paths were characterised as equivalent volume velocity sources using the measured velocity under the source excitation. The acoustic FRF's linking the path vibration to the pressure at a receiver point was then measured through a novel inverse process using accelerance and vibroacoustic FRF's. This allows measurement of the acoustic FRF in situations where acoustic FRF's cannot be measured directly or reciprocally. This forms the novel I-PCA (Inverse Path Contribution Analysis) methodology (Section 3.6.2). For the test case of cavity backed panel, the I-PCA methodology was applied to measure the path contributions. The accuracy of the I-PCA was found to be the same as I-ASCA. The path contributions highlighted the contributions of different regions (centre, corners, and edges) in different frequency regions and conform to the theoretical observations from the literature. A limitation of the I-PCA is that inverse measurement of acoustic FRF's can be tedious and prone to inversion errors, but is necessary when a direct or reciprocal measurement is not possible.

*In summary, the I-PCA method outlines a novel method for measuring the path contributions which are a diagnostic property of the path. A novel inverse measurement of acoustic FRF's is laid out for when direct or reciprocal measurement cannot be conducted. The accuracy of prediction is same as I-ASCA and the sampling follows  $x \leq \lambda_b/2$  criterion.*

Next, in Chapter 4, the application of I-ASCA, I-PCA methods on a dual leaf partition (with one point connection and absorption in cavity) was tested. I-ASCA for a structure borne case shows that the method has potential for source localisation, but can be tedious. The predicted pressure in receiver cavity was within 3.5 dB from 100 Hz to 1 kHz, which is the frequency limit set by the  $\lambda_b/2$  rule for the used grid size. Using I-PCA it was also estimated that removing the point connection contribution from the total pressure provided a decrease in sound transmission above 500 Hz till 1 kHz. This shows that the point connection (structural path) indeed acts a strong element of sound transfer or a sound bridge.

For airborne excitation case, the validation of the method was initially difficult (due to flanking) and was thus performed in a transmission suite facility. Also the cavity absorption was removed thereby increasing the sound transmission through airborne paths. The validation from I-ASCA shows the prediction was within 2 dB in 100 Hz-1 kHz range. Using I-PCA method, it was also found that the path contribution of the sound bridge path compared to individual acoustic path in the cavity was generally high above 200 Hz however; on aggregate the contribution of one structural path compared to the total acoustic path contributions is negligible. This is because having a non-absorbent cavity increased the sound transmission through the acoustic paths. Thus it was estimated that the effect of removing the point connection would be negligible. This was also confirmed by a predicting the sound insulation of the structure with and without single point connection in a transfer matrix model. In practice where multiple point connections or studs are used with cavity absorption, the contributions of the structural path could be significant. From the case studies it was also evident that the measurement time for all the vast number of FRF's for discrete paths was enormous.

In Chapter 5, a critique of I-ASCA and I-PCA methods was presented which suggested that for the diagnosis to be practical, the measurement time should be vastly reduced. As the inverse approach of source characterisation is tedious, a direct measurement approach was investigated. It was concluded that a direct blocked pressure characterisation was suitable. Three different characterisation approaches (existing and novel) were discussed which shows that blocked pressures can be approximated by contact pressures measured directly against the interface for  $Z_{partition} \gg Z_{air}$  where,  $Z$  represents the mechanical impedance. The contact forces (contact pressure x path area) can thus be used to measure the source contributions approximately. This formed the D-ASCA (Direct-Airborne Source Contribution Analysis) approach. Thus, as opposed to I-ASCA, the D-ASCA process is direct and does not require any accelerance measurements for source characterisation which provides a tremendous time advantage.

To validate D-ASCA experimentally, a test was conducted on an un baffled and baffled single leaf panel where the response was predicted by contact forces and inversely measured blocked forces. It was found that while I-ASCA introduces large inverse errors in some high frequency bands, the prediction from D-ASCA is far better (within 1 dB for un baffled panel and within 3.6 dB for baffled panel). Additionally, inverse errors are not introduced in the D-ASCA prediction as opposed to I-ASCA prediction. For a dual leaf partition, the pressure prediction is within 3 dB in 63-1000 Hz region. Using these contact pressures, the source contributions were also measured relatively easily. Like I-ASCA, one limitation of the D-ASCA process is that path contributions cannot be measured.

The difference between the contact pressure and the blocked pressure is a radiated pressure term which has been shown to be negligible in the literature. It was found that a conservative estimate of radiated pressure can be predicted using contact pressure which will be greater than the actual radiated pressure. But this would serve as a check to identify if contact pressure approximation is inaccurate. Additionally, a semi-analytical semi-experimental model was conceived to calculate the radiated pressure from the partition. This represents a novel application where the operational volume velocities are combined with the acoustic FRF's (derived from room modal model) to predict the radiated pressure

from the partition on source side. Using this technique, it was found that for the case of the dual leaf partition, the radiated pressure is negligible. For practical multi-layered partitions where the impedance of the panels is similar, the radiated pressure may then be neglected. This presents an added novelty to the objective (1) which deals with airborne source characterisation.

*The D-ASCA method thus approximates the blocked pressure of the airborne excitation on the paths by their contact pressure and the prediction accuracy (on average) is within 3 dB of the measured pressure. The sampling criterion for D-ASCA is the same as I-ASCA ( $x \leq \lambda_b/2$ ). Using D-ASCA, the source contributions can be measured but the path contribution cannot be measured. The radiated pressure was also found to be negligible*

The advantages of the D-ASCA over I-ASCA method can now be summarised as follows,

- 1) A significant reduction in measurement time can be achieved compared to I-ASCA method as the source characterisation and source contributions are measured directly without the need of measuring the accelerance or mobility FRF's.
- 2) Unlike I-ASCA, D-ASCA does not employ an inverse process-thus is not prone to any inverse errors in characterisation or source contributions.
- 3) In I-ASCA, FRF's on the whole structure have to be measured to diagnose a single source contribution. In D-ASCA, a single source contribution can be calculated without characterising the source for the complete interface, thus the method is local.
- 4) D-ASCA can be potentially made fully automated and non-invasive if the vibroacoustic FRF can be measured reciprocally using a laser vibrometer and volume velocity excitation.

To highlight how the diagnostic results can complement the SRI data, a combined insulation and diagnostic test were applied to a single and double casement window case. The D-ASCA approach was first applied to double casement window case and the accuracy of prediction was within 2.5 dB in 63-1000 Hz. The coupling between the frame and the glazing was assumed negligible due to resilient seals installed in between. Accordingly, the path contributions were estimated by the source contributions and the weak paths of sound

insulation were assessed. These contributions were discussed with the SRI measurement which shows the potential of the complementing diagnostic results with the SRI. This fulfilled the objective statement (3).

An investigation was made into predicting the SRI using the diagnostic measurements. It was found that under the case of a pressure doubling at the surface, the incident sound power can be measured from the blocked pressures. The novelty of the approach is that by measuring the radiated pressure one can assess if a pressure doubling occurs on the partition. This ultimately was used to measure the SRI of the single and double casement window and the error between the measured and predicted SRI was found to be within 3 dB. This fulfils the aim of the objective (4).

In total, the work presented three novel applications for diagnosing the airborne sound transmission through building partitions –the I-ASCA, I-PCA and D-ASCA method. Using these methods, the diagnostic source and path contributions can be measured in-situ. These methods are also not limited to building partitions but in principle can be applied to other structures such as a car window/door. These methods show potential in identifying the weak sound insulation paths, which can be a useful complement to the standard SRI results for R&D purposes. Finally, to have the combined in-situ application of sound insulation and diagnostic testing, a new measurement approach for sound insulation measurement was also outlined which in principle can be applied in-situ on any building partition. This demonstrates the versatility and potential of a combined in-situ SRI and diagnostic testing application developed in the work.

---

# FURTHER WORK

---

The methods developed in the thesis opens explore new applications of TPA methods in building acoustics. The methods were tested and validated in the tested frequency range and used to measure the source and path contributions. Following are the future steps in which the methods can be developed more.

1) The approaches developed in the thesis essentially represent the pressure excitation by an equivalent set of discrete point forces. While pressure excitation ranges from a normal to grazing incidence angles, the equivalent representation employed here is normal forces acting at the interface. For building acoustics applications in reverberant rooms, the energy distribution at grazing is usually minimal compared to angles close to normal incidences so this representation is sufficient as evidenced by the pressure validation in the transmission suite. However, this may not be the case for critical frequencies in the higher frequency region ( $\sim 2\text{-}4$  kHz). Such representation may also cause issues for cases when the excitation source is parallel to the partition essentially around grazing incidence angles. Therefore, an investigation can be made to assess whether grazing incidence transmission are predicted by the current methodology. If not, it would be advisable to measure additional FRF's (with excitation parallel to interface) to account for the grazing incidence transmission.

2) While the D-ASCA offers a significant improvement over the I-ASCA approach in measuring the source contributions relatively faster, it cannot be used to measure the path contributions. The path contributions at best can be approximated by the source contributions for elements which are decoupled from each other by resilient elements (for example, the frame and glazing in a window are relatively isolated from each other by seals between them). Therefore a more accurate method to measure the path contributions directly would be the next step forward from this research.

3) For partitions with structural elements such as studs/point connectors, etc. the path contributions (structure-borne and airborne) as well as the source contributions can be

measured. These contributions are what determine the sound insulation performance of the partition. Then an attempt can be made to optimise the location of structural elements within the partition for achieving the desired response. If the impedances of the structural elements can be measured in-situ, then these impedances can be adjusted in a global impedance matrix of the structure to virtually assess the performance of the new configuration.

4) The sound insulation of the partition can be measured in-situ for partitions using the new method but has not yet been applied to complex structures like a car window. Here, it is desirable to separate out the structural flanking for assessing the airborne transmission only. In principle the methods described in the present work would allow one to separate the transmissions, but practical studies into such cases is required to allow for the validation of these methods outside of building acoustics applications.



---

# APPENDIX I

---

## In-situ blocked force characterisation of structure-borne sources

The following derivation is taken from Moorhouse et al. [139]. Consider a source receiver assembly as shown in Figure I.1. The source substructure 'A' is coupled to the receiver substructure 'B' at the interface 'c'. C denotes the coupled assembly.

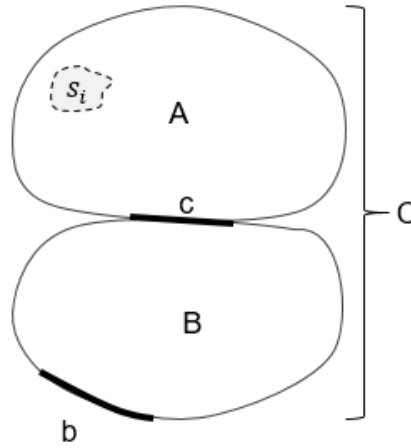


*Figure I.1* Assembled structure C comprising of source substructure A and receiver substructure B.  $b$  represents the DOF on the receiver and  $c$  represents the DOF on the interface,  $s_i$  represents the internal forces of the source

At first, we can write the operational velocity in 'B' using contact forces applied by the source at  $c$  as,

$$\mathbf{v}_b = \mathbf{Y}_{B,bc} \mathbf{f}_c \quad (\text{I.1})$$

Here, small letters in bold refer to a vector while capital letters in bold refer to a matrix. Eq. (I.1) represents the prediction using contact forces, which is used in classical TPA approaches. The contact forces can also be written in terms of the free velocity of the source as,

$$\mathbf{f}_c = [\mathbf{Y}_{A,cc} + \mathbf{Y}_{B,cc}]^{-1} \mathbf{v}_{fs} \quad (I.2)$$

The free velocity of the source is an independent property of the source which can be related to the blocked forces of the source as,

$$\mathbf{v}_{fs} = \mathbf{Y}_{A,cc} \mathbf{f}_{bl} \quad (I.3)$$

Substituting Eq. (I.3) into Eq. (I.2) we get,

$$\mathbf{f}_c = [\mathbf{Y}_{A,cc} + \mathbf{Y}_{B,cc}]^{-1} \mathbf{Y}_{A,cc} \mathbf{f}_{bl} \quad (I.4)$$

Substituting the above in Eq. (I.1), we get,

$$\mathbf{v}_b = \mathbf{Y}_{B,bc} [\mathbf{Y}_{A,cc} + \mathbf{Y}_{B,cc}]^{-1} \mathbf{Y}_{A,cc} \mathbf{f}_{bl} \quad (I.5)$$

Now let us consider the case of the passive assembly excited by a forces  $\mathbf{f}'$ . The resulting velocity then at 'c' can be written as,

$$\mathbf{v}'_c = \mathbf{Y}_{C,cc} \mathbf{f}' \quad (I.6)$$

Where, the prime indicates excitation at 'c'. Under the same excitation, the velocity at c and b in the assembly can be related to the interface force as,

$$\mathbf{f}'_c = \mathbf{Y}_{B,bc}^{-1} \mathbf{v}'_b = \mathbf{Y}_{B,cc}^{-1} \mathbf{v}'_c \quad (I.7)$$

From Eq. (I.6) and Eq. (I.7), we can obtain,

$$\mathbf{v}'_b = \mathbf{Y}_{B,bc} \mathbf{Y}_{B,cc}^{-1} \mathbf{Y}_{C,cc} \mathbf{f}' \quad (I.8)$$

We can now make use of the fact that the impedance of the coupled assembly is a sum of impedances of the individual substructures:

$$\mathbf{Y}_{C,cc}^{-1} = \mathbf{Y}_{A,cc}^{-1} + \mathbf{Y}_{B,cc}^{-1}$$

This identity can be substituted in Eq. (I.8) to obtain,

$$\mathbf{v}'_b = \mathbf{Y}_{B,bc} \mathbf{Y}_{B,cc}^{-1} (\mathbf{Y}_{A,cc}^{-1} + \mathbf{Y}_{B,cc}^{-1})^{-1} \mathbf{f}' = [\mathbf{Y}_{B,bc} (\mathbf{Y}_{A,cc} + \mathbf{Y}_{B,cc})^{-1} \mathbf{Y}_{A,cc}] \mathbf{f}' \quad (\text{I.9})$$

The matrix in the square brackets transforms the vector of forces applied at c to the velocity at b. Therefore, it must be equal to the generalised transfer mobility matrix of the coupled structure. Therefore, we get,

$$\left[ \mathbf{Y}_{B,bc} (\mathbf{Y}_{A,cc} + \mathbf{Y}_{B,cc})^{-1} \mathbf{Y}_{A,cc} \right] = \mathbf{Y}_{C,bc} = \mathbf{Y}_{C,cb}^T \quad (\text{I.10})$$

So now, we can write the Eq. (I.1) as,

$$\begin{aligned} \mathbf{v}_b &= \mathbf{Y}_{C,cb}^T \mathbf{f}_{bl} \\ \therefore \mathbf{f}_{bl} &= [\mathbf{Y}_{C,cb}^T]^{-1} \mathbf{v}_b \end{aligned} \quad (\text{I.11})$$

This means that the blocked forces can be conveniently measured in-situ from the couple mobility matrix of the source receiver assembly. This is especially advantageous over the classical TPA approaches where the mobilities have to be measured for the receiver substructure by physically removing the source. Another important advantage of Eq. (I.11) is that the source can be characterised by an independent quantity –the blocked force.

---

# APPENDIX II

---

## Measurement of material properties

To measure the material properties of a test structure, the following methodology was used and the relations have been taken from Cremer [37]. The bending wavelength in a solid panel of thickness ' $h$ ' at frequency ' $f$ ' can be found as,

$$\lambda_b \approx \sqrt{\frac{1.8c_{LI}h}{f}} \quad (\text{II.1})$$

where,  $c_{LI}$  is the longitudinal wave velocity in the panel. To measure  $c_{LI}$  we make use of the following relation,

$$c_{LI} = \sqrt{\frac{E}{\rho(1 - \mu^2)}} \quad (\text{II.2})$$

where,  $E$  is the modulus of elasticity,  $\rho$  is material density and  $\mu$  is the Poisson's ratio. The modulus of elasticity can be determined from the propagation velocity of quasi longitudinal waves in a beam of the same material as,

$$c_{LII} = \sqrt{\frac{E}{\rho}} \quad (\text{II.3})$$

$$\therefore E = c_{LII}^2 \rho$$

Therefore to determine the material properties and the bending wavelength in the test panel which is made from Perspex, the propagation velocity  $c_{LII}$  was first measured in a Perspex beam. To measure the propagation velocity the first longitudinal mode in the beam was measured by capturing the accelerance FRF from one end of the beam to the other end. The schematic of the experiment is shown below.

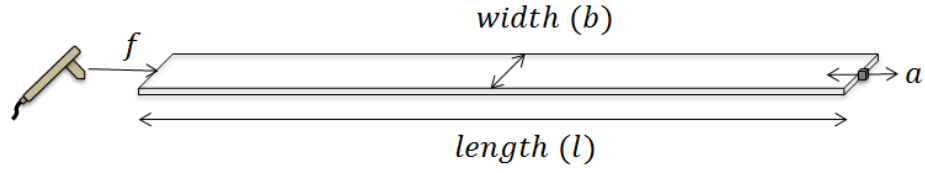


Figure II.1: Schematic of test on a Perspex beam ( $l = 1\text{ m}$ ,  $b = 0.05\text{ m}$ , thickness  $0.096\text{ m}$ ) for measuring the accelerance FRF (impact at one end and measuring the accelerance at other end)

The FRF obtained is shown in the figure below,

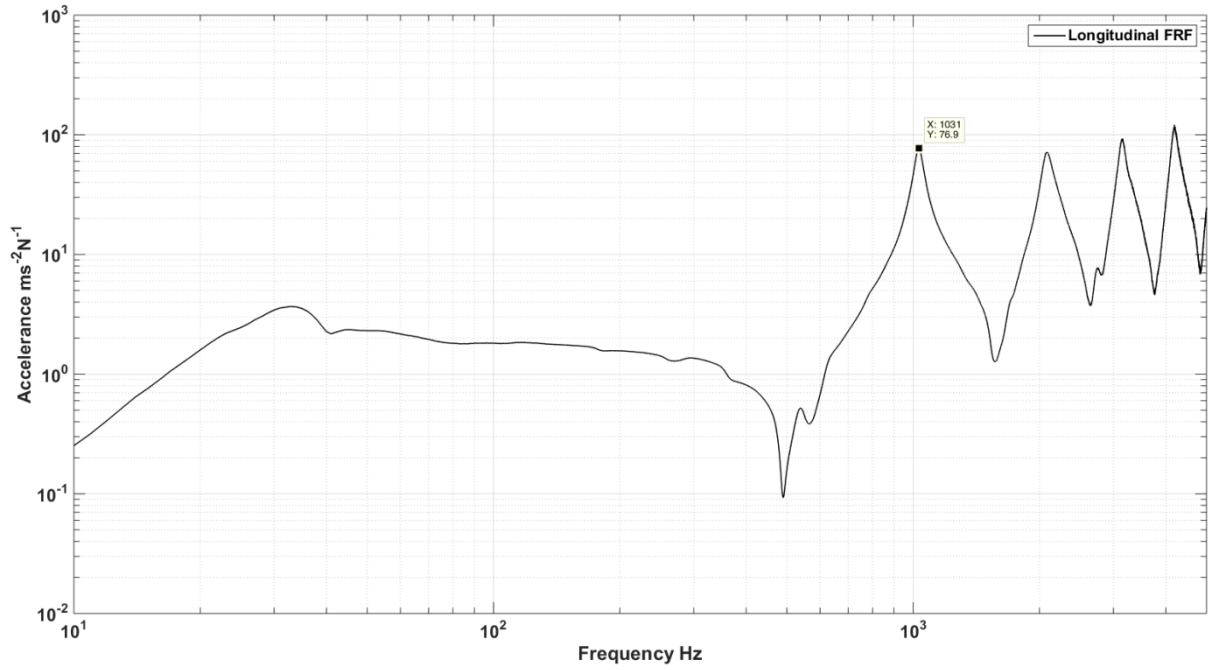


Figure II.2: Accelerance measured in the longitudinal direction of the beam as per Figure II.1

The peaks in the FRF correspond to the longitudinal modes in the beam. The first peak in the FRF at  $1031\text{ Hz}$  corresponds to the first longitudinal mode ( $f_1$ ) in the structure which relates to the propagation velocity as,

$$c_{LII} = f_1 \cdot 2l \quad (\text{II.3})$$

Table A.II.1: Measured material properties of Perspex

|   |           |         |
|---|-----------|---------|
| Length of sample (m)                                | $l$       | 1       |
| Width of sample (m)                                 | $b$       | 0.05    |
| Thickness of sample (m)                             | $h$       | 0.096   |
| Density (kg/m <sup>3</sup> )                        | $\rho$    | 1180    |
| First longitudinal mode in the beam (Hz)            | $f_1$     | 1031    |
| Propagation velocity in beam (m/s)                  | $c_{LII}$ | 2062    |
| Modulus of Elasticity (GPa)                         | $E$       | 5.02    |
| Longitudinal wave velocity on panel structure (m/s) | $c_{LI}$  | 2229.22 |
| Poisson's ratio                                     | $\mu$     | 0.38    |

Now we can plot, the longitudinal wave velocity in air and bending wavelength in the structure with respect to frequency. Additionally to identify the minimum grid size dimension for a particular frequency (according to  $x \leq \frac{\lambda}{2}$  criterion) a line corresponding to  $\lambda_b/2$  below critical frequency and  $\lambda_a/2$  above the critical frequency is also plotted.

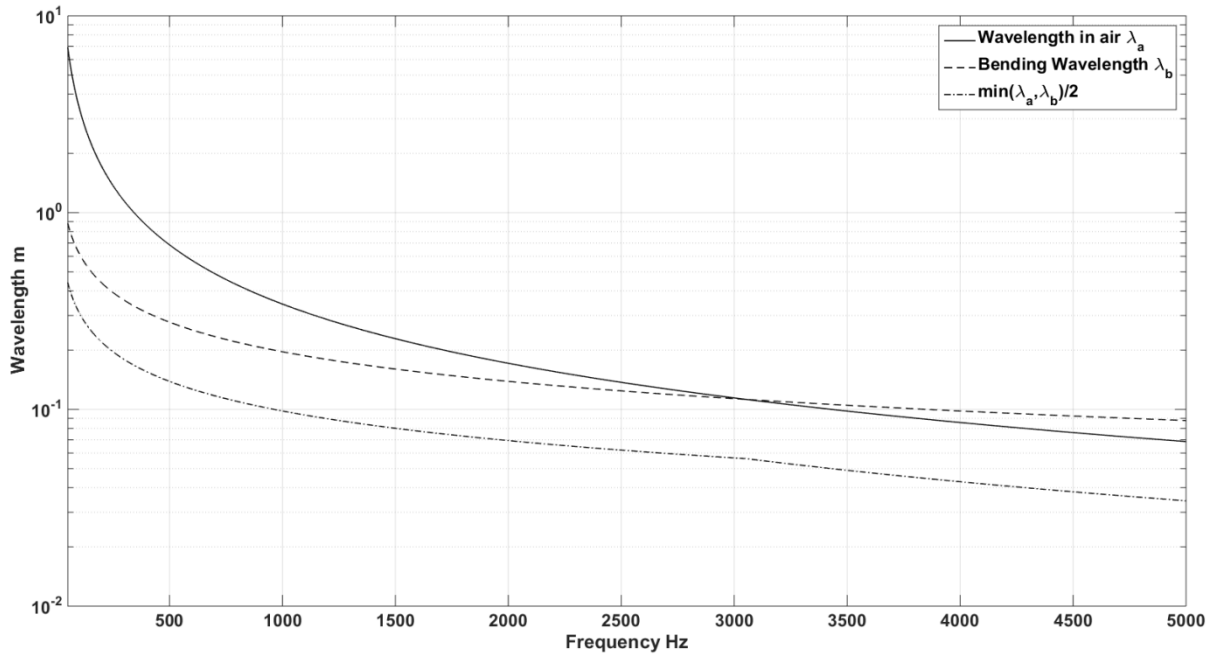


Figure II.3: Wavelength in air and Perspex panel plotted against frequency (50-5000 Hz) and the grid size line (•-•-) specifying minimum grid size according to  $x \leq \lambda/2$  sampling criterion

---

# APPENDIX III

---

## Blocked pressure formulation –Smith’s theory

This appendix outlines the formulation for blocked pressure on a partition as devised by Smith [108]. According to Smith, the blocked pressure of the airborne source is the pressure it applies on the partition when its motion is blocked. Then the blocked pressure can be related to the operational pressure as,

$$\mathbf{p} = \mathbf{p}_b + \mathbf{p}_{rad} \quad (\text{III.1})$$

where,  $p$  is the operational pressure acting on the partition when the partition is free to respond to the incident sound field,  $p_b$  is the blocked pressure and  $p_{rad}$  is the pressure radiated by the partition when the partition is driven by actuators which create an identical modal field similar to the operational velocity field in the partition.

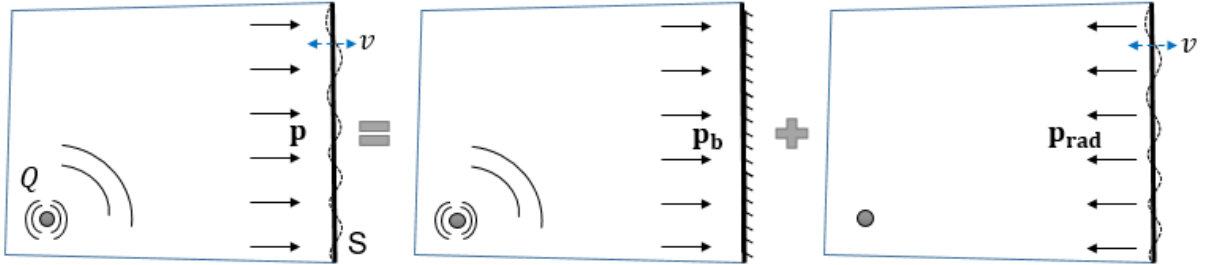


*Figure III.1* Operational pressure ( $\mathbf{p}$ ) acting on a partition ‘S’ due to an active volume velocity source  $Q$  represented as a result of the total blocked pressure ( $\mathbf{p}_b$ ) acting on the partition plus the pressure radiated by the partition ( $\mathbf{p}_{rad}$ ) when it vibrates with the operational velocity  $v$

The derivation can be explained using a conceptualised experiment. At first, the operational pressure acting on the partition can be measured under the action of the active source. Keeping the source unchanged, the blocked pressure can then be measured by blocking the motion of the partition. Next, the source is switched off and the partition is made to vibrate



with velocity amplitude that would be equal in magnitude to the operational velocity of the partition. The pressure radiated ( $p_{rad}$ ) by the partition can then be measured.

In other words, this is similar to imagining two sources that contribute to the pressure in the source volume. The first source is the original airborne source and the other is the partition source. By principle of superposition, the combined action of the two sources operating simultaneously is equal to the sum of individual sources activated independently. Smith did not provide a measurement results for the radiated pressure.

---

# APPENDIX IV

---

## Blocked pressure measurement –boundary value problem approach

Bobrovnitskii [129] outlined a general theorem for the solution of forced vibration problem expressed as a sum of solutions of two simple auxiliary boundary value problems. A short summary of the approach is presented here. Let's consider 'a' and 'b' as the two subsystems coupled at an interface 'S' with responses  $u$  and  $v$  respectively as shown in Figure IV.1 (left graphic).

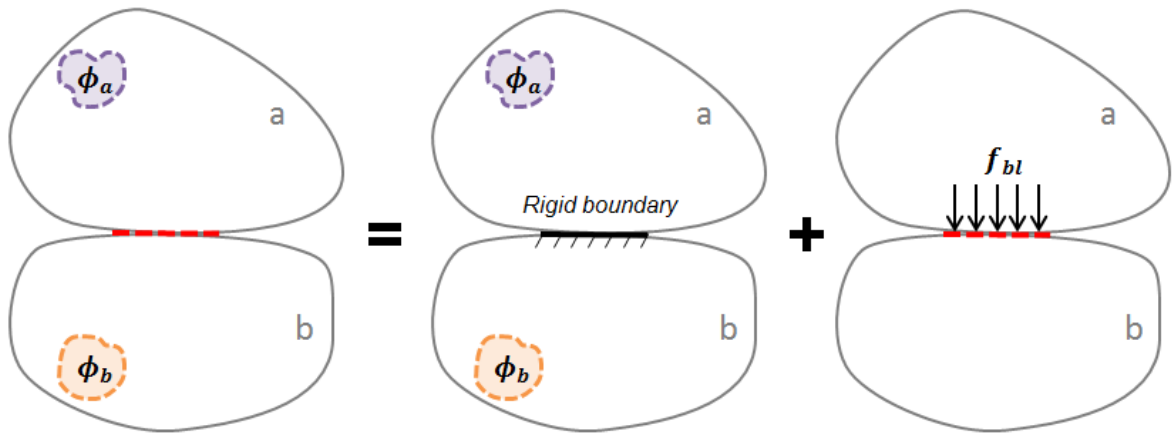


*Figure IV.1* Representation of the forced vibrations of a system (left) as a resultant of two boundary value problems (middle and right)

Let  $\phi_a$  and  $\phi_b$  be the external forces or the sources acting in the subsystems a and b. Under the action of these sources,  $f$  and  $g$  are the internal forces/stresses that develop at the interface S in subsystems a and b. Also,  $u$  and  $v$  are the responses of the subsystems a and b respectively. The responses of the subsystems to the external forces can be written as,

$$\begin{aligned} L_a u &= \phi_a \\ L_b v &= \phi_b \end{aligned} \tag{IV.1}$$

$L_a$  and  $L_b$  are the differential operators that relate the responses to the external stimuli. Similarly the internal forces ( $f$  and  $g$ ) developed at the interface are related to the responses through differential operators  $l_a$  and  $l_b$  respectively as,

$$\begin{aligned} f &= l_a u \\ g &= l_b v \end{aligned} \tag{IV.2}$$

The solution for this problem can be broken down as solutions to two simple auxiliary problems as,

$$\begin{aligned} u &= u_0 + u_1 \\ v &= v_0 + v_1 \end{aligned} \tag{IV.3}$$

Response  $u_0$  and  $v_0$  refer to the solution of first auxiliary problem where the interface S is blocked whilst  $u_1$  and  $v_1$  refer to the solution of the second auxiliary problem when the blocked reaction obtained from the first problem act at interface 'S' and the source is inactive. The equations for the first problem can then be written as,

$$\begin{aligned} L_a u_0 &= \phi_a \\ L_b v_0 &= \phi_b \\ f_0 &= l_a u_0 \\ g_0 &= l_b v_0 \end{aligned} \tag{IV.4}$$

$f_0$  and  $g_0$  are the reaction forces acting in blocked conditions. If the boundary conditions for the first problem were assumed to be blocked, the boundary conditions for the second problem can be determined by comparing Eq. (IV.1-IV.4). We get,

$$\begin{aligned} L_a u_1 &= 0 \\ L_b v_1 &= 0 \end{aligned} \tag{IV.5}$$

Thus in the second auxiliary problem, there is no external excitation (or the external sources are switched off). The responses for the second problem at interface 'S' are,

$$\begin{aligned} u &= u_0 + u_1 = u_1 \\ v &= v_0 + v_1 = v_1 \end{aligned} \tag{IV.6}$$

The interface in the first problem is blocked hence,  $u_0 = v_0 = 0$ . Applying the response continuity equation ( $u = v$ , at S) we get,

$$u_1 = v_1 \tag{IV.7}$$

Applying force continuity equations at interface 'S', we get,

$$f + g = 0 \tag{IV.8}$$

$$\begin{aligned} l_a u_0 + l_a u_1 + l_b v_0 + l_b v_1 &= 0 \\ f_0 + l_a u_1 + g_0 + l_b v_1 &= 0 \end{aligned} \tag{IV.9}$$

$$l_a u_1 + l_b v_1 = -(f_0 + g_0) = -f_b$$

This second problem thus represents the system where there are no external forces acting on the subsystems and the response at the surface S is equal to response of the system with the source activated. The forces acting on the surface S are the reaction forces from the first auxiliary problem in blocked condition (blocked forces). Therefore the response of the system under the action of an active source can be defined with the source inactive and blocked forces of the source acting on the interface 'S'.

---

# APPENDIX V

---

## Comparison of eigen/modal frequencies of a non-rectangular and rectangular room

The non-rectangular source room was modelled in COMSOL to calculate its modal frequencies. Additionally, the approximate rectangular model used for the comparison is also shown in the Figure V.1 below. The approximate room is found by having a rectangular room of the same volume as the non-rectangular room.

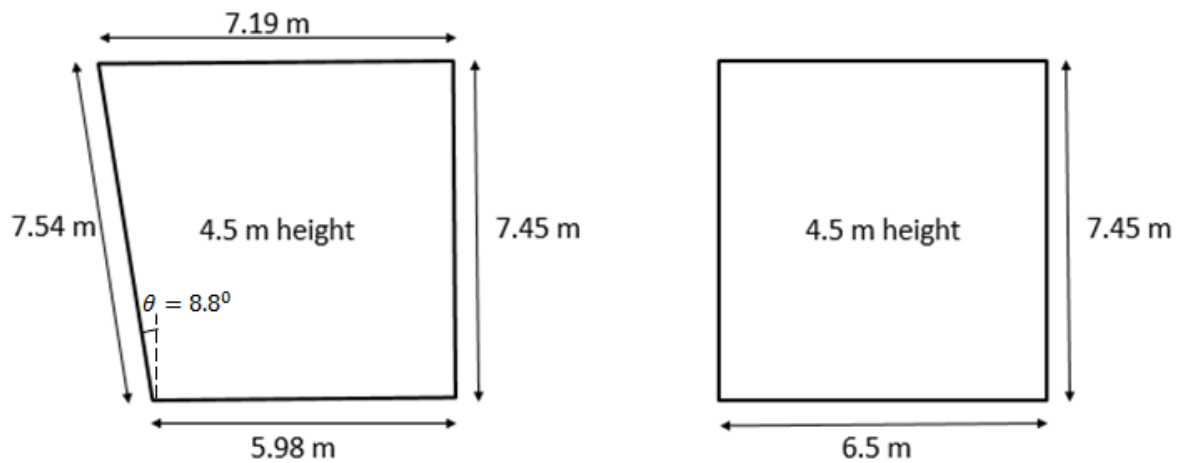


Figure V.1 The real geometry modelled in COMSOL (on left) and the approximate rectangular geometry (on right) modelled using analytical method

Once the modes were calculated for both cases, the modal frequencies were plotted together and the results are shown below.

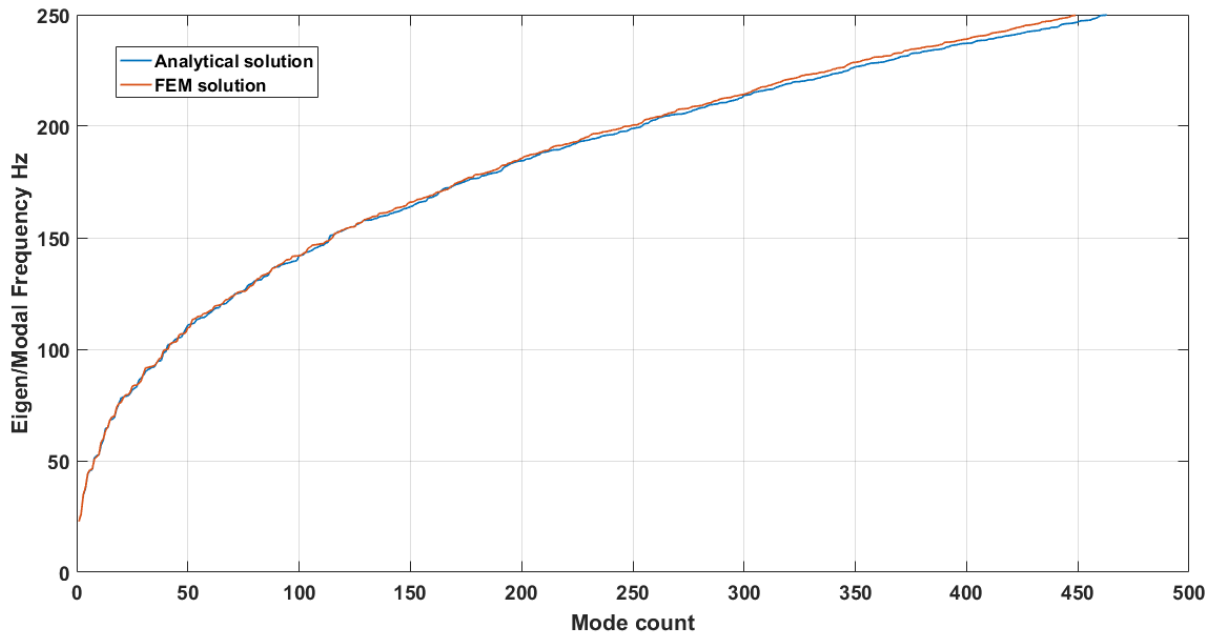


Figure V.2 Calculated modal frequencies for the configurations shown in Figure V.1.

Analytical solution is for the rectangular room while FEM solution is for the non-rectangular room

The way to interpret Figure V.2 is to look at the number of modes (mode count) under a given frequency of interest (y-axis). The results presented in Figure V.2 are below Schroeder Frequency above which the sound field in the room can be considered diffuse. For the source room, the Schroeder frequency is about 248 Hz. Even below this frequency, we can see the modal frequencies of the non-rectangular room are similar to the approximate rectangular room. For the rectangular room, the number of modes is slightly higher (15 modes) than the non-rectangular counterpart. This is because not all axial modes are excited in a non-rectangular room which is why we see less number of modes than a rectangular room of the same volume. Overall, the similarity in the modal frequency results provide confidence in the rectangular room approximation to be used in the current case of the non-rectangular room for calculating the acoustic FRF's in Section 5.5.3.

---

# REFERENCES

---

- [1] Balazova, I., Clausen, G., Rindel, J. H., Poulsen, T., & Wyon, D. P. (2008). Open-plan office environments: a laboratory experiment to examine the effect of office noise and temperature on human perception, comfort and office work performance. *Proceedings of indoor air, 2008*.
- [2] Paradis R., (2016, January 9), *Acoustic Comfort*. Retrieved from-  
<http://www.wbdg.org/resources/acoustic-comfort>
- [3] Tiller, D. K., Wang, L. M., Musser, A., & Radik, M. J. (2010). Combined effects of noise and temperature on human comfort and performance. In *2010 ASHRAE Annual Conference*.
- [4] Skånberg, A., & Öhrström, E. (2002). Adverse health effects in relation to urban residential soundscapes. *Journal of Sound and Vibration, 250*(1), 151-155.
- [5] Ouis, D. (2001). Annoyance from road traffic noise: a review. *Journal of environmental psychology, 21*(1), 101-120.
- [6] Beaman, C. P. (2005). Auditory distraction from low-intensity noise: a review of the consequences for learning and workplace environments. *Applied Cognitive Psychology, 19*(8), 1041-1064.
- [7] Leather, P., Beale, D., & Sullivan, L. (2003). Noise, psychosocial stress and their interaction in the workplace. *Journal of Environmental Psychology, 23*(2), 213-222.
- [8] Mak, C. M., & Lui, Y. P. (2012). The effect of sound on office productivity. *Building Services Engineering Research and Technology, 33*(3), 339-345.
- [9] Suter, A. H. (2002). Construction noise: exposure, effects, and the potential for remediation; a review and analysis. *AIHA Journal, 63*(6), 768-789.
- [10] Waye, K. P., & Rylander, R. (2001). The prevalence of annoyance and effects after long-term exposure to low-frequency noise. *Journal of sound and vibration, 240*(3), 483-497.
- [11] Bolin, K., Bluhm, G., Eriksson, G., & Nilsson, M. E. (2011). Infrasound and low frequency noise from wind turbines: exposure and health effects. *Environmental research letters, 6*(3), 035103.
- [12] Berglund, B., Hassmen, P., & Job, R. S. (1996). Sources and effects of low-frequency noise. *The Journal of the Acoustical Society of America, 99*(5), 2985-3002.
- [13] Gibbs, B. M., Qi, N., & Moorhouse, A. T. (2007). A practical characterisation for vibro-acoustic sources in buildings. *Acta Acustica united with Acustica, 93*(1), 84-93.
- [14] Rasmussen, B. (2010). Sound insulation between dwellings—Requirements in building regulations in Europe. *Applied Acoustics, 71*(4), 373-385.
- [15] ISO, E. (2010). 10140-2: 2010. *ISO Acoustics--Laboratory measurement of sound insulation of building elements--Part 2: Measurement of airborne sound insulation, 1-13*.

- [16] ISO, I. (2000). 15186-1: 2000. *Acoustics—Measurement of sound insulation in buildings and of building elements using sound intensity—Part, 1*, 1-20.
- [17] ISO, I. (2011). 16283: 1. *Acoustics—Field measurement of sound insulation in buildings and of building elements—Part 1: Airborne sound insulation*.
- [18] ISO, E. (2006). 717-1: 1996. *Acoustics—Rating of sound insulation in buildings and of building elements—Part, 1*, 717-1.
- [19] Park, H. K., & Bradley, J. S. (2009). Evaluating standard airborne sound insulation measures in terms of annoyance, loudness, and audibility ratings. *The Journal of the Acoustical Society of America*, 126(1), 208-219.
- [20] Neubauer, R. O. (2005, July). Airborne sound insulation in dwellings and its subjective estimation. In *Proc. 12th International Congress on Acoustics-ICSV* (Vol. 12).
- [21] Hopkins, C., & Turner, P. (2005). Field measurement of airborne sound insulation between rooms with non-diffuse sound fields at low frequencies. *Applied Acoustics*, 66(12), 1339-1382.
- [22] Government of Scotland, *Noise, Part 1 Technical Handbook*, Retrieved from, [www.gov.scot/resource/buildingstandards/2013NonDomestic/chunks/ch06.html](http://www.gov.scot/resource/buildingstandards/2013NonDomestic/chunks/ch06.html)
- [23] Beranek, L. L. (1954). *Acoustics* New York.
- [24] Sabine, W. C. (1922). *Collected papers on acoustics*. Harvard university press.
- [25] Buckingham, E. (1925). *Theory and interpretation of experiments on the transmission of sound through partition walls* (No. 506). Govt. Print. Off..
- [26] Davis, A. H. (1926). XLVII. The basis of acoustic measurements by reverberation methods. *The London, Edinburgh, and Dublin Philosophical Magazine and Journal of Science*, 2(9), 543-556.
- [27] Davis, A. H. (1925). VI. Reverberation equations for two adjacent rooms connected by an incompletely soundproof partition. *The London, Edinburgh, and Dublin Philosophical Magazine and Journal of Science*, 50(295), 75-80.
- [28] Jacobsen, F. (2011). The sound field in a reverberation room. *Technical University of Denmark, Lyngby, Denmark*.
- [29] Wentle, E. C., & Bedell, E. H. (1930). A chronographic method of measuring reverberation time. *The Journal of the Acoustical Society of America*, 1(3A), 422-427.
- [30] Schroeder, M. R. (1965). New Method of Measuring Reverberation Time. *The Journal of the Acoustical Society of America*, 37(6), 1187-1188.
- [31] ISO, E. (1993). 9614-1. *Acoustics—Determination of sound power levels of noise sources using sound intensity—Part 1: Measurement at discrete points* (ISO 9614, 1).
- [32] Pascal, J. C., & Carles, C. (1982). Systematic measurement errors with two microphone sound intensity meters. *Journal of Sound and Vibration*, 83(1), 53-65.



- [33] Jacobsen, F., & Jaud, V. (2006). A note on the calibration of pressure-velocity sound intensity probes a. *The Journal of the Acoustical Society of America*, 120(2), 830-837.
- [34] Jacobsen, F., & de Bree, H. E. (2005). A comparison of two different sound intensity measurement principles a. *The Journal of the Acoustical Society of America*, 118(3), 1510-1517.
- [35] Halliwell, R. E., & Warnock, A. C. C. (1985). Sound transmission loss: Comparison of conventional techniques with sound intensity techniques. *The Journal of the Acoustical Society of America*, 77(6), 2094-2103.
- [36] Schroeder, M. (1954). Die statistischen Parameter der Frequenzkurven von großen Räumen. *Acta Acustica united with Acustica*, 4(5), 594-600.
- [37] Cremer, L., Heckl, M., & Ungar, E. E. (1975). Structure-borne sound. *Physics Today*, 28, p 545.
- [38] Utley, W. A. (1968). Single leaf transmission loss at low frequencies. *Journal of Sound and Vibration*, 8(2), 256-261.
- [39] Mulholland, K. A., & Lyon, R. H. (1973). Sound insulation at low frequencies. *The Journal of the Acoustical Society of America*, 54(4), 867-878.
- [40] Sewell, E. C. (1970). Transmission of reverberant sound through a single-leaf partition surrounded by an infinite rigid baffle. *Journal of Sound and Vibration*, 12(1), 21-32.
- [41] ISO, I. (2014). 12999. *Acoustics– Determination and application of measurement uncertainties in building acoustics -- Part 1: Sound insulation*.
- [42] Simmons, C. (2007). Uncertainty of measured and calculated sound insulation in buildings- Results of a Round Robin Test. *Noise control engineering journal*, 55(1), 67-75.
- [43] Simmons, C. (1999). Measurement of sound pressure levels at low frequencies in rooms. Comparison of available methods and standards with respect to microphone positions. *Acta Acustica united with Acustica*, 85(1), 88-100.
- [44] D. B., Roland, J., Raabe, G., & Maysenhölder, W. (2000). Measurement of the low-frequency sound insulation of building components. *Acta Acustica united with Acustica*, 86(3), 495-505.
- [45] Hoffmeyer, D., & Jakobsen, J. (2010). Sound insulation of dwellings at low frequencies. *Journal of Low Frequency Noise, Vibration and Active Control*, 29(1), 15-23.
- [46] Dijckmans, A., & Vermeir, G. (2012). Numerical investigation of the repeatability and reproducibility in building acoustical measurements. *Department of Civil Engineering, KU Leuven, Kasteelpark Arenberg*, 40.
- [47] Mašović, D., Mijić, M., & Pavlović, D. Š. (2012, November). Comparison of New measurement methods in building acoustics at low frequencies. In *Telecommunications Forum (TELFOR), 2012 20th* (pp. 1232-1235). IEEE.

- [48] Prato, A., Casassa, F., & Schiavi, A. (2016). Reverberation time measurements in non-diffuse acoustic field by the modal reverberation time. *Applied Acoustics*, 110, 160-169.
- [49] De Tricaud, P. (1975). Impulse techniques for the simplification of insulation measurement between dwellings. *Applied Acoustics*, 8(4), 245-256.
- [50] Balilah, Y. A., & Gibbs, B. M. (1988). The measurement of the transmission loss of single leaf walls and panels by an impulse method. *Journal of sound and vibration*, 123(2), 229-245.
- [51] Viveiros, E. B., Gibbs, B. M., & Gerges, S. N. Y. (2002). Measurement of sound insulation of acoustic louvres by an impulse method. *Applied Acoustics*, 63(12), 1301-1313.
- [52] ISO, I. (2006). 18233. *Acoustics -- Application of new measurement methods in building and room acoustics*.
- [53] Venegas, C. R., Nabuco, M., & Massarani, P. (2006). Sound insulation evaluation using transfer function measurements. *Building Acoustics*, 13(1), 23-31.
- [54] Satoh, F., Hayashi, Y., Hirano, J., & Sakamoto, S. (2011). Sound insulation measurement using 10 minute Swept-Sine signal. *Proc. Inter-Noise 2011*, 428950.
- [55] de AC Duarte, E., Moorhouse, A., & Viveiros, E. B. (2012). Indirect measurement of acoustic power into a small room at low frequencies. *Applied Acoustics*, 73(3), 248-255.
- [56] Roozen, N. B., Labelle, L., Rychtáriková, M., & Glorieux, C. (2015). Determining radiated sound power of building structures by means of Laser Doppler vibrometry. *Journal of Sound and Vibration*, 346, 81-99.
- [57] Williams, E. G., & Maynard, J. D. (1982). Numerical evaluation of the Rayleigh integral for planar radiators using the FFT. *The Journal of the Acoustical Society of America*, 72(6), 2020-2030.
- [58] Piana, E. A. (2016). A method for determining the sound reduction index of precast panels based on point mobility measurements. *Applied Acoustics*, 110, 72-80.
- [59] Robin, O. (2016, August). Alternative Methods for the Measurement of Panel Transmission Loss under Diffuse Acoustic Field Excitation. In *INTER-NOISE and NOISE-CON Congress and Conference Proceedings* (Vol. 253, No. 6, pp. 2120-2129). Institute of Noise Control Engineering.
- [60] Nishida, E. (2010). Sound transmission loss estimation method by impact testing. *Noise Control Engineering Journal*, 58(5), 551-556.
- [61] Prato, A., & Schiavi, A. (2015). Sound insulation of building elements at low frequency: A modal approach. *Energy Procedia*, 78, 128-133.
- [62] Dowell, E. H., & Voss, H. M. (1963). The effect of a cavity on panel vibration. *AIAA journal*, 1(2), 476-477.
- [63] Guy, R. W., & Bhattacharya, M. C. (1973). The transmission of sound through a cavity-backed finite plate. *Journal of Sound and Vibration*, 27(2), 207IN7217-216IN8223.

- [64] Pretlove, A. J. (1966). Forced vibrations of a rectangular panel backed by a closed rectangular cavity. *Journal of Sound and vibration*, 3(3), 252-261.
- [65] Kihlman, T. (1967). Sound radiation into a rectangular room. Applications to airborne sound transmission in buildings. *Acta Acustica united with Acustica*, 18(1), 11-20.
- [66] Nilsson, A. C. (1972). Reduction index and boundary conditions for a wall between two rectangular rooms. Part I: Theoretical results. *Acta Acustica united with Acustica*, 26(1), 1-18.
- [67] Hopkins, C. (2012). *Sound insulation*. Routledge.
- [68] Hongisto, V. (2000). *Airborne sound insulation of wall structures: measurement and prediction methods*. Helsinki University of Technology.
- [69] Mak, C. M., & Wang, Z. (2015). Recent advances in building acoustics: An overview of prediction methods and their applications. *Building and Environment*, 91, 118-126.
- [70] Crocker, M. J., & Price, A. J. (1969). Sound transmission using statistical energy analysis. *Journal of Sound and Vibration*, 9(3), 469-486.
- [71] Tadeu, A., & António, J. M. P. (2002). Acoustic insulation of single panel walls provided by analytical expressions versus the mass law. *Journal of sound and vibration*, 257(3), 457-475.
- [72] Sharp, B. H. (1973). *A study of techniques to increase the sound insulation of building elements*. US Department of Commerce, National Technical Information Service (NTIS).
- [73] Ng, C. F., & Zheng, H. (1998). Sound transmission through double-leaf corrugated panel constructions. *Applied Acoustics*, 53(1-3), 15-34.
- [74] London, A. (1949). Transmission of reverberant sound through single walls. *J. Research Nat. Bur. of Stand*, 42(605), 2.
- [75] London, A. (1950). Transmission of reverberant sound through double walls. *The journal of the acoustical society of America*, 22(2), 270-279.
- [76] Kang, H. J., Ih, J. G., Kim, J. S., & Kim, H. S. (2000). Prediction of sound transmission loss through multilayered panels by using Gaussian distribution of directional incident energy. *The Journal of the Acoustical Society of America*, 107(3), 1413-1420.
- [77] Guy, R. W. (1979). The steady state transmission of sound at normal and oblique incidence through a thin panel backed by a rectangular room—A multi-modal analysis. *Acta Acustica united with Acustica*, 43(5), 295-304.
- [78] Brunskog, J. (2012). The forced sound transmission of finite single leaf walls using a variational technique a. *The Journal of the Acoustical Society of America*, 132(3), 1482-1493.
- [79] Trevathan, J. W., & Pearse, J. R. (2005). The significance of the incident sound field on the sound transmission loss of a finite panel. *Building Acoustics*, 12(4), 225-235.

- [80] Brutel-Vuilmet, C., Guigou-Carter, C., Villot, M., & Jean, P. (2006). Measurement of the sound reduction index as a function of the incidence angle by two different methods. *Building Acoustics*, 13(1), 33-48.
- [81] Hopkins, C. (2004). Airborne Sound Insulation of Beam and Block Floors: Direct and Flanking Transmission. *Building Acoustics*, 11(1), 1-25.
- [82] Clasen, D., & Langer, S. (2007). Finite element approach for flanking transmission in building acoustics. *Building Acoustics*, 14(1), 1-14.
- [83] Warnock, A. C. C. (1982). Influence of specimen frame on sound transmission loss measurement. *Applied Acoustics*, 15(4), 307-314.
- [84] Craik, R. J. M., Nightingale, T. R. T., & Steel, J. A. (1997). Sound transmission through a double leaf partition with edge flanking. *The Journal of the Acoustical Society of America*, 101(2), 964-969.
- [85] Stani, M. M., Muellner, H., Plotizin, I., & Zlabinger, K. (2005, July). Sound insulation of plasterboard walls and airflow resistivity: an empirical examination with respect to practical applications. In *Proc. Forum Acusticum* (pp. 1987-1992).
- [86] Wang, J., Lu, T. J., Woodhouse, J., Langley, R. S., & Evans, J. (2005). Sound transmission through lightweight double-leaf partitions: theoretical modelling. *Journal of sound and vibration*, 286(4), 817-847.
- [87] Poblet-Puig, J., Rodríguez-Ferran, A., Guigou-Carter, C., & Villot, M. (2009). The role of studs in the sound transmission of double walls. *Acta Acustica united with Acustica*, 95(3), 555-567.
- [88] Bradley, J. S., & Birta, J. A. (2001). On the sound insulation of wood stud exterior walls. *The Journal of the Acoustical Society of America*, 110(6), 3086-3096.
- [89] Muellner, H., & Plotizin, I. (2002). The influence of the screw position on the airborne sound insulation of plasterboard walls. In *Proceedings of forum acusticum 2002*.
- [90] Roozen, N. B., Muellner, H., Labelle, L., Rychtáriková, M., & Glorieux, C. (2015). Influence of panel fastening on the acoustic performance of light-weight building elements: study by sound transmission and laser scanning vibrometry. *Journal of Sound and Vibration*, 346, 100-116.
- [91] Ten Wolde, T. (1973). Reciprocity experiments on the transmission of sound in ships.
- [92] Ten Wolde, T. (2010). Reciprocity measurements in acoustical and mechano-acoustical systems. Review of theory and applications. *Acta Acustica united with Acustica*, 96(1), 1-13.
- [93] Verheij, J. W. (1982). Multi-path sound transfer from resiliently mounted shipboard machinery: Experimental methods for analyzing and improving noise control.
- [94] Verheij, J. W. (1997). Inverse and reciprocity methods for machinery noise source characterization and sound path quantification. Part 1: Sources. *International Journal of Acoustics and Vibration*, 2(1), 11-20.

- [95] Späh, M. M., & Gibbs, B. M. (2009). Reception plate method for characterisation of structure-borne sound sources in buildings: Assumptions and application. *Applied Acoustics*, 70(2), 361-368.
- [96] Blau, M. (1999). Indirect measurement of multiple excitation force spectra by FRF matrix inversion: influence of errors in statistical estimates of FRFs and response spectra. *Acta Acustica united with Acustica*, 85(4), 464-479.
- [97] Van der Linden, P., & Floetke, H. (2004, September). Comparing inverse force identification and the mount stiffness force identification methods for noise contribution analysis. In *ISMA 2004 Conference Proceedings* (pp. 2971-2985).
- [98] Elliott, A. S. (2009). *Characterisation of structure borne sound sources in-situ* (Doctoral dissertation, University of Salford).
- [99] Verheij, J. W., Janssens, M. H., & Charlier, P. J. (1995, July). Using pseudo-forces for characterization of structure-borne sound sources. In *INTER-NOISE and NOISE-CON Congress and Conference Proceedings* (Vol. 1995, No. 3, pp. 559-562). Institute of Noise Control Engineering.
- [100] Janssens, M. H. A., & Verheij, J. W. (2000). A pseudo-forces methodology to be used in characterization of structure-borne sound sources. *Applied Acoustics*, 61(3), 285-308.
- [101] Thite, A. N., & Thompson, D. J. (2003). The quantification of structure-borne transmission paths by inverse methods. Part 1: Improved singular value rejection methods. *Journal of Sound and Vibration*, 264(2), 411-431.
- [102] Janssens, M. H., Verheij, J. W., & Thompson, D. J. (1999). The use of an equivalent forces method for the experimental quantification of structural sound transmission in ships. *Journal of sound and vibration*, 226(2), 305-328.
- [103] Elliott, A., & Moorhouse, A. T. (2008). Characterisation of structure borne sound sources from measurement in-situ. *Journal of the Acoustical Society of America*, 123(5), 3176.
- [104] Elliott, A. S., Moorhouse, A. T., Huntley, T., & Tate, S. (2013). In-situ source path contribution analysis of structure borne road noise. *Journal of Sound and Vibration*, 332(24), 6276-6295.
- [105] Mondot, J. M., & Petersson, B. (1987). Characterization of structure-borne sound sources: the source descriptor and the coupling function. *Journal of sound and vibration*, 114(3), 507-518.
- [106] Moorhouse, A. T. (2001). On the characteristic power of structure-borne sound sources. *Journal of sound and vibration*, 248(3), 441-459.
- [107] ISO, E. (2010). 3744 Acoustics. *Determination of sound power levels of noise sources using sound pressure. Engineering method in an essentially free field over a reflecting plane (ISO 3744: 1994)*.

- [108] Smith Jr, P. W. (1962). Response and radiation of structural modes excited by sound. *The Journal of the Acoustical Society of America*, 34(5), 640-647.
- [109] Fahy, F. J. (2003). Some applications of the reciprocity principle in experimental vibroacoustics. *Acoustical Physics*, 49(2), 217-229.
- [110] Bobrovnikskii, Y. I., & Pavic, G. (2003). Modelling and characterization of airborne noise sources. *Journal of sound and vibration*, 261(3), 527-555.
- [111] Pavić, G. (2010). Air-borne sound source characterization by patch impedance coupling approach. *Journal of Sound and Vibration*, 329(23), 4907-4921.
- [112] Magrans, F. X. (1981). Method of measuring transmission paths. *Journal of Sound and Vibration*, 74(3), 321-330.
- [113] Magrans, F. X., Rodriguez, P. V., & Cousin, G. C. (2005). Low and mid-high frequency advanced transmission path analysis. In *Proceedings of the Twelfth International Congress on Sound and Vibration ICSV12*.
- [114] Zafeiropoulos, N., Moorhouse, A., Mackay, A., & Senapati, U. (2013, April). A comparison of two in-situ transfer path analysis methods. In *RASD 2013 11th International Conference on Recent Advances in Structural Dynamics 1st-3rd July 2013*.
- [115] Lohrmann, M., & Hohenberger, T. (2008). Operational transfer path analysis: comparison with conventional methods. *Journal of the Acoustical Society of America*, 123(5), 3534.
- [116] Gajdatsy, P., Janssens, K., Gielen, L., Mas, P., & Van Der Auweraer, H. (2008). Critical assessment of Operational Path Analysis: effect of coupling between path inputs. *Journal of the Acoustical Society of America*, 123(5), 3876-3876.
- [117] Janssens, K., Gajdatsy, P., Gielen, L., Mas, P., Britte, L., Desmet, W., & Van der Auweraer, H. (2011). OPAX: A new transfer path analysis method based on parametric load models. *Mechanical Systems and Signal Processing*, 25(4), 1321-1338.
- [118] Guasch, O., & Magrans, F. X. (2004). The global transfer direct transfer method applied to a finite simply supported elastic beam. *Journal of sound and vibration*, 276(1), 335-359.
- [119] Schevenels, P., van der Linden, P. J., & Vermeir, G. (2010). An inverse force measurement method to determine the injected structure-borne sound power from an installation into a building element. *Building Acoustics*, 17(3), 199-219.
- [120] Geebelen, N. (2008). Structure-Borne Sound Sensitivity of Building Structures-Assessment of the Acoustic Performances of Multilayered Structures by Simulation and Measurement Techniques. *Doctoral Thesis*. Katholieke Universiteit Leuven
- [121] Squicciarini, G., Putra, A., Thompson, D. J., Zhang, X., & Salim, M. A. (2015). Use of a reciprocity technique to measure the radiation efficiency of a vibrating structure. *Applied Acoustics*, 89, 107-121.

- [122] Heilmann, G., Meyer, A., & Döbler, D. (2008). Time-domain beamforming using 3D-microphone arrays. *Proceedings of the BeBeC*.
- [123] Patil, N., WongMcSweeney, B. M., Fitton, R., Elliott, A., & Waddington, D. (2016). Feasibility study on using acoustic camera for acoustic imaging to detect air leaks in a structure. In *Proceedings of the IOA conference, Kenilworth, UK*.
- [124] *Panel Noise Contribution Analysis*. Retrieved from-  
<http://www.microflown.com/library/publications/panel-noise-contribution-analysis.html>
- [125] Hendricx, W., Choi, Y. B., Ha, S. W., & Lee, H. K. (1997). *Experimental body panel contribution analysis for road induced interior noise of a passenger car* (No. 971913). SAE Technical Paper.
- [126] Fahy, F. J. (1995). The vibro-acoustic reciprocity principle and applications to noise control. *Acta Acustica united with Acustica*, 81(6), 544-558.
- [127] Pavić, G., & Totaro, N. (2008). Noise source characterisation using patch impedance technique. *The Journal of the Acoustical Society of America*, 123(5), 3310-3310.
- [128] Chazot, J. D., & Guyader, J. L. (2007). Prediction of transmission loss of double panels with a patch-mobility method. *The Journal of the Acoustical Society of America*, 121(1), 267-278.
- [129] de Klerk, D., Rixen, D. J., & Voormeeren, S. N. (2008). General framework for dynamic substructuring: history, review, and classification of techniques. *AIAA journal*, 46(5), 1169.
- [130] Magrans Fontrodona, F. X., Arcas, K., Vicens Rodríguez, P., Poblet-Puig, J., & Rodríguez Ferran, A. (2017). Experimental numerical correlation of subsystem contributions in the advanced transfer path analysis framework. In *24th International Congress on Sound and Vibration* (pp. 1-8).
- [131] Comesaña, D. F., & Wind, J. (2011). *A scanning method for source visualization and transfer path analysis using a single probe* (No. 2011-01-1664). SAE Technical Paper.
- [132] Bobrovnikskii, Y. I. (2001). A theorem on the representation of the field of forced vibrations of a composite elastic system. *Acoustical Physics*, 47(5), 507-510.
- [133] Ouisse, M., Maxit, L., Cacciolati, C., & Guyader, J. L. (2005). Patch transfer functions as a tool to couple linear acoustic problems. *Journal of vibration and acoustics*, 127(5), 458-466.
- [134] Moorhouse, A. T., & Elliott, A. S. (2012, April). Indirect measurement of frequency response functions applied to the problem of substructure coupling. In *INTER-NOISE and NOISE-CON Congress and Conference Proceedings* (Vol. 244, No. 1, pp. 814-820). Institute of Noise Control Engineering.
- [135] Bauer, M., Moorhouse, A., & Alber, T. (2011). Virtual Acoustic Prototyping for electrical steering systems. *DAGA*.

- [136] Aucejo, M., Maxit, L., Totaro, N., & Guyader, J. L. (2010). Convergence acceleration using the residual shape technique when solving structure–acoustic coupling with the patch transfer functions method. *Computers & Structures*, 88(11-12), 728-736.
- [137] Roozen, N. B., Leclere, Q., Rychtarikova, M., & Glorieux, C. (2015). A global error estimator for the uncertainty of a multi-channel spectral analysis. *Applied Acoustics*, 87, 57-63.
- [138] Thite, A. N., & Thompson, D. J. (2003). The quantification of structure-borne transmission paths by inverse methods. Part 2: Use of regularization techniques. *Journal of Sound and Vibration*, 264(2), 433-451.
- [139] Crocker, M. J., & Price, A. J. (1969). Sound transmission using statistical energy analysis. *Journal of Sound and Vibration*, 9(3), 469-486.
- [140] Pezerat, C., & Guyader, J. L. (2000). Force analysis technique: reconstruction of force distribution on plates. *Acta Acustica united with Acustica*, 86(2), 322-332.
- [141] Schroeder, M. R. (1996). The “Schroeder frequency” revisited. *The Journal of the Acoustical Society of America*, 99(5), 3240-3241.
- [142] Craik, R. J. M., & Smith, R. S. (2000). Sound transmission through double leaf lightweight partitions part I: airborne sound. *Applied Acoustics*, 61(2), 223-245.
- [143] Massaglia, J. F. (2017). *Modelling the sound insulation of corrugated roof structures: an extended transfer matrix approach* (Doctoral dissertation, University of Salford).
- [144] Demmel, J. W. (1987). On condition numbers and the distance to the nearest ill-posed problem. *Numerische Mathematik*, 51(3), 251-289.
- [145] Yoon, S. H., & Nelson, P. A. (2000). Estimation of acoustic source strength by inverse methods: Part II, experimental investigation of methods for choosing regularization parameters. *Journal of sound and vibration*, 233(4), 665-701.
- [146] Hine, M. J. (1973). Acoustically induced vibrations of slender rods in a cylindrical duct. *Journal of Applied Mechanics*, 40(2), 459-463.
- [147] Guy, R. W. (1979). The steady state transmission of sound at normal and oblique incidence through a thin panel backed by a rectangular room—A multi-modal analysis. *Acta Acustica united with Acustica*, 43(5), 295-304.
- [148] Moorhouse, A. T., Elliott, A. S., & Evans, T. A. (2009). In situ measurement of the blocked force of structure-borne sound sources. *Journal of Sound and Vibration*, 325(4), 679-685.
- [149] Lennström, D., Olsson, M., Wullens, F., & Nykänen, A. (2016). Validation of the blocked force method for various boundary conditions for automotive source characterization. *Applied Acoustics*, 102, 108-119.



- [150] Pietrzyk, A. (1998, October). Computer modeling of the sound field in small rooms. In *Audio Engineering Society Conference: 15th International Conference: Audio, Acoustics & Small Spaces*. Audio Engineering Society.
- [151] Cooper, I. J., & Pollard, H. F. (1978). Low-Frequency Resonances in Unsymmetrical Enclosures. *Acta Acustica united with Acustica*, 41(2), 86-93.
- [152] Kuttruff, H. (2016). *Room acoustics*. Crc Press.
- [153] Papagiannopoulos, G. A., & Hatzigeorgiou, G. D. (2011). On the use of the half-power bandwidth method to estimate damping in building structures. *Soil Dynamics and Earthquake Engineering*, 31(7), 1075-1079.
- [154] Vorländer, M. (1995). Revised relation between the sound power and the average sound pressure level in rooms and consequences for acoustic measurements. *Acta Acustica united with Acustica*, 81(4), 332-343.
- [155] Moorhouse, A., & Ramadoray, R. (2006). Measurement of the average sound pressure level in a room at low frequency. In *Proceedings of 13th International Congress on Sound and Vibration*.
- [156] Schoenwald, S., & Pedersoli, S. (2016, August). Applicability of measurement method according to ISO 16283 in small rooms at low frequencies. In *INTER-NOISE and NOISE-CON Congress and Conference Proceedings* (Vol. 253, No. 5, pp. 3334-3345). Institute of Noise Control Engineering.
- [157] Marchetto, C., Maxit, L., Robin, O., & Berry, A. (2017). Vibroacoustic response of panels under diffuse acoustic field excitation from sensitivity functions and reciprocity principles. *The Journal of the Acoustical Society of America*, 141(6), 4508-4521.